Faculty of Engineering and Science

Experimental Investigation of Emulsions Formation and Evolution in Pipeline Flow

Wong Siew Fan

This thesis is presented for the Degree of
Doctor of Philosophy
of
Curtin University

June 2017

Declaration

To the best of my knowledge and belief this thesis contains no material previously published by any other person except where due acknowledgement has been made.

This thesis contains no material which has been accepted for the award of any other degree or diploma in any university.

Signature:

Date: 20/06/2017

List of Publications

Following are the journal papers that have been published from current work:

1. Wong, S.F., Lim, J.S. and Dol, S.S., 2015. Crude oil emulsion: a review on formation, classification and stability of water-in-oil emulsions. *Journal of Petroleum Science and Engineering*, *135*, pp.498-504.
2. Wong, S.F., Law, M.C., Samyudia, Y. and Dol, S.S., 2015. Rheology study of water-in-crude oil emulsions. *Chemical Engineering Transactions*, *45*, pp.1411-1416.
3. Lim, J.S., Wong, S.F., Law, M.C., Samyudia, Y. and Dol, S.S., 2015. A review on the effects of emulsions on flow behaviours and common factors affecting the stability of emulsions. *Journal of Applied Sciences*, *15*, pp.167-172.

Acknowledgement

First and foremost, I would like to express my sincere gratitude to my main supervisor, Associate Professor Dr. Sharul Sham bin Dol for his encouragement and endless guidance throughout my Ph.D. degree. I am very grateful to him for providing me with this golden opportunity to work on this project. It would be impossible for me to complete my research without his constant care and motivation.

My sincere thanks also go to my co-supervisor, Dr. Wee Siaw Khur, whose help has provided valuable ideas during my research period. Her vital support, assistance and encouragement have made it possible for me to achieve the goal.

I would also like to pay my tribute and appreciation to the persons below who have assisted and supported me during the research period.

Laboratory technicians, Mr. Aspindy and Mr. Michael Ding and my research partner, Jason Lim have been very helpful. Their services for the fabrication, construction, installation and set-up of the research equipment are very much appreciated.

MCOT (Miri Crude Oil Terminal) Team, for giving me access and clearance to obtain valuable crude oil for my academic purpose is owed my thanks.

My beloved Mom and Dad, without them I am nothing; they not only assisted me financially, but also extended their support morally and emotionally.

The Ministry of Higher Education, for providing me with the Exploratory Research Grant Scheme (Grant no. L8-1034). Without their opportunity and funding, it would be impossible for me to achieve my success.

Faculty of Engineering and Science, Curtin University, Malaysia for the tuition fee support. I would not be able to involve in this project without their valuable financial support.

Abstract

In the oil production industry, emulsification – two immiscible liquids mix together, is unavoidable as crude oil is usually produced together with water from the reservoir. The presence of emulsions brings numerous undesirable effects to the industry; it affects the flow regimes and flow behaviour, reduces the quality of crude oil, requires longer retention time in the separation vessels, causes corrosion to the transport system, contaminates catalyst used in the refining process that leads to huge economic losses. So, it is essential to investigate the formation of emulsions and to study the flow behavior in the pipeline so that proper method can be recommended for the control of the effect of emulsions. It is important to remark that the formation of emulsions through flow shear using lab-scale flow rig has been less researched. This leads to the objectives of this study, which are: first, to characterize the formation of water-in-crude oil (W/O) emulsions formed through the constriction in the pipeline; second, to investigate the effects of W/O emulsions to pipeline flow transport; and third, to analyze the roles of turbulent energy in emulsions formation and flow transport in the pipeline system.

First, a lab-scale flow loop was designed and fabricated, in which the emulsification was induced by the pipeline constriction solely through flow shear to mirror industrial environment. Three parameters, namely, water cuts (WC), Reynolds number and pipeline constrictions were studied. For each of the parameters, the regions of study are: 0 to 40% WC; laminar ($1100 < Re < 1800$) and transitional ($2400 < Re < 2800$) flow regimes; and gradual contraction with a contraction ratio of 0.50 and 0.75 (GC 0.50 and GC 0.75) and sudden contraction with a contraction ratio of 0.50 and 0.75 (SC 0.50 and SC 0.75). An ultrasonic velocity profiler (UVP) was used to measure the flow behavior.

The rheology analysis was used to investigate the rheological behaviour of pure crude – Miri Light Crude (MLC) and water-oil emulsions. As the rheological behaviour of water-oil emulsions shows that phase inversion from W/O emulsions to O/W emulsions happens at 40% WC, subsequent study was carried out up to 40% WC only as this study focused only on W/O emulsions. Through visual observation, the results show that the stability and the amount of emulsions formed increases with the increase in the water cuts and the

Reynolds number. Next, the results also show that emulsions produced from GC 0.50 and SC 0.50 are more stable than the GC 0.75 and SC 0.75.

Next, the wall shear stress (τ_w) examination, supported with the energy dissipation analysis as well as analysis on the amount and stability of emulsions, was carried out. The results show that the τ_w increases with the increase in water cuts up to 10% and then started to decrease with further increase in the water cuts up to 40%. It was also determined that inlet flow with higher velocity results in the lower τ_w. Furthermore, the study shows that GC 0.50 and SC 0.50 results in a lower τ_w as compared to the GC 0.75 and SC 0.75, with the gradual contraction results in lower τ_w than the sudden contraction.

Next, Reynolds stress and turbulence intensity analysis show that turbulence activities and transport influence the formation of emulsions and it is induced from the constriction of pipeline. The largest amount of fluctuating components are observed nearest to the constriction and the turbulence is diminishing as the flow flows further away from the constriction.

This research work enables the oil industry to provide a better strategy in treating the emulsification phenomena in the pipeline transportation system. In the industry, optimum conditions can be obtained from the combination of Reynolds number and types of pipeline constriction in order to result in the lowest wall shear stress so that the energy losses during the transportation of crude in the pipeline can be minimized.

Nomenclature

Symbols

D	Inner pipe diameter
f	Friction factor
k	Flow consistency coefficient
K_L	Loss coefficient
ℓ_e	Entrance length
L	Length
n	Flow behaviour index
n_r	Emulsions relative viscosity
p	Pressure
R	Pipe radius
Re	Reynolds number
u	Velocity in *x*-direction
u'	Fluctuating component of *x*-velocity
U	Instantaneous velocity
V	Velocity
x	Location in the *x*-direction
y	Location in the *y*-direction

Greek symbols

ε	Dissipation energy rate
μ	Dynamic viscosity

ϑ	Kinematic viscosity
ϕ	Volume fraction of dispersed droplets
ρ	Density
τ	Shear stress
τ_w	Wall shear stress

Abbreviations

BS&W	Basic sediments and water
Ch Dist	Channel distance
Cyc/Pulse	Cycles per pulse
End Ch	Distance of last channel
First Ch	Distance of first channel
GC	Gradual constriction
L	Litre
LVR	Linear viscoelasticity region
MCOT	MCOT Miri Crude Oil Terminal
MLC	MLC Miri Light Crude
NL	Noise level
O/W	Oil-in-water
O/W/O	Oil-in-water-in-oil
Rep/Prof	Number of profile repetitions
RF Gain	Echo signal
RMS	Root-mean-square
RSS	Root-sum-square
SARA	SARA Saturates, Aromatics, Resins, and Asphaltenes

SC	Sudden constriction
SS	Stainless steel
US	Ultrasonic
UVP	Ultrasonic velocity profiler
Vac	Vac Voltage Alternating Current
Vdc	Vdc Voltage Direct Current
Vel Range	Velocity range
WAT	Wax appearance temperature
W/O	Water-in-oil
W/O/W	Water-in-oil-in-water

List of Figures

List of Tables

Table of Contents

CHAPTER 1

INTRODUCTION

1.1 Introduction

In Malaysia, oil and gas industry plays a very important role in contributing to support the country's economy. To date, proven reserves oil are about 28.35 billion barrels and the average current production rate of crude oil products is about 730,000 barrels per day [1]. According to the Malaysian Investment Development Authority, Malaysia's oil and gas industries contribution to gross national income (GNI) of Malaysia in the year 2009 was RM110 billion and it is expected to increase up to RM1.7 trillion by the year 2020 [2].

Crude oil from oil and gas reservoir has to be processed and refined into more useful finished products in the oil production industries before they are sent to end users. In the oil and gas industry, emulsification in the pipeline flow is unavoidable as crude oil usually comes together with water from the reservoir. **Figure 1.1** shows the simplified process flow diagram of crude oil processing. As can be seen in **Figure 1.1**, crude oil must pass through different processes before it is processed and refined into more useful products such as gasoline, petroleum, liquefied petroleum gas, lubricating oil, asphalt, paraffin wax, diesel fuel, bitumen and etcetera. Those processes include heating (in heater and pre-heat train unit), salt removing (in desalter unit), separation of water from crude oil (in separator), separation of crude oil into different fractions (crude unit) and other refinery processes. In the oil and gas industry, these processes which involve converting or processing the collected materials during the upstream stage (locating underground oil reserves process) into useful end products is characterized as the downstream process. Throughout all these processes, the agitation, mixing as well as the turbulence energy formed through downhole wellbores, surface chokes, valves, pumps, and pipes will directly lead to the formation of emulsion in the crude oil flow [3].

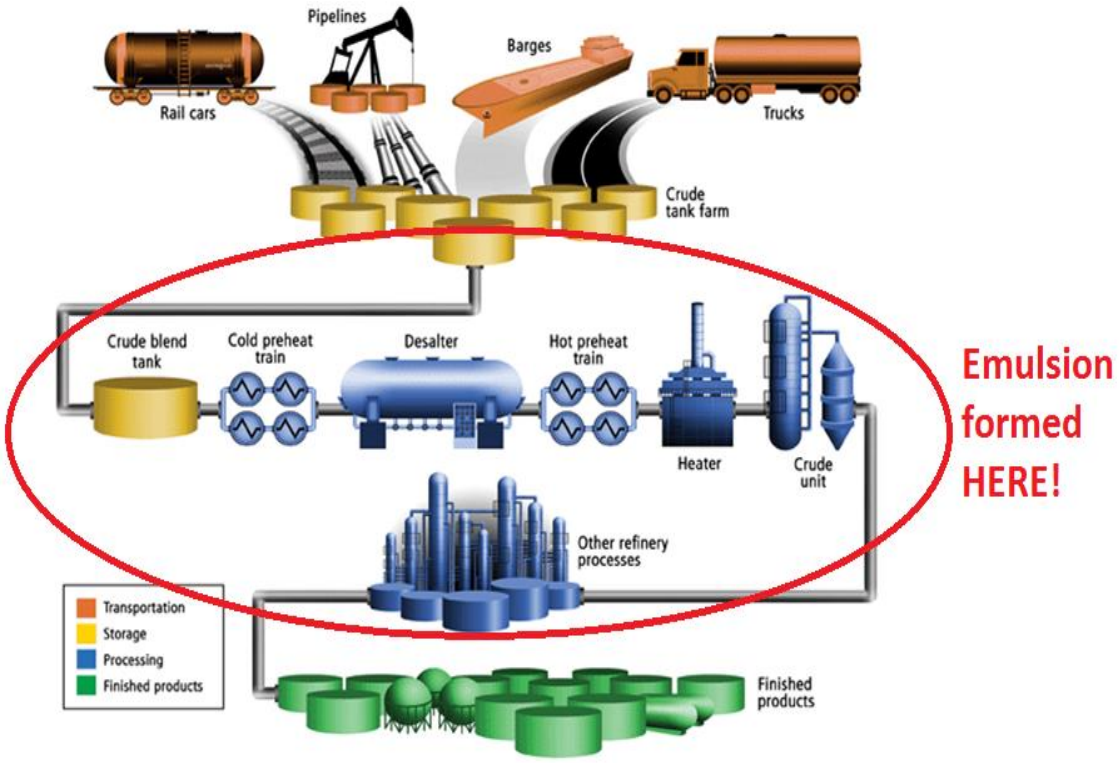

Figure 1.1: Simplified process flow diagram of crude oil processing [4].

An emulsion is defined as a system, whereby one immiscible liquid phase is dispersed as globules (dispersed phase) in the second phase of immiscible liquid (continuous phase) [3]. There are three types of emulsions: they are, water-in-oil (W/O) emulsion, oil-in-water (O/W) emulsion and multiple emulsion [5]. Multiple emulsion includes water-in-oil-in-water (W/O/W) emulsion and oil-in-water-in-oil (O/W/O) emulsion [6]. These emulsions can be found in many areas either as a desirable type or an undesirable type. For the O/W emulsion and W/O emulsions, they can be easily found in the petroleum industry [7], in food matrices [8] as well as pharmaceutical field [9]. Types of emulsion formed depend on the volumetric amount of the phases [10]. However, the formation of emulsions is undesirable in the oil and gas industry because emulsification brings a number of problems; it affects the flow regimes and flow behaviour, reduces the crude oil's quality, occupies a volume in the pipeline, reduces the mass flow rate, requires longer retention time in the separation vessels, causes corrosion to the transport system, contaminates catalyst used in the refining process and increases operating cost. Yet, this is unavoidable because oil will always be produced together with water from the reservoir

and towards the end of the reservoir life, with the increasing amount of water especially if the reservoir is driven by water aquifer [3].

In Malaysia, the oil quality is determined by basic sediments and water parameter (BS&W), where the BS&W must not exceed 0.5 volume % [11]. It has been reported that oil producers have to lower the selling price of their oil for not meeting the required crude oil quality [11]. It was reported that the presence of emulsions in crude oil will affect the flow of the crude oil in the pipeline, which will directly affect the capacity of separators, pumps and pipeline [3]. Besides that, higher concentration of emulsions is also correlated with larger values of pressure drop [12-14]. Higher pressure drop requires higher pumping power or lower flow rate and this in turn incurs a higher operating cost and more oil deferment [3]. It has been discovered that the presence of emulsions also can affect the general flow behaviour of the mixture, the friction factor of the flow, as well as the viscosity of the mixture and pressure drop along the pipeline [3]. A more detailed literature review on the effects of emulsions are presented in Chapter 3.1.

Behaviour of pure crude and emulsions is complex. They are shown to behave differently given different types of pure crude and different conditions. According to Keleşoğlu *et al*. [15], pure crude oil is a Newtonian fluid at temperatures of 15℃ and above, below than that, the crude oil displays shear thinning behaviour. Keleşoğlu *et al*. [15] also reported that W/O emulsions show strong shear thinning behaviour at low temperatures and the shear thinning behaviour becomes stronger at aqueous volume fractions above 0.55.

It is essential to understand the rheology of pure crude and emulsions if they are Newtonian or non-Newtonian fluid. This is because if they are non-Newtonian fluid, the viscosity of the fluid depends on the shear rate. The viscosity will increase with the shear rate (shear-thickening behaviour) or decrease with the shear rate (shear-thinning behaviour). This has an effect on the flowing fluid, such as, in controlling the flow regime of the flowing fluid (Reynolds number which is based on viscosity) and in determining the shear stress of the flowing fluid (shear stress is the production of viscosity and shear rate). This will add complexity to the study if the crude and emulsions are non-Newtonian fluids.

Figure 1.2 describes the relationship between the shear stress and shear rate (velocity gradient) for Newtonian and non-Newtonian fluid.

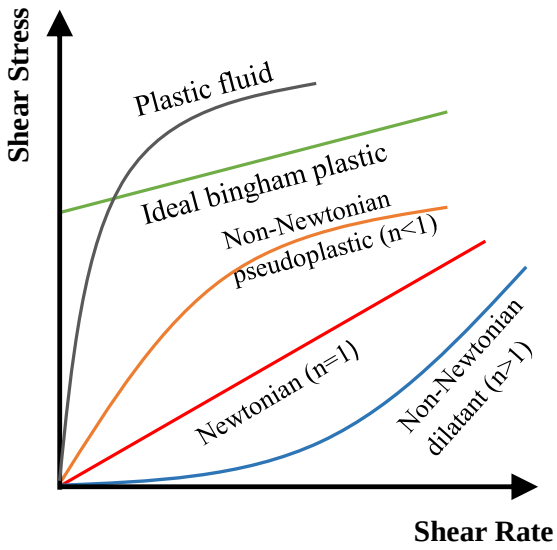

Figure 1.2: Shear stress and shear rate of Newtonian and non-Newtonian [16].

For a Newtonian fluid, the shear stress is linearly dependent on the shear rate, provided the viscosity is constant. The straight line plot of shear stress versus shear rate will pass through the origin or it displays as a straight line with a slope of unity on a log-log plot [17]. The relationship of shear stress and shear rate can be described by Equation 1.1 below, which obeys the Newton law of viscosity [17]:

$$\tau = \mu \frac{du}{dy} \tag{1.1}$$

where τ is the shear stress, μ is the viscosity and du/dy is the shear rate.

For non-Newtonian fluid, it does not obey Newton law of viscosity. The relationship of shear stress and shear rate for non-Newtonian fluid can be described using a Power-Law model or Ostwald-de Waele model as shown in Equation 1.2 [17]:

$$\tau = k\left(\frac{du}{dy}\right)^{n} \tag{1.2}$$

where τ is the shear stress, k is the flow consistency coefficient, n is the flow behaviour index, and du/dy is the shear rate. For shear-thinning fluid, the flow behaviour index should be less than 1; for shear-thickening fluid, the flow behaviour index should be greater than 1 [17].

In the existing literature, various studies have been conducted to understand the formation of emulsions. However, almost all of these studies on the emulsification are due to the application of an external force such as stirring, shaking, blending and whisking. Besides, most of these studies were carried out in batch processes, which means emulsions were formed inside a beaker or a tank, instead of using continuous process. To the author's best knowledge, only Nädler and Mewes [14], Keleşoğlu *et al*. [15] and Plasencia *et al*. [18] had carried out a study on the formation of water-in-oil emulsions solely from flow shear using a lab-scale pipeline. Less attention has been paid to the pipeline flow of W/O emulsions. Therefore, one of the attempts of this research study is to investigate the formation of W/O emulsions using a continuous flow loop, where the emulsification process is induced by the flow shear and turbulence effects such as the pipeline constriction disturbance in the flow loop.

1.2 Problem Statement

In the existing research studies in the emulsification field, less emphasis has been placed on the usage of flow loop to replicate the emulsification process in the real practical field conditions. Existing experimental studies on emulsification were mainly focused on the membrane emulsification, forming emulsions using external forces as well as emulsification studies based on batch processes. These existing emulsification studies poorly represent the emulsification process in real practical field, where the mixture of crude oil and water are transported in a continuous process. Also, emulsions in the field are formed through choke valves, pumps and pipes, not by applying external force such as stirring. Besides, the real focus on the emulsions treatment was based on using chemical compounds, such as, concentration of asphaltenes and resins, concentration of volatile aromatic components, salt concentration and etcetera. But, mechanical effects to the emulsification process has not yet been established. Also, study on relating the effect of

emulsions to the friction/wall shear stress (WSS) in the pipeline has not yet been carried out. Moreover, the roles of turbulent flow generated in the pipeline in emulsification process has not yet been understood.

1.3 Objectives and Scopes of Study

This research is to perform an in-depth study of the behaviours of water-in-crude oil emulsions in the pipeline flow. The main objectives of this research are:

1. To characterize the formation of water-in-crude oil (W/O) emulsions formed through the constriction in the pipeline.
    - Characteristics study is carried out by analyzing the rheological behaviour of W/O emulsions and stability of the W/O emulsions.
    - Amount of emulsions formed is examined in order to identify the effects of flow regime, water cuts and types of constriction on the formation of emulsion.

2. To investigate the effects of water-in-crude oil emulsion to pipeline flow transport.
    - By varying the types of pipeline constriction, water cuts and flow regime, the wall shear stress of the flowing fluid in the pipeline are examined.

3. To analyze the roles of turbulent energy in emulsions formation and flow transport in the pipeline system.
    - Kinetic energy budget equation is used for the study of turbulence.
    - Energy dissipation is calculated.
    - Reynolds stress and turbulence intensity are analysed and discussed.

Limitations of the study:

- The chosen controlling parameter – Reynolds number (inlet flow velocity) is only limited to laminar and transitional flow regimes.
- The study does not determine the droplet sizes of the emulsions formed.

1.4 Novelty, contribution and significance

No work has been done yet to explore the flow-induced emulsification through a 90 ° bend pipeline constriction using a model lab-scale continuous flow rig. The 90 ° bend constriction is used so as to replicate a choke valve in the real industries. Existing work mostly focused on membrane emulsification and emulsification formation with the application of external forces such as stirring. So, this research study on flow-induced emulsification by using pipeline constriction can better reflect the real practical industry conditions.

Besides, the findings in this research are able to tackle or handle the emulsions mechanically, as different types of 90 ° bend pipeline constriction are used to study the effect of those pipeline constrictions to the emulsification process. Previous studies on emulsification was mainly focused on the study of emulsions formation chemically.

Next, this study is capable of relating the effects of emulsions downstream of the 90 ° bend pipeline constriction to the friction or wall shear stress in the pipeline flow. This has not yet been established in the existing research works.

Another significance of this study is the contribution to Malaysia's oil and gas industry. This is because local offshore crude oil, which is Miri Light Crude (MLC) blend is used in this research. Emulsification behaviours as well as the evolution in the pipeline flow of this type of crude are studied and analyzed.

In addition, completing this research will be a significant contribution to the economics of oil and gas industry as the outcome of this research can aid in the design of pipelines in the field to allow less emulsion formation and provide better strategy in treating them. By reducing the amount of emulsified crude oil, the industry is able to increase the revenue.

Finally, the roles of turbulence in the formation of emulsions can be understood from this study. This will then broadly contribute to the transportation of crude, *i.e.* with less emulsions formation, as the energy for the formation of emulsions can be controlled accordingly with the understanding on the roles of turbulence activities in the emulsification process.

1.5 Overview of the thesis

This thesis is divided into the following chapters:

The **first** chapter introduces the challenges faced by oil and gas industries as well as the objectives and significance of this research study.

The **second** chapter presents the background of this study, which introduces the formation of emulsions, types of emulsions, classification of Newtonian and non-Newtonian fluid and also discusses the theory of turbulence.

The **third** chapter provides the literature review on the effects of emulsions, stability of emulsions, factors influencing the stability of emulsions as well as the experimental studied done based emulsification process. The research gap of this study is also included in this chapter.

The **fourth** chapter describes the design of the flow loop and designs of the pipeline constrictions used for the experiments, the materials and resources used in this research study, experimental set-up and experimental methodology. This chapter also presents the calibration results and uncertainty analysis of the current research.

The **fifth** chapter commences with the results and discussion on the rheological behaviour of pure crude oil. Subsequently, the experimental results and discussions on the characterization of water-in-oil emulsions based on the rheological behaviour of the emulsions and the stability of the emulsions are presented. The amount of emulsions formed at different parameters is also compared and discussed in this chapter.

The **sixth** chapter provides the experimental results on the wall shear stress of the horizontal pipeline with the effect of different water cuts, different Reynolds number (flow rates) and different type of pipeline constriction. The changes of wall shear stress along the pipeline is also presented. Dissipation energy is presented to support the results presented in this chapter.

The **seventh** chapter discusses on the roles of turbulent energy in the formation of emulsions based on the turbulence analytical results, which are, Reynolds stress and turbulence intensity.

The **last** chapter concludes the results of the experimental research from the research and presents some recommendations further to this study.

Then, the literature sources that were used in this thesis are listed. The very last section of this thesis are appendixes.

CHAPTER 2

THEORETICAL BACKGROUND

This chapter presents the fundamental background on emulsions, including the formation, the type as well as classification of emulsions. Classification of types of flowing fluid is discussed in this chapter as well. The governing equations are discussed to understand the physics for emulsification. All the topics being presented in this chapter will serve as a comprehensive knowledge to aid in the understanding of the fundamental of this research.

2.1 Emulsions Formation

An emulsion can be defined as a system, whereby one immiscible liquid phase is dispersed as globules (dispersed phase) in the second phase of immiscible liquid (continuous phase) [3]. There are three types of emulsions, namely, water-in-oil (W/O) emulsion, oil-in-water (O/W) emulsion and multiple emulsion. W/O emulsion is formed when water globules are dispersed throughout the oil continuous phase, as shown in **Figure 2.1**. O/W emulsion is formed when oil globules are dispersed throughout the water continuous phase, as shown in **Figure 2.2**. A multiple emulsion is a complex emulsion system, whereby W/O or O/W emulsions are dispersed throughout another immiscible phase [19]. Multiple emulsion includes water-in-oil-in-water (W/O/W) emulsion and oil-in-water-in-oil (O/W/O) emulsion [6].

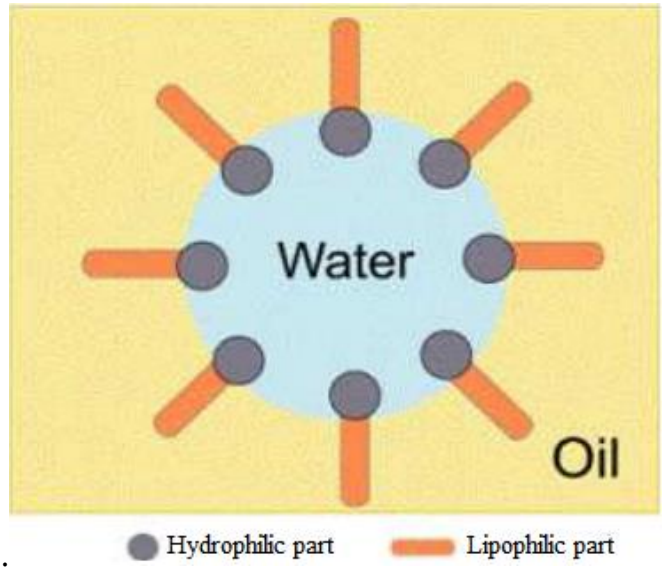

Figure 2.1: W/O emulsion [19].

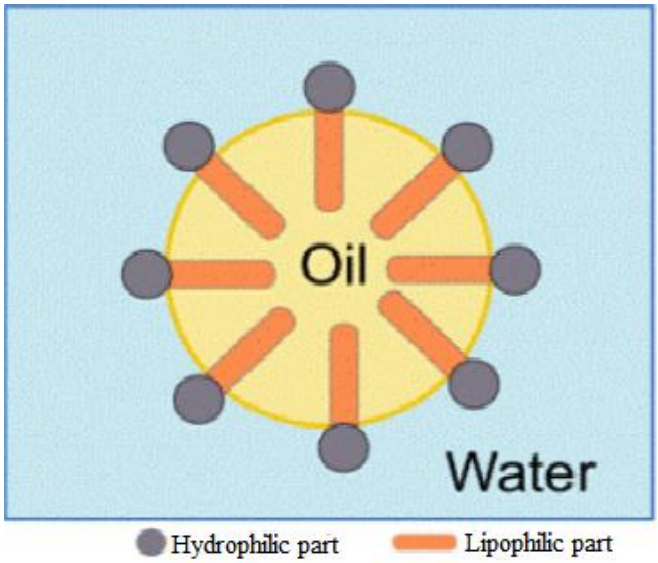

Figure 2.2: O/W emulsion [19].

Emulsification is the process of formation of emulsions. In the oil and gas industries, emulsification problem is mostly due to W/O emulsion. W/O emulsion is also known as "chocolate mousse" or "mousse" among oil spill workers [20-22]. According to Fingas and Fieldhouse [20], the majority of researchers agreed that emulsification is the next most crucial behavioural characteristics of oil after the evaporation characteristics because emulsification significantly influences the nature of oil spills at sea as well as clean-up response. Besides that, in the upstream oil production industries, pipeline emulsification

flow is a very common occurrence. As crude oil continues to be produced towards the end of the reservoir life, the amount of producing water increases as well, especially if the reservoir is driven by water aquifer [3]. Although crude oil and water are initially presented in two separated phases, the turbulence, mixing, as well as agitation through downhole wellbore, surface chokes, valves, pumps and pipes will cause emulsions to form [10]. **Figure 2.3** gives an overview of surface facilities for producing crude oil, from oil wellhead to the pipeline.

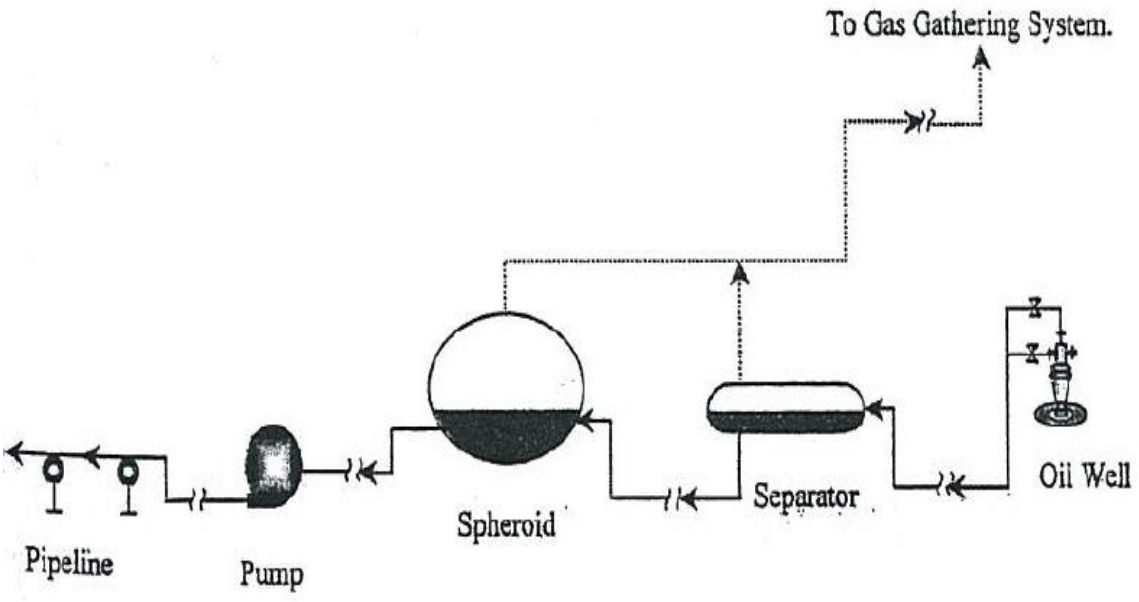

Figure 2.3: Overview of crude oil surface production facilities [23].

Due to emulsification, the properties and characteristics of oil spill will be altered to a significant extent, especially the volume of spilled materials, density and viscosity of oil [20-22]. It has been reported that the emulsification caused the volume of spilled materials to increase from two to five times of the original volume, the density increased up to 1.03 g/ml from the original density of around 0.80 g/ml while the viscosity increased from an original of a few hundred mPa.s to as high as one hundred thousand mPa.s [20-22]. This will then lead to the production of a liquid, which is a heavy, semi-solid material [20-22].

Figure 2.4 shows the process of the water-in-oil emulsion formation. Oil and water are two immiscible phases which are incapable of mixing together. However, due to the factors mentioned above, water will disperse into the oil phase and form the water-in-oil emulsions.

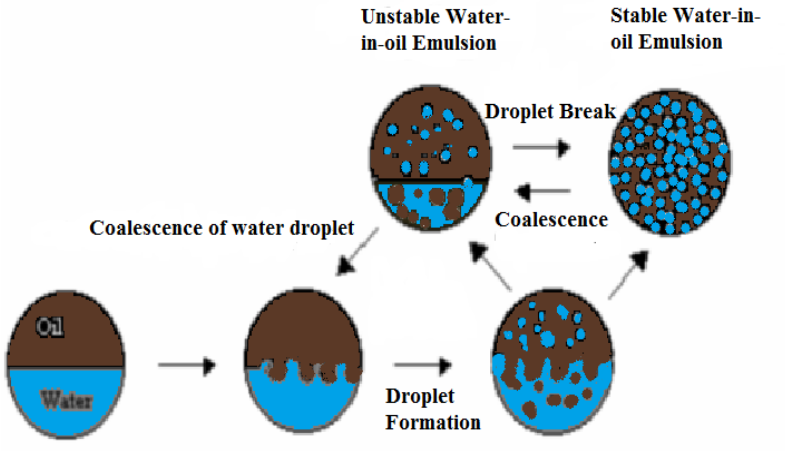

Figure 2.4: Formation of water-in-oil emulsions [11].

Many researchers have studied as well as reviewed in the emulsion formation process and their research studies are in general agreement on emulsion formation. They have reviewed that emulsion formation mainly correlated with the oil compositions, mainly asphaltenes and resins. Asphaltenes and resins are natural emulsifying agents that can be found in crude oil [24]. Berridge *et al.* [25] has declared that asphaltenes and resins are the main reason for emulsion formation. Likewise, a number of researchers in the 1980s reviewed that emulsion formation is mainly correlated with the oil compositions; mainly asphaltenes and resins [25-30]. According to Canvari [31], these natural emulsifying agents prevent dispersed water droplets from coalescing because these agents will be attached to the surface of the water droplets and resist water droplets from rupturing and then coalescing with the droplets around it. Besides, other researchers have reported that one of the main criteria for the formation of emulsions is the presence of asphaltenes and resins in crude oil [32]. Merv Fingas [33] has reported that asphaltenes are the main content in crude oil that stabilize W/O emulsions and resins are the content that solvate the asphaltenes.

Another factor that leads to the formation of emulsions is the increase in turbulence or mixing energy. Researchers in the 1970s concluded that the primary reason leading to the emulsion formation was the increase in turbulence or mixing energy [34, 35]. This finding is supported by Schubert and Armbruster [32] which stated that turbulence plays an important role in the distribution and mixing of the phases in the pipeline flow of water/oil system. They also mentioned that turbulence suppression will result in the turbulent flow of emulsions when the emulsions (dispersed phase) interact with the continuous phase [32]. Turbulence suppression is the occurrence where the local kinetic energy in single-phase flow becomes larger than that in two-phase flow at the same averaged liquid flux [32]. The local kinetic energy in the two-phase flow is smaller because part of the eddy's energy in the continuous phase is imparted to the emulsions/droplets. This causes the turbulent energy contained in the eddy in the continuous phase to transform into the kinetic energy of the particle and hence the turbulent intensity is reduced [32]. Turbulence intensity is a measure of the energy contained in the eddies [32].

Although earlier researchers had found out that turbulence energy causes emulsions to be formed, they did not carry out an in-depth study on the contribution of turbulence energy in the formation of emulsions. Therefore, one of the focuses of this research study is to analyze the roles of turbulent energy in emulsion formation and flow transport.

2.2 Classification of Emulsion

W/O mixtures can be divided or grouped into four classes: they are, stable W/O emulsions, mesostable W/O emulsions, entrained water, and unstable W/O emulsions [20, 36, 37]. According to Fingas and Fieldhouse [20], the states of W/O can be classified into four classes by studying the stability, the appearance as well as the rheological measurements of different water-in-oil samples.

According to Fingas and Fieldhouse [20, 21], stable W/O emulsions are the emulsions that remained unbroken for more than a week in the laboratory and those emulsions that remained intact for at least four weeks: it means that the emulsions do not break into water and free oil. The stable emulsions appeared as a brown or reddish semi-solid materials.

On the first day the stable emulsions are formed, they have an average water content of about 80% and stayed about the same after a week [20, 21]. This led Fingas and Fieldhouse [20] to discover the properties of the starting oil needed for the formation of the stable emulsions. Those properties included: viscosity 15–10,000 mPa.s; density 0.85–0.97 g/ml; asphaltene content 3–20%; resin content 5–30%; asphaltene-to-resin ratio 0.74; and average increase in viscosity, 1100 mPa.s on day of emulsion formed and 1500 mPa.s a week later.

Mesostable W/O emulsions are the emulsions that remained unbroken for less than three days in laboratory conditions [20, 21]. They are separated into water and free oil in around one to three days of time [20]. According to Fingas and his co-workers [36], it was reported that the mesostable emulsions displayed the properties between the stable and unstable emulsion. The mesostable emulsions appeared as a black or brown liquid. On the first day the mesostable emulsions formed, they had an average water content of about 70% and reduced to around 30% after one week [21]. Hence, Fingas and Fieldhouse [20] duly discovered the properties of the starting oil needed for the formation of the mesostable emulsion. Those properties included: viscosity 6–23,000 mPa.s; density 0.84–0.98 g/ml; asphaltene content 3–17%; resin content 6–30%; asphaltene-to-resin ratio 0.47; and average increase in viscosity, 45 mPa.s on day of emulsion formed and 3 a week later.

Entrained W/O is not characterized as emulsion [21]. The entrained water appeared as a black liquid [21]. On the first day the entrained water formed, it had an average water content of about 40% and reduced to around 15% after one week [21]. In laboratory conditions, the entrained water stayed in such condition for less than one day [21]. Once again, Fingas and Fieldhouse [20] had found out the average properties of the starting oil needed for the formation of the entrained water. Those properties included: viscosity 2000-60,000 mPa.s; density 0.97–0.99 g/ml; asphaltene content 3–22%; resin content 15–30%; asphaltene-to-resin ratio 0.62; and average increase in viscosity, 13 mPa.s on day of emulsion formed and 30 a week later.

Unstable W/O state is typified when oil does not hold a significant amount of water, even when the oil does hold a significant amount of water, the water stays for a very short period of time [21]. By comparing with the other three types of water-in-oil states, the

unstable water-in-oil displays a much larger range in the properties of the starting oil needed for its formation [21].

2.3 Classification of Different Types of Fluid Flow in Pipes

As mentioned earlier in the introduction, fluid can be grouped as Newtonian or non-Newtonian. Both the Newtonian and non-Newtonian fluid flow can be classified as laminar, transitional or turbulent flow depending on its Reynolds number. Reynolds number is the most important dimensionless parameter used in identifying the flow properties, *i.e.* the flow regime. It is described as the ratio of inertial forces to viscous forces, as shown in Equation 2.1 below:

$$\mathrm{Re} = \frac{\rho VD}{\mu} = \frac{VD}{\vartheta} \tag{2.1}$$

where ρ is the density of the fluid, V is the mean velocity of the fluid flow, D is the internal diameter of the pipe, μ is the dynamic viscosity of the fluid, and ϑ is the kinematic viscosity of the fluid.

In this research and industrial application, flow in a round pipe is of interest. For flow in a round pipe, it is considered as laminar when the Reynolds number is less than 2100, and when the Reynolds number is more than 4000, it is considered as turbulent. For the Reynolds number ranges from 2100 to 4000, the flow is considered as transitional flow.

2.3.1 Flow of Newtonian Fluid

For laminar flow of Newtonian fluid in a pipe, the friction losses can be determined using the Hagen-Poiseuille in Equation 2.2 [38, 39]:

$$f = \frac{16}{\mathrm{Re}} \tag{2.2}$$

where f is the friction factor and *Re* is the Reynolds number.

The friction factor is independent of the surface roughness of the pipe due to the thickness of laminar sublayer, which has covered the surface roughness and irregularities [16]. The friction factor also can be described as in Equation 2.3 and Equation 2.4 [17]:

$$f = \frac{2\tau_w}{\rho V^2} \tag{2.3}$$

$$f = \frac{D}{2\rho V^2}\left(\frac{\Delta P}{L}\right) \tag{2.4}$$

where τ_w is the wall shear stress of the pipe, ρ is the fluid density, V is the average velocity in the pipe, D is the diameter of the pipe and $\Delta P / L$ is the pressure gradient.

For laminar flow, the pipe wall shear rate, du/dy can be determined using Equation 2.5 [17]:

$$\frac{du}{dy} = -\left.\frac{du(r)}{dr}\right|_{r=\frac{D}{2}} \tag{2.5}$$

where $u(r)$ is the local fluid velocity and r is the radial position.

For fully developed steady flow of a Newtonian fluid in laminar region, the velocity profile is as shown in Equation 2.6 [17]:

$$u(r) = \left(\frac{\Delta P}{L}\right)\left(\frac{R^2}{4\mu}\right)\left[1-\left(\frac{r}{R}\right)^2\right] \tag{2.6}$$

where R is the pipe radius and μ is the fluid viscosity.

Combining Equation 2.3, 2.4, 2.5 and 2.6, the shear rate at the pipe wall can be expressed as in Equation 2.7 [17]:

$$\frac{du}{dy} = \frac{8V}{D} \tag{2.7}$$

For fully developed turbulent flow of Newtonian fluid in a smooth pipe, the friction factor can be obtained using Equation 2.8, the Blasius equation or Equation 2.9, the Prandtl-Karman equation [17, 38, 39]:

$$f = \frac{0.079}{\mathrm{Re}^{0.25}} \tag{2.8}$$

$$\frac{1}{\sqrt{f}} = 4.0\log_{10}(\mathrm{Re}\sqrt{f}) - 4.0 \tag{2.9}$$

For fully developed turbulent flow of Newtonian fluid in a rough pipe, wall roughness are taken into account when calculating the friction factor. Colebrook modified the Prandtl-Karman equation in order to indicate the effect of wall roughness. The equation is given as follows [38, 39]:

$$\frac{1}{\sqrt{f}} = -4.0\log_{10}\left[\frac{\varepsilon/D}{3.7} + \frac{1.255}{\mathrm{Re}\sqrt{f}}\right] \tag{2.10}$$

where ε/D is the surface roughness.

2.3.2 Flow of Non-Newtonian Fluid

For laminar flow of non-Newtonian shear thinning fluid in a pipe, the friction losses can be determined using Equation 2.11 as suggested by Metzner and Reed [38, 39].

$$f = \frac{16}{\mathrm{Re}'} \tag{2.11}$$

where Re' is the Metzner-Reed modified Reynolds number.

Metzner-Reed modified Reynolds number, Re' can be defined as:

$$\mathrm{Re}' = \frac{D^{n'}V^{2-n'}\rho}{k'(8)^{n'-1}} \tag{2.12}$$

where ρ is the fluid density, V is the average velocity in the pipe, D is the diameter of the pipe, n' and k' are the Metzner-Reed modified power law constants for pipe flow, whereby they are related to the power law constants obtained with a Viscometer as follows [38, 39]:

$$n' = n \tag{2.13}$$

$$k' = k\left[\frac{1+3n}{4n}\right]^n \tag{2.14}$$

For laminar flow, the pipe wall shear rate in a smooth pipe can be determined using Equation 2.15.

$$\frac{du}{dy} = \frac{8V}{D}\left[\frac{1+3n}{4n}\right] \tag{2.15}$$

For turbulence flow, Dodge and Metzner developed the following equation to calculate the turbulence friction factor by including the power law non-Newtonian fluid [38]:

$$\frac{1}{\sqrt{f}} = \frac{4}{n'^{0.75}}\log_{10}(\mathrm{Re}\, f^{1-\frac{n'}{2}}) - \frac{0.4}{n'^{1.2}} \tag{2.16}$$

2.4 Governing Equations

The turbulence theories which are important to this research study are introduced to aid in the understanding of the present work. It includes characteristics of turbulence and Kinetic Budget Equations.

2.4.1 Turbulence Characteristics

Turbulence is defined by four main characteristics, which are irregularity, diffusivity, rotationality and dissipation actions. These characteristics are described as follows [40]:

I. Irregularity –Turbulent flow is always irregular and chaotic. However, not all chaotic flows are categorized as turbulent flow. The flow consists of turbulent eddies of different sizes.

II. Diffusivity – Turbulent flow tends to increase the diffusivity action of fluid mixtures due to the presently available energy supply in turbulent flow. The increase in diffusivity will increase the rates of mass, momentum and energy transport in the flow.

III. Rotationality – Turbulent flow is always unsteady, three-dimensional and rotational. This is because turbulent flow involves vortex stretching, whereby, vortices are subjected to stretching and eventually breaking down to vortices that are small enough for the transformation of vortices' kinetic energy into heat energy.

IV. Dissipation – Turbulence will dissipate rapidly. This is because the kinetic energy in the flow is converted into heat/thermal energy. The transferring of energy (known as a turbulent energy cascade process) is from the largest turbulent eddies to the smallest turbulent eddies and eventually gets dissipated by viscosity. Capital energy is gained from the mean flow.

Figure 2.5 shows the turbulent flow behind a cylinder obstacles. From the figure, the above mentioned characteristics of turbulence are demonstrated, where behind the obstacles, the flow is shown to be chaotic, unsteady and rotational.

Figure 2.5: The turbulent flow behind a cylindrical obstacle [41].

2.4.2 Kinetic Budget Equations

As mentioned in section 2.1, turbulence energy is one of the main factors that lead to the formation of emulsions in the crude oil. However, there is no in-depth study that presents the effect of turbulence energy that causes the emulsions to be formed. Since the emulsions formation needed energy, transfer of energy in the turbulent flow has to be studied. Kinetic Energy Budget equations are the equations that explain the sources and sinks of the energy transfer in a turbulent flow. Kinetic Energy Budget Equations can be divided into the Kinetic Energy Budget of Mean Flow and the Kinetic Energy Budget of Turbulent Flow. Kinetic Energy Budget of Mean Flow describes the energy transfer in the main flow, as shown in Equation 2.31 [42].

$$\frac{D}{Dt}\left(\frac{1}{2}U_i^2\right) = \frac{\partial}{\partial x_j}\left(-\frac{PU_j}{\rho_0} + 2\nu U_i E_{ij} - \overline{u_i u_j} U_i\right) - 2\nu E_{ij}E_{ij} + \overline{u_i u_j}\frac{\partial U_i}{\partial x_j} - \frac{g}{\rho_0}\overline{\rho} U_3 \quad (2.17)$$

where $\frac{D}{Dt}\left(\frac{1}{2}U_i^2\right)$ represents the rate of change of the mean kinetic energy, $\frac{\partial}{\partial x_j}\left(-\frac{PU_j}{\rho_0} + 2\nu U_i E_{ij} - \overline{u_i u_j} U_i\right)$ represents the transport term of mean kinetic energy, whereby, the first term represents the mean pressure, the second term represents the mean viscous stresses and the third term represents the Reynolds stresses. These three transport terms describe the transportation of energy from one region to the other region and can neither be generated nor dissipated. $2\nu E_{ij}E_{ij}$ represents the viscous dissipation term of mean kinetic energy. It refers to the energy loss at every point in the flow due to the viscosity. This lost energy will go to the agency that generates the viscous stress and ended up as heat. $\overline{u_i u_j}\frac{\partial U_i}{\partial X_j}$ represents the "loss to turbulence" term of mean kinetic energy. It refers to the energy that losses to the agency that generates the turbulent stress. Hence, this lost energy will reappear in the Kinetic Energy Budget of Turbulent Flow, which is the turbulent fluctuating field. $\frac{g}{\rho_0}\overline{\rho} U_3$ represents the "loss to potential energy" term of mean kinetic energy. It refers to the work done by gravity on the mean vertical motion. In other word, it means that the mean kinetic energy is converted to potential energy when the motion is against the gravitational force direction.

Meanwhile, in the turbulent regime, the kinetic energy is described by the Kinetic Energy Budget of Turbulent Flow. Equation 2.32 shows the Kinetic Energy Budget of Turbulent Flow [42].

$$\frac{D}{Dt}(\frac{1}{2}u_i^2) = \frac{\partial}{\partial x_j}(-\frac{1}{\rho_0}\overline{pu_j} + \frac{1}{2}\overline{u_i^2 u_j} - 2\nu\overline{u_i e_{ij}}) - 2\nu\overline{e_{ij}e_{ij}} - \overline{u_i u_j}\frac{\partial U_i}{\partial x_j} + g\alpha\overline{\omega T'} \quad (2.18)$$

where, $\frac{D}{Dt}\overline{\left(\frac{1}{2}u_i^2\right)}$ represents the rate of change of turbulent kinetic energy, $-\frac{\partial}{\partial x_j}\left(\frac{1}{\rho_0}\overline{pu_j} + \frac{1}{2}\overline{u_i^2 u_j} - 2\nu\overline{u_i e_{ij}}\right)$ represents the transport term of turbulent kinetic energy, whereby the first refers to the transport of energy by the pressure force, the second term refers to the transport of energy by the turbulence itself and the third term refers to the viscous transport. This transport term does not create or destroy turbulent kinetic energy, it only redistributes turbulent kinetic energy from one location to another location. $2\nu\overline{e_{ij}e_{ij}}$ represents the viscous dissipation term of turbulent kinetic energy. $\overline{u_i u_j}\frac{\partial U_i}{\partial X_j}$ represents the shear production term, which also means the rate of generation of turbulent kinetic energy. This term can be found in Equation 2.31 too, but of opposite sign. This is because in Equation 2.31 this term represents a loss of mean kinetic energy and in Equation 2.32, this term represents a gain of turbulent kinetic energy. $g\alpha\overline{\omega T'}$ represents the buoyant production term, provided that the turbulent heat flux is upward, $\overline{\omega T'} > 0$. Opposite of this condition, when the turbulent heat flux is downward, $\overline{\omega T'} < 0$, this term refers to the rate of turbulent energy loss. The potential energy generated in the mean field is lowered by the buoyant production of the turbulent field.

As a whole, Kinetic Energy Budget Equations are very important in the study relating to the turbulent flow as its transport equation can provide insight into the flow physics. In the present research study, Kinetic Energy Budget Equations are used to serve as a fundamental to the understanding of the formation of emulsions. For example, the formation and dissipation of energy described by the Kinetic Energy Budget Equations can be used as an aid in understanding the flow transport in the pipeline.

2.5 Summary of Chapter

This chapter introduces the necessary background as well as the governing equations significantly important in the study in order to aid one with the understanding of the current research. First, the very basic yet an important character in the research – the emulsions, is introduced. Different types of emulsions have been identified. An overview of how emulsification process has taken place in the oil and gas industries; and the process of emulsification are presented too. It is also recognized that the various researchers have carried out studies on the emulsion formation process and their research studies are in general agreement on the criteria as well as the factors leading to the formation of emulsions.

This chapter is then followed by the introduction on classification of water-in-oil (W/O) emulsions as only this type of emulsions is being studied in the current research. It is recognized that they can be divided into four groups: they are stable W/O emulsions, mesostable W/O emulsions, entrained water and unstable W/O emulsions. Each group of mixtures has its own characteristics in the form of its stability, appearance and rheological properties. Next, the basic concept of identifying types of fluid flow in the pipeline is introduced. It is important to determine if the flowing fluid is Newtonian or non-Newtonian as they behave differently in the pipeline. Then, characteristics of turbulence are presented as turbulence is the main focus of the study on the formation of emulsions. Lastly, Kinetic Budget Equations are introduced to discuss the sources and sinks of the energy transfer in a turbulent flow.

Next chapter will be focusing on the literature review of the current research.

CHAPTER 3

LITERATURE REVIEW

This chapter presents an overview on the existing research studies on emulsification, which includes effects of emulsions and its stability, and the factors that influence it. The last part of the review will be on the experimental studies that have been done on the emulsification process. The review is done so that the research gaps can be addressed based on the current research objectives.

3.1 Effects of Emulsions

As mentioned earlier, the presence of emulsions significantly affects the flow behavior as well as flow properties. This section reviews the existing research studies on the effects of emulsions on the general flow behavior, friction factor as well as viscosity and pressure drop.

3.1.1 The Effect of Emulsions on General Flow Behaviour

At low concentration of emulsion droplets, the emulsion system can be assumed to behave as Newtonian fluid. However, as the concentration of emulsion droplets is increased, the emulsion system will start to exhibit non-Newtonian behaviours. In a research done by Pal, the oil-in-water emulsion system was Newtonian when the oil droplets concentration was less than 55.14% in volume. But, as the oil droplets concentration was further increased, the emulsion system became non-Newtonian pseudoplastic. The viscosity decreased when higher shear stress was applied [43].

Omer and Pal [44] reported there was a significant delay in the transition from laminar to turbulent regime in water-in-oil emulsions flow. The delay became even greater with bigger pipe diameter. But, interestingly, such transitional delay was not observed in the case of oil-in-water emulsions.

3.1.2 The Effect of Emulsions on Friction Factor

Cengel *et al.* [45] has studied the effect of emulsions on the flow friction factor. The results were re-confirmed by Pal [13], Pal [46] as well as Omer and Pal [47]. Friction factor data on emulsions flow were compared against the calculated values of single-phase Hagen-Poiseuille and Blasius equations. Hagen-Poiseuille equation is valid for laminar of Newtonian fluids, and it is given by Equation 3.1 [38, 39]:

$$f = \frac{16}{\mathrm{Re}} \tag{3.1}$$

Blasius equation is an empirical relationship for turbulent flow of Newtonian fluids in smooth pipes, and it is given by Equation 3.2 [38, 39]:

$$f = 0.079 \cdot \mathrm{Re}^{-0.25} \tag{3.2}$$

The results showed different behaviours between unstable emulsions and surfactant-stabilized emulsions at the turbulent flow regime. For unstable emulsions in turbulent flow, the measured friction factor data were much lower than the calculated values of single-phase Blasius equation. This phenomenon is known as drag-reduction behaviour, and it was aggravated with increased concentration of emulsion droplets [45].

However, for surfactant-stabilized emulsions in turbulent flow, little or no drag-reduction behaviour is observed. The only exception to this observation is documented in a research conducted by Zakin *et al.* [48], where they reported the occurrence of drag-reduction behaviour in surfactant-stabilized emulsions. They worked on non-Newtonian oil-in-water emulsions, and they postulated viscoelasticity to be a reason for that behaviour, but Pal questioned the significance of droplet viscoelasticity's role in drag-reduction, and doubted the existence of droplet-droplet microstructure in high shear rates of turbulent flow. Pal [13] further suggested that the emulsions may not have been fully stabilized, thus causing drag-reduction behaviour to be observable.

More recent studies by Omer and Pal [44, 47], Pal [46] and Pal [13] all agree that drag-reduction behaviour is only exhibited in unstable emulsions. According to Pal [13],

unstable emulsions experience frequent and dynamic break-up as well as a coalescence of dispersed droplets, and this may have suppressed the turbulence, eventually causing the drag-reduction behaviour. Pal [13] also compared the extent of drag-reduction between water-in-oil emulsions and oil-in-water emulsions. He found out that the extent of drag-reduction was higher for water-in-oil emulsions. He attributed this to the more frequent coalescence activities occurring for water-in-oil emulsions, as water droplets tend to coalesce rapidly in the non-polar continuous oil phase due to negligible potential energy barrier [49]. Conversely, for oil-in-water emulsions, the coalescence activities are less frequent, due to resistance from electrical double-layer effect on the continuous water phase [49, 50].

Little or no drag-reduction behaviour is observed for the case of surfactant-stabilized emulsions, as the dispersed droplets are smaller (due to lower interfacial tension), so they flow along with turbulent eddies and do not affect the turbulence suppression, resulting in negligible drag-reduction. This is especially true when the dispersed droplets are smaller than the scale of turbulence [44].

Ashrafizadeh *et al.* [51] gave an alternative explanation of the reason of no drag-reduction behaviour of surfactant-stabilized emulsions, by virtue of the higher viscosity. They found out that the viscosity of emulsions increased with higher surfactant concentration. This observation agrees with a previous work done by Otsubo and Prud'homme [52]. One possible cause is the higher surfactant concentration resulted in smaller dispersed droplets, leading to more interaction energy among the droplets.

The drag-reduction phenomenon can be interpreted as reduced emulsion viscosity, which in turn will lead to less pressure drop of the flow.

3.1.3 The Effect of Emulsions on Viscosity and Pressure Drop

For water-in-oil emulsions, prior to the phase inversion point, the increase of the water volume fraction will cause the viscosity of emulsions to increase, and subsequently result in a higher pressure drop [15]. For either Newtonian or non-Newtonian flow, emulsions

relative viscosity can be correlated to the volume fraction or the concentration of dispersed droplets using an empirical equation developed by Pal and Rhodes [53]:

$$n_r = \left[1 + \frac{(\phi / \phi^*)}{1.187 - (\phi / \phi^*)}\right]^{2.49} \tag{3.3}$$

where n_r is the relative viscosity (emulsion viscosity is directly proportional to the continuous phase viscosity), ϕ is the concentration of dispersed droplets, and ϕ^* is the concentration of dispersed droplets at which relative viscosity becomes 100. Besides the water volume fraction, the viscosity of emulsions is also affected by single phase viscosities of oil and water, temperature, droplet size distribution, amount of solids in the crude and the applied shear rate [54].

The increment of emulsions viscosity can be understood from the hydrodynamic forces working on the emulsion droplets. As the droplets experience shear flow, hydrodynamic forces cause two droplets to make a doublet rotating around their mutual center of mass [55, 56]. The rotating doublets dissipate more energy as the amount of emulsion droplets increase, contributing to higher emulsion viscosity.

However, as the water volume fraction is increased further beyond the phase inversion point (the inversion from water-in-oil emulsions to oil-in-water emulsions occurs), Charles *et al*. [57] and Nadler and Mewes [14] found that the pressure drop will decrease, to as low as the pressure drop of pure water. Nadler and Mewes [14] explained this observation as a drag-reduction behaviour, where a continuous water layer is flowing at the lower section of the pipe wall, and this water layer minimises the viscous dissipation effects of the emulsions. This phenomenon has been greatly leveraged to facilitate the transportation of heavy and viscous crude oil via pipelines, by emulsifying the oil to be concentrated oil-in-water emulsions [58-60]. The practical application of this idea has been implemented in Indonesia (20-in diameter and 283-km long pipeline) as well as California (8-in diameter and 20.9-km long pipeline) [61, 62].

The viscosity of concentrated oil-in-water emulsions can be several orders of magnitude lower than the viscosity of the single-phase oil. This shows that the emulsions viscosity

strongly depends on the viscosity of the continuous phase [63]. Yaghi and Al-Bemani [64] claimed that in some cases, the viscosity could be reduced by up to 90%, while Zhang *et al*. [65] reported that the pressure drop could be as much as 30% lower. Messick [66] recommended that for the purpose of feasible crude transportation via pipeline, the viscosity of the flow should not be more than 200 cP.

3.2 Stability of Emulsion

The stability of W/O emulsion is described as the dispersed water droplets resistance against coalescence [67]. Coalescence means that diverse particles/droplets unite together and form a larger droplet. The adverse and beneficial effects of emulsions can be realized only if the emulsions are stable. If the emulsions are unstable, they will soon separate into two distinguished phases of water and oil, and thus the effects discussed earlier may no longer be applicable. The stability of emulsion interestingly ranges from a few minutes up to a number of years [68] and the stability performance is dictated by the structure as well as the rigidity of the emulsion droplets' interfacial films. A few common factors which influence the stability of emulsions are discussed.

3.2.1 Concentration of Asphaltenes and Resins

According to Ortega *et al.* [69], the adsorption of surface active molecules such as asphaltenes and resins at the interface has been found to determine the emulsion stability. However, with the presence of resins alone, they cannot stabilize the emulsions. Stable emulsions will only be formed with the presence of both asphaltenes and resins [24]. Aguilera *et. al.* [70] concluded that an increase in asphaltenes concentration increases the emulsion stability. Joseph and Peter [71] found out that the stability of emulsions is governed by the asphaltenes solubility in the crude oil. Nghiem *et. al.* [72] reported that stabilizing layer of emulsions is due to asphaltenes which tends to form aggregates with aromatic resins. In order for asphaltenes and resins to stabilize an emulsion, a minimum mass percentage of 3% for either one of the compositions is needed [73-75]. Other

components in crude oil such as waxes, porphyrins and others do not show to play a vital role in emulsion formation and stabilization [73-75].

3.2.2 Concentration of Volatile Aromatic Components

Volatile aromatic components, BTEX (benzene, toluene, ethylbenzene, xylenes) in crude oil are found to be able to solubilize asphaltenes and polar compounds. The amount of volatile aromatic to solubilize asphaltenes and polar compounds in order to prevent them from stabilizing emulsion is about 3% [73-75]. This means that the mass percentage of volatile aromatic components have to be equal to or more than the total mass percentage of asphaltenes and resins in order to forbid the formation of emulsions.

3.2.3 Elastic modulus (G') and Viscous modulus (G'')

Apart from asphaltenes and polar compounds, the storage or elastic modulus (G') and loss or viscous modulus (G'') is found to be the factors affecting the stability of emulsions. Torres and coworkers reported that when the viscous behaviour of the fluid is less than the elastic behaviour ($G'' < G'$) of the fluid, the emulsions are said to be comparatively stable, provided that both of the parameters are independent of the frequency in the linear viscoelasticity region [69]. Linear viscoelasticity region (LVR) is the region where a system does not break down due to applied stress. The larger the linear viscoelasticity region, the higher is the system's stability. When the elastic modulus (G') and viscous modulus (G'') do not change with respect to frequency and they are within LVR, the system is said to be independent of the frequency in the linear viscoelasticity region. **Figure 3.1** shows the linear viscoelasticity system with which the elastic modulus (G') is the greater viscous modulus (G'').

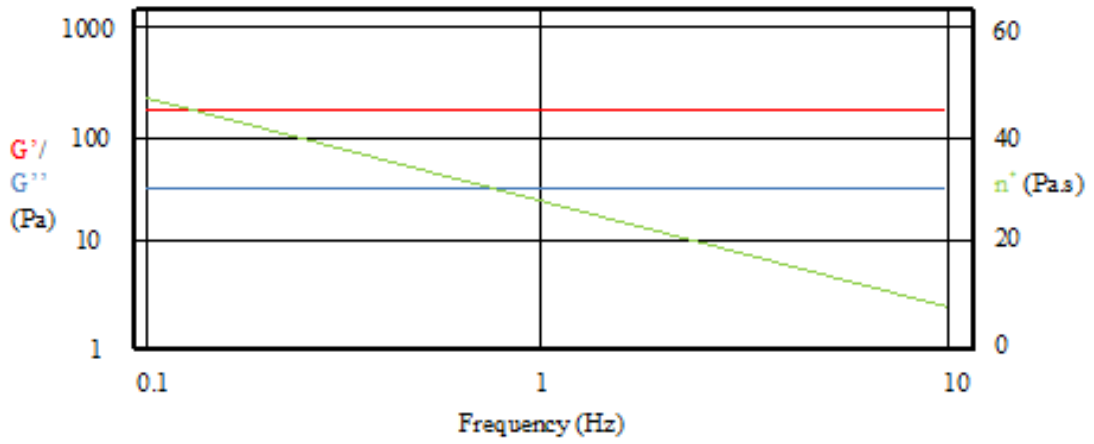

Figure 3.1: A well-structured system [76].

Elastic modulus is directly affected by the natural surfactant of crude oil, such as asphaltenes, resins and naphthenates. This statement is based on the results done by Maia Filho *et al.* [77] which reported that adsorption of these surfactants on water-oil (emulsion) interface will lead to intermolecular interactions, which will work against any strain on the water-oil emulsion interface (Gibbs-Marangoni Effect), and hence increasing the elastic behaviour of the emulsions. This finding is supported by Derkach [78] study, which concluded that when shear stress is applied onto the emulsion, the surfactants adsorbed on the surface of the emulsion will generate a stress gradient, resulting in the elastic component (G') in the complex modules (G^*) of the emulsion getting increased. In other words, it can be said that increases in elastic behaviour will lead to decreases in coalescence mechanism among the emulsions, and thereby producing the stable emulsions.

3.2.4 Time

Next factor affecting the stability of emulsions is the period of time after the emulsions have been formed. In indicating the stability of water-in-oil emulsions, water content at formation is not a decisive aspect [20, 21]. This is because the initial water content is prone to error due to the "excess" water that may exist. About one week after the emulsions were formed, the water content was found to be more reliable because emulsions that are less stable will be separated [20].

3.2.5 Mixing Speed and Mixing Duration

Generally, higher mixing speed and longer mixing duration would produce smaller sizes of emulsion droplets, which have higher interfacial area and droplet-to-droplet interaction, resulting in more stable emulsions [63, 79, 80]. In studies conducted by Ashrafizadeh and Kamran [63], fully stabilized emulsions (no separated water observed in 24 hours) were achieved by mixing at more than 10,000 rpm for longer than 30 minutes. Apart from stabilized emulsions, smaller emulsion droplets with higher interaction would also increase the viscosity of the emulsions [81].

3.2.6 pH of Solution

Sakka [82] and Yang *et al*. [83] suggested that higher pH (alkaline) would give more stability to the emulsions. According to Yang *et al*. [83], for oil-in-water emulsions, higher pH would promote more affinity of surfactant molecules towards aggregation, resulting in more stable emulsions. Sakka [82] attributed the emulsion stability to the increased absolute value of zeta potential of the droplets in the alkaline region, i.e. pH 9.

However, Tambe and Sharma offered a different observation. Tambe and Sharma [84] maintained that in their studies, low pH values of 4 – 6 favoured oil-in-water emulsions, while high pH values of 8 – 10 favoured water-in-oil emulsions. They found out that for the case of oil-in-water emulsions, the stability was increased as the pH was increased from 4 to 6. But beyond pH 6 to pH 10, oil-in-water emulsions became less stable, and on the flip side, water-in-oil emulsions were favoured.

Sjoblom *et al*. [85] put forward another point of view, which generally believed that intermediate pH would cause instability, while either very high or very low pH values would help in stabilizing the emulsions.

3.2.7 Temperature of Solution

Higher temperatures will first reduce the emulsions viscosity, eventually destabilizing and breaking the emulsions. This thermal method is well practised in the oil refinery industry [11]. According to Grace [86], temperature above 50 °C – 65 °C may completely destabilize the emulsions. Mat *et al*. [11] highlighted that the rate of droplet film drainage is directly proportional to the temperature.

3.2.8 Salt Concentration

There are various conflicting ideas and theories surrounding the effects of salt concentration on the characteristics of emulsions. Nevertheless, the presence of salt in oilfield emulsions is real and should not be neglected, as the formation water produced together with crude oil does contain a certain amount of salt, known as oilfield brine.

In a research conducted by Bink [87], he claimed that higher salt concentration resulted in oil-in-water droplets to increase in size, while water-in-oil droplets to decrease in size. He showed that higher salt concentration would destabilize oil-in-water emulsions, but stabilize water-in-oil emulsions.

However, later research by Ahmed *et al*. does not agree with Bink. Ahmed *et al*. [62] found out that higher salt concentration would result in lower interfacial tension of the oil droplets and the continuous water phase, facilitating the formation of smaller oil droplets. Smaller oil droplets make the oil-in-water emulsions to be more stable.

Ashrafizadeh and Kamran [63] echo the views by Ahmed *et al*., where they reported that at higher salinity of the water phase, the viscosity of oil-in-water emulsions was increased, and the amount of separated water was reduced as well. Oil-in-water emulsions became more stable at higher salinity of the water phase. Ashrafizadeh and Kamran [63] postulated that the phenomenon could be caused by salt ions acting as barriers among the oil droplets and the continuous water phase, thus increasing the emulsions stability.

More recently, Ashrafizadeh *et al*. [51] contributed additional info in this interesting discussion, by showing the effects of chemical reactions between the salt (NaCl) ions and the surfactants. The stability of emulsions is not affected by the salt concentration alone, but its chemical reactions with the surfactants playing an important role. In their research, sodium carbonate (Na_2CO_3) was used as the surfactant, where the formed carboxylate ions would be adsorbed at the interface of oil/water, promoting the reduction of the oil droplets mean diameter and increasing the emulsions stability. But, as the salt (NaCl) concentration was increased, the excess sodium ions would induce the precipitation of carboxylate ions as sodium carboxylate, thus hindering the carboxylate ions from acting as good surfactant. So, in this special case, high salt concentration would destabilize the oil-in-water emulsions.

3.3 Experimental-Based Emulsification Process

This section deliberates and reviews the existing research studies and findings concerning emulsification process. Both the water-in-oil emulsification and oil-in-water emulsification forming from stirring or mixing (external forces) and from flow shear are reviewed.

In 1997, Nadler and Mewes [14] experimentally investigated the flow of water and oil without any added surfactant in a horizontal pipe using a lab-scale pipeline (as shown in **Figure 3.2**) to determine the effect of input water fraction, mixture velocity as well as the viscosity ratio on emulsification and phase inversion. The input water fraction used in the study were ranging from 0.1 to 1.0; the mixture velocity ranging from 0.3 m/s to 1.5 m/s; the viscosity ratio ranging from 28 to 35. From this study, it was found out that phase inversion is observed at the input water fractions between 10% and 20%. It is observed that the maximum pressure drop in the pipeline flow is in the case of water-in-oil emulsions. On the other hand, the minimum pressure drop is determined in the case of pure water phase. Meanwhile, in the case of oil-in-water emulsions flowing in the pipeline, the pressure drop is between the pressure drop for the flow of pure oil phase and the flow of pure water phase in the pipeline. Nadler and Mewes [14] also determined that the viscosity ratio has no significant effect on the emulsification process.

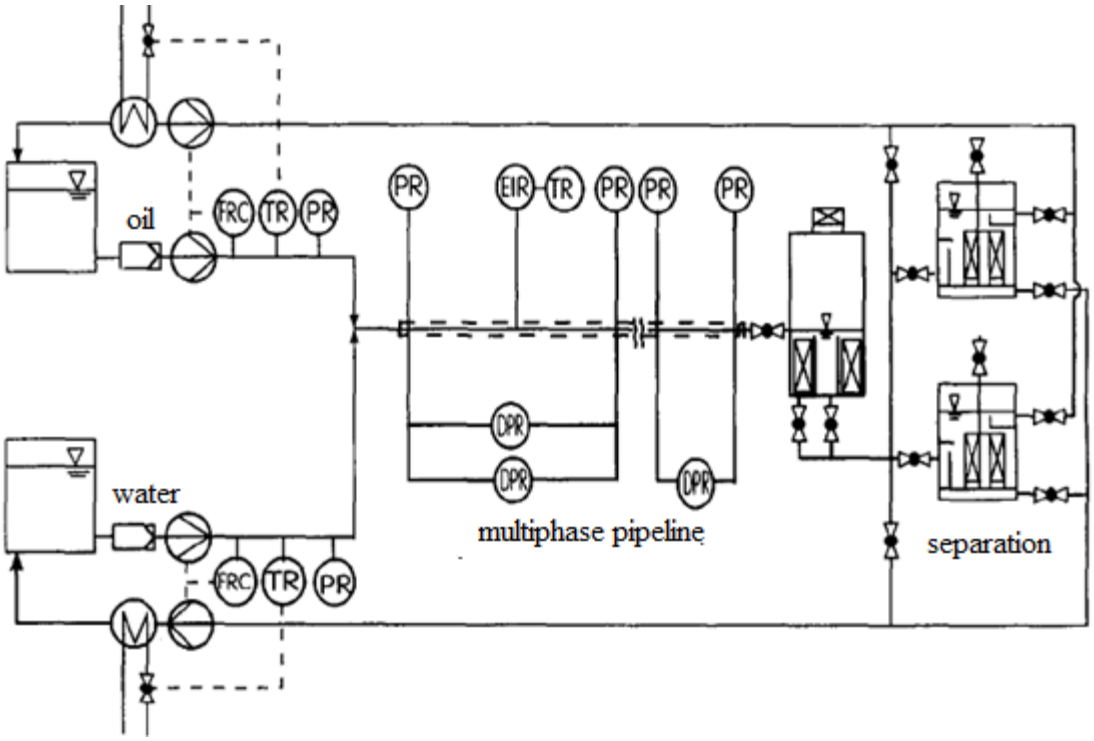

Figure 3.2: Illustration of experimental lab scale flow rig [14].

In 2002, Kobayashi *et al.* [88] had carried out an experimental study of membrane emulsification process, where an emulsion is formed by feeding the dispersed phase into the continuous phase through the membrane pores. They performed the study on the effect of the flow velocity of the continuous phase and the effect of different types of surfactants to the membrane emulsification behaviours. The membrane emulsification behaviours analysed in their study were the average diameter of the emulsion formed, the suitability of the surfactants in achieving O/W membrane emulsification, as well as the stability of emulsions formed while using different types of surfactants. Although this research performed by Kobayashi *et al.* was on emulsification, it is actually a lot different from the author's research on emulsification. Kobayashi et al. were focused on forming O/W emulsions using a membrane emulsification process. Meanwhile, the author of this thesis focuses on the flow-induced W/O emulsions through a horizontal pipeline (no membrane is included).

In 2005, Chen and Tao [67] investigated the stability of O/W emulsions experimentally. They distinguished the stability by checking the relative volume of O/W emulsions after

24 hours. The oil being tested was commercial oil in China. Emulsifier was used to form the O/W emulsions. In the study, the experimental conditions were emulsifier dosage ranging from 0.25% to 0.50%, oil to water ratio ranging from 9:1 to 5:5, stirring intensity ranging from 1000 rpm to 3000 rpm, mixing temperature of 30 ℃ to 70 ℃ and mixing time of 3 min to 5 min. From the study, they concluded that the optimum conditions for producing stable O/W emulsions were emulsifier dosage of 0.5%, oil to water ratio of 1:1, stirring intensity of 2500 rpm and mixing temperature of 30 ℃.

In 2003, Johnsen and Ronningsen [89] had performed experimental works to study the viscosity of W/O emulsions using seven different North Sea oils which were ranging from light to heavy crudes. The experimental conditions used in the study were temperature ranging from 50 ℃ to 70 ℃, flow velocities ranging from 0.7 m/s to 3 m/s, water cuts ranging from 0 to 90% and saturation pressure ranging from 12 bar to 100 bar. Their results showed that although the viscosity of the selected crude oils was quite big, the changes in the relative viscosity of W/O emulsions were quite small for water cuts up to 70%. Higher than that, the changes in the relative viscosity of W/O emulsions could be quite significant.

In 2005, Marco *et al.* [90] performed an experimental study on the effect of the volume fractions of dispersed phase, temperatures and shear rates on the viscosity of W/O emulsions. In the study, six different types of crude oils with density ranging from 15° to 40° API were tested at temperature from 8 ℃ to 50 ℃, dispersed phase volume percentage from 0 to 40% and shear rate of 10 s^{-1} to 80 s^{-1}. Their results showed that W/O emulsions showed Newtonian behaviour with higher temperature and higher dispersed phase volume percentage. At temperatures lower than that of wax appearance temperature (WAT), the W/O emulsions showed Bingham plastic behaviour at all the measured shear rates in this study.

In 2006, Dan and Jing [91] carried out experimental works to study the viscosity of W/O emulsions in order to validate the results obtained from the improved P&R model for predicting non-Newtonian emulsions. Seven sets of W/O emulsions were formed using crude oils from different oil fields. Those crude oils were heavy oil and waxy oil. The experimental conditions used in the study were processing temperature of 60 ℃ for heavy

oil and 30 ℃ for waxy oil, water cuts ranging from 0 to 60% and shear rates ranging from 15 s^{-1} to 600 s^{-1}. Their results showed that W/O emulsions formed using crude oils of different density behaves differently. They concluded that W/O emulsions formed using heavy and waxy crude oil show non-Newtonian behaviour, meaning the viscosity changes with time. On the other hand, W/O emulsions formed using light crude oils show Newtonian behaviour, meaning the viscosity remains unchanged.

Although the studies done by Johnsen and Ronningsen [89], Marco *et al.* [90] and Dan and Jing [91] were on W/O emulsions which is the same with the thesis author, the focus of the studies are different. Marco *et al.*, Johnsen and Ronningsen, and Dan and Jing were focused on the viscosity of the W/O emulsions but the author of this thesis focuses on the behaviours of W/O emulsions formation. Another main difference is that all of these previous researchers [89-91] formed W/O emulsions by applying external forces such as stirring and rotating, but this author uses flow-induced emulsions formation.

In 2007, Broboana and Balan [7] investigated the rheological behaviour of W/O emulsions experimentally. The crude oil studied was asphaltic Romanian crude oil with 30% water cuts and paraffinic Romanian crude oil with 6% water cuts. The experiments were performed at temperature of 5℃, pressure of atmospheric pressure and shear rate from 1 s^{-1} to 1000 s^{-1} using model MC 300 and MC 1 Physica rheometers. Their results showed that both samples displayed a non-Newtonian, shear thinning behaviour.

In 2010, Ilia Anisa and Abdurahman Nour [92] presented an experimental study on the effects of phase ratios, effects of temperature and effects of stirring speed to the viscosity and the average droplet diameter of W/O emulsions. Three types of crude oil obtained from Petronas Refinery Melaka with API gravity of 29.27 °, 33.82 ° and 26.48 ° respectively were tested in their study. The experimental parameters tested in the study were phase ratios of 20 – 80% and 50 – 50% W/O emulsions, temperature of 25 ℃ to 90 ℃ and stirring speed of 500 to 2000 rpm. Ilia Anisa and Abdurahman Nour concluded that the viscosity of W/O emulsions increased with the increase in the phase ratio, decreased in the temperature and increased in the stirring speed. They also concluded that the average droplet diameter of W/O emulsions greatly depended on the viscosity as well as the behavior of the emulsions if they are Newtonian or non-Newtonian.

In 2012, Maia Filho *et al.* [77] carried out an experimental study on the effect of the aging of the W/O emulsions on the emulsions stability. The crude oil examined in their study was crude oil obtained from the Brazilian field with API gravity of 28.3 °, which can be considered as medium crude oil. Six sets of W/O emulsions were formed at different oil phases using a Polytron PT 3100 homogenizer. The results showed that the emulsions elastic behaviour has the greatest effect on the emulsions stability. Although this study was about W/O emulsions, the focus of the study was different from the author study. This study was about the aging of the W/O emulsions on the emulsions stability and the author of this study is focused on the flow behaviours of W/O emulsions in the horizontal pipeline.

Keleşoğlu *et al*. [15] studied the flow properties of water-in-North Sea heavy crude oil emulsions using a lab scale flow rig as shown in **Figure 3.3** at different aqueous phase volume fractions from 0.0 to 0.50 and flow rates from $0.10\ \mathrm{m/s}$ to $0.70\ \mathrm{m/s}$ for 50 ℃. The corresponding Reynolds number for the studied aqueous phase volume fraction, flow rates and temperature was in between 9 to 292, which means that the flow of the emulsions in the pipeline is in the laminar flow regime. The results from the study showed that pressure gradients ($\Delta P/L$) along the pipeline test section increased as a function of flow rate and volume fraction of water. Keleşoğlu *et al*. [15] determined that the calculated viscosities of the emulsions remained constant with respect to the shear rate at the wall of the pipe and increased with the increased in the aqueous phase volume fraction. Keleşoğlu *et al*. [15] explained that the calculated viscosities of the emulsions did not increase with the increase in the flow rate was due to measurement errors in pressure drop data.

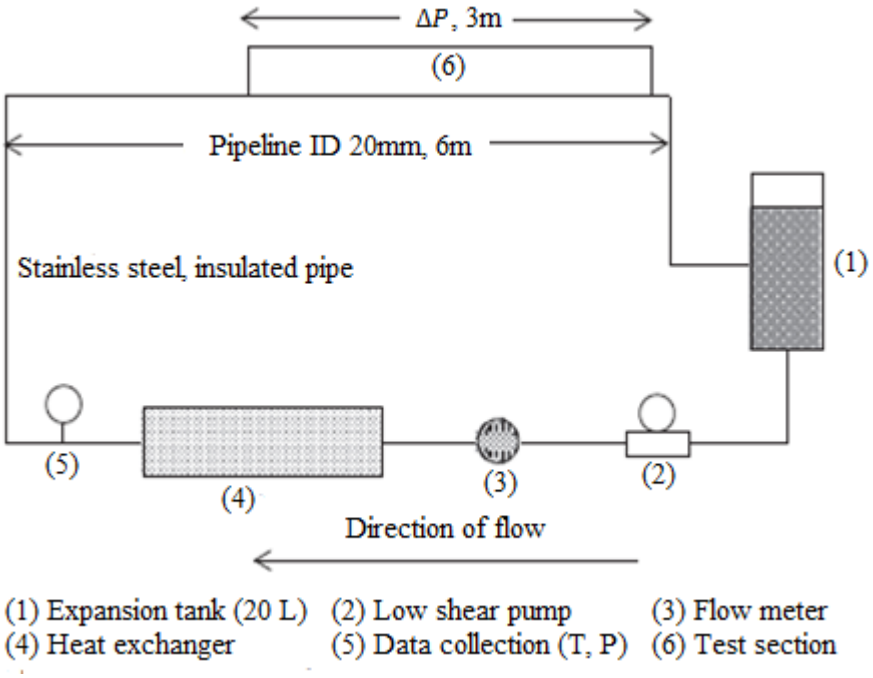

Figure 3.3: Illustration of experimental lab scale flow rig [15].

Plasencia *et al.* [18] carried out a study on the flow induced emulsification in a small scale close loop system as shown in **Figure 3.4**. The focus of this study was on the effective viscosity, inversion point and droplet size distribution of the emulsions formed by circulating the mixture of oil and water in the flow loop. Six different types of crude oils with viscosities ranging from 4.8 to 23.5 mPa.s and salt water with 3.5% NaCl w/v, pH 7.3 were used in the study. From the study, Plasencia *et al.* concluded that the effective viscosities of the six water-in-crude oil emulsions present a similar increase with water cuts up to 30% and larger differences are observed at higher water cuts. They also determined that different types of oils have a different inversion point. For the study on droplet size distribution, they observed that droplet sizes decrease with increasing flow rate and decreasing interface tension.

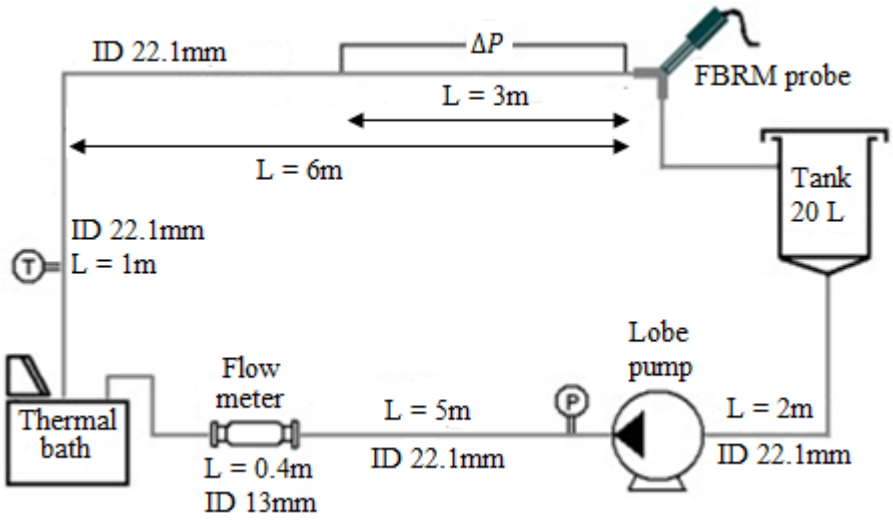

Figure 3.4: Illustration of experimental small scale close loop system [18].

3.4 Summary of Chapter

This chapter covers the literature review on the effects of emulsions, factors affecting the stability of emulsions and emulsification process. From the review on the effects of emulsions on the general flow behaviours, friction factor as well as viscosity and pressure drop, it can be concluded that the presence of emulsions significantly affects these flow properties. Also, it has been understood that the stability of emulsions is affected by the total mass percentage of asphaltenes and resins, the total mass percentage of volatile aromatic components, the elastic modulus (G') and viscous modulus (G'') of the fluid, as well as the duration time after the emulsions has been formed. Other than that, earlier researchers also have concluded that the stability of emulsions is affected by the mixing speed and mixing duration, pH of a solution, temperature of the solution and salt concentration. The focus of the current studies on the emulsification study is determined as well and hence the research gaps are addressed accordingly.

3.5 The research gap

Throughout the review of the existing experimental study on emulsification, it can be understood that the focuses were on the membrane emulsification, forming emulsions

using external forces, viscosity of emulsions and stability of emulsions (mostly based on the study of chemical compounds). Also, the study on formation of W/O emulsions through flow shear using lab-scale pipeline has been paid very little attention. To the author's best knowledge, only Nädler and Mewes [14], Keleşoğlu *et al*. [15] and Plasencia *et al*. [18] had done research on this. However, Keleşoğlu *et al*. [15] used North Sea heavy crude oil and the study focused on laminar flow only. In other words, the results cannot be applied in the real flow field because the flow regime used in the real flow field is turbulent flow. Plasencia *et al*. [18] on the other hand only studied on the effective viscosity, inversion point and droplet size distribution.

It is important to remark that the prediction of emulsions formation, where the emulsions are formed while the multiphase fluid passes through a 90 ° bend constriction using a model lab-scale continuous flow rig, has not yet been established. Besides, emulsion study using Miri crude oil has not yet been carried out as well. So, the current research is conducted using a model lab-scale continuous flow rig with the presence of a 90 ° bend pipeline constriction (to replicate the choke valve in the real industries) and Miri crude oil in order to mirror the real field conditions.

Emulsification study using different types of 90 ° bend constrictions is able to fill in the research gap in handling the emulsions formation mechanically, by suppressing or control the emulsions formation using different types of pipeline constrictions. Also, the study to relate the effect of emulsions formed downstream of the pipeline constriction to the friction or wall shear stress of the pipe in the pipeline flow has not yet been established.

Furthermore, the turbulence role in the formation of emulsions can be understood through this research.

CHAPTER 4

RESEARCH METHODOLOGY

This chapter provides the research methodology of the study. This study consists of rheology, wall shear stress and turbulence characteristics studies. The rheology studies were carried out to investigate the rheological behavior of Miri Light Crude and Miri Light Crude with water emulsions. For the wall shear stress and turbulence characteristics studies, velocity measurements experiments carried out using Ultrasonic Velocity Profiler (UVP) were involved. Before carrying out the velocity measurement experimental works, a lab-scale closed-circuit flow loop was designed and fabricated, serving as the experimental flow rig for the study. The results obtained from the UVP were then used for the wall shear stress and turbulence characteristics analysis.

The chapter is divided into 6 main sections. In the first section of this chapter, the design considerations and methodology for fabricating a lab-scale pipeline closed-circuit flow loop are provided. Description for the sizing of the flow loop and storage tank, technical selection of pump and flow meter, type of transport pipe used for the flow loop construction, measurement segments of the flow loop, transducer holder as well as control and safety instrumentation will be elucidated.

In the second section, the fluids used in this study and the properties of the fluid will be fully described accordingly.

The third section of this chapter seeks to provide an illustrated calibration of the experiments. The calibration of rheometer has been presented. Verification of the experiment is essential to ensuring the accuracy of results relating to the later stage of the study.

The forth section is the description of the experimental methodology of the measurement of crude oil rheology. This part of experiment is needed in order to characterize the crude oil before proceeding with the later stage experiments.

The fifth section of this chapter describes the experimental setup and methodology of the velocity measurement in the pipeline. Detailed information on the Ultrasonic Velocity Profiler (UVP), which is used for the velocity measurement, is presented in the velocity measurement methodology.

The last section of this chapter analyzes the uncertainty and error associated with the results. This is done to ensure the integrity of the results.

4.1 Design of Experimental Flow Loop

The main aim of this study is to perform an in-depth study of the behaviours of water-in-crude oil emulsions in the pipeline flow where the emulsification is induced by the flow shear instead of applying external forces to form emulsions with the purpose of replicating the emulsification process in the real practical. In order to achieve flow-induced emulsification, a closed-circuit flow loop with 90 ° bend pipeline constriction was designed. Also, since different types of pipeline constrictions are involved in the study, the pipeline constriction section was designed to be detachable so that it can be attached and detached from the flow loop as per user experiments request.

Next, for the fabrication of the flow loop, the following design considerations are covered:

a) Sizing of the flow loop
b) Sizing of the water and oil storage tank
c) Technical selection of the flow meter
d) Overall pressure drop estimation and technical selection of the pump

4.1.1 Layout and Sizing of the Flow Loop

The model continuous closed-circuit flow loop is one of the main facilities needed in this research. It is a test loop designed for the study of water-in-crude oil (W/O) emulsions. As can be seen in **Figure 4.1** and **Figure 4.2**, the designed flow loop is a closed-circuit loop and it is divided into two main loops. First loop is from P → O → N → M → L → K → J → I →H → F→ E → D. Second loop is from P → O → N → M → L → K → J → I → H

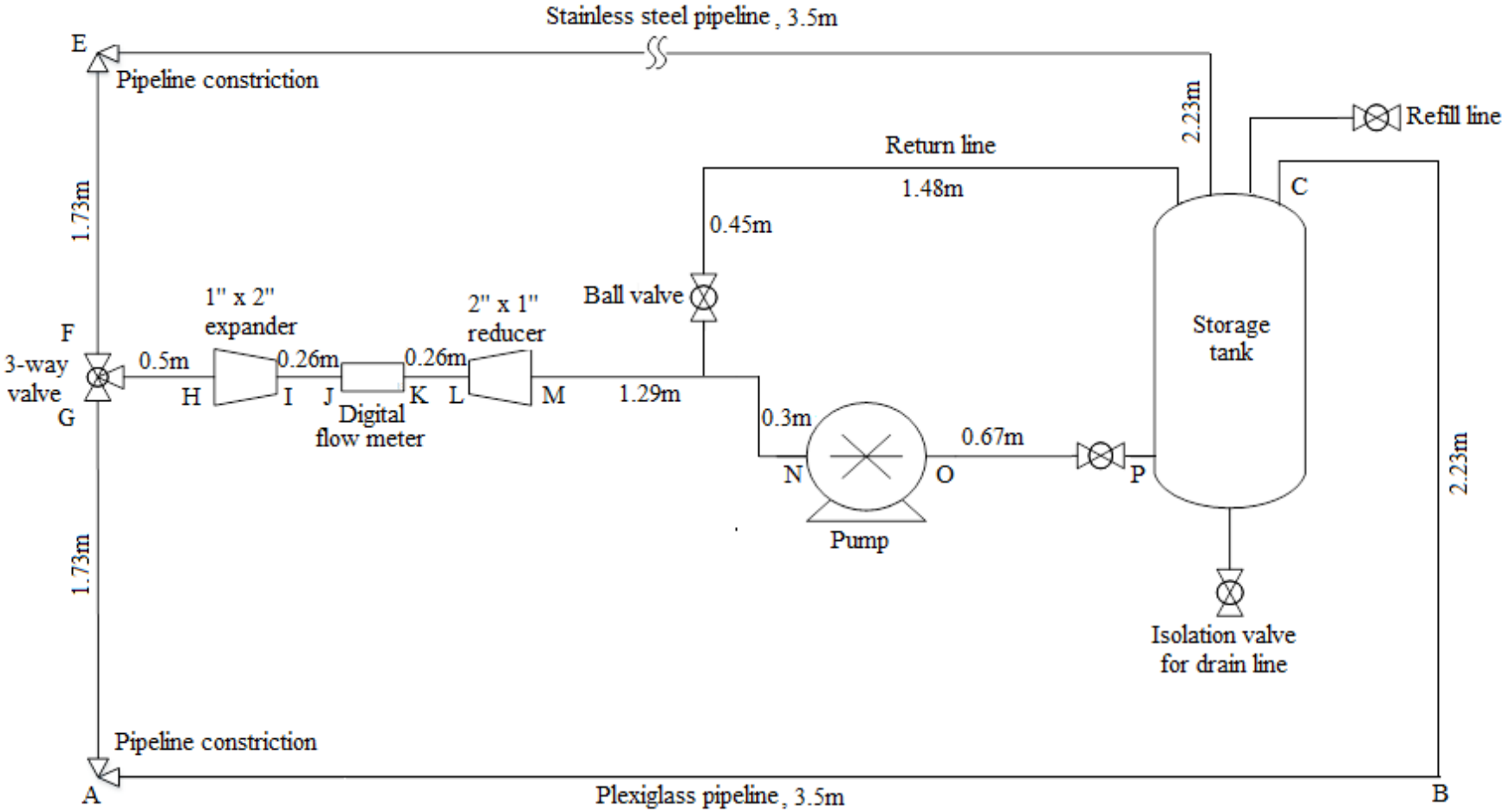

Figure 4.1: Flow sheet of the lab-scale continuous closed-circuit flow loop.

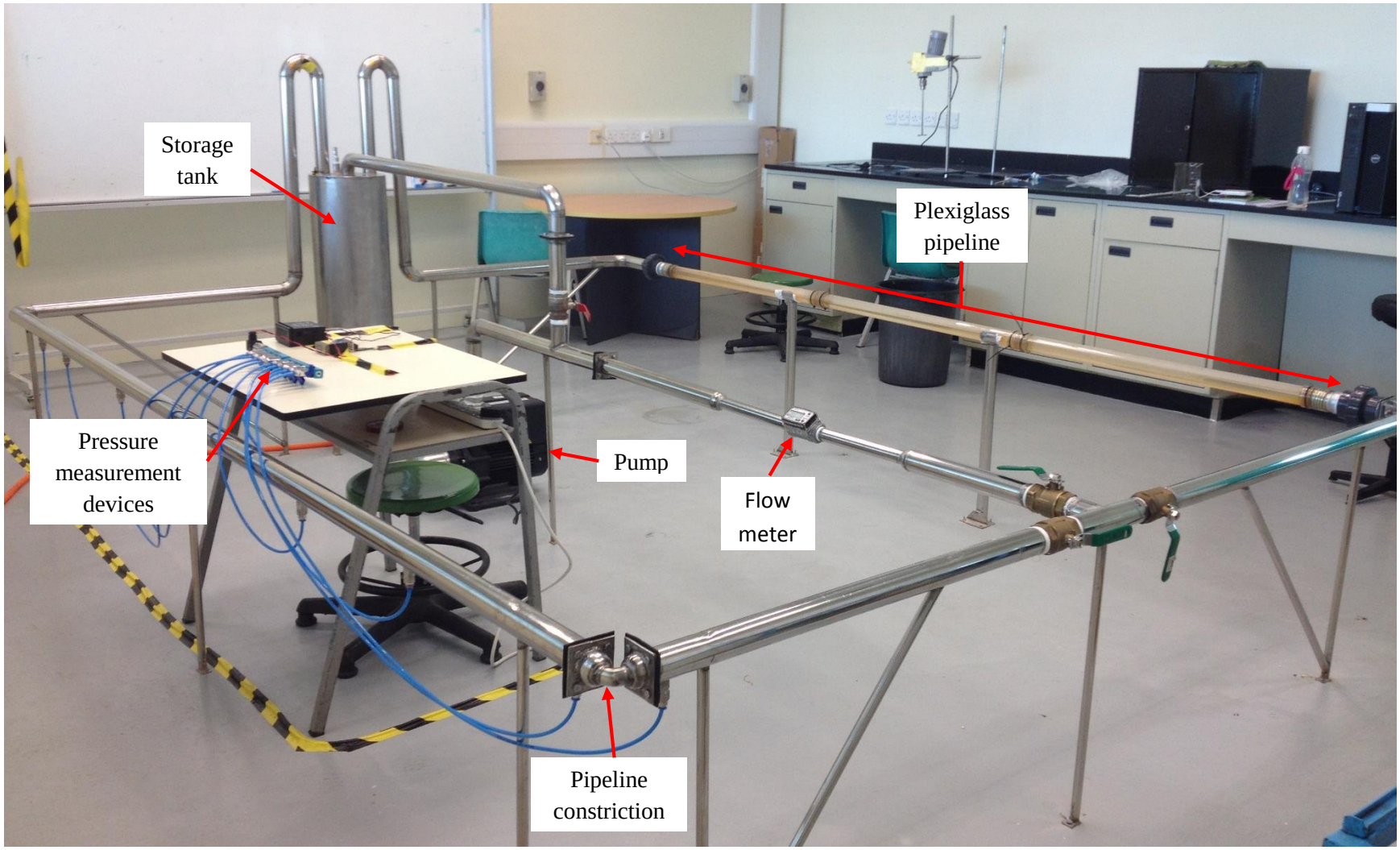

Figure 4.2: Actual photo of the lab-scale continuous closed-circuit flow loop (Test Loop).

→ G→ A → B → C. The difference between these two loops is the material used to construct the test segment ED and test segment AB. Test segment ED was constructed using stainless steel pipe whereas test segment AB was constructed using plexiglass tube. The test segment ED was used for the pressure drop measurement along the pipeline; meanwhile, the test segment AB was used for the velocity profile measurement and visualization of mixture along the pipeline. In this model continuous closed-circuit flow loop, a pump was used to circulate the liquid in the flow loop starting from the tank, through a flow meter and measurement segment, finally back to the tank. A bypass line was provided right after the pump to circulate the liquid back to the tank in order to control the flow rate.

The sizing of the flow loop was based on the space availability of the laboratory room and the length of the test section. It was made to ensure that the length of the test section is sufficient for the flow in the pipeline to be fully developed. In order to fulfill this criteria, the entrance length was calculated as flow beyond the entrance flow region is considered as fully-developed flow. Entrance length for laminar flow and turbulent flow can be obtained by Equation 4.1 and Equation 4.2, respectively [93]:

$$\frac{\ell_e}{D} = 0.06\, Re \text{ for laminar flow (Re} \leq 2100) \tag{4.1}$$

$$\frac{\ell_e}{D} = 4.4\, Re^{1/6} \text{ for turbulent flow (Re} \geq 4000) \tag{4.2}$$

where ℓ_e is the entrance length; D is the diameter of the pipe; Re is the Reynolds number.

Table 4.1 shows the entrance length for 0.044 m and 0.0762 m pipe's diameter at their respective volume fraction of water and Reynolds number. The entrance lengths were calculated for each of the experimental parameters as shown in **Table 4.1**. From the table, it can be clearly seen that the entrance length for pipe with 0.044 m diameter is shorter than the one of 0.0762 m diameter. Due to the space limitation of the laboratory room, the pipe with 0.044 m diameter was selected as it gives shorter entrance length as compared to the 0.0762 m diameter pipe. In order to have the pressure and velocity profile measurement at the fully-developed flow region (entrance length of transitional flow was

Table 4.1: Comparison of entrance length between 2'' and 3'' pipe.

Volume fraction of water (%)	Flow regime	Entrance length, ℓ_e for 2'' or 0.044 m pipe (m)	Entrance length, ℓ_e for 3'' or 0.0762 m pipe (m)
0	Laminar	2.90	5.00
5	Laminar	4.01	6.91
	Transitional	0.73	1.25
10	Laminar	4.29	7.39
	Transitional	0.73	1.26
15	Laminar	4.02	6.92
	Transitional	0.73	1.26
20	Laminar	3.48	6.00
	Transitional	0.71	1.23
25	Laminar	4.81	8.29
30	Laminar	4.30	7.41
35	Laminar	4.19	7.23
40	Laminar	2.88	4.96

considered), it was decided to design the measurement segment to be 3.50 m long horizontally, where it gives about 2.8 m long of fully-developed region measurement. It is important to remark that although the selected pipe diameter is unable to replicate the real pipe diameter being used in the real practical field, the results obtained in this study can still be applied to the real practical field. This is because the study is carried out based on dimensionless number, which are, Reynolds number, y/D location (dimensionless pipe's diameter), *x/D* location (dimensionless pipe's length) and $\frac{\tau_w D}{\mu U}$ (dimensionless wall shear stress). Using non-dimensional number, the dynamic similarity between the prototype used in this study and the one in the real practical field can be achieved.

As can be seen in **Table 4.1**, given the same flow regime, the entrance length is different at different volume fractions of water. This is because the density and the dynamic viscosity are different at different volume fraction of water. The density and dynamic viscosity used in the calculation are given in **Table 4.2**. The density for different water fractions of water was calculated based on the fraction of water and crude oil presence multiply by their respective density, where the density of water and pure crude oil are 995 kg/m^3 and 876.8 kg/m^3, respectively, at 25 ℃. For example, at 5% volume fraction of water, the density calculation is:

$$\rho_{5\%} = (0.05)\left(995\,\frac{\text{kg}}{\text{m}^3}\right) + (0.95)\left(876.8\,\frac{\text{kg}}{\text{m}^3}\right) = 882.71\,\frac{\text{kg}}{\text{m}^3}$$

Meanwhile, the dynamic viscosity for different volume fractions of water was obtained from the rheology study.

Table 4.2: Density and dynamic viscosity for 0 – 40% volume fraction of water.

Volume fraction of water (%)	**Density, ρ (kg/m^3)**	**Dynamic viscosity, μ (Pa.s)**
0	876.80	0.00732
5	882.71	0.00898
10	888.62	0.01103
15	894.53	0.01329
20	900.44	0.01680
25	906.35	0.01683
30	912.26	0.02039
35	918.17	0.02408
40	924.08	0.02792

The main components of this continuous closed-circuit flow loop are:

- Water and oil storage tank
- Pump
- Flow meter
- Transport pipes
- Horizontal test sections
- Pipeline constriction
- Ultrasonic velocity profiler (UVP) probe holder
- Control and safety instrumentation

All of these components are described in the following sections.

4.1.2 Water and Oil Storage Tank

The storage tank is made of stainless steel, with a diameter of 0.285 m and height of 0.865 m, which gives a total volume of about 55.18 L. The storage tank is supported by three stands to make it 0.18 m from the ground. In that way, an isolation valve can be connected below the tank for an easier draining purpose. There are four inlets for the storage tank which are located at the top of the tank. One of the inlets is the inlet for filling the fluid into the tank. Another two inlets are the inlets for the continuous flow fluid in the loop back to the storage tank. The fourth inlet is the inlet for the by-pass loop as can be seen in **Figure 4.1**. The liquid level in the tank is indicated using a transparent pipe connected at the drain line which is positioned to be parallel to the tank. The size of the tank is designed based on the total expected volume of fluid circulated in the flow loop. The size of the tank (based on volume) should be about the same with the total expected volume of fluid circulated in the flow loop. Neither a smaller tank nor a larger tank is desired. This is because a smaller tank will not be able to store the total volume of fluid that is required to fill the entire flow loop, and a larger tank will increase the residence time of fluid in the tank. High residence time of fluid is unwanted in this research study because the research is about the study of emulsions effects to the pipeline flow transport. High residence time

of emulsions fluid in the tank will allow the unstable emulsions to settle out into two distinct phases.

The total expected volume of fluid is the total volume of segments, which can be calculated using Equation 4.3.

$$V_{total} = (\pi \cdot r^2) \times L_{total} \tag{4.3}$$

where πr^2 denotes the cross-sectional area of the pipe and L_{total} denotes the total length of the pipeline segments. The total length of the pipeline segments of the closed-circuit flow loop is 20.115 m and the cross-sectional area of pipe is 0.00181 m^2. Hence, the total volume of all the segments in the flow loop gives about 36.40 L. With 50% of contingency, the tank size should be 54.60 L, with which the final fabrication gives the actual tank size of 55.18 L.

4.1.3 Pump

The pump selected is a positive displacement pump, model TQ 1500 manufactured by Walrus Pump Co (Walrus). The specifications of the selected pump are as follow:

- Power – 2 HP
- Cycle – 60 Hz
- Maximum height – 134 ft
- Maximum flow rate – 250 L/min
- Maximum pump pressure – 58 psi
- Maximum inlet pressure – 48 psi
- Maximum discharge head – 32 m

This pump was selected mainly because the maximum discharge pressure of the pump is able to overcome the total pressure loss in the flow loop. The total pressure loss can be calculated using Equation 4.4.

$$\Delta P_L = \Delta P_{L,major} + \Delta P_{L,\min or} \tag{4.4}$$

where $\Delta P_{L,major}$ denotes major pressure drops and $\Delta P_{L,\min or}$ denotes minor pressure drops. $\Delta P_{L,major}$ and $\Delta P_{L,\min or}$ can be obtained from Equation 4.5 and Equation 4.6 respectively. Major loss is due to the pressure drop when fluid flows across a straight pipe whereas minor loss is due to the pressure drop when fluid flows across a pipe component. Typical pipe components include entrance and exit, enlargements and contractions, bends, as well as fittings such as tees, elbows, union and valves.

$$\Delta P_{L,major} = f \frac{L}{D} \frac{\rho V^2}{2} \tag{4.5}$$

$$\Delta P_{L,\min or} = K_L \frac{\rho V^2}{2} \tag{4.6}$$

where f denotes friction factor, L denotes pipe equivalent length, D denotes pipe's diameter, ρ denotes density of fluid, V denotes average flow velocity, K_L denotes loss coefficient. The friction factor can be obtained from Moody's chart and the loss coefficient can be obtained from literature or textbook sources.

Besides, this pump was selected because it tends to provide constant flow or fixed volume of fluid from the pump inlet pressure section to the pump discharge section. Also, this type of pump is designed for pumping non-aggressive water and solid particles free water, which is suitable for this research. Moreover, the power requirement for this pump is 1.5 kW which is compatible with the existing laboratory electrical power supply. All in all, the specifications of this pump satisfy the requirements of this study.

4.1.4 Flow Meter

The selected flow meter is a 1" turbine flow meter, model GPI® A100 digital type flow meter. The specifications of the selected flow meter are as follow:

- Accuracy – $\pm$ 1.5 %
- Repeatability – $\pm$ 0.2 %

- Flow range – 10 L/min to 190 L/min
- Temperature limit – −40 ℃ to 121 ℃
- Maximum pressure it can withstand – 300 psi
- Maximum pressure drops across the flow meter – 5 psi

This flow meter was selected mainly because its measurable flow range meet the requirements for this research study and price valuation. Also, it is suitable for use in crude oil service. **Table A.1** in the appendix shows all the flow meter models used for comparisons, with which flow meter number 2 is selected.

The installation of the flow meter considered two requirements. First, since the bore size of the flow meter is 1" (2.54 cm) and the transportation pipeline is 2" (5.08 cm), a 26 cm long (10 times of flow meter bore diameter) straight horizontal 1" pipes are connected to both the inlet and outlet of the flow meter. The 1" pipes are then connected to the 2" transportation pipeline. The installation of 26 cm long straight horizontal pipes is to provide an adequate straight-run horizontal pipes before and after the flow meter to avoid the swirl in the flow from affecting the accuracy of the flow meter. Second, the flow meter is installed more than 6" away from other electronic equipment to prevent interference from other possible electromagnetic sources. This is to ensure the accuracy of the flow meter is sustained.

4.1.5 Transport Pipes

All the transportation pipings used in this test loop circuit are made of 2" stainless-steel (SS) pipes with an inner diameter of 48 mm and a wall thickness of 2 mm. The total length of the stainless-steel piping is about 15 meters. SS pipe was selected to be used as the transportation piping for the test loop circuit in order to replicate the metal pipeline used in the oil and gas industry. SS pipe was chosen instead of other types of metal because SS pipe is less prone to corrosion and stains as well as to prevent the galvanic corrosion. Galvanic corrosion can be prevented because the selected pump and flow meter for the test loop are provided with SS joints. The use of same metals gives similar electro-potentials and hence no galvanic current which can cause the galvanic corrosion [94].

4.1.6 Pipe Measurement Segments

As mentioned in section 4.1.1, there are two segments; they are test segment ED (made of stainless-steel) and test segment AB (made of plexiglass). The test segment stainless steel pipe has the same size as the transportation pipes and the test segment plexiglass pipe has an inner diameter of 44 mm and wall thickness of 1 mm. Both the test pipes are about 3.5 meters long respectively.

The stainless-steel pipe test segment is for the measurements of pressure. Eight pressure tapings are located on the stainless-steel test pipe test segment. The plexiglass test segment is for the flow pattern visualization as well as for the velocity profile measurements.

The entry region is made long enough to allow the flow to be fully-developed. The entry region length was calculated before the flow loop was constructed as described in section 4.1.1.

4.1.7 Pipeline constrictions

Four pipeline constrictions with different contraction ratios and designs were used in the present study. As presented in **Table 4.3**, there are sudden constrictions with contraction ratio of 0.50 and 0.75, and gradual constrictions with contraction ratio of 0.50 and 0.75 respectively. The contraction ratio is the ratio of the internal diameter of the constriction to the internal diameter of the transport pipeline. The drawings of the constriction are not up to scale. These pipeline constrictions are connected at Section A and E as shown in **Figure 4.1**. Section A and E of the flow loop were designed to be detachable so that all these constrictions can be attached and detached from the flow loop as per user experiments request.

Table 4.3: Geometry of the pipeline constrictions.

Description	Geometry of Constriction
Sudden contraction ratio 0.5 Degree of bend: 90° Internal diameter of constriction: 2.2 cm Length: 4.5 cm × 4.5 cm Thickness: 0.1 cm	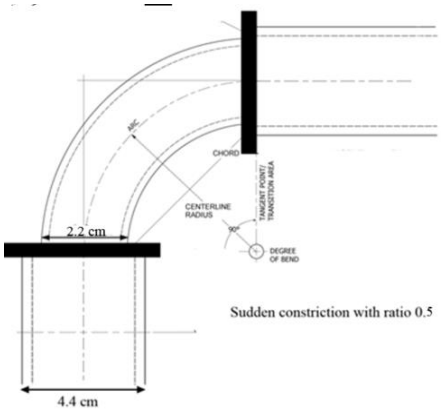 Sudden constriction with ratio 0.5
Gradual contraction ratio 0.5 Degree of bend: 90° Internal diameter of constriction: 4.4 cm to 2.2 cm Length: 4.5 cm × 4.5 cm Thickness: 0.1 cm	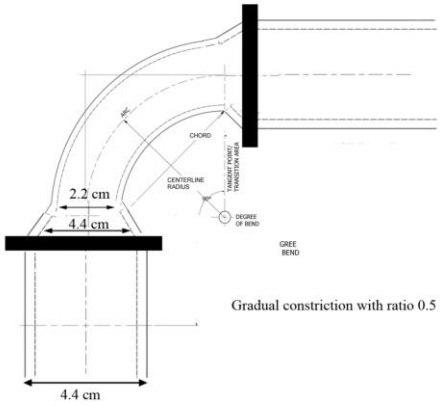 Gradual constriction with ratio 0.5
Sudden contraction ratio 0.75 Degree of bend: 90° Internal diameter of constriction: 3.3 cm Length: 4.5 cm × 4.5 cm Thickness: 0.1 cm	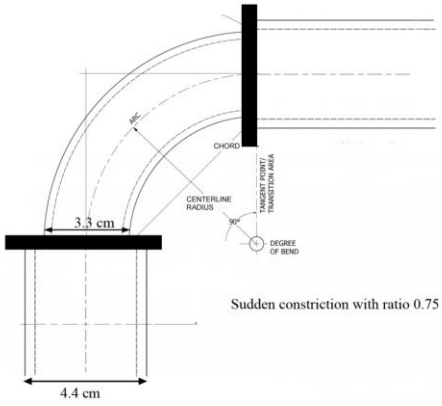 Sudden constriction with ratio 0.75

Table 4.3: Geometry of the pipeline constrictions (continued).

Description	Geometry of Constriction
Gradual contraction ratio 0.75 Degree of bend: 90° Internal diameter of constriction: 4.4 cm to 3.3 cm Length: 4.5 cm × 4.5 cm Thickness: 0.1 cm	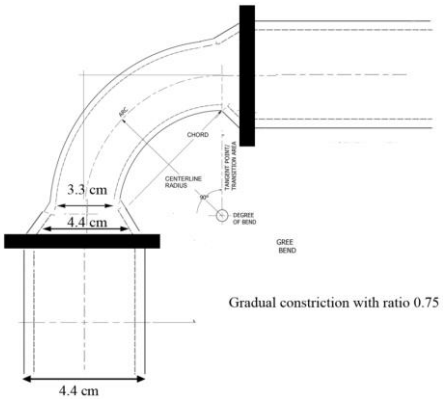

4.1.8 Ultrasonic Velocity Profiler (UVP) Transducer/Probe Holder

Five UVP transducer holders are attached on the horizontal plexiglass pipeline. This is to ease the velocity measurement using UVP. All the transducer holders are designed to have an incident angle of 10 degrees from the normal. The incident angle of 10 degrees is chosen due to a few facts. First, the critical angles of incidence for coupling gel (water-based) and plexiglass is about 30 degrees. So, the chosen angle of incidence cannot be greater than 30 degrees. Next, although a smaller angle of incidence can reduce the sound pressure lost at the pipe wall [95], the incident angle of zero cannot be used. This is because the incidence angle of zero cannot detect the velocity of the axial flow component. Therefore, as a compromise, the incidence angle of 10 degrees is chosen to be used in this research study.

These transducer holders are attached at 45 cm (13 *x/D*), 90 cm (24 *x/D*), 135 cm (38 *x/D*), 180 cm (51 *x/D*) and 215 cm (63 *x/D*) on the plexiglass pipeline after the pipe constriction, respectively. The design of the transducer holder is as shown in **Figure 4.3**. This transducer design was inspired by the thesis of Thomas Geisler [96] with some

modifications. **Figure 4.4** shows the positioning of the transducer with an incidence angle of 10 degrees.

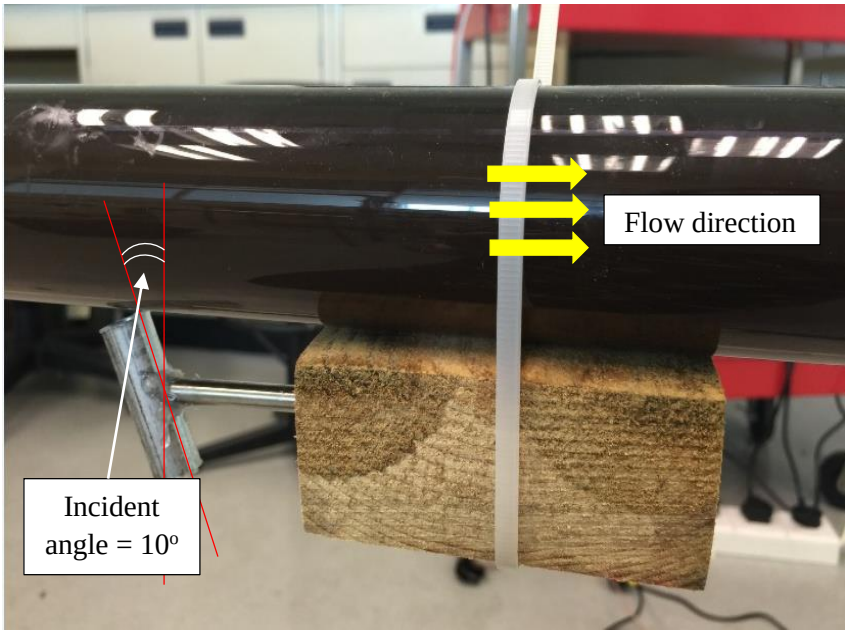

Figure 4.3: UVP probe holder.

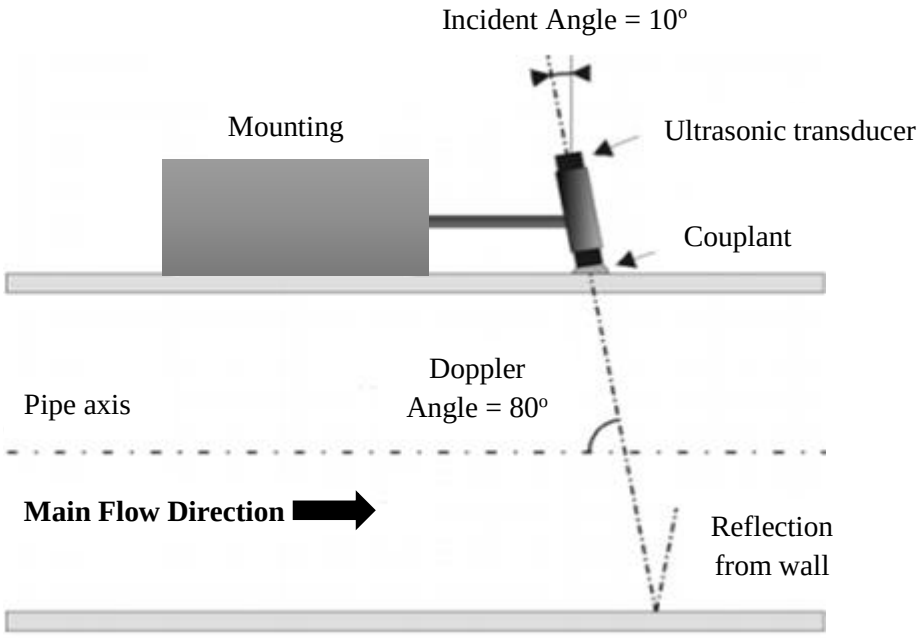

Figure 4.4: Positioning of the transducer [96].

4.1.9 Control and Safety Instrumentation

Temperature

The temperature of the test section pipe was measured from time to time using electronic digital infrared thermometer temperature sensor gun, model IRT537. The measurement range of the infrared thermometer is -20 ℃ to 537 ℃. Measuring temperature was to make sure that the temperature rise of the flow is within a few degrees Celsius only. This is because the change in temperature will change the fluid properties as well. The temperature rise is due to the operation of pump especially when the pump is operating at high speed. The changes in temperature cannot be controlled in this study. Hence, experiments were terminated once the increase in temperature is more than 15 ℃. The temperatures measured during the experiments were recorded.

Pressure

Static pressures of the flow were measured by installing pressure tappings along the test section pipe. Along the test section pipe, eight pressure tappings are located on the pipe. One pressure tapping is located before the pipe constriction and another seven pressure tappings are located after the pipe constriction. The purpose of locating pressure tappings in this way is to study the pressure change due to the pipe constriction. All the pressure tappings are connected to a manifold via impulse lines and the manifold is connected to a digital pressure transmitter. As can be seen in **Figure 4.5**, at the manifold, there are 9 valves provided to allow the user to select the required pressure point to be measured. 8 of the valves are connected to the pressure tapping points via impulse line and 1 of the valves is the drain line. The measured output unit of the digital pressure transmitter is in milliamps (mA). Hence, the digital pressure transmitter is connected to a digital pressure indicator to convert the pressure measurement reading into an appropriate pressure measurement unit, which is in unit bar.

The model of digital pressure transmitter used is BCM 130C. The pressure measurement range of this type of transmitter is from 0 bar to 4 bar and the allowable operating

temperature ranges from -40 ℃ to 125 ℃. BCM 130C digital pressure transmitter has an accuracy of $\pm$ 0.5% of the full-scale output. The allowable voltage supply for this type

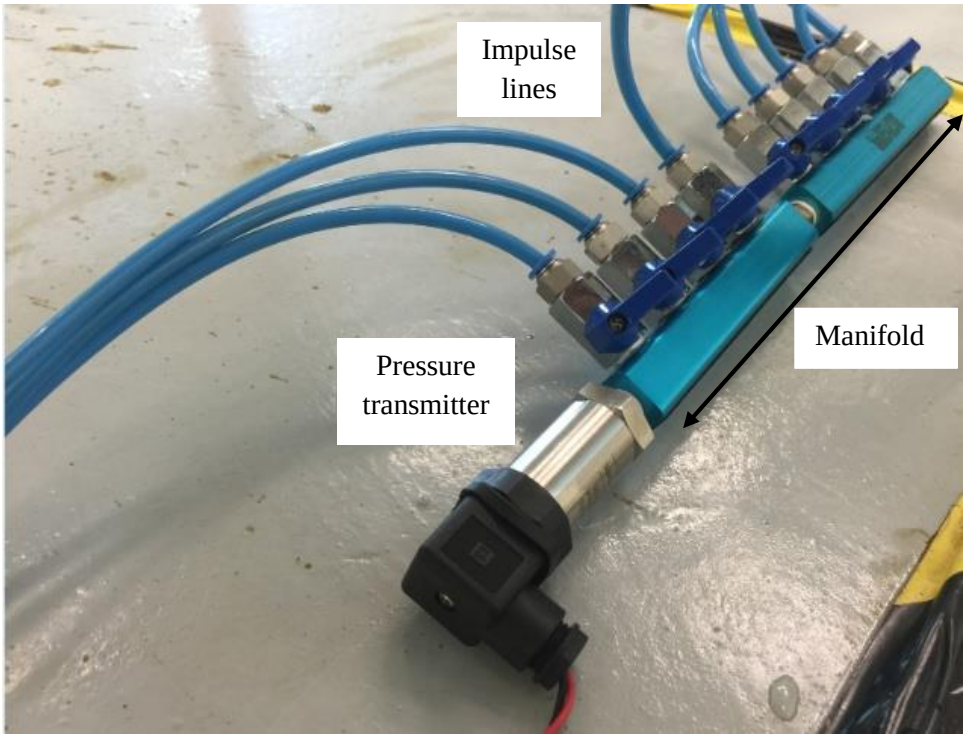

Figure 4.5: A photograph of manifold connected to pressure transmitter (model BCM 130C).

of transmitter is only 12 Vdc to 36 Vdc, but the laboratory power supply voltage is 240 Vac. Hence, a 24 Vdc voltage convertor was used to convert the power supply voltage from 240 Vac to 24 Vdc. The allowable measured output of this transmitter ranges from 4 mA to 20 mA. **Figure 4.5** shows the BCM 130C digital pressure transmitter.

The digital pressure indicator model used was the Autonics MT4W-DA-41 digital pressure indicator. As mentioned earlier, it was used to convert the input current signal from BCM 130C pressure transmitter in mA to the output of pressure measurement unit in bar. Autonics MT4W-DA-41 digital pressure indicator has an output range of 0.00 bar to 4.00 bar, with sensitivity of 2 decimal points. The allowable operating temperature for this pressure indicator is -10 ℃ to 50 ℃. **Figure 4.6** shows the Autonics MT4W-DA-41 pressure indicator.

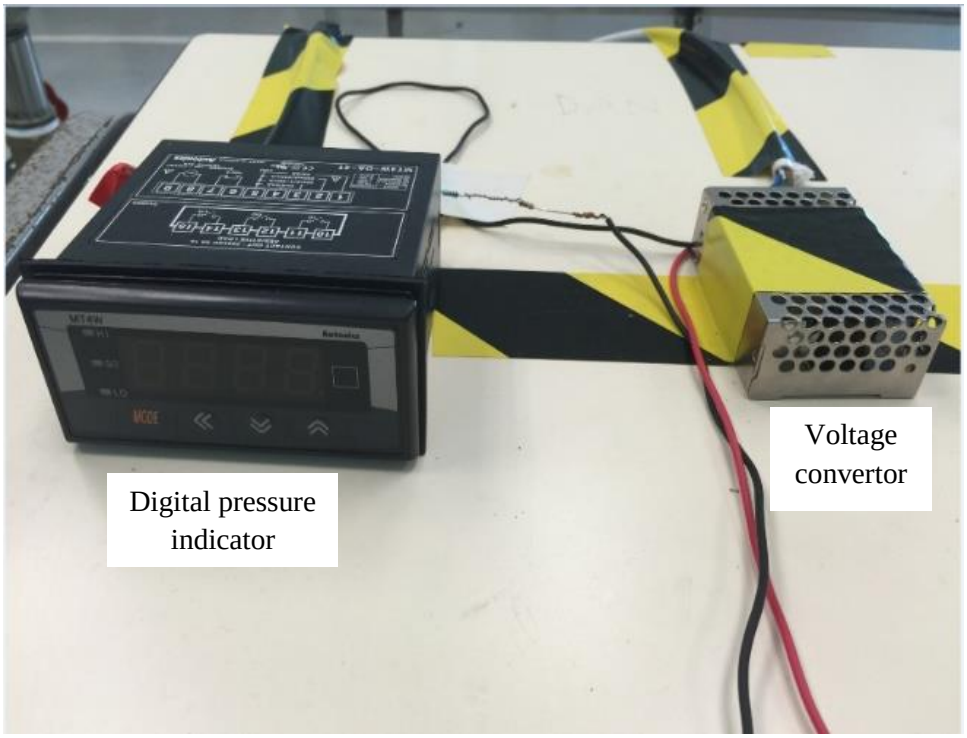

Figure 4.6: A photograph of 24 Vdc voltage convertor wire connected to digital pressure indicator (model Autonics MT4W-DA-41).

Flow rate

Flow rate was measured using turbine flow meter, model A 100 GPI digital type meter. The flow meter is installed 1.25 m after the pump as can be seen in **Figure 4.1**. It has an accuracy of $\pm 1.5\%$ and repeatability of $\pm\, 0.2\%$. The flow range of this flow meter is $10 - 190$ L/min. The temperature limit for the flow meter is 121 ℃ and the maximum pressure is 300 psi. This model of flow meter was selected because its specifications meet the requirement of the study.

4.2 Fluids

The fluids used for this research study were crude oil stock and filtered tap water. Crude oil stocks were provided by PETRONAS Miri Crude Oil Terminal (MCOT). The crude oil stock is known as "Miri Light Crude (MLC)" because the crude stock has an API gravity of 29.79°. Presented in **Table 4.4** is the physicochemical properties and content

of the MLC. The analysis of the MLC was performed by external industrial laboratory - Petrotechnical Inspection (M) Sdn. Bhd., which is located in Labuan.

Filtered water was obtained by filtering the tap water from local municipal water supply. The purpose of filtering the water is to remove the unwanted rust and sediment particles.

Table 4.4: Physicochemical properties and content of the crude oil.

No.	Parameter	Test Method	Unit	Result
1	Density @ 15 °C	ASTM D 5002	g/cm3	0.8768
2	API Gravity @ 60 °F	Calculated	Degree	29.79
3	Total Sulphur	ASTM D 4294	wt %	0.0771
4	Nitrogen Content	ASTM D 5762	ppm wt	255
5	Total Acid Number	ASTM D 664	mgKOH/g	0.24
6	Nickel (Ni)	ASTM D 5863	ppm wt	< 1.0
7	Vanadium (V)	ASTM D 5863	ppm wt	1
8	Flash Point	IP 170	°C	< -20
9	Pour Point	ASTM D 5853	°C	-30
10	Colour ASTM	ASTM D 1500	-	D 8.0
11	Reid Vapor Pressure @ 37.8°C	ASTM D 5191	kPa	9.2
12	Salt Content	ASTM D 3230	lb/1000bbl s	3.5
13	Ash Content	ASTM D 482	wt %	0.002
14	Mercaptan Sulphur	UOP 163	ppm wt	23
15	MCRT - 100% Sample	ASTM D 4530	wt %	0.23
16	Wax Content	UOP 46	wt %	4.5
17	Kinematic Viscosity @ 25°C	ASTM D 445	cSt	4.785
18	Kinematic Viscosity @ 40°C	ASTM D 445	cSt	3.958
19	Kinematic Viscosity @ 70°C	ASTM D 445	cSt	2.303
20	Characterisation Factor	UOP 375	-	11.5
21	Gross Calorific Value	ASTM D 240	MJ/kg	44.482
22	Asphaltenes	IP 143	wt %	0.43

Table 4.4: Physicochemical properties and content of the crude oil (continued).

No.	Parameter	Test Method	Unit	Result
23	Sodium (Na)	ASTM D 5863	ppm wt	14
24	Potassium (K)	ASTM D 5863	ppm wt	< 1.0
25	Copper (Cu)	ASTM D 5863	ppm wt	< 1.0
26	Lead (Pb)	ASTM D 5863	ppm wt	< 1.0
27	Iron (Fe)	ASTM D 5863	ppm wt	1.2
28	Basic Sediment & Water	ASTM D 4007	vol. %	0.05
29	Water Content	ASTM D 4006	vol. %	0.10

4.3 Calibration

Preliminary experiments were conducted to verify the performance of rheometer. The verification experiments were done to ensure that the measurement systems are able to produce accurate results as well as acting as the basis for the experiments presented later in the thesis.

4.3.1 Calibration of Rheometer

The experiment was done to verify the functionality of rheometer. A rheometer model AR 1500 was used for the study of viscoelastic properties of the test liquids. Calibration of rheometer was done before it was used for measuring the mixtures of this research study. The experiments were carried out using water as water is well-known as Newtonian fluid, with which viscosity is independent of shear rate and shear stress is directly proportional to shear rate. The data attained from the rheometer are plotted in **Figure 4.7** and **Figure 4.8**. As can be seen in **Figure 4.7**, the viscosity does not change with shear rate. It remained constant at 0.001 Pa. s, which is the typical value of water viscosity. As shown in **Figure 4.8**, the calibration curve is linear, in which shear stress is directly proportional to shear rate. The equation that can be used to attain shear stress values from shear rate is $y = 0.001x$, wherein y and x represents shear stress (Pa) and shear rate $(1/\mathrm{sec})$ respectively. The coefficient of determination (R^2) of the graph shows a value 0.9885 which is extremely close to 1. This means that the regression line fits the data very well.

The conclusion from this experiment is the rheometer gives satisfactory results compared to the expectations.

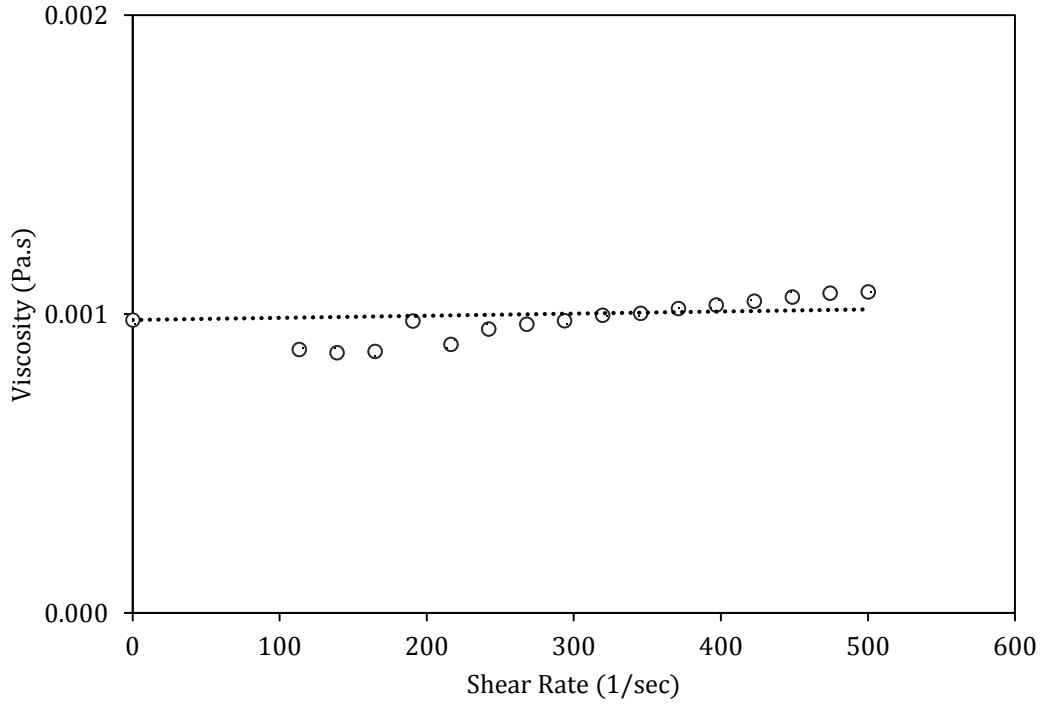

Figure 4.7: Viscosity versus shear stress of water.

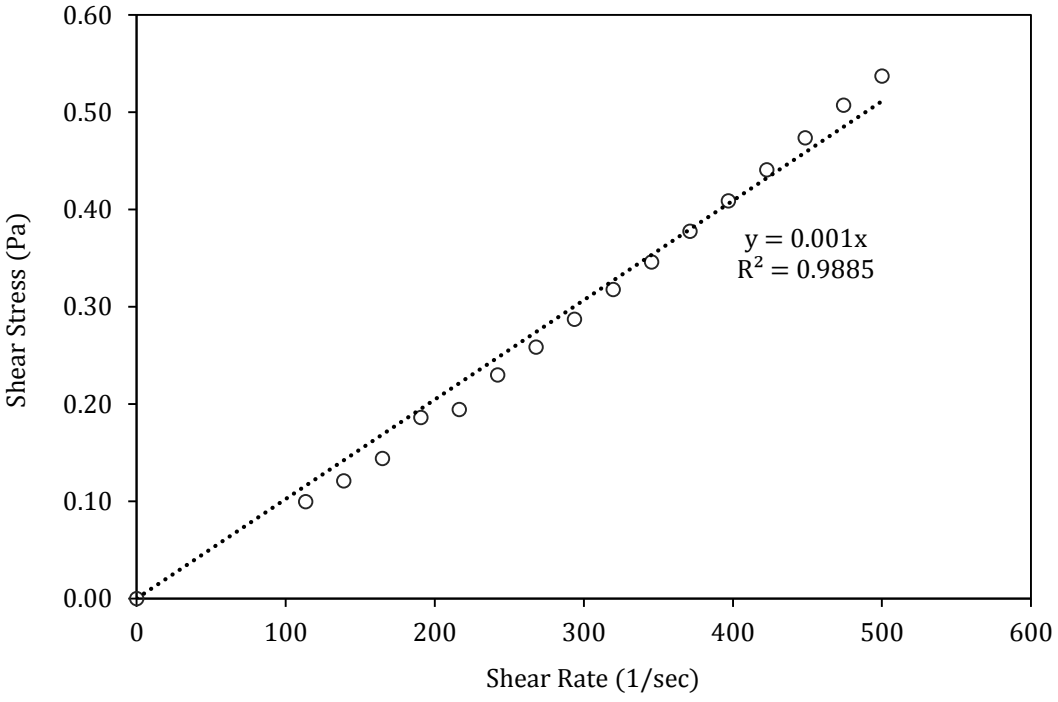

Figure 4.8: Shear stress versus shear rate of water.

4.4 Rheology Measurement

Rheology study was carried out to characterize the crude oil and crude oil with water emulsions used in this research before proceeding to study the water-in-oil emulsions formation in the pipeline. The rheological behavior can be divided into Newtonian and non-Newtonian, which is sub-divided into shear thinning and shear thickening.

4.4.1 Experimental Setup

An overhead stirrer model OST 20 digital supplied by Yellow Line was used to stir water in the crude oil phase to form crude oil with water emulsions. **Figure 4.9** shows the overhead stirrer used for the experiment. This type of stirrer automatically adjusts the speed through microprocessor controlled technology within the speed range of 30 – 2,000 rpm. The overhead stirrer gives a constant speed because a continuous comparison of shaft speed to desired speed is maintained and variations are adjusted automatically.

Figure 4.9: Overhead stirrer model OST 20 digital.

A rheometer model AR 1500 supplied by TA instruments was used to test the rheological characterization of crude oil and crude oil with water emulsions. It uses air-bearing technology, drag-cup motor for stress application and optical encoder for displacement/strain measurement. It is armed with a temperature controller to control the temperature in the range of -40 ^{o}C to 200 ^{o}C. The cone and plate geometry was used for the experiment. The diameter of the cone was 60 mm and the cone angle was 2 degrees. The gap in between the cone and plate for sample fluid was set to be 61 mm. The rheometer is connected to a computer data acquisition system to read the output signals. It is equipped with a Peltier plate which controls and measures the temperature from a range of $-40\,℃$ to $200\,℃$ with an accuracy of $\pm\,0.1\,℃$. To operate the rheometer, operating temperature (℃), operating range of shear rate $(1/s)$, operating mode and points per decade were designated. Operating mode refers to the type of graph to be plotted, either log or linear plot; points per decade refers to the number of readings to be taken. **Figure 4.10** shows the rheometer used for the experiments.

(a)

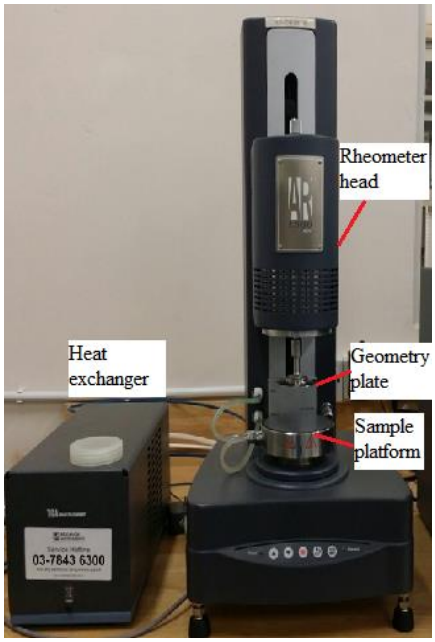

(b)

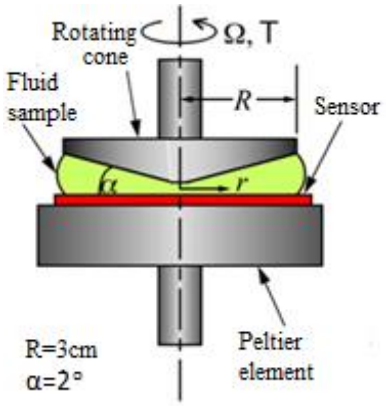

(c)

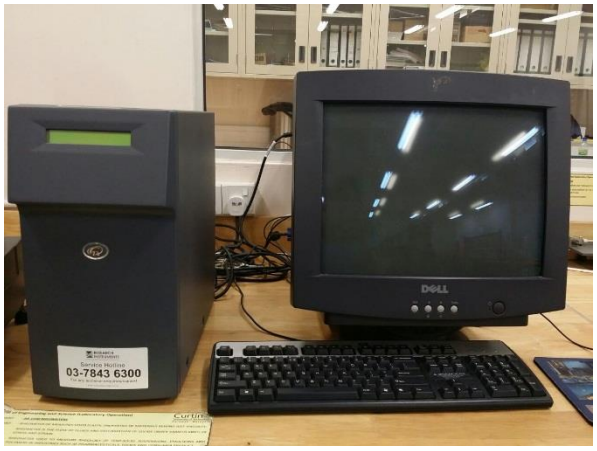

Figure 4.10: (a) Rheometer model AR 1500 (b) Cone and plate geometry (c) Rheometer data acquisition system.

4.4.2 Experimental Methodology

All emulsions samples were prepared in the beakers. Water was poured into the beaker filled with crude oil at desired water cut. Water cut in this study refers to the ratio of water compared to the volume of total liquids. The volume of total liquids used in this study was 100 ml (taken as 100%). Then, the solution was allowed to stir for 60 seconds using the overhead stirrer at a speed of 500 rpm [97]. In the present study, the water cuts was varied from 0% to 100%. Water cuts from 0% to 100% were selected so that fluids in all range – from pure crude to pure water as well as from W/O emulsions to O/W emulsions, were covered. Then, the mixed mixture was used for rheology measurements using viscometer. **Table 4.5** presents the operating conditions used for the experiments in this study.

Table 4.5: Operating conditions for the experiments.

Operating	Unit	Operating conditions
Pressure	atm	1
Temperature	℃	40
Range of shear rate	s^{-1}	0 – 1000 [7] [98-100]
Mode	-	Linear
Points per decade	-	30
Water cuts	%	0 - 100

4.5 Velocity Measurement

4.5.1 Experimental Setup

The experimental setup for velocity measurement experiments consists of the designed closed-circuit flow loop (as discussed earlier in section 4.1.1) and an ultrasonic velocity profiler (UVP) device. A schematic diagram of the experimental setup is illustrated in **Figure 4.11**.

The working principle of UVP system is it uses pulsed ultrasonic Doppler Effect together with the echography relationship, as shown in **Figure 4.12**. The ultrasonic (US) transducer transmits short US pulses into flowing fluid along transducer axis. The same transducer acts as US receiver to receive the echoes, which occurs when part of the US energy is reflected from minuscule particles scattered in the flowing fluid. The reflected signal is Doppler-shifted to provide the velocity information. The Doppler shift frequency is proportional to particle (and liquid) velocity. Besides, the reflected signal comes back to the transducer with a certain delay. This allows the system to provide the position information by capturing the time duration between the pulse emission and the instant of echo reception, thus recording the position from where the echo is reflected. The delay is proportional to particle position in the time of pulse reflection. By space separation of many measurement points, UVP system is capable of capturing a complete velocity profile in the flowing liquid.

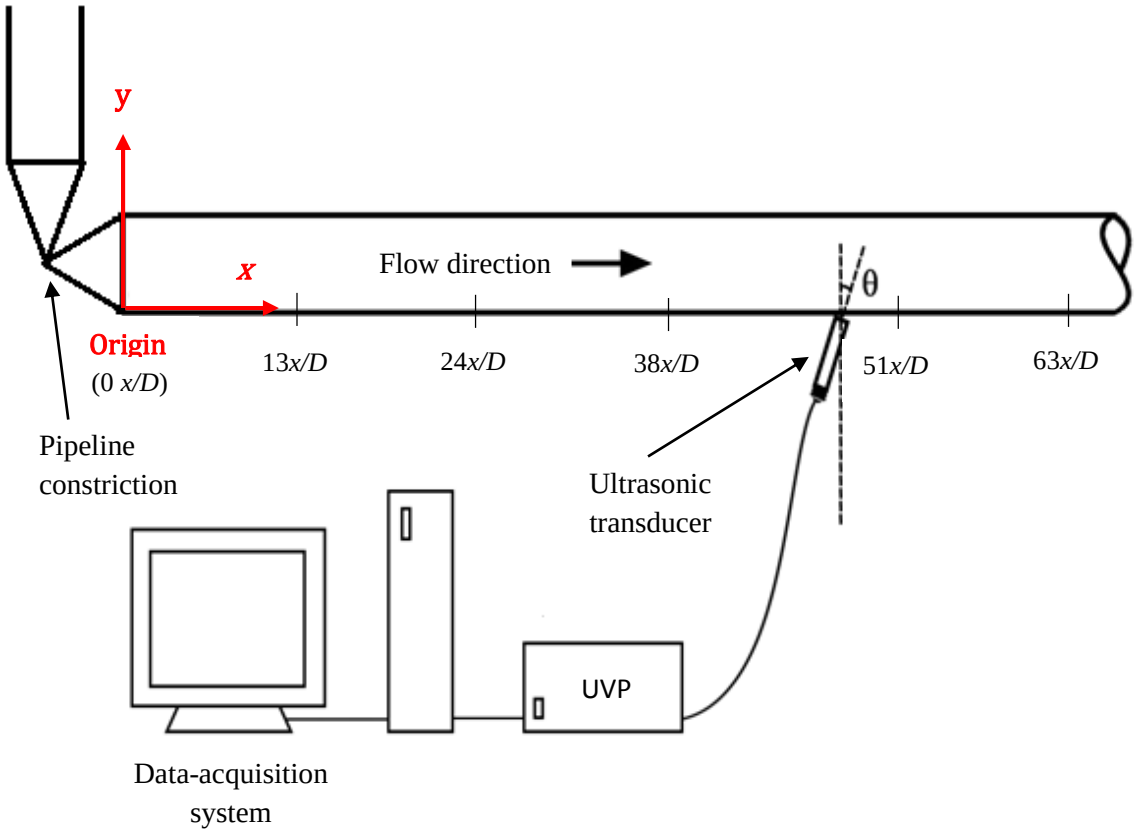

Figure 4.11: Schematic diagram of the experimental setup.

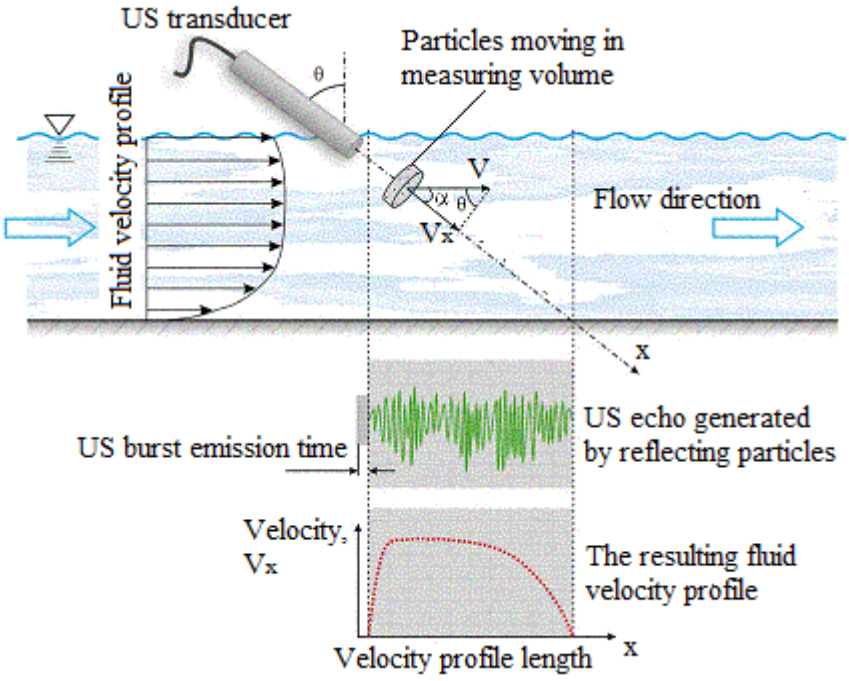

Figure 4.12: Working principles of UVP monitor [95].

As mentioned earlier in Section 4.1.8, the velocity measurement using UVP were conducted at an incident angle of 10 degrees. In order to obtain the velocity perpendicular to the pipe wall, Equation 4.7 [96] is used:

$$v = \frac{v_x}{\cos \alpha} \tag{4.7}$$

where v denotes velocity of particle (m/s), v_x denotes velocity component along transducer axis (m/s), and α denotes Doppler angle.

It is important to note that the Doppler angle is not the same as the incident angle. As the incident angles is 10 degrees, the Doppler angle is 80 degrees. By substituting Doppler angle and the velocity measured along the transducer axis using the UVP probe, the velocity perpendicular to the pipe wall can be achieved.

4.5.2 Experimental Methodology

The measurement of velocity is carried out at the transparent plexiglass pipe segment, which is test segment AB (as discussed in section 4.1.6). UVP probe holders are fixed along the plexiglass pipe at the measurement points. There are five measurement points along the plexiglass pipe, which are located at 58cm, 104cm, 168cm, 224cm and 279cm downstream of the constriction. In term of *x/D*, these measurement locations are at 13, 24, 38, 51 and 63 downstream of the pipeline constriction (as shown in **Figure 4.11**). When carrying out the velocity measurement experiments, the test segment ED can be neglected as this test segment is for pressure measurement.

Prior to the experiments, the water and crude oil were filled into the storage tank at a desired volume fraction, with the total amount of 35 L. The volume of water and crude oil with a total volume of 35 L were calculated for each of the water cuts (WC) examined in this study. For example, volume of water and crude oil for 5% WC were calculated as follow:

$$\text{Volume of water}_{5\%\,\text{WC}} = (0.05)(35\text{L}) = 1.75\text{L}$$

$$\text{Volume of crude oil}_{5\%\,\text{WC}} = (1 - 0.05)(35\text{L}) = 33.25\text{L}$$

This amount of liquid is enough to fully occupy the pipeline as it was pre-calculated. Water and crude oil were filled into the storage tank as two separated liquids instead of emulsified mixture. This is because the aim of this research is to study the formation of emulsions via constriction in the flow loop. The mixture was then allowed to circulate in the flow loop for 15 minutes at the desired flow rate. This was to make sure the formation of emulsions has taken placed due the turbulence effect or flow shear of the constriction in the flow loop.

At the same time, the UVP setup was prepared. The transducer was placed on the holder with an angle of incidence of 10° at the measurement location, starting from measurement location 13 *x/D* to 63 *x/D* (as shown in **Figure 4.11**). In order to obta Pipe wall ıwise velocity gradient ($\frac{\partial U}{\partial X}$), the velocity of the flowing fluid was measured across the direction y, which is perpendicular to the direction of the flowing fluid in the pipeline (direction x) - as illustrated in **Figure 4.13**.

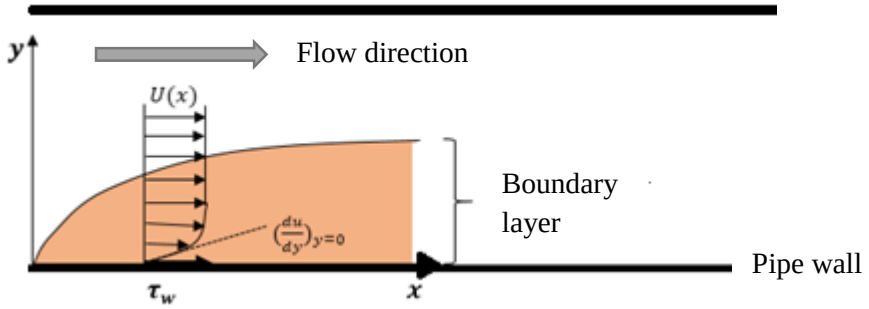

Figure 4.13: du/dy at the pipe wall.

Software parameters were set accordingly. The software parameters used for the velocity measurement are presented in **Table 4.6**. These settings were believed to yield the best results after a test phase. The size of the measurement window was adjusted so as to investigate a complete velocity profile by altering the channel distance (Ch Dist). Channel distance of 0.74 mm was used because this is the smallest value with no overlapping situations. Overlapping situation was avoided as overlapping can be critical for flows with strong variation in the velocity gradient. The velocity range (Vel Range) was set to the value nearest to the expected velocity. The pulse length was set to the recommended

minimum of 4 cycles per pulse (Cyc/Pulse) to achieve high spatial resolution. With shorter pulses, the shape of the ultrasonic beam deteriorates and echo generation becomes difficult [95]. The noise level (NL) filter was set to 4. The number of profile repetitions (Rep/Prof) was increased up to 96 to improve the estimates of the measured velocity. The time dependent amplification of the echo signal (RF Gain) was set to the recommended default values.

During the experiments, the temperature was monitored from time to time to make sure that the temperature rise was not more than 15 ℃. Higher temperature may affect the results as the viscosity of fluid varies with the temperature. Since the temperature cannot be controlled in this study, experiments were terminated once the increase in temperature was more than 15 ℃.

Table 4.6: Met-Flow software parameters.

Input water (%)	**Window Parameter**				**Signal Parameter**			**RF Gain**	
	First Ch (mm)	Ch Dist (mm)	End Ch (mm)	Vel Range (mm/s)	Cyc/ Pulse (-)	NL (-)	Rep/Prof (-)	Start (-)	End (-)
0	3.7	0.74	453.99	300.1	4	4	96	3	6
5	3.7	0.74	226.07	599.7	4	4	96	3	6
10	3.7	0.74	169.09	799.1	4	4	96	3	6
15	3.7	0.74	58.09	2284	4	4	96	3	6
20	3.7	0.74	58.09	2284	4	4	96	3	6
25	3.7	0.74	58.09	2284	4	4	96	3	6
30	3.7	0.74	58.09	2284	4	4	96	3	6
35	3.7	0.74	58.09	2284	4	4	96	3	6
40	3.7	0.74	58.09	2284	4	4	96	3	6

Same steps were repeated for other variables, according to the variables matrix presented in **Table 4.7**. As shown in the table, there are a total of four constrictions for each of the input water fraction, which are gradual constriction with constriction ratio of 0.50, gradual

constriction with constriction ratio of 0.75, sudden constriction with constriction ratio of 0.50 and sudden constriction with constriction ratio of 0.75. The input water fraction being studied in this research was from 0 to 0.40. The calculation for input water fraction has been presented in the above section. Reynolds number being studied for each input water fraction is presented in **Table 4.7**. Reynolds number was calculated using Equation 4.7.

$$\mathrm{Re} = \frac{\rho V D}{\mu} \tag{4.7}$$

where ρ is the density of the fluid, V is the inlet velocity of the fluid flow, D is the internal diameter of the pipe and μ is the dynamic viscosity of the fluid.

It is important to remark that the density and the dynamic viscosity of the fluid for each of the water cuts are different. As has been mentioned earlier in this chapter, the density for each of the water cuts was calculated based on the fraction of water and crude oil multiply by their respective density. On the other hand, the dynamic viscosity for different water cuts was obtained from the rheology study.

For each repeat of different types of constriction and different input water fraction, new mixtures of separated water and crude oil were used. The purpose of doing this was to rule out the presence of existing emulsions.

Table 4.7: Experiment variables matrix.

Input water fraction	Types of constriction	Ratio of constriction diameter to pipeline diameter	Reynolds number	
0	Gradual constriction	0.50 : 1 0.75 : 1	1095	-
	Sudden constriction	0.50 : 1 0.75 : 1		
0.05	Gradual constriction	0.50 : 1 0.75 : 1	1510	2709
	Sudden constriction	0.50 : 1 0.75 : 1		
0.10	Gradual constriction	0.50 : 1 0.75 : 1	1616	2857
	Sudden constriction	0.50 : 1 0.75 : 1		
0.15	Gradual constriction	0.50 : 1 0.75 : 1	1514	2825
	Sudden constriction	0.50 : 1 0.75 : 1		
0.20	Gradual constriction	0.50 : 1 0.75 : 1	1312	2442
	Sudden constriction	0.50 : 1 0.75 : 1		
0.25	Gradual constriction	0.50 : 1 0.75 : 1	1812	-
	Sudden constriction	0.50 : 1 0.75 : 1		
0.30	Gradual constriction	0.50 : 1 0.75 : 1	1620	-
	Sudden constriction	0.50 : 1 0.75 : 1		
0.35	Gradual constriction	0.50 : 1 0.75 : 1	1561	-
	Sudden constriction	0.50 : 1 0.75 : 1		
0.40	Gradual constriction	0.50 : 1 0.75 : 1	1062	-
	Sudden constriction	0.50 : 1 0.75 : 1		

4.6 Uncertainty Analysis

Experiments inherently have errors, e.g., due to instrumentation, data acquisition and reduction limitations, and facility and environmental effects. Due to these reasons, estimation for experimental errors is required to estimate the magnitude of the individual uncertainties. Generally, these experimental errors are divided into bias errors (fixed or systematic errors) and precision error (random errors) [101].

Bias errors are repeatable errors which represents a systematic distortion in a measurement. Bias error is a non-compensating error and arises due to flaw in measurement instrument, flaw in the method of selecting sample, flaw in the technique of estimating a parameter and subjectivity of operators [102]. It is a fixed error that can be reduced by calibration.

Precision errors are non-repeatable errors which are invariably present in every measurement [102]. They are random errors and will have different values for each measurement. When repeated measurements are made for fixed test conditions, precision errors are observed as the scatter of the data. Precision errors are due to limitations on repeatability of the measurement system and to facility and environmental effects [101]. This error can be reduced by obtaining multiple measurements.

To determine the overall uncertainty, U_R, the bias and precision limit, W_R and P_R, have to be combined using the root-sum-square (RSS) method [103].

$$U_R = \left({W_R}^2 + {P_R}^2\right)^{0.5} \tag{4.8}$$

To obtain bias limit, W_R, all the factors causing the bias error in a measured variable has to be identified first. For measurement variable X_K, their 95% confidence bias limits are determined as $(W_K)_1$, $(W_K)_2$, …, $(W_K)_M$. Then, the overall bias limit W_K is given by the RSS expression:

$$W_K = [(W_K)_1^2 + (W_K)_2^2 + \cdots + (W_K)_M^2]^{0.5} \tag{4.9}$$

Then, data reduction equation is taken to determine how the bias limits $(W_1, W_2, \ldots, W_K)$ for the individual variables propagate:

$$R = R(X_1, X_2, \ldots, X_K) \tag{4.10}$$

It is assumed that this relation is continuous and has continuous derivatives in the domain of interest and that the bias limits W_i for the measurement variables are independent of one another. With these conditions, the bias limit can be calculated using Equation 4.10 where partial derivatives is performed.

$$\left(\frac{W_R}{R}\right)^2 = \left(\frac{1}{2}\frac{\partial R}{\partial X_1}W_1\right)^2 + \left(\frac{1}{2}\frac{\partial R}{\partial X_2}W_2\right)^2 + \ldots + \left(\frac{1}{2}\frac{\partial R}{\partial X_K}W_K\right)^2 \tag{4.11}$$

Precision limit, $P_{\bar{r}}$ for the average result can be estimated by [101]:

$$P_{\bar{r}} = \frac{tS_{\bar{r}}}{\sqrt{M}} \tag{4.12}$$

where t is determined with M-1 degrees of freedom ($t = 2$ for $M \geq 10$) and $S_{\bar{r}}$ is the standard deviation of the M "sample" distribution of results [101].

$$S_{\bar{r}} = \left[\sum_{k=1}^{M} \frac{(r_k - \bar{r})^2}{M-1}\right]^{0.5} \tag{4.13}$$

Alternatively, $P_{\bar{r}}$ can be estimated by the RSS of the precision limits for the measurements of the individual variables. The procedure is similar to that discussed previously for the determination of the bias limit.

4.6.1 UVP – Velocity Measurement Accuracy

Using the above explained methods, the uncertainty of the UVP measurement is determined based on its bias error and precision error. The velocity of mixture was measured using ultrasonic velocity profiler (UVP), which has a velocity resolution of $\pm$ 0.4% of velocity range. This velocity resolution is accounted for the bias error for the measurement done. Meanwhile, the precision error of the velocity measurement is determined using Equation 4.11. Since different parameters (eg. Reynolds number, input water fractions, type and ratio of pipe constriction) are used in this study, the precision

error for each of the cases is different as well. Hence, precision error for each of the cases was calculated accordingly, as shown in **Table 4.8**. The highest precision error investigated among all the cases was then used to calculate the overall uncertainty. Using Equation 4.8, overall uncertainty (highest uncertainty among all the experiments) is 4.77% at a 95% confidence level. The measured velocity can then be written as, *e.g.* 0.78 ± 0.04 m/s. For cases with lower precision error, the overall uncertainty would be lower.

4.6.2 Reynolds Number, Re

Reynolds number, $Re = \frac{\rho VD}{\mu}$ is one of the main parameter to be controlled in this work. Since the Reynolds number is a function of measured variables (ρ, V, D and μ), root-sum-square (RSS) method was used for uncertainty estimation. Velocity, V is measured with a flow meter, diameter of the plexiglass, D is measured with a Vernier caliper, dynamic viscosity, μ is measured with rheometer.

The density of crude oil was tested using Test Method D 5002 by Petrotechnical Inspection (M) Sdn. Bhd., an external industrial laboratory. The precision error of this test method is reported to be $\pm 0.105\%$ and no statement as to bias error can be made [104].

Table 4.8: Precision error estimation for measured velocities using UVP.

Water cuts (%)	Type of constriction	Constriction diameter: pipeline diameter (Ratio)	Precision Limit, P_i (%)	
			Laminar	Transitional
0	Gradual constriction	0.50 : 1	1.23	-
		0.75 : 1	1.81	
	Sudden constriction	0.50 : 1	1.25	
		0.75 : 1	1.46	
5	Gradual constriction	0.50 : 1	2.71	3.90
		0.75 : 1	2.45	3.80
	Sudden constriction	0.50 : 1	2.91	4.75
		0.75 : 1	1.37	4.10
10	Gradual constriction	0.50 : 1	2.50	3.40
		0.75 : 1	2.10	2.15
	Sudden constriction	0.50 : 1	2.01	2.65
		0.75 : 1	2.17	2.61
15	Gradual constriction	0.50 : 1	3.80	4.30
		0.75 : 1	3.21	4.62
	Sudden constriction	0.50 : 1	2.94	4.18
		0.75 : 1	3.49	4.43
20	Gradual constriction	0.50 : 1	2.62	3.72
		0.75 : 1	2.60	3.88
	Sudden constriction	0.50 : 1	2.87	3.76
		0.75 : 1	3.09	3.96
25	Gradual constriction	0.50 : 1	2.84	-
		0.75 : 1	2.77	
	Sudden constriction	0.50 : 1	2.71	
		0.75 : 1	2.96	
30	Gradual constriction	0.50 : 1	2.96	-
		0.75 : 1	2.48	
	Sudden constriction	0.50 : 1	3.02	
		0.75 : 1	2.85	
35	Gradual constriction	0.50 : 1	2.66	-
		0.75 : 1	2.19	
	Sudden constriction	0.50 : 1	2.22	
		0.75 : 1	2.41	
40	Gradual constriction	0.50 : 1	2.20	-
		0.75 : 1	2.13	
	Sudden constriction	0.50 : 1	2.40	
		0.75 : 1	2.49	

The density of water (specifically tap water) was obtained from available online source [13]. The density of water is dependent on temperature. Hence, the available online data was used to plot a graph in order to obtain the equation for the density and temperature relations, as shown in **Figure 4.14**. Equation obtained from the graph is then substituted into Equation 4.10 to calculate the bias limit of the density of tap water. The calculation for the bias limit of the density of tap water is as follow:

$$\left(\frac{W_\rho}{\rho}\right)^2 = \left(\frac{1}{\rho}\frac{\partial \rho}{\partial T} W_T\right)^2 \tag{4.14}$$

where $\rho = -3 \times 10^{-6}T^2 - 8 \times 10^{-5}T + 1.003$ (from **Figure 4.14**)

$$\left(\frac{W_\rho}{\rho}\right)^2 = \left[\frac{1}{\rho}\left(\frac{\partial(-3 \times 10^{-6}T^2 - 8 \times 10^{-5}T + 1.003)}{\partial T} W_T\right)\right]^2$$

$$\left(\frac{W_\rho}{\rho}\right)^2 = \left[\frac{1}{\rho}(-6 \times 10^{-6}TW_T - 8 \times 10^{-5}W_T)\right]^2$$

$$\left(\frac{W_\rho}{\rho}\right)^2 = \left[\frac{(-6 \times 10^{-6}TW_T - 8 \times 10^{-5}W_T)}{-3 \times 10^{-6}T^2 - 8 \times 10^{-5}T + 1.003}\right]^2$$

where bias error of temperature, W_T is taken based on last significant digit which is 1 ℃. Since the uncertainty calculated using the above equation would be bigger with increasing temperature, the uncertainty analysis was done here for the maximum allowable temperature in the experiment, which is 40 ℃.

$$\left(\frac{W_\rho}{\rho}\right)^2 = \left[\frac{(-6 \times 10^{-6}(40)(1) - 8 \times 10^{-5}(1))}{-3 \times 10^{-6}(40)^2 - 8 \times 10^{-5}(40) + 1.003}\right]^2$$

$$\frac{W_\rho}{\rho} = 0.000322 \approx 0.032\%$$

There is no precision error for the density of tap water as only one set of data is available.

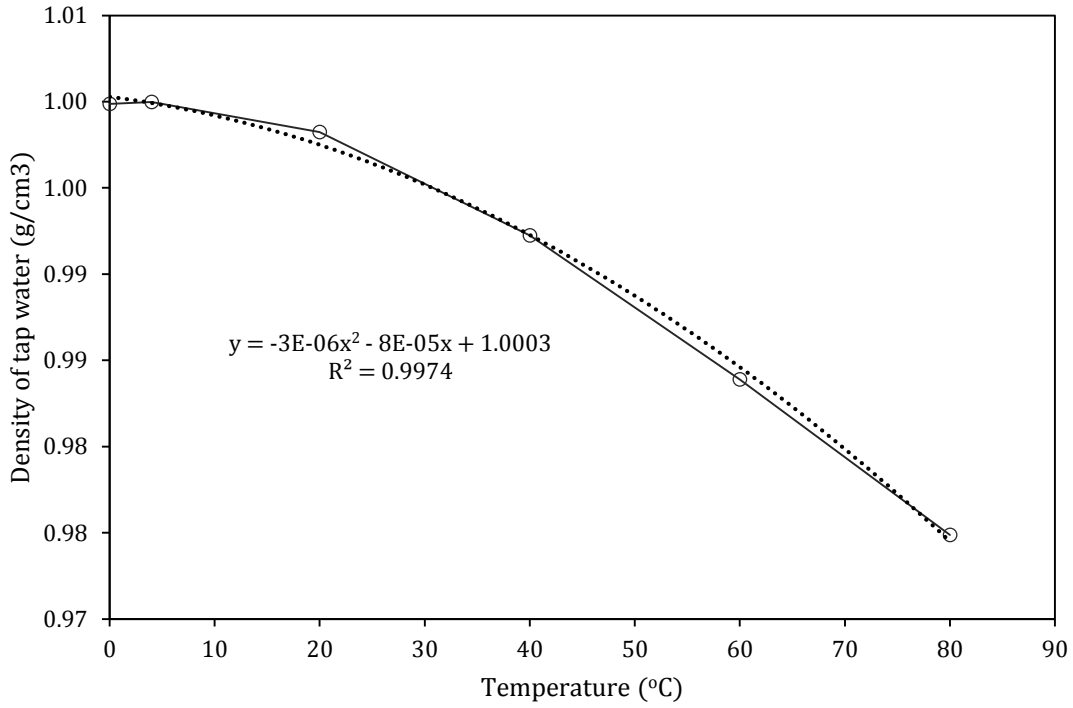

Figure 4.14: Density of tap water with respect to temperature [13].

The diameter of the plexiglass, D measured using Vernier caliper has a resolution of $\pm$ 0.05 mm which is equivalent to $\pm$ 0.11%, bias error in percentage. As for precision error of diameter of the plexiglass, Equation 4.11 was employed and it was determined to be 0.053 mm or $\pm$ 0.12%. The total uncertainty is then evaluated to be 0.073 mm using Equation 4.7, which is $\pm$ 0.17% of nominal diameter.

The dynamic viscosity of crude oil, μ_{oil} was tested using rheometer. The bias error of the dynamic viscosity of crude oil was based on the last significant digit that the rheometer capable of measuring, which is $\pm$ 0.0000001 Pa. s. The precision error of the dynamic viscosity of crude oil is $\pm$ 0.000013 Pa. s which was calculated using Equation 4.11. The total uncertainty is then evaluated to be $\pm$ 0.000013 Pa. s using Equation 4.7.

The dynamic viscosity of water, μ_{water} was tested using rheometer too. The bias error of the dynamic viscosity of water was based on the last significant digit that the rheometer capable of measuring, which is $\pm$ 0.000001 Pa. s. The precision error of the dynamic

viscosity of water is $\pm$ 0.0000103 Pa. s which was calculated using Equation 4.11. The total uncertainty is then evaluated to be $\pm$ 0.0000103 Pa. s using Equation 4.7.

The bias and precision error for velocity measured using UVP has been explained in section 4.6.1. The precision error of velocity showed in **Table 4.9** is the maximum error investigated among all the cases.

Table 4.9: Uncertainty estimation.

Measured Variable, X_i	**Nominal value**	**Bias Limit, W_i**	**Precision Limit, P_i**	**Overall uncertainty, U_i**
Density of crude oil, ρ_{oil} (kg/m^3)	876.8	–	$\pm$ 0.105 %	$\pm$ 0.105 %
Density of water, ρ_{water} (kg/m^3)	996.425	$\pm$ 0.032 %	–	$\pm$ 0.032 %
Plexiglass Diameter, D (mm)	44.212	$\pm$ 0.05	$\pm$ 0.053	$\pm$ 0.073
Dynamic viscosity of crude oil, μ_{oil} (Pa.s)	0.00733	$\pm$ 0.0000001	$\pm$ 0.000013	$\pm$ 0.000013
Dynamic viscosity of water, μ_{water} (Pa.s)	0.001067	$\pm$ 0.0000001	$\pm$ 0.0000103	$\pm$ 0.0000103
Velocity, V (mm/s)	791.5	$\pm$ 0.4 %	$\pm$ 3.8 %	$\pm$ 3.82 %

Then, the bias limit of Reynolds number, W_{Re} can be determined through the following calculation:

$$Re = \rho V D \mu^{-1} \tag{4.15}$$

Using Equation 4.10 gives,

$$\left(\frac{W_{Re}}{Re}\right)^2 = \left(\frac{1}{Re}\frac{\partial Re}{\partial \rho}W_\rho\right)^2 + \left(\frac{1}{Re}\frac{\partial Re}{\partial V}W_V\right)^2 + \left(\frac{1}{Re}\frac{\partial Re}{\partial D}W_D\right)^2 + \left(\frac{1}{Re}\frac{\partial Re}{\partial \mu}W_\mu\right)^2$$

Computing the derivatives:

$$\frac{1}{Re}\frac{\partial Re}{\partial \rho}W_\rho = \left(\frac{1}{\rho VD\mu^{-1}}\right)(VD\mu^{-1})(W_\rho) = \frac{W_\rho}{\rho}$$

$$\frac{1}{Re}\frac{\partial Re}{\partial V}W_V = \left(\frac{1}{\rho VD\mu^{-1}}\right)(\rho D\mu^{-1})(W_V) = \frac{W_V}{V}$$

$$\frac{1}{Re}\frac{\partial Re}{\partial D}W_D = \left(\frac{1}{\rho VD\mu^{-1}}\right)(\rho V\mu^{-1})(W_D) = \frac{W_D}{D}$$

$$\frac{1}{Re}\frac{\partial Re}{\partial \mu}W_\mu = \left(\frac{1}{\rho VD\mu^{-1}}\right)(-\rho VD\mu^{-2})(W_\mu) = \frac{-W_\mu}{\mu}$$

Substituting into the uncertainty expression for W_{Re}:

$$\left(\frac{W_{Re}}{Re}\right)^2 = \left(\frac{W_\rho}{\rho}\right)^2 + \left(\frac{W_V}{V}\right)^2 + \left(\frac{W_D}{D}\right)^2 + \left(\frac{W_\mu}{\mu}\right)^2 \quad (4.16)$$

Substituting in the numerical values from **Table 4.9**.

$$\left(\frac{W_{Re}}{Re}\right)^2 = 0 + (0.004)^2 + \left(\frac{0.05}{44.212}\right)^2 + \left(\frac{0.0000001}{0.0073}\right)^2$$

$$\frac{W_{Re}}{Re} = 4.16 \times 10^{-3} \approx 0.42\%$$

Now considering the precision limits, the uncertainty expression for P_{Re} is:

$$\left(\frac{P_{Re}}{Re}\right)^2 = \left(\frac{1}{Re}\frac{\partial Re}{\partial \rho}P_\rho\right)^2 + \left(\frac{1}{Re}\frac{\partial Re}{\partial V}P_V\right)^2 + \left(\frac{1}{Re}\frac{\partial Re}{\partial D}P_D\right)^2 + \left(\frac{1}{Re}\frac{\partial Re}{\partial \mu}P_\mu\right)^2 \quad (4.17)$$

Substituting the derivatives from previous part into the uncertainty expression for P_{Re}:

$$\left(\frac{P_{Re}}{Re}\right)^2 = \left(\frac{P_\rho}{\rho}\right)^2 + \left(\frac{P_V}{V}\right)^2 + \left(\frac{P_D}{D}\right)^2 + \left(\frac{P_\mu}{\mu}\right)^2 \quad (4.18)$$

Substituting in the numerical values from **Table 4.9**.

$$\left(\frac{P_{Re}}{Re}\right)^2 = (0.00105)^2 + (0.038)^2 + \left(\frac{0.053}{44.212}\right)^2 + \left(\frac{0.000092}{0.0073}\right)^2$$

$$\frac{P_{Re}}{Re} = 0.04 = 4\%$$

Lastly, combining the bias and precision limits by the RSS method:

$$\frac{U_{Re}}{Re} = \left[\left(\frac{W_{Re}}{Re}\right)^2 + \left(\frac{P_{Re}}{Re}\right)^2\right]^{0.5} \tag{4.19}$$

$$\frac{U_{Re}}{Re} = [(4.16 \times 10^{-3})^2 + (0.04\ )^2]^{0.5}$$

$$\frac{U_{Re}}{Re} = 0.0402 = 4.02\%$$

All-in-all, the total uncertainty in the Reynolds number is 4.02% at a 95% confidence level.

4.6.3 Shear Stress, τ

Shear stress is one of the main finding in this study. Since the shear stress is a function of measured variables, *e.g.* velocity V, distance y and dynamic viscosity μ, the root-sum-square (RSS) method was used for uncertainty estimation.

Velocity, V and distance y here were measured using UVP with an accuracy of $\pm$ 0.4%, which accounts for the bias error. The precision error for both V and y are calculated using Equation 4.11. Dynamic viscosity, μ was measured with a rheometer. The bias error of the dynamic viscosity was based on the last significant digit that the rheometer was capable of measuring, which is $\pm$ 0.0000001 Pa. s. The precision error of the dynamic viscosity of is calculated using Equation 4.11.

Using Equation 4.7, overall uncertainties for each of the cases was determined. All the uncertainty estimates are as shown in **Table 4.10.**

Table 4.10: Summary of error contribution in shear stress calculation.

Measured Variable, X_i	**Water cuts**	**Nominal value**	**Bias Limit, W_i**	**Precision Limit, P_i**	**Overall uncertainty, U_i**
Dynamic viscosity of w/o mixture, $\mu_{w/o}$ $(Pa.s)$	0%	0.00732731	$\pm$ 0.001 %	$\pm$ 0.17 %	$\pm$ 0.17 %
	5%	0.00895820	$\pm$ 0.001 %	$\pm$ 0.42 %	$\pm$ 0.42 %
	10%	0.01109600	$\pm$ 0.001 %	$\pm$ 0. 75%	$\pm$ 0.75 %
	15%	0.01332400	$\pm$ 0.0008 %	$\pm$ 0. 48%	$\pm$ 0.48 %
	20%	0.01688500	$\pm$ 0.0006 %	$\pm$ 1.06 %	$\pm$ 1.06 %
	25%	0.01699550	$\pm$ 0.0006 %	$\pm$ 1.54 %	$\pm$ 1.54 %
	30%	0.02069900	$\pm$ 0.0005 %	$\pm$ 2.91 %	$\pm$ 2.91 %
	35%	0.02407450	$\pm$ 0.0004 %	$\pm$ 1.00 %	$\pm$ 1.00 %
	40%	0.02792400	$\pm$ 0.0004 %	$\pm$ 1.37 %	$\pm$ 1.37 %
Distance, y (mm)	10% to 40%	0.73	$\pm$ 0.4 %	0	$\pm$ 0.4 %
Velocity, V (mm/s)	0%	497.5	$\pm$ 0.4 %	$\pm$ 1.46 %	$\pm$ 1.51 %
	5%	892.1	$\pm$ 0.4 %	$\pm$ 1.37 %	$\pm$ 1.43 %
	10%	951.9	$\pm$ 0.4 %	$\pm$ 2.17 %	$\pm$ 2.21 %
	15%	802.7	$\pm$ 0.4 %	$\pm$ 3.49 %	$\pm$ 3.51%
	20%	922.7	$\pm$ 0.4 %	$\pm$ 3.09 %	$\pm$ 3.11 %
	25%	1096.5	$\pm$ 0.4 %	$\pm$ 2.96 %	$\pm$ 2.98 %
	30%	1179.4	$\pm$ 0.4 %	$\pm$ 2.85 %	$\pm$ 2.88 %
	35%	1375.2	$\pm$ 0.4 %	$\pm$ 2.41 %	$\pm$ 2.44 %
	40%	1258.6	$\pm$ 0.4 %	$\pm$ 2.49 %	$\pm$ 2.52 %

Next, the bias limit and precision limit for shear stress were calculated using Equation 4.13 and Equation 4.14, which were derived from Equation 4.10.

$$\left(\frac{W_\tau}{\tau}\right)^2 = \left(\frac{W_\mu}{\mu}\right)^2 + \left(\frac{W_V}{V}\right)^2 + \left(\frac{W_y}{y}\right)^2 \tag{4.20}$$

$$\left(\frac{P_\tau}{\tau}\right)^2 = \left(\frac{P_\mu}{\mu}\right)^2 + \left(\frac{P_V}{V}\right)^2 + \left(\frac{P_y}{y}\right)^2 \tag{4.21}$$

RSS method was then used to combine the bias limit and precision limit to get the overall uncertainty for shear stress. The total error on the shear stress was estimated to be in between 1.54% to 4.11%. The errors for shear stress in each of the studied cases (at different water cuts) are summarized in **Table 4.11**

Table 4.11: Uncertainty estimation for shear stress.

Variable	**Water cuts**	**Bias Limit, W_i**	**Precision Limit, P_i**	**Overall uncertainty, U_i**
Shear stress (Pa)	0%	± 0.57 %	± 1.47 %	± 1.58 %
	5%	± 0.57 %	± 1.43 %	± 1.54 %
	10%	± 0.57 %	± 2.30 %	± 2.37 %
	15%	± 0.57 %	± 3.52 %	± 3.57 %
	20%	± 0.57 %	± 3.27 %	± 3.32 %
	25%	± 0.57 %	± 3.34 %	± 3.39 %
	30%	± 0.57 %	± 4.07 %	± 4.11 %
	35%	± 0.57 %	± 2.61 %	± 2.67 %
	40%	± 0.57 %	± 2.84 %	± 2.90 %

4.7 Summary of Chapter

In this chapter, the main subjects being discussed were the design on the experimental flow rig, the calibration of the equipment, the experimental methodology and the uncertainty analysis. Each part of the flow rig, namely storage tank, pump, flow meter, transport pipes and pipeline constriction are presented in terms of their material, size and specifications. Results on the calibration of rheometer and pressure measurement devices are presented. This is done to verify the performance of these equipment. Next, the steps and methods to carry out experiment for rheology and velocity measurement are listed. Lastly, methods to perform uncertainty analysis as well as the end results for uncertainty analysis are presented.

The results of these experimental studies will be analyzed and discussed in the following chapters.

CHAPTER 5

WATER-IN-OIL (W/O) EMULSIONS CHARACTERIZATION

The first section in this chapter provides the rheological behaviour study of pure crude oil and crude oil with water emulsions. A study on the rheological behavior of crude oil emulsions is important due to their complex behaviors. Crude oil emulsions are an immensely complex colloidal systems containing oil and aqueous phases, emulsifying agents, organic and inorganic additives and natural amphiphilic compounds from crude oil [104]. Ariffin et al. and Wong et al. reported that light crude oil emulsions exhibit non-Newtonian flow behaviour at low shear rate and Newtonian flow behaviour at high shear rate [105, 106]. A few other studies [107-109] reported that crude oil emulsions can display either a Newtonian or a shear thinning rheological behavior, which indicates the complexity of crude oil emulsions behavior.

Since crude oil emulsions formed from different types of crudes behave differently and thus far no study has been done or reported on the rheological behaviors of Miri crude with water emulsions, it is important to determine the rheological behaviors of the mixtures beforehand. From the rheological behavior study, the viscosity for each of the crude oil emulsions with different water cuts are determined. The viscosity of the emulsion mixture is one of the important properties in the study as it will be used in the study at later stage. For example, in determining the Reynolds number of the flow in the pipeline as well as aiding in the wall shear stress determination. Hence, the rheological behavior study is carried out as the rheological results are crucial in correlating with the study of the flow regime of crude oil and water mixture in pipeline transportation. Besides, emulsions are characterized based on their stability as well.

The next section of this chapter discusses the formation of water-in-oil emulsion (amount of emulsions formed) at different conditions. Comparisons are made between different inlet flow regime (laminar and transitional flow regime), different water cuts (5% to 40%) and different types of pipeline constriction (gradual contraction with a contraction ratio of 0.50, gradual contraction with a contraction ratio of 0.75, sudden contraction with a contraction ratio of 0.50 and sudden contraction with a contraction ratio of 0.75). The

results obtained in this section will serve as a measure to identify the effects of flow regime, water cuts and types of constriction on the formation of emulsion, *i.e.* the amount of emulsions formed.

5.1 Measurement of Crude Oil Rheology

As mentioned earlier, rheological behavior of the tested crude oil has to be determined beforehand as different types of crude oil has its own rheological behaviour – either Newtonian or non-Newtonian. So, the crude oil being used in this study – Miri Light Crude (MLC) is examined. **Figure 5.1** and **Figure 5.2** show the results of pure crude oil rheology study. From **Figure 5.1**, it is clearly shown that the viscosity does not change with respect to shear rate. It remains constant at 0.00733 Pa. s. In **Figure 5.2**, it is demonstrated that the shear stress is directly proportional to shear rate. With the increasing of shear rate from $0\ s^{-1}$ to $1000\ s^{-1}$, the shear stress of the pure crude increases gradually from 0 to 7.4 Pa. The result demonstrates that the tested Miri light crude oil is a Newtonian fluid as it obeys the Newton's law of viscosity, where viscosity is independent of the shear rate. Newton's law of viscosity describes the relationship between the shear stress and shear rate of a fluid subjected to a mechanical stress [105]. Hence, in the following study, properties of Newtonian fluid flow are taken into account.

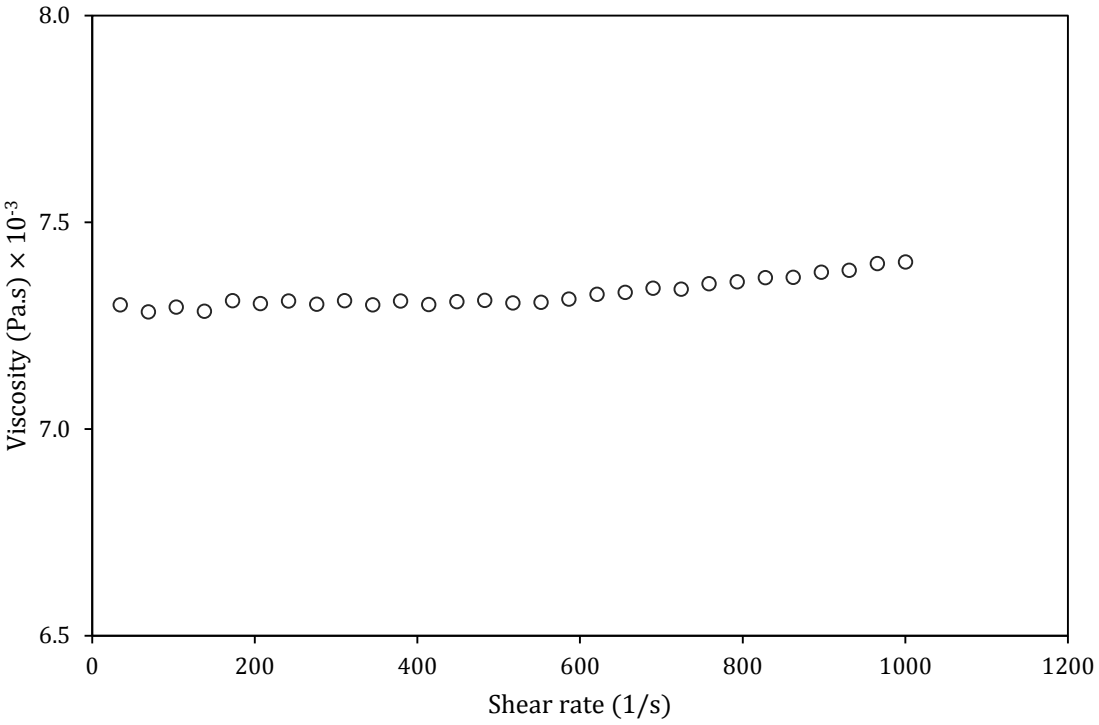

Figure 5.1: Viscosity versus shear rate of crude oil.

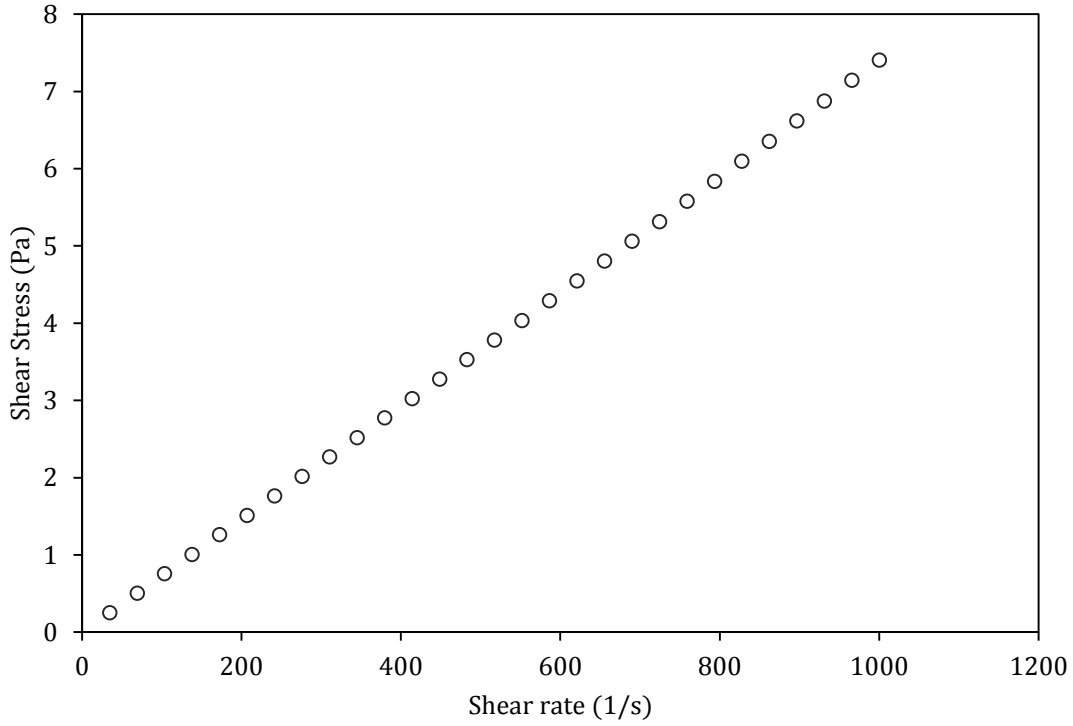

Figure 5.2: Shear stress versus shear rate of crude oil.

5.2 Characterization of Water-in-Oil Emulsion

To characterize an emulsion, one way is to study the emulsion rheology. A fluid is considered as a non-Newtonian fluid when the viscosity of the fluid is a function of shear rate. When the viscosity of the fluid is constant for all shear rates, it is a Newtonian fluid.

As mentioned earlier in Chapter 2, water-in-oil (W/O) emulsion can be categorized into stable, mesostable or unstable emulsion. Each type of these emulsions has their own characteristics. In the present study, categorization of water-in-oil (W/O) emulsions is done by observing the relative volume of emulsions to study the stability of the emulsion, of which it will be explained in detail in the next section.

Experiments were carried out at water cuts of 5% to 40%, sudden and gradual constriction with a contraction ratio of 0.50 and 0.75, respectively, as well as Reynolds number which covers laminar and transitional flow. In this study, laminar flow is referred to $1100 < Re < 1800$ and transitional flow is referred to $2400 < Re < 2800$. Findings on the rheology of emulsion and the stability of emulsions are presented in the next section.

5.2.1 Measurement of Emulsion Rheology

To test the rheological behaviour of crude oil with water emulsions, Miri light crude oil was mixed with water to form crude oil with water emulsions. Crude oil with water emulsions can either be water-in-oil emulsions or oil-in-water emulsions depending on crude oil or water staying as a continuous or dispersed phase.

In **Figure 5.3**, the viscosity of crude oil with water emulsions for water cuts from 5% up to 90% is generally seen to decrease with the increase in shear rate from 0 to 1,000 s^{-1}. This trend demonstrates that the tested crude oil with water emulsion is a non-Newtonian fluid, displaying a shear thinning fluid property. This finding can be supported by a few researchers [104, 105] who proclaimed that water-in-crude oil emulsion is a non-Newtonian fluid with shear thinning behavior, with which viscosity of the fluid decreases with the increase of shear rate.

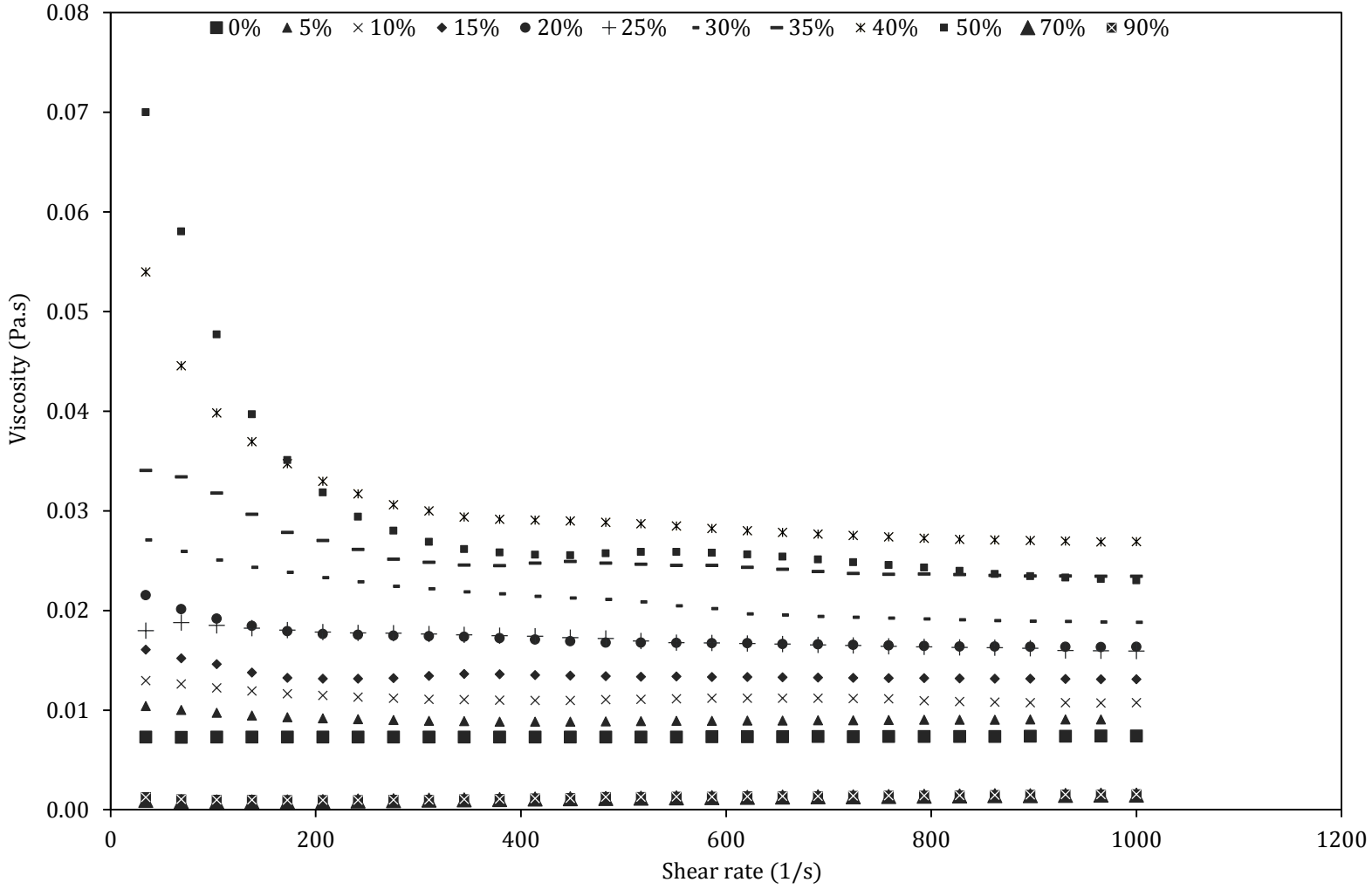

Figure 5.3: Viscosity versus shear rate data for emulsions.

However, the changes in the viscosity are inconsequential, from the shear rate of 200 s^{-1} onwards for emulsions with water cuts of 5% to 30%. Meanwhile, for emulsions with water cuts of 35% to 90%, the changes in the viscosity are insignificant from the shear rate of 350 s^{-1} onwards. In other words, beyond shear rate of 200 s^{-1} and 350 s^{-1} for the respective water cuts, the fluids are said to be exhibiting Newtonian behavior. For these respective shear rates, the mixtures at all water cuts except for 70% and 90% water cuts correspond to the laminar flow (Reynolds number below 2,100), as presented in **Table 5.1**. As demonstrated in **Table 5.1**, the corresponding Reynolds number for shear rate of 200 s^{-1} for emulsions with water cuts of 5%, 10%, 15%, 20%, 25% and 30% are 1207, 972, 853, 639, 638 and 490, respectively. And the corresponding Reynolds number for shear rate of 350 s^{-1} for mixture with water cuts of 35%, 40%, 50%, 70% and 90% are 822, 693, 788, 21004 and 20668, respectively.

Table 5.1: Reynolds number with respect to shear rate of 200 s^{-1} and 350 s^{-1} for respective water cuts.

Water Cuts (%)	Corresponding Reynolds Number
5	1207
10	972
15	853
20	639
25	638
30	490
35	822
40	693
50	788
70	21004
90	20668

This shows that the mixtures with water cuts of 5% to 50% has already shown Newtonian behavior in laminar flow. Meanwhile, for the mixtures with water cuts of 70% and 90%, the mixtures exhibit shear thinning (non-Newtonian) behavior in laminar flow and only display Newtonian behaviour in moderately high turbulent flow (Re > 21000). However, shear thinning will not be an issue in this study. This is because parameters studied in this research are Reynolds number below 4200 and water cuts of 0% to 40%, which correspond to the Newtonian flow behavior. In general, crude oil with water emulsions at all water cuts except for 70% and 90% behaves as a Newtonian fluid in turbulent flow.

As can be seen in **Figure 5.4**, different water cuts result in different viscosity. The viscosity of crude oil with water emulsions increases with the water cuts from 0% up to 40%, then decreases with a further increase in the volume of water cuts up to 100%. From 0% to 40% water cuts, increase in the viscosity can be explained by the increase in the amount of dispersed phase water droplets as the amount of water cuts increases. Increase in the amount of dispersed water droplets with the increase in water cuts is evidenced by the photos shown in **Table 5.2**, where higher water cuts resulted in emulsions with lighter colour as there are more finely dispersed water droplets in the mixture. The increase in viscosity with the water cuts is also observed by Taju Ariffin et. al. [106]. Taju Ariffin et. al. [106] suggested that the number of dispersed water droplet and hydrogen bond increase with the increase in water cuts and this directly leads to an increase in hydrodynamic forces between the droplets and hence, increase in the viscosity.

Meanwhile, for 50% to 90% WC, the dispersed phase water droplets start to coalesce and form larger droplets causing the surface area per unit volume to decrease and hence, the friction among the droplets is reduced, which leads to a decrease in viscosity.

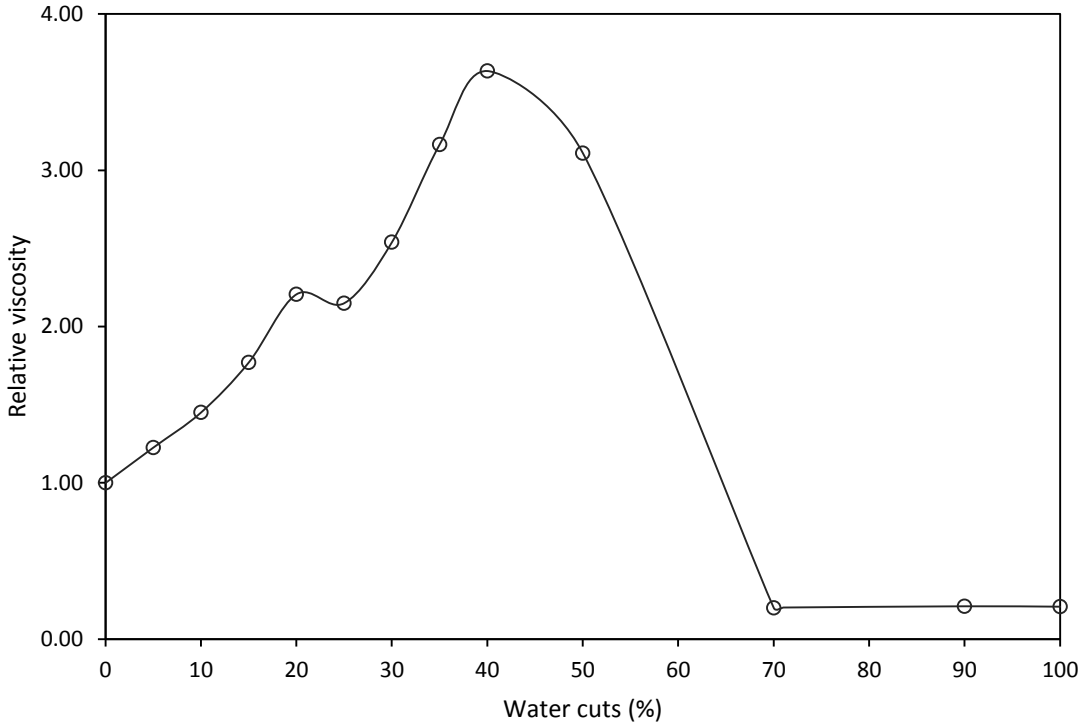

Figure 5.4: Relative viscosity of emulsions at a shear rate 1000 1/s.

Table 5.2: In site observation before emulsions is settled out.

Pure crude	10% Water cut	20% Water cut	30% Water cut	40% Water cut
				
Decreasing in color intensity as water content increases in the crude oil.				

Decreases in viscosity for mixture with water cuts beyond 40% also can be explained by the occurrence of phase inversion, where water-in-oil emulsions inverts to oil-in-water emulsions. Oil-in-water emulsions has lower viscosity than water-in-oil emulsions, where its viscosity eventually decreases to almost the same as the viscosity of pure water. This is because water, which has lower viscosity than pure crude remains as the continuous phase in oil-in-water emulsions. This is proven by the results shown in **Figure 5.4**, where the relative viscosity of pure crude is 1 and the relative viscosity of pure water is 0.21. Besides, a few studies on the transportation of heavy crude oil have reported that the oil is dispersed in the aqueous phase to form oil-in-water emulsions in order to reduce the viscosity of the fluid and hence reduce the pumping energy during transportation [97, 107, 108]. This proves that oil-in-water emulsions has lower viscosity compared to water-in-oil emulsions; hence, it resulted in the reduction of viscosity from 40% water cuts where phase inversion has taken place. Phase inversion taking place at water cuts of 40% has been proven by Ronningsen [109]; who has stated that the highest viscosity is found at the inversion point (from water-in-oil to oil-in-water emulsions). From **Figure 5.4**, it can be seen that the highest viscosity is found at 40% water cuts.

5.2.2 Stability of Emulsion

Stability of W/O emulsion is defined as the resistance by the dispersed water droplets against coalescence [67]. As discussed earlier in Chapter 3, stability of emulsions is affected by a few main factors – concentration of asphaltenes and resins, mixing speed, mixing time, the pH of the fluid, temperature of the fluid and the concentration of salt. The mixing time is kept constant and temperature of the fluid is kept controlled within a range for all set of experiments, and the same crude oil is used for all the experiments (same pH). So, in the present study, the mixing time, pH and the temperature of the fluid is not an affecting factor for the results observed. On the other hand, the concentration of asphaltenes and resins, and mixing speed is the main contributing factor to the emulsion stability.

In this emulsions stability analysis, samples were collected in a 50 mL measuring cylinder. Visual observation was made to examine the amount of emulsion, oil and separated water.

Three observations were made; they are on the spot observation, observation after 24 hours and observation after 48 hours. On the spot observation was made so as to obtain the actual representation of emulsions in the flow loop. And, observations made after 24 hours and 48 hours were with the purpose of determining the stability of the emulsions, which is after the unstable emulsions had settled out. The emulsification observations made for all the water cuts are as shown in **Table 5.5** to **Table 5.16**. In these tables, the amount of emulsions, amount of separated water and amount of initial water in terms of photos were presented.

24 hours is chosen to analyze the stability of emulsions as this is the common practice of previous researchers in studying the stability of emulsions [63, 67]. According to Chen and Tao [67], stability of emulsions is measured based on the relative volume of emulsions, which is the ratio of volume of emulsions to the total volume of the mixture used for the emulsions preparation after 24 hours. In the present study, this method is used for the emulsions stability characterization. Total volume of mixture was the volume of sample collected for the stability test, which was 50 mL. An example for the calculation of relative volume of emulsion (for 10% WC – refer to **Table 5.7**) is:

$$\text{Relative volume of emulsion}_{10\%\text{WC}} = \frac{\text{volume of emulsion (in mL)}}{\text{total volume of sample (in mL)}}$$

$$= \frac{5\ \text{mL}}{50\ \text{mL}} \times 100\% = 10\%$$

5.2.2.1 Effect of Water Cuts

Eight water cuts ranging from 5% to 40% with an interval of 5% in between were studied. **Table 5.3** presents the relative volume of emulsions for all the water cuts being studied, for both laminar and transitional flow. For laminar flow, as the water cuts increases from 5% to 40%, the relative volume of emulsions increases from 0% to 44%. Meanwhile, for transitional flow, as the water cuts increases from 5% to 20%, the relative volume of emulsions increases from 0% to 23%. From the obtained results, it can be clearly seen that

the analyzed relative volume of emulsions increases with the increase in the water cuts. This indicates that the stability of emulsions increases with the increase in the water cuts.

Stability of emulsions increases with the increase of water cuts can be explained as higher water cuts produces a higher volume fraction of water dispersed phase. This would lead to the increase in the compactness of the emulsions (dispersed droplets) as well as the viscosity of the emulsions, and hence heighten the stability of the emulsions. Besides, higher stability at higher water cuts is also because of, with the presence of more water dispersed droplets, the total surface area of oil-water interface that was being aggregated and adsorbed by asphaltenes is increased. Adsorption of asphaltene precipitates at the interface of oil-water (emulsion interface) would strengthen the interfacial film, resulting in the formation of more stable emulsion droplets. From the SARA (Saturates, Aromatics, Resins and Asphaltenes) analysis, it is proven that the Miri Light Crude used in the present study contains 0.43 wt% of asphaltenes and 3.65 wt% of resins. SARA analysis is widely used for crude oil classification as it separates crude oil into four main categories, namely, Saturates, Aromatics, Resins and Asphaltenes [110]. Fingas and Fieldhouse [20] have stated that asphaltenes films act as a barrier to prevent the coalescence of water emulsion droplets as they are highly viscoelastic. Previous study also showed that mixture containing higher asphaltenes content produces emulsions with higher stability [77]. Hence, with the presence of more asphaltenes precipitated dispersed water droplets, the stability is improved. The results also show agreement with Al-Yaari *et. al.* [111] finding, which concluded that stability of W/O emulsions increases with the increase in the water cuts.

5.2.2.2 Effect of Reynolds number

Next, a comparison is made in between the emulsion formed at a different flow rate of the fluid. As has been mentioned earlier, laminar flow is referred to $1100 < Re < 1800$ and transitional flow is referred to $2400 < Re < 2800$. By comparing the emulsion stability of different flow rate or different flow regime (laminar and transitional), it is found that the relative volume of emulsions increases as the flow rate increases, *i.e.* from laminar flow regime to transitional flow regime, as presented in **Table 5.3**. For 10% water cuts, the

Table 5.3: Relative volume of emulsion (%) after 24 hours of settling.

Water Cuts (%)	Types of Constrictions	1100 < *Re* < 1800	2400 < *Re* < 2800
5	GC 0.50	0	0
	GC 0.75	0	0
	SC 0.50	0	0
	SC 0.75	0	0
10	GC 0.50	10	13
	GC 0.75	10	13
	SC 0.50	10	13
	SC 0.75	10	13
15	GC 0.50	20	22
	GC 0.75	20	22
	SC 0.50	20	22
	SC 0.75	20	22
20	GC 0.50	22	23
	GC 0.75	22	23
	SC 0.50	22	23
	SC 0.75	22	23
25	GC 0.50	28	-
	GC 0.75	28	-
	SC 0.50	28	-
	SC 0.75	28	-
30	GC 0.50	32	-
	GC 0.75	32	-
	SC 0.50	32	-
	SC 0.75	32	-
35	GC 0.50	36	-
	GC 0.75	36	-
	SC 0.50	36	-
	SC 0.75	36	-
40	GC 0.50	44	-
	GC 0.75	44	-
	SC 0.50	44	-
	SC 0.75	44	-

relative volume of emulsions in laminar regime is 10% and in transitional regime it is 13% (as shown in **Table 5.3**). This shows that the relative volume of emulsions is increased by 3% as the flow evolves from laminar to transitional regime. Meanwhile, for 15% and 20% water cuts, the relative volume of emulsions is increased by 2% and 3%, respectively. This indicates that the stability of emulsions increases with the increase in the fluid flow rate.

The obtained observation of the increase of stability of emulsions with the increase in the flow rate, is consistent with what was reported by Ahmed *et. al.* [62], Ashrafizadeh and Kamran [63] and Chen and Tao [67]. The increase of emulsions stability with the flow rate is believed to be caused by the reduction in the dispersed droplets size as a result of more energy (higher flow rate) is provided for the emulsification process. Higher mixing speed (more mechanical energy) results in smaller droplets size, *i.e.* dispersed phase, have been consistently reported in a few studies [62, 63, 67, 79, 80]. With smaller dispersed water droplets, the emulsion is tighter and hence increases its stability.

5.2.2.3 Effect of Types and contraction ratios of pipeline constriction

The stability of emulsions was also studied for two different types of pipeline constriction, which are, gradual constriction and sudden constriction. For each type of pipeline constriction, two contraction ratios, which are 0.50 and 0.75, was used. All these constrictions, namely, gradual constriction with a contraction ratio of 0.50 (GC 0.50), gradual constriction with a contraction ratio of 0.75 (GC 0.75), sudden constriction with a contraction ratio of 0.50 (SC 0.50), and sudden constriction with a contraction ratio of 0.75 (SC 0.75), were examined at water cuts of 5% to 40% and inlet flow regime of laminar and transitional. Since the amount of emulsions being examined after 24 hours was the same for all types of constriction, the settling period was extended to after 48 hours. This was done to allow the emulsions for further separation in order to obtain the stability difference due to the effect of different pipeline constrictions.

As can be seen from **Table 5.4**, for 5% and 10% WC, the relative volume of emulsions is the same for all types of constriction. Effect of different types of constriction could not be

Table 5.4: Relative volume of emulsion (%) after 48 hours of settling.

Water Cuts (%)	Types of Constrictions	1100 < *Re* < 1800	2400 < *Re* < 2800
5	GC 0.50	2	4
	GC 0.75	2	4
	SC 0.50	2	4
	SC 0.75	2	4
10	GC 0.50	10	13
	GC 0.75	10	13
	SC 0.50	10	13
	SC 0.75	10	13
15	GC 0.50	17	21
	GC 0.75	16	20
	SC 0.50	17	21
	SC 0.75	16	20
20	GC 0.50	7	9
	GC 0.75	6	8
	SC 0.50	7	9
	SC 0.75	6	8
25	GC 0.50	8	-
	GC 0.75	7	-
	SC 0.50	8	-
	SC 0.75	7	-
30	GC 0.50	7	-
	GC 0.75	6	-
	SC 0.50	7	-
	SC 0.75	6	-
35	GC 0.50	6	-
	GC 0.75	6	-
	SC 0.50	6	-
	SC 0.75	6	-
40	GC 0.50	8	-
	GC 0.75	8	-
	SC 0.50	8	-
	SC 0.75	8	-

determined in 5% and 10% WC. This is most likely due to the amount of emulsions formed was too little to demonstrate a significant difference in its stability.

For water cuts of 15% to 30%, it is found out that the relative volume of emulsions for GC 0.50 and SC 0.50 is identical to each other. Meanwhile, for GC 0.75 and SC 0.75, the relative volume of emulsions is equivalent to each other. On the other hand, by comparing the relative volume of emulsions of GC 0.50 and SC 0.50 with GC 0.75 and SC 0.75, the results show that the relative volume of emulsions in GC 0.50 and SC 0.50 is higher than that of GC 0.75 and SC 0.75. This indicates that emulsions formed from GC 0.50 and SC 0.50 exhibit higher stability than that of GC 0.75 and SC 0.75.

For water cuts of 35% and 40%, although the relative volume of emulsions is the same for all types of constriction made for comparison, the stability can be determined visually. As can be seen in **Table 5.15** and **Table 5.16**, the samples from GC 0.75 and SC 0.75 showed a very clear layer of separated water at the bottommost of the cylinder, but not in GC 0.50 and SC 0.50. This indicates that GC 0.50 and SC 0.50 produced emulsions with higher stability.

From the above observations, it can be concluded that the emulsions formed from the pipeline constriction type GC 0.50 and SC 0.50 are more stable than the emulsions formed from GC 0.75 and SC 0.75. Therefore, it is logical to suggest that the types of constriction, *i.e.* gradual constriction and sudden constriction, does not affect the stability of the emulsions. On the contrary, the contraction ratio of the pipeline constriction, *i.e.* 0.50 and 0.75, has a significant effect on the stability of emulsions.

Table 5.5: Emulsions after 24 hours and 48 hours for 5% water cuts (Laminar regime – *Re* 1510).

Gradual contraction 0.50	**Gradual contraction 0.75**	**Sudden contraction 0.50**	**Sudden contraction 0.75**
After 24 hours	After 24 hours	After 24 hours	After 24 hours
			
Emulsion: 0 mL	Emulsion: 0 mL	Emulsion: 0 mL	Emulsion: 0 mL
Sep. water: 0 mL	Sep. water: 0 mL	Sep. water: 0 mL	Sep. water: 0 mL
After 48 hours	After 48 hours	After 48 hours	After 48 hours
			
Emulsion: 1 mL, 2%	Emulsion: 1 mL, 2%	Emulsion: 1 mL, 2%	Emulsion: 1 mL, 2%
Sep. water: 0 mL, 0%	Sep. water: 0 mL, 0%	Sep. water: 0 mL, 0%	Sep. water: 0 mL, 0%
Initial water: 2.5 mL	Initial water: 2.5 mL	Initial water: 2.5 mL	Initial water: 2.5 mL

Table 5.6: Emulsions after 24 hours and 48 hours for 5% water cuts (Transitional regime – *Re* 2709).

Gradual contraction 0.50	**Gradual contraction 0.75**	**Sudden contraction 0.50**	**Sudden contraction 0.75**
After 24 hours	After 24 hours	After 24 hours	After 24 hours
			
Emulsion: 0 mL	Emulsion: 0 mL	Emulsion: 0 mL	Emulsion: 0 mL
Sep. water: 0 mL	Sep. water: 0 mL	Sep. water: 0 mL	Sep. water: 0 mL
After 48 hours	After 48 hours	After 48 hours	After 48 hours
			
Emulsion: 2 mL, 4%	Emulsion: 2 mL, 4%	Emulsion: 2 mL, 4%	Emulsion: 2 mL, 4%
Sep. water: 0 mL, 0%	Sep. water: 0 mL, 0%	Sep. water: 0 mL, 0%	Sep. water: 0 mL, 0%
Initial water: 2.5 mL	Initial water: 2.5 mL	Initial water: 2.5 mL	Initial water: 2.5 mL

Table 5.7: Emulsions after 24 hours and 48 hours for 10% water cuts (Laminar regime – *Re* 1616).

Gradual contraction 0.50	**Gradual contraction 0.75**	**Sudden contraction 0.50**	**Sudden contraction 0.75**
After 24 hours	After 24 hours	After 24 hours	After 24 hours
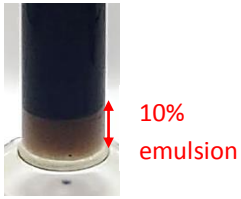			
Emulsion: 5 mL	Emulsion: 5 mL	Emulsion: 5 mL	Emulsion: 5 mL
Sep. water: 0 mL, 0%	Sep. water: 0 mL, 0%	Sep. water: 0 mL, 0%	Sep. water: 0 mL, 0%
After 48 hours	After 48 hours	After 48 hours	After 48 hours
			
Emulsion: 5 mL, 10%	Emulsion: 5 mL, 10%	Emulsion: 5 mL, 10%	Emulsion: 5 mL, 10%
Sep. water: 0 mL, 0%	Sep. water: 0 mL, 0%	Sep. water: 0 mL, 0%	Sep. water: 0 mL, 0%
Initial water: 5 mL	Initial water: 5 mL	Initial water: 5 mL	Initial water: 5 mL

Table 5.8: Emulsions after 24 hours and 48 hours for 10% water cuts (Transitional regime – *Re* 2857).

Gradual contraction 0.50	**Gradual contraction 0.75**	**Sudden contraction 0.50**	**Sudden contraction 0.75**
After 24 hours	After 24 hours	After 24 hours	After 24 hours
			
Emulsion: 6.5 mL, 13%	Emulsion: 6.5 mL, 13%	Emulsion: 6.5 mL, 13%	Emulsion: 6.5 mL, 13%
Sep. water: 0 mL, 0%	Sep. water: 0 mL, 0%	Sep. water: 0 mL, 0%	Sep. water: 0 mL, 0%
After 48 hours	After 48 hours	After 48 hours	After 48 hours
			
Emulsion: 6.5 mL, 13%	Emulsion: 6.5 mL, 13%	Emulsion: 6.5 mL, 13%	Emulsion: 6.5 mL, 13%
Sep. water: 0 mL, 0%	Sep. water: 0 mL, 0%	Sep. water: 0 mL, 0%	Sep. water: 0 mL, 0%
Initial water: 5 mL	Initial water: 5 mL	Initial water: 5 mL	Initial water: 5 mL

Table 5.9: Emulsions after 24 hours and 48 hours for 15% water cuts (Laminar regime – *Re* 1514).

Gradual contraction 0.50	**Gradual contraction 0.75**	**Sudden contraction 0.50**	**Sudden contraction 0.75**
After 24 hours	After 24 hours	After 24 hours	After 24 hours
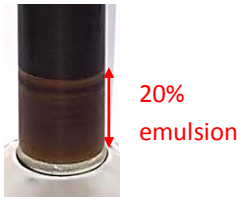			
Emulsion: 10 mL, 20%	Emulsion: 10 mL, 20%	Emulsion: 10 mL, 20%	Emulsion: 10 mL, 20%
Sep. water: 0 mL, 0%	Sep. water: 0 mL, 0%	Sep. water: 0 mL, 0%	Sep. water: 0 mL, 0%
After 48 hours	After 48 hours	After 48 hours	After 48 hours
			
Emulsion: 8.5 mL, 17%	Emulsion: 8 mL, 16%	Emulsion: 8.5 mL, 17%	Emulsion: 8 mL, 16%
Sep. water: 1.5 mL, 3%	Sep. water: 2 mL, 4%	Sep. water: 1.5 mL, 3%	Sep. water: 5 mL, 4%
Initial water: 7.5 mL	Initial water: 7.5 mL	Initial water: 7.5 mL	Initial water: 7.5 mL

Table 5.10: Emulsions after 5 hours and 48 hours for 15% water cuts (Transitional regime – *Re* 2825).

Gradual contraction 0.50	**Gradual contraction 0.75**	**Sudden contraction 0.50**	**Sudden contraction 0.75**
After 24 hours	After 24 hours	After 24 hours	After 24 hours
			
Emulsion: 11 mL, 22%	Emulsion: 11 mL, 22%	Emulsion: 11 mL, 22%	Emulsion: 11 mL, 22%
Sep. water: 0 mL, 0%	Sep. water: 0 mL, 0%	Sep. water: 0 mL, 0%	Sep. water: 0 mL, 0%
After 48 hours	After 48 hours	After 48 hours	After 48 hours
			
Emulsion: 10.5 mL, 21%	Emulsion: 10 mL, 20%	Emulsion: 10.5 mL, 21%	Emulsion: 10 mL, 20%
Sep. water: 0.5 mL, 1%	Sep. water: 1 mL, 2%	Sep. water: 0.5 mL, 1%	Sep. water: 1 mL, 2%
Initial water: 7.5 mL	Initial water: 7.5 mL	Initial water: 7.5 mL	Initial water: 7.5 mL

Table 5.11: Emulsions after 48 hours for 20% water cuts (Laminar regime – *Re* 1312).

Gradual contraction 0.50	**Gradual contraction 0.75**	**Sudden contraction 0.50**	**Sudden contraction 0.75**
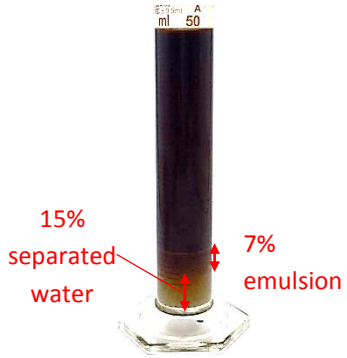			
Emulsion: 3.5 mL, 7%	Emulsion: 3 mL, 6%	Emulsion: 3.5 mL, 7%	Emulsion: 3 mL, 6%
Sep. water: 7.5 mL, 15%	Sep. water: 8 mL, 16%	Sep. water: 7.5 mL, 15%	Sep. water: 8 mL, 16%
Initial water: 10 mL	Initial water: 10 mL	Initial water: 10 mL	Initial water: 10 mL

[Note: Emulsions after 24 hours is the amount of emulsions before further separation, 11 mL, which is summation of amount of emulsions and separated water]

Table 5.12: Emulsions after 48 hours for 20% water cuts (Transitional regime – *Re* 2442).

Gradual contraction 0.50	**Gradual contraction 0.75**	**Sudden contraction 0.50**	**Sudden contraction 0.75**
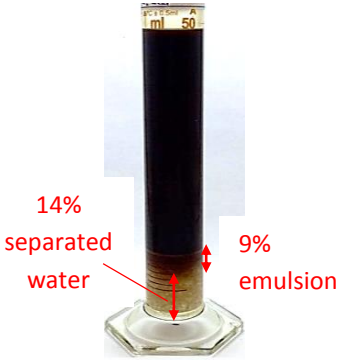			
Emulsion: 4.5 mL, 9%	Emulsion: 4 mL, 8%	Emulsion: 4.5 mL, 9%	Emulsion: 4 mL, 8%
Sep. water: 7 mL, 14%	Sep. water: 7.5 mL, 15%	Sep. water: 7 mL, 14%	Sep. water: 7.5 mL, 15%
Initial water: 10 mL	Initial water: 10 mL	Initial water: 10 mL	Initial water: 10 mL

[Note: Emulsions after 24 hours is the amount of emulsions before further separation, 11.5 mL, which is summation of amount of emulsions and separated water]

Table 5.13: Emulsions after 48 hours for 25% water cuts.

Gradual contraction 0.50	Gradual contraction 0.75	Sudden contraction 0.50	Sudden contraction 0.75
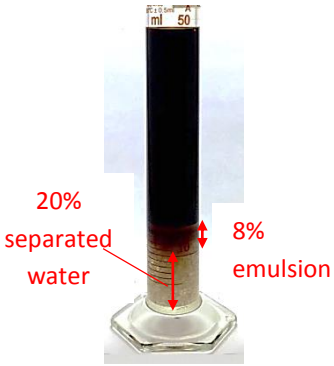			
Emulsion: 4 mL, 8% Sep. water: 10 mL, 20% Initial water: 12.5 mL	Emulsion: 3.5 mL, 7% Sep. water: 10.5 mL, 21% Initial water: 12.5 mL	Emulsion: 4 mL, 8% Sep. water: 10 mL, 20% Initial water: 12.5 mL	Emulsion: 3.5 mL, 7% Sep. water: 10.5 mL, 21% Initial water: 12.5 mL

[Note: Emulsions after 24 hours is the amount of emulsions before further separation, 14 mL, which is summation of amount of emulsions and separated water]

Table 5.14: Emulsions after 48 hours for 30% water cuts.

Gradual contraction 0.50	Gradual contraction 0.75	Sudden contraction 0.50	Sudden contraction 0.75
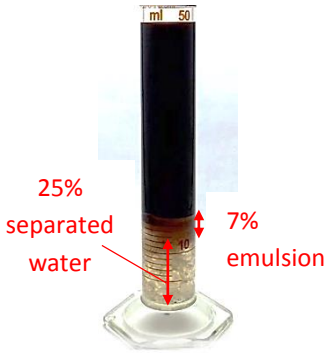			
Emulsion: 3.5 mL, 7%	Emulsion: 3 mL, 6%	Emulsion: 3.5 mL, 7%	Emulsion: 3 mL, 6%
Sep. water: 12.5 mL, 25%	Sep. water: 13 mL, 26%	Sep. water: 12.5 mL, 25%	Sep. water: 13 mL, 26%
Initial water: 15 mL	Initial water: 15 mL	Initial water: 15 mL	Initial water: 15 mL

[Note: Emulsions after 24 hours is the amount of emulsions before further separation, 16 mL, which is summation of amount of emulsions and separated water]

Table 5.15: Emulsions after 48 hours for 35% water cuts.

Gradual contraction 0.50	Gradual contraction 0.75	Sudden contraction 0.50	Sudden contraction 0.75
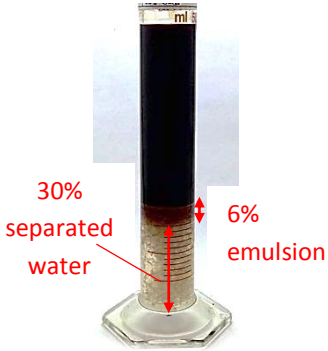	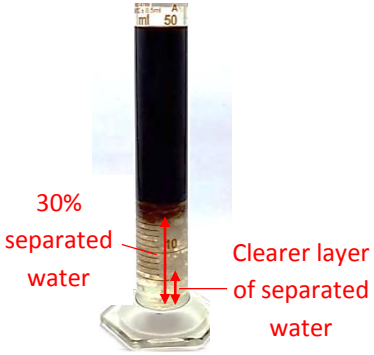		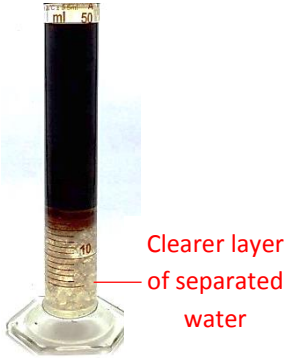
Emulsion: 3 mL, 6% Sep. water: 15 mL, 30% Initial water: 17.5 mL	Emulsion: 3 mL, 6% Sep. water: 15 mL, 30% Initial water: 17.5 mL	Emulsion: 3 mL, 6% Sep. water: 15 mL, 30% Initial water: 17.5 mL	Emulsion: 3 mL, 6% Sep. water: 15 mL, 30% Initial water: 17.5 mL

[Note: Emulsions after 24 hours is the amount of emulsions before further separation, 18 mL, which is summation of amount of emulsions and separated water]

Table 5.16: Emulsions after 48 hours for 40% water cuts.

Gradual contraction 0.50	Gradual contraction 0.75	Sudden contraction 0.50	Sudden contraction 0.75
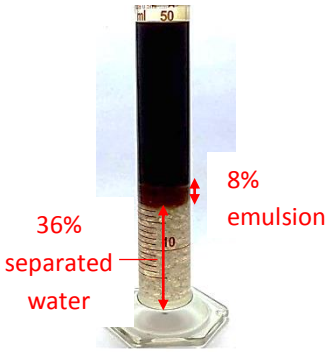	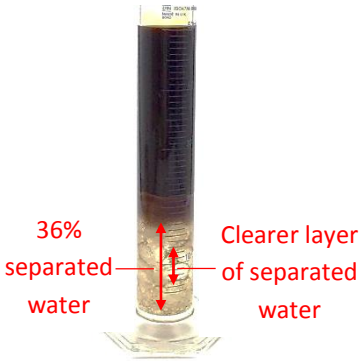		
Emulsion: 4 mL, 8% Sep. water: 18 mL, 36% Initial water: 20 mL	Emulsion: 4 mL, 8% Sep. water: 18 mL, 36% Initial water: 20 mL	Emulsion: 4 mL, 8% Sep. water: 18 mL, 36% Initial water: 20 mL	Emulsion: 4 mL, 8% Sep. water: 18 mL, 36% Initial water: 20 mL

[Note: Emulsions after 24 hours is the amount of emulsions before further separation, 22 mL, which is summation of amount of emulsions and separated water]

5.3 Formation of Water-in-Oil Emulsions

In this section, the formation of water-in-oil emulsions is discussed based on the amount of emulsions formed at all the parameters examined in this study, *i.e.* water cuts, flow rate and types of pipeline constriction.

In the formation of water-in-oil emulsions study, samples were collected in a 50 mL measuring cylinder and visual observation was made after 24 hours of settling time. Volumetric amount of emulsion after 24 hours of settling time is chosen for the determination of the amount of emulsions formed because, for the samples that have undergone 48 hours of settling time, separation of water from the mixture has already taken place. This causes the amount of emulsions being determined no longer represents the emulsions formed in the flow loop. Although immediate observation of the samples is best representing the amount of emulsions in the flow loop, it is not used for the determination of the amount of emulsions formed either. This is because emulsions are still dispersed all over in the mixture when it was just collected from the flow loop, causing visual observation of the amount of emulsions being impossible. Hence, 24 hours were used for the determination of the amount of emulsions formed; when the emulsions had settled out and yet water separation has not yet happened.

5.3.1 Effect of Reynolds Number

Table 5.17 presents the volumetric amount of emulsions observed after 24 hours of settling time for all the water cuts, except 5% water cuts that the volumetric amount of emulsion was observed after 48 hours. This is because for 5% water cuts, emulsion could not be visualized after 24 hours of settling time, as has been explained in the previous section.

In order to examine the amount of emulsion formed with respect to different flow rate, the amount of emulsion formed is plotted as a function of Reynolds number for each of the water cuts. The plotted results for 5%, 10%, 15% and 20% water cuts are as shown in **Figure 5.5** to **Figure 5.8**, respectively.

Table 5.17: Volumetric amount of emulsions (%).

Water cuts (%)	**Types of Pipeline Constrictions**	**1100 < *Re* < 1800**	**2400 < *Re* < 2800**
5	GC 0.50	2	4
	GC 0.75	2	4
	SC 0.50	2	4
	SC 0.75	2	4
10	GC 0.50	10	13
	GC 0.75	10	13
	SC 0.50	10	13
	SC 0.75	10	13
15	GC 0.50	20	22
	GC 0.75	20	22
	SC 0.50	20	22
	SC 0.75	20	22
20	GC 0.50	22	23
	GC 0.75	22	23
	SC 0.50	22	23
	SC 0.75	22	23
25	GC 0.50	28	-
	GC 0.75	28	
	SC 0.50	28	
	SC 0.75	28	
30	GC 0.50	32	-
	GC 0.75	32	
	SC 0.50	32	
	SC 0.75	32	
35	GC 0.50	36	-
	GC 0.75	36	
	SC 0.50	36	
	SC 0.75	36	
40	GC 0.50	44	-
	GC 0.75	44	
	SC 0.50	44	
	SC 0.75	44	

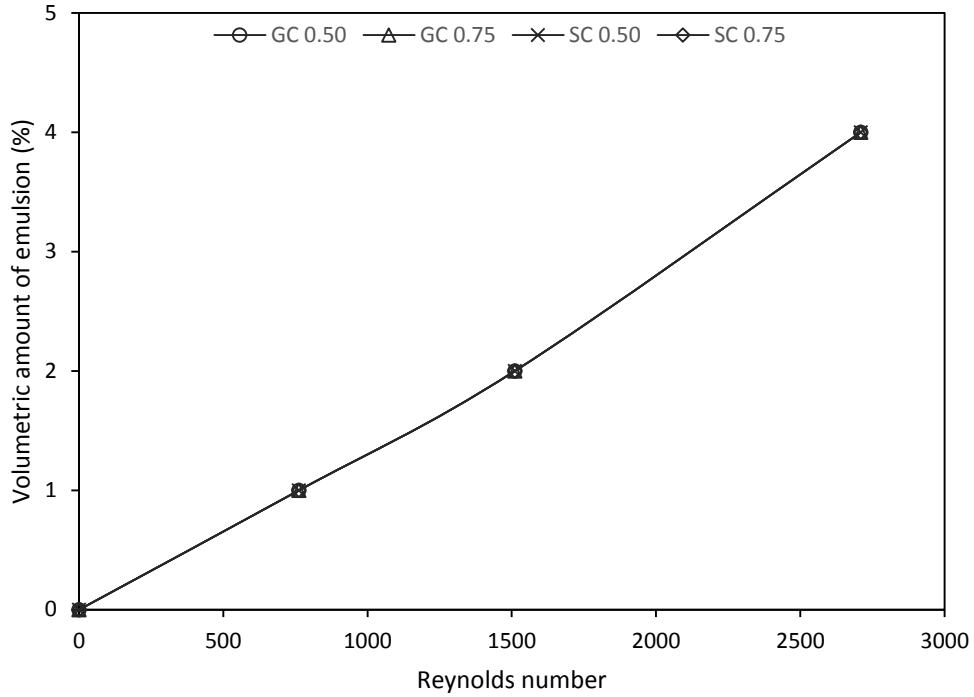

Figure 5.5: Amount of emulsion formed with respect to the changes in Reynolds number for 5% water cuts.

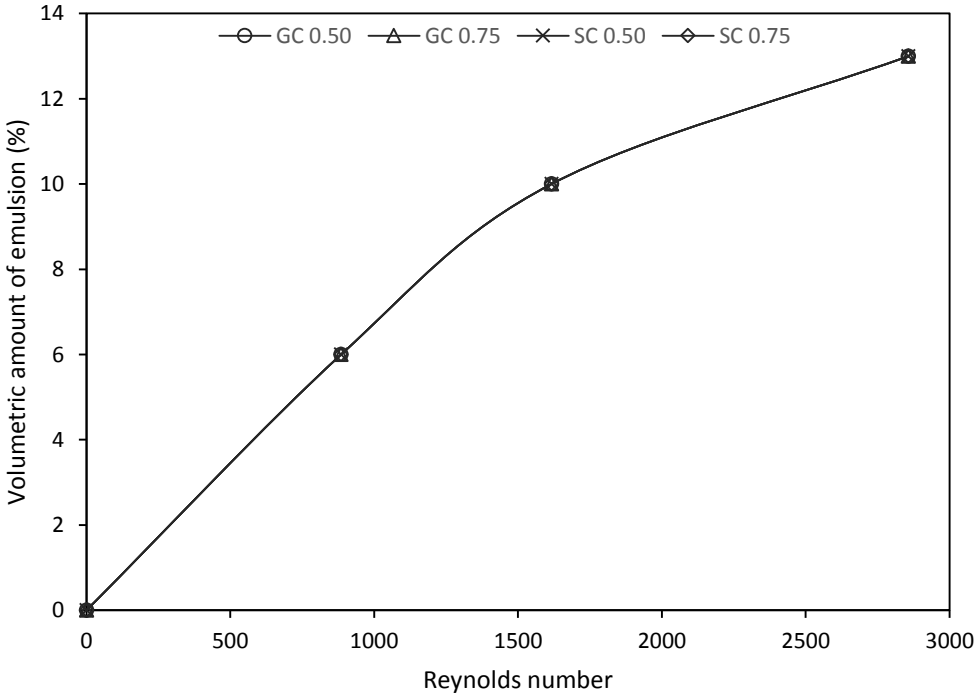

Figure 5.6: Amount of emulsion formed with respect to the changes in Reynolds number for 10% water cuts.

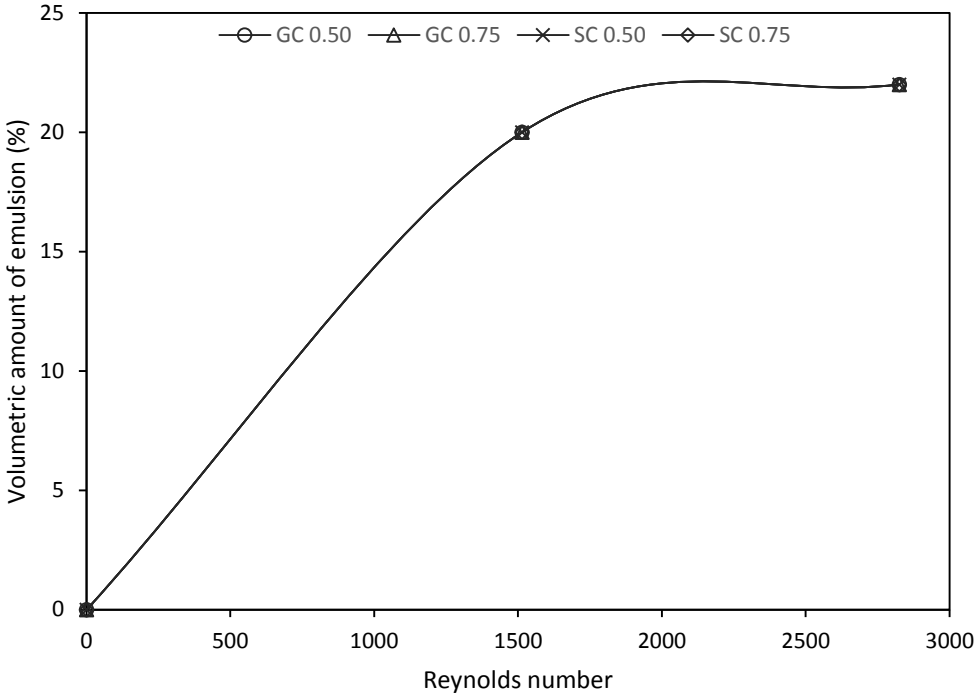

Figure 5.7: Amount of emulsion formed with respect to the changes in Reynolds number for 15% water cuts.

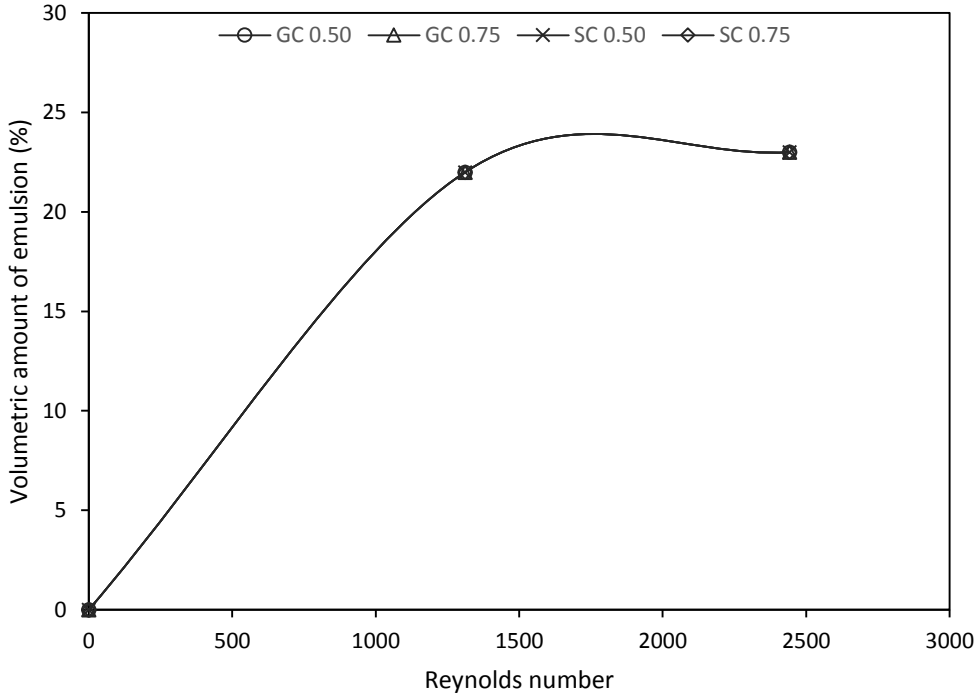

Figure 5.8: Amount of emulsion formed with respect to the changes in Reynolds number for 20% water cuts.

From the figures, it is noticed that the emulsification trend is similar for all the examined water cuts. The results show that the amount of emulsion formed increases with the increase in the Reynolds number. In other words, an increase in the velocity of the fluid flow in the pipeline lead to an increase in the amount of emulsions formed. This is because with the increase in the velocity of the flow in the pipeline, the shearing rate is also increased. An increase in the shearing rate has directly led to an increase in the shear stress. It was reported that shear stresses are accounted for dissipation rate [98-100]. In other words, higher fluid flow rate brings on to a higher dissipation rate. With higher dissipation rate, more energy is dissipated into the flow given a specific time. Johnsen and Ronningsen [89] have stated that energy dissipation is the energy accounts for the formation of emulsions, *i.e.* dispersed droplets, in a pipe flow where formation of emulsions is achieved via flow shear. The dissipation energy is obtained from **Equation 5.1**.

$$\varepsilon = 2f\frac{U^3}{D} \tag{5.1}$$

where f is the Fanning friction factor, U is the average flow velocity and D is the inner diameter of the pipe.

From the above discussion, it is logical to say that higher amount of emulsions formed at higher Reynolds number is due to the presence of higher dissipation energy in the flow. In order to confirm this postulation – higher dissipation energy (higher flow rate) leads to higher amount of emulsions formed, the dissipation energy at different flow regime (different flow rates) for each of the water cuts being studied is analyzed. The analyzed results are plotted in **Figure 5.9, Figure 5.10, Figure 5.11** and **Figure 5.12.** From these figures, it is clearly demonstrated that transitional flow gives higher dissipation energy compared to the one from laminar flow. This finding has served as a strong evidence for the above discussion, where higher flow rates cause higher dissipation energy. Aside from supporting evidence from the present study, the results also can be supported by previous findings, which proclaimed that higher shear rate would produce more dissipation energy, which results in emulsion droplets of smaller sizes [63, 79, 80].

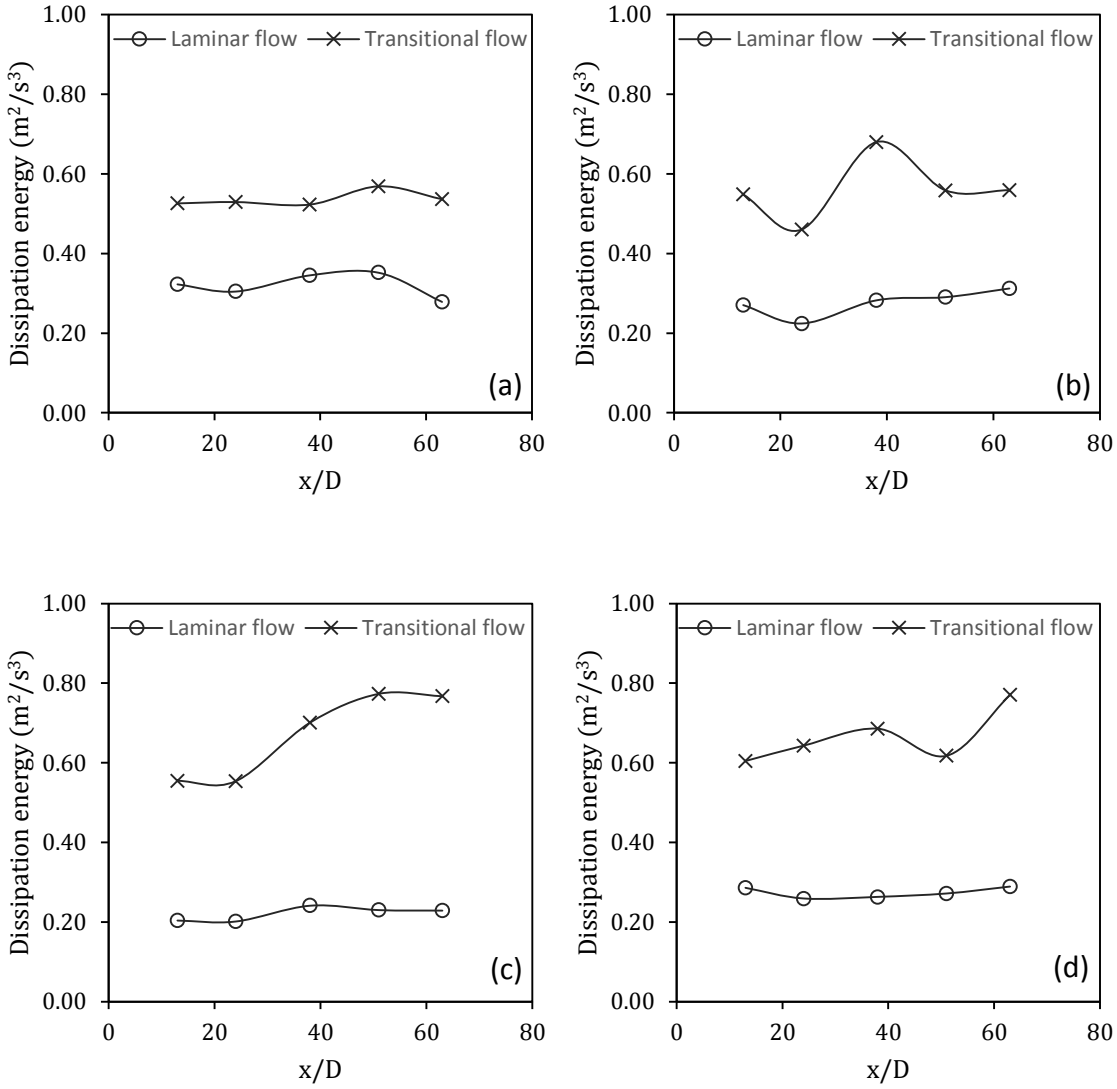

Figure 5.9: Dissipation energy at different flow regime (different flow rate) for 5% water cuts types of constriction of (a) GC 0.50 (b) GC 0.75 (c) SC 0.50 (d) SC 0.75.

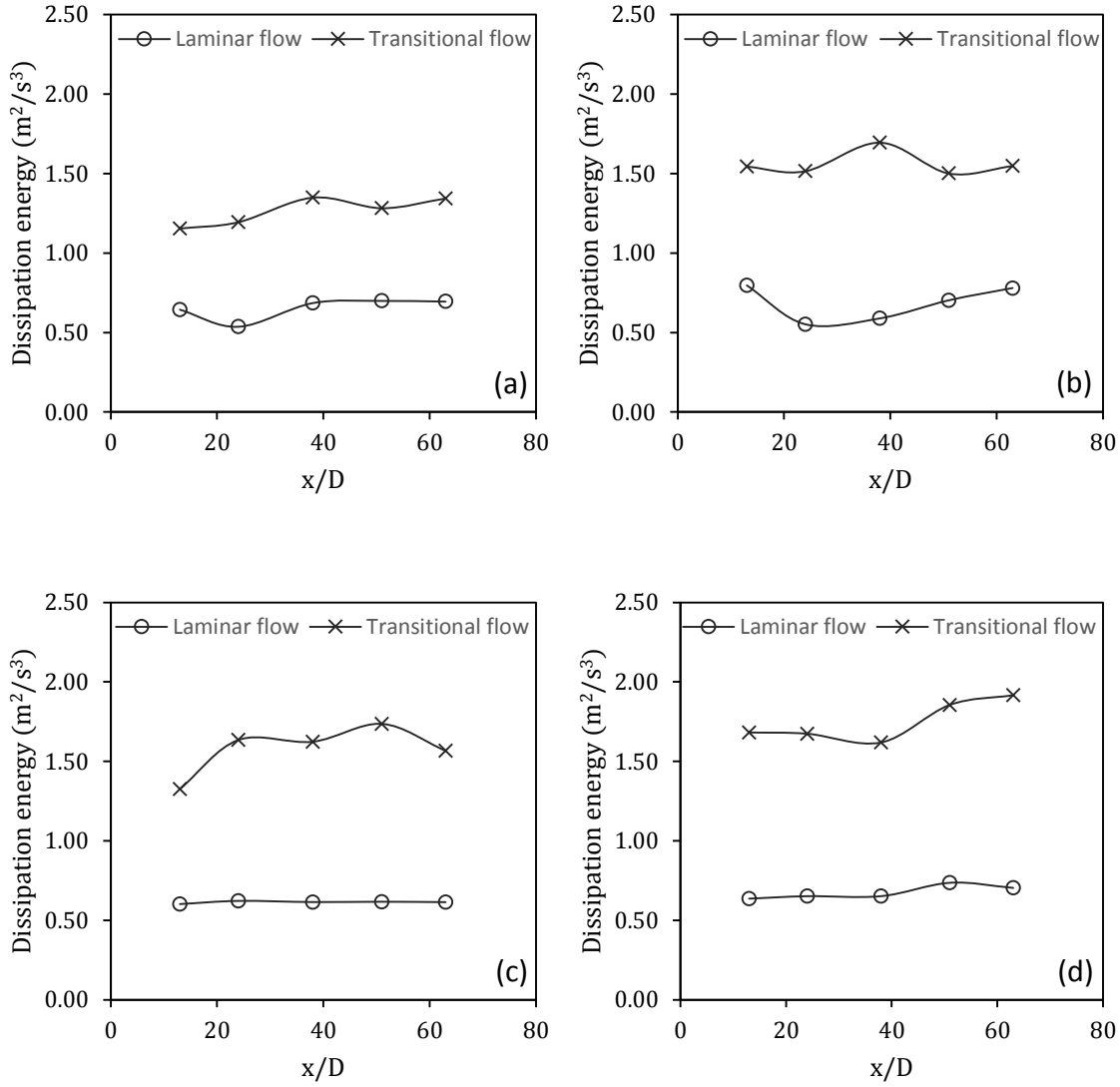

Figure 5.10: Dissipation energy at different flow regime (different flow rate) for 10% water cuts types of constriction of (a) GC 0.50 (b) GC 0.75 (c) SC 0.50 (d) SC 0.75.

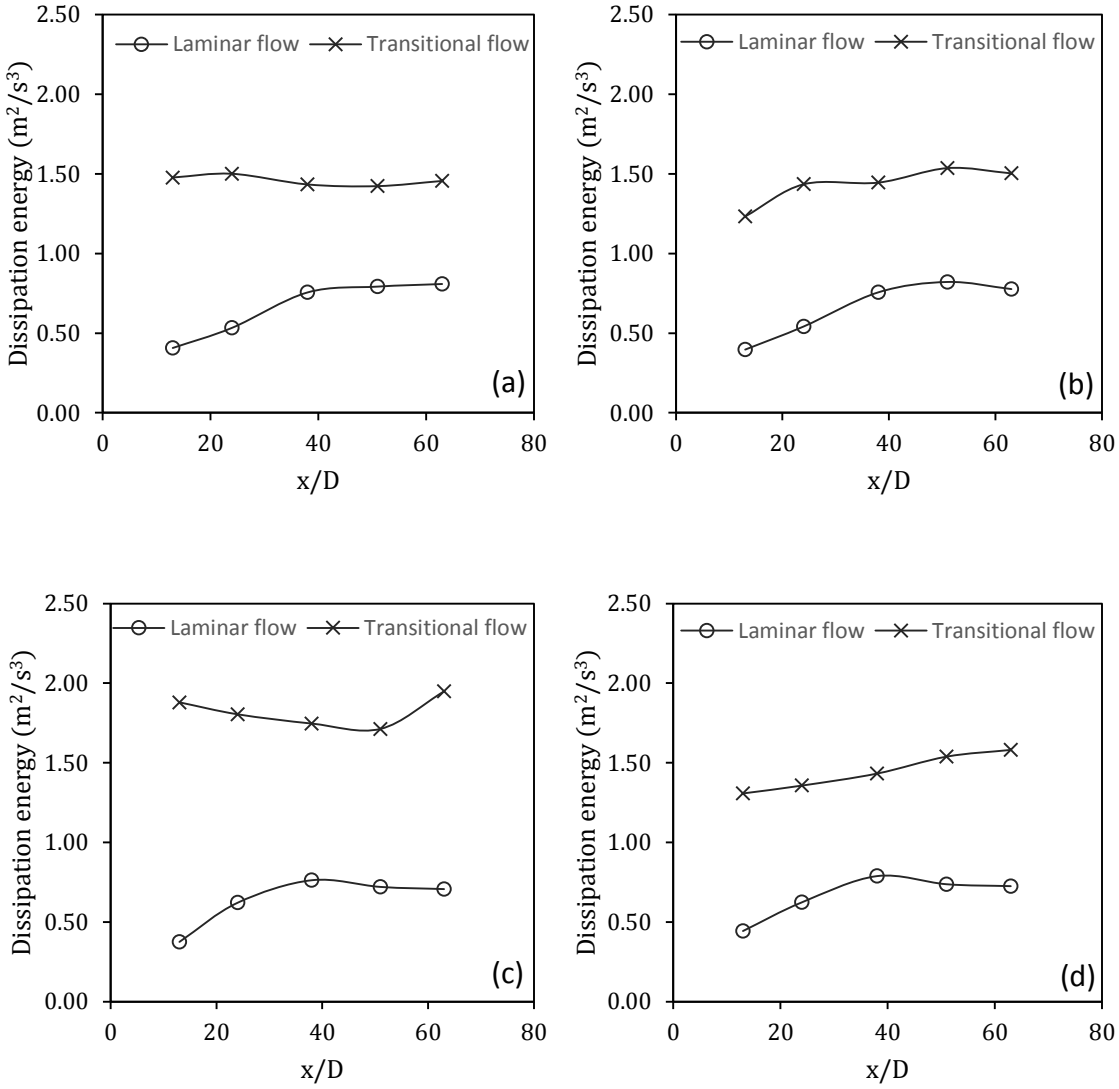

Figure 5.11: Dissipation energy at different flow regime (different flow rate) for 15% water cuts at types of constriction of (a) GC 0.50 (b) GC 0.75 (c) SC 0.50 (d) SC 0.75.

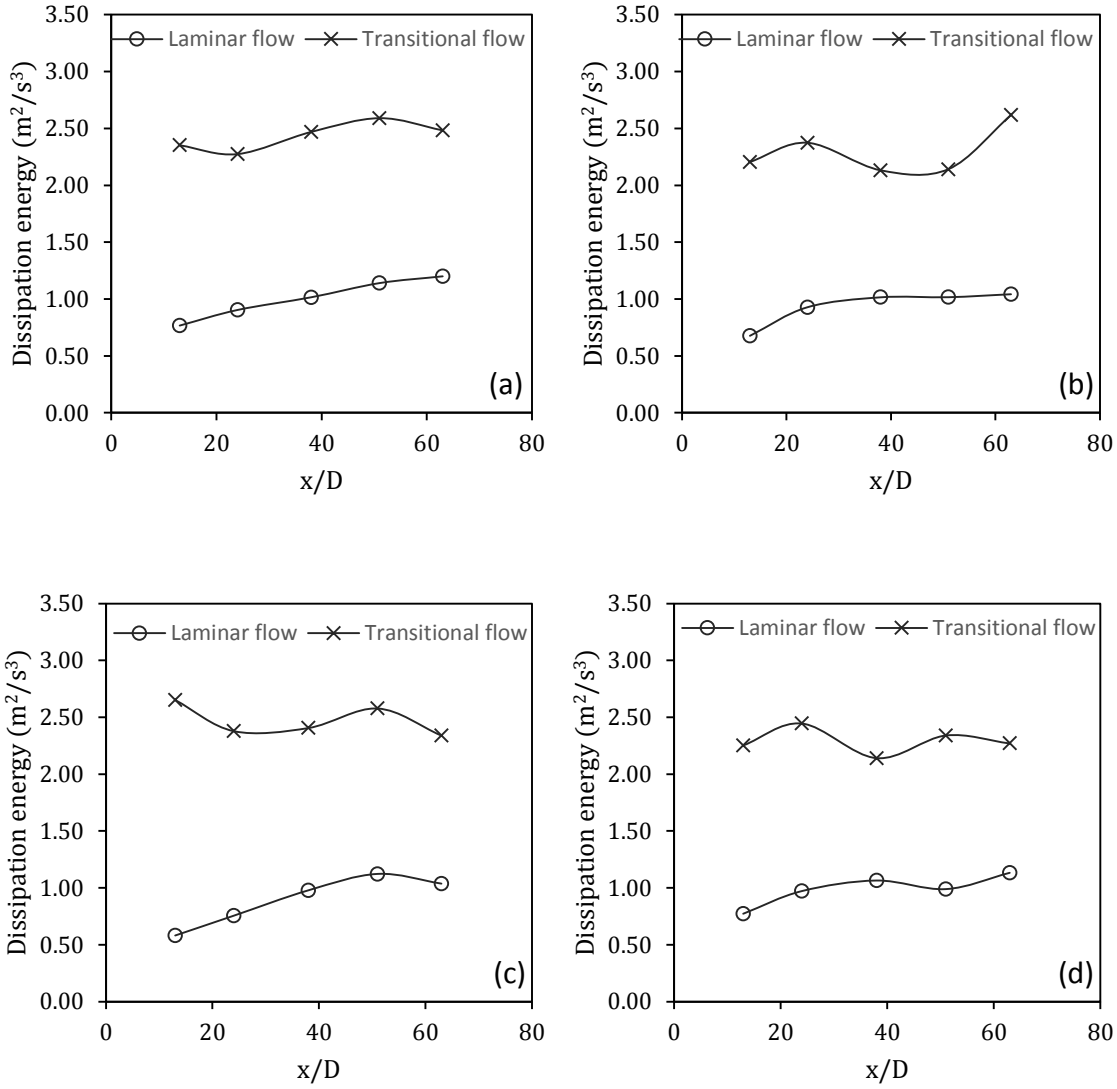

Figure 5.12: Dissipation energy at different flow regime (different flow rate) for 20% water cuts at types of constriction of (a) GC 0.50 (b) GC 0.75 (c) SC 0.50 (d) SC 0.75.

5.3.2 Effect of Water Cuts

For laminar flow, eight water cuts ranging from 5% to 40% with an increment of 5% in between are examined. The results are as shown in **Figure 5.13**. From the presented results, it can be clearly seen that the volumetric amount of emulsions formed increases with the increase in water cuts.

For transitional flow, four water cuts, which are 5%, 10%, 15% and 20% were studied. The obtained results are presented in **Figure 5.14**. Same as the one in laminar flow, the results also show that increase in the water cuts leads to an increase in the amount of emulsion formed.

With the increase in water cuts, there is more water available in the flow to be dispersed as water droplets (emulsion) in the continuous oil phase. This finding can be supported with Arrifin et. al. studies, which concluded that increase of water content leads to the increase in the number and volume of dispersed water droplets in the continuous phase (crude oil) [106].

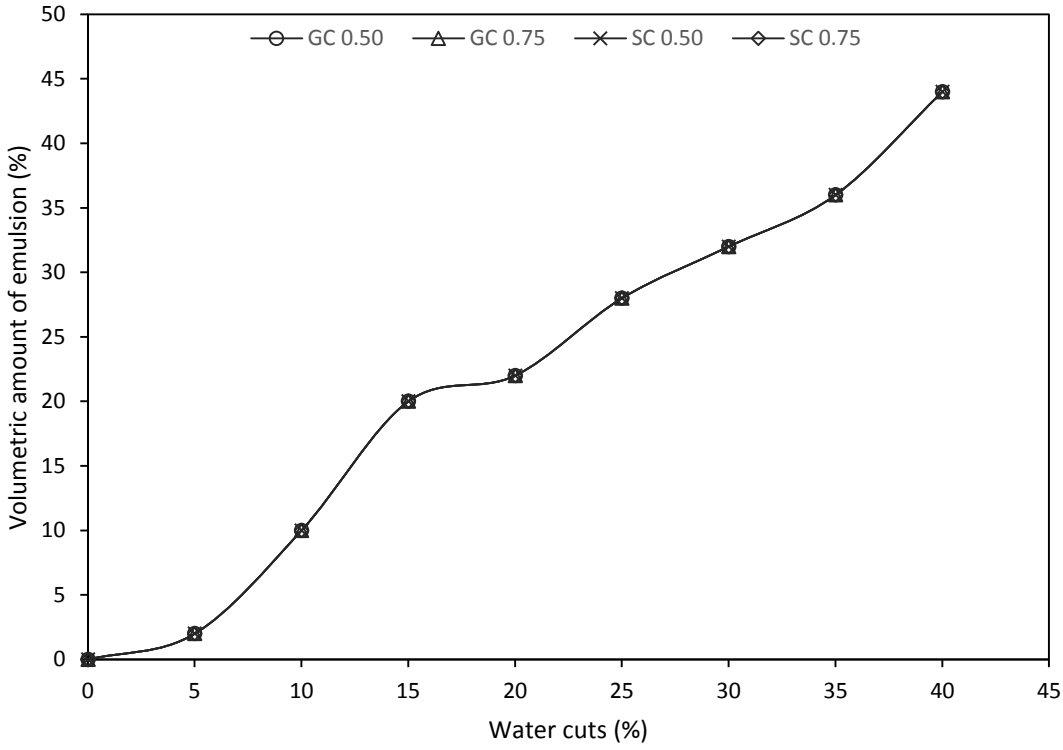

Figure 5.13: Amount of emulsions formed at the respective water cuts (Laminar flow).

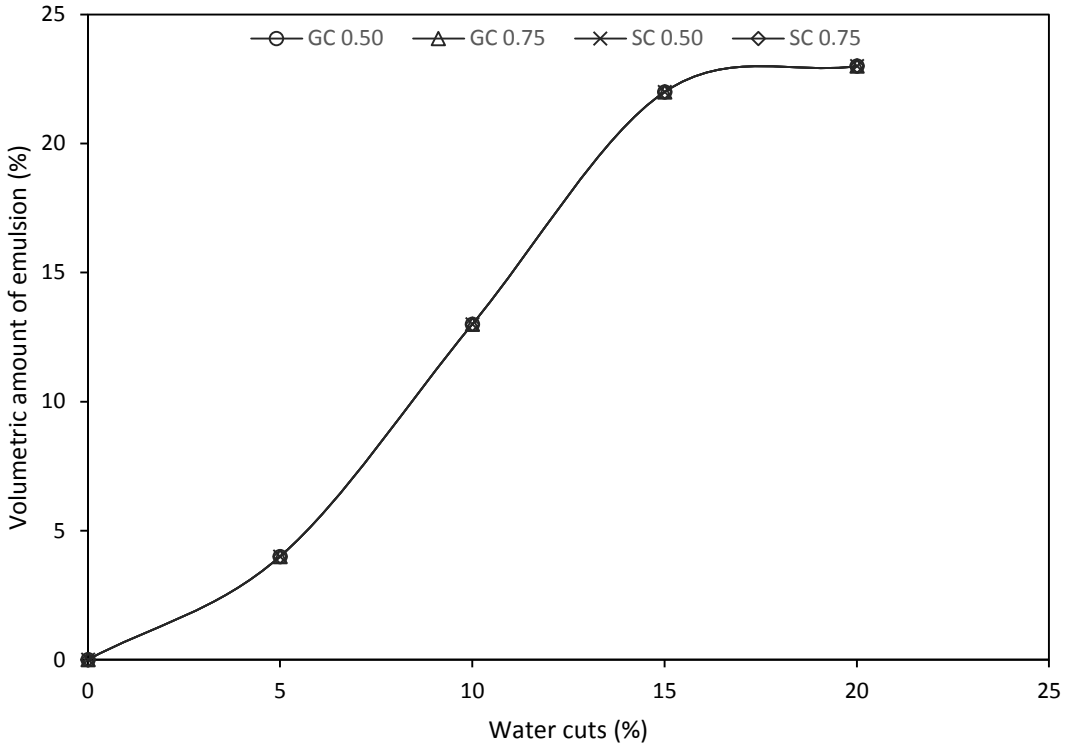

Figure 5.14: Amount of emulsions formed at the respective water cuts (Transitional flow).

5.3.3 Effect of Types of Pipeline Constriction

Four different types of pipeline constrictions, which are gradual contraction with a contraction ratio of 0.50 (GC 0.50), gradual contraction with a contraction ratio of 0.75 (GC 0.75), sudden contraction with a contraction ratio of 0.50 (SC 0.50) and sudden contraction with a contraction ratio of 0.75 (SC 0.75) are compared in the current study. The results are as presented in **Table 5.17**.

From the results obtained, it is observed that all the four types of pipeline constriction produced the same amount of emulsions. Kinsey [112] reported that sudden change in pipe diameter has higher energy loss compared to the gradual one. With higher energy loss, there is more energy to be dissipated. These lost energies will get dissipated by viscous dissipation as well as dissipated by shear stresses within the flow [93]. Viscous dissipation, which is the transformation of kinetic energy lost into internal energy of the fluid (heating up the fluid), is the same for the case being compared as the fluid being used

for the experiment is with the same viscosity. Meanwhile, part of the lost energy gets dissipated by shear stresses. Shear stress dissipation is through eddies generated by the sudden change in pipeline diameter, which are responsible for energy transfer and at the same time exert shear on the water interface. Once the shear exerts by these eddies on the water interface exceeds the cohesive forces of the water, the water gets separated into smaller droplets and eventually forming emulsions. Since there is a higher energy loss in sudden contraction, there will be more energy for emulsification. However, the results show that the amount of emulsions formed through all the four different types of pipeline constrictions are the same with one another. The results suggest that it is most likely that visual observation is not possible for capturing the difference in the amount of emulsions formed for the study of the effect of pipeline constrictions. This is most probably due to the difference in the amount of emulsions is being too small to be captured visually.

5.4 Summary of Chapter

In this chapter, the rheological results of Miri light crude oil are presented and discussed. It is determined that the Miri light crude oil is a Newtonian fluid, with a viscosity of 0.00733 Pa. s. Next, the W/O emulsions characteristics study is based on analyzing the rheological behaviour of W/O emulsions and stability of the W/O emulsions. Based on the analysis, it is determined that emulsions have a very interesting rheological behaviour, where the emulsions exhibit a non-Newtonian, e.g. shear-thinning behaviour, at shear rates below 200 s^{-1} (for 5-30% WC) and 350 s^{-1} (for 35 – 90% WC) and behaves as a Newtonian fluid beyond the respective shear rates. Also, it is determined that phase inversion from W/O emulsions to O/W emulsions happens at 40% WC. Furthermore, the stability of W/O emulsions at different controlling parameters is identified. With the increase in the water cuts, the stability of the emulsions is increased; with the increase in the flow rate, the stability of emulsions is increased; the emulsions formed from the pipeline constriction type GC 0.50 and SC 0.50 is more stable than the emulsions formed from GC 0.75 and SC 0.75. In addition, the amount of emulsions formed at different affecting parameters are presented. The results concluded that – amount of emulsions formed increase with the increase in the flow rate; amount of emulsions formed increase

with the increase in the water cuts; amount of emulsions formed are the same for different types of pipeline constriction.

The above discussed topic serves not only as to understand the characteristics of emulsions formed using Miri Light Crude, but also as a useful essential evidence in the next chapter.

CHAPTER 6

EFFECTS OF WATER-IN-OIL (W/O) EMULSIONS ON WALL SHEAR STRESS

This chapter starts with a discussion on the time-averaged streamwise velocity. Following that, the chapter will analyze and discuss the effects of W/O emulsions to pipeline flow transport, by varying three parameters, namely, water cuts, Reynolds number (flow regime) and pipeline constrictions. For each of the parameters, the regions of study are: 5 to 40% WC; laminar and transitional flow regime; and gradual contraction with a contraction ratio of 0.50 (GC 0.50), gradual contraction with a contraction ratio of 0.75 (GC 0.75), sudden contraction with a contraction ratio of 0.50 (SC 0.50) and sudden contraction with a contraction ratio of 0.75 (SC 0.75). Here, water cuts is referred to as the percentage of the volume of water present in the total liquids. The effects of W/O emulsions to pipeline flow will be examined based on the wall shear stress (τ_w) of the flowing fluid in the pipeline.

6.1 Time-Averaged Velocity Distribution

Figure 6.1 to **Figure 6.5** show the streamwise average velocity profile for input of water cuts 0%, 10%, 20%, 30% and 40% at pipeline constrictions type GC 0.50 and SC 0.75. 13 *x/D*, 24 *x/D*, 38 *x/D*, 51 *x/D* and 63 *x/D* in the figures, which illustrate the measurement location after the pipeline constriction, along the horizontal pipeline. It should be noted that the inlet average velocity corresponds to the laminar flow regime ($1100 < Re < 1800$). The average streamwise velocity profiles of different types of pipeline constriction does not differ much from each other. Hence, the velocity profiles for pipeline constriction type GC 0.75 and SC 0.75 are presented in the appendix **Figure B.1** to **Figure B.9**.

Figure 6.1 shows the average streamwise velocity profile of pure crude. From the figure, it is shown that the flow has fully developed at location 51 *x/D* as the average velocity profiles at location 51 *x/D* and 63 *x/D* remains the same. The velocity profile near to the pipeline constriction is shown to be flat in the center of the pipe. This is because the flow

is disturbed at the constriction and it develops after the constriction. Besides, **Figure 6.1** also shows that the fully developed average velocity profiles follow the laminar parabolic profile relatively well. This indicates that the crude oil flow in the horizontal pipeline remains in the laminar regime after passing through the constriction (disturbance of the flow).

As the input water cuts increases, it is observed that the average streamwise velocity profiles become flatter or fuller as compared to the profiles of lower input water cuts. For an input of 5% to 15% WC, the disturbed parabolic profiles are observed (refer to appendix **Figure B.2** to **Figure B.4**) as compared to the parabolic profiles of pure crude. At the input of 20% to 40% WC, the results show that in the middle of the pipe, the average velocity profiles are completely flat (as shown in **Figure 6.3** to **Figure 6.5**). From the observation of these results, it can be deduced that the higher the amount of dispersed water droplets, the flatter the velocity profile in the middle of the pipe. Hence, it is logical to suggest that the presence of dispersed water droplets (emulsions) in the flow leads to the changes in the velocity profiles.

As stated earlier, the inlet flow corresponds to the laminar flow regime. However, the results on the average streamwise velocity profiles of water-oil emulsions flow appear to develop a turbulent flow velocity profile (flatter profile) as the input of water cuts increases. This suggests that the presence of emulsions induces the flow to turbulent flow. Therefore, in Chapter 7, the turbulence characteristics of the water-oil emulsions flow will be examined and discussed.

Next, from these average streamwise velocity profiles, the velocity gradient at the pipe wall will be obtained. Likewise, from the velocity gradient, the wall shear stress will be determined; and discussed accordingly in the next section of this chapter.

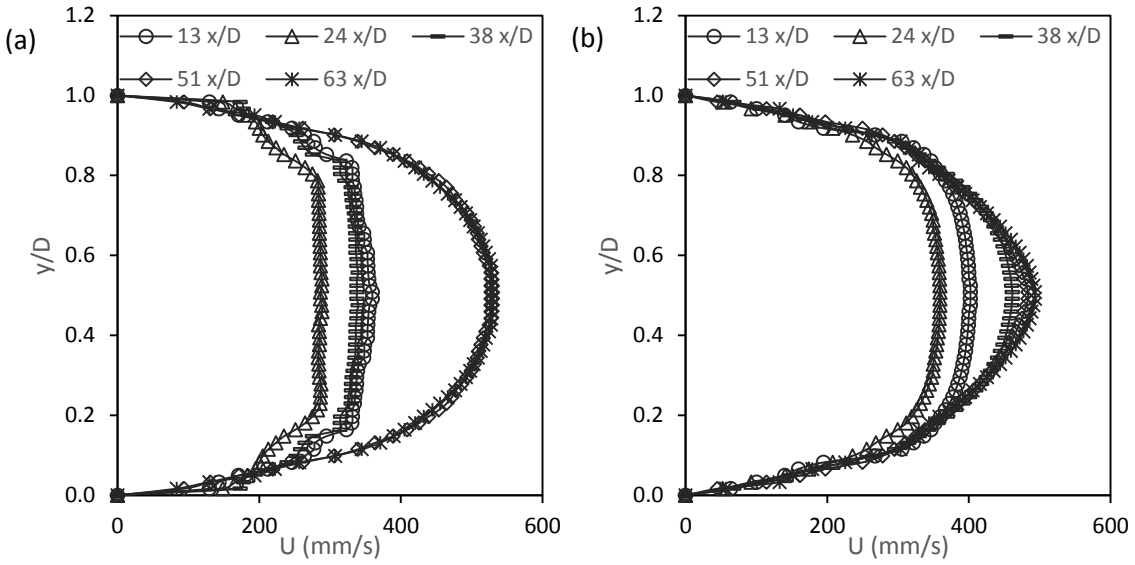

Figure 6.1: Time-average streamwise velocity profile for flow with pure crude at pipeline constriction of (a) GC 0.50 (b) SC 0.50.

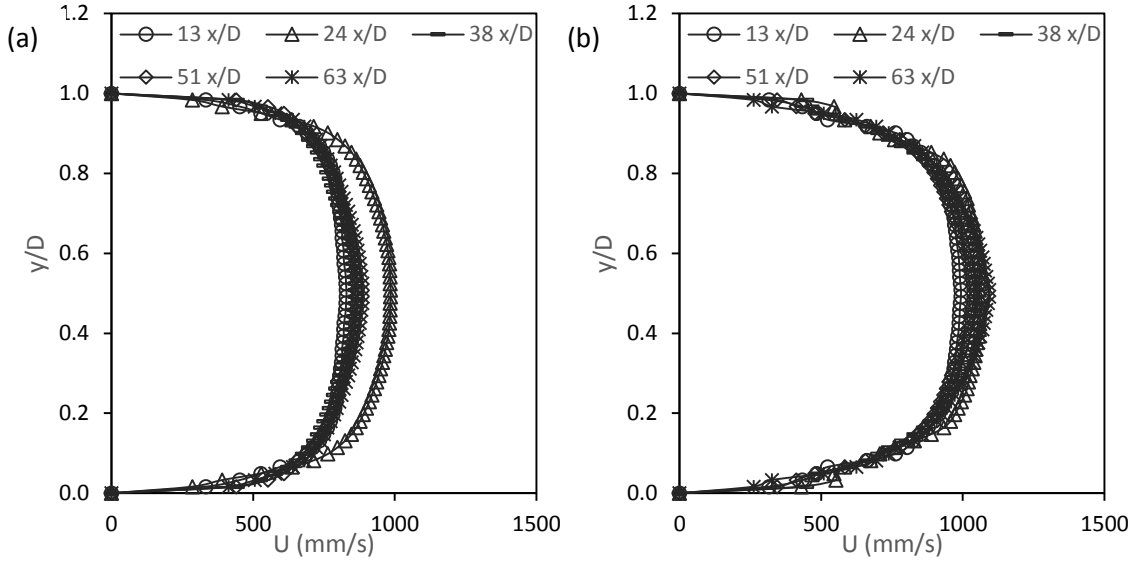

Figure 6.2: Time-average streamwise velocity profile for flow with 10% water cuts at pipeline constriction of (a) GC 0.50 (b) SC 0.50.

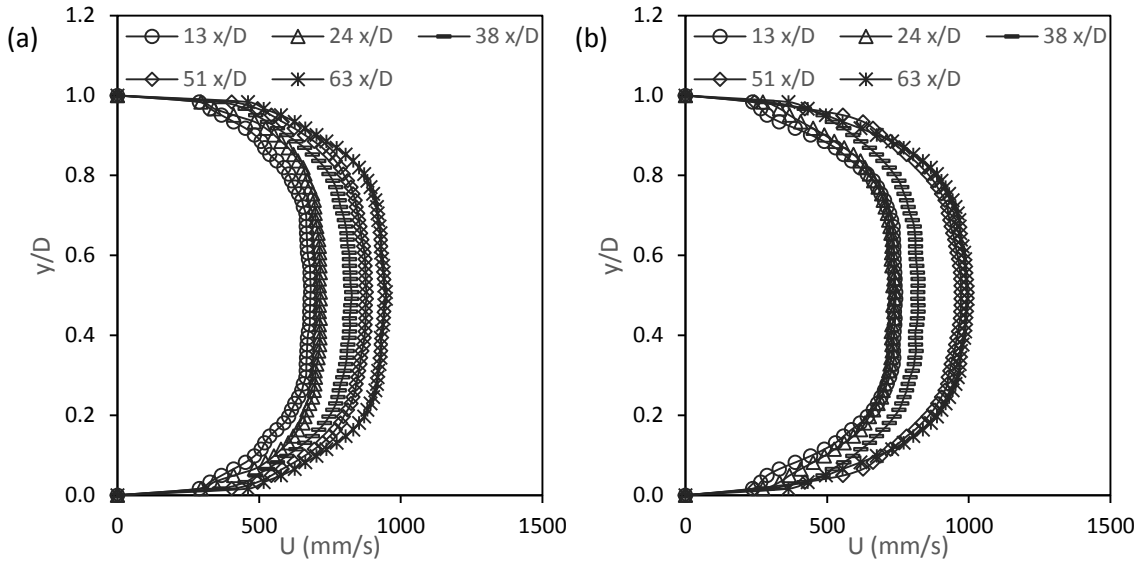

Figure 6.3: Time-average streamwise velocity profile for flow with 20% water cuts at pipeline constriction of (a) GC 0.50 (b) SC 0.50.

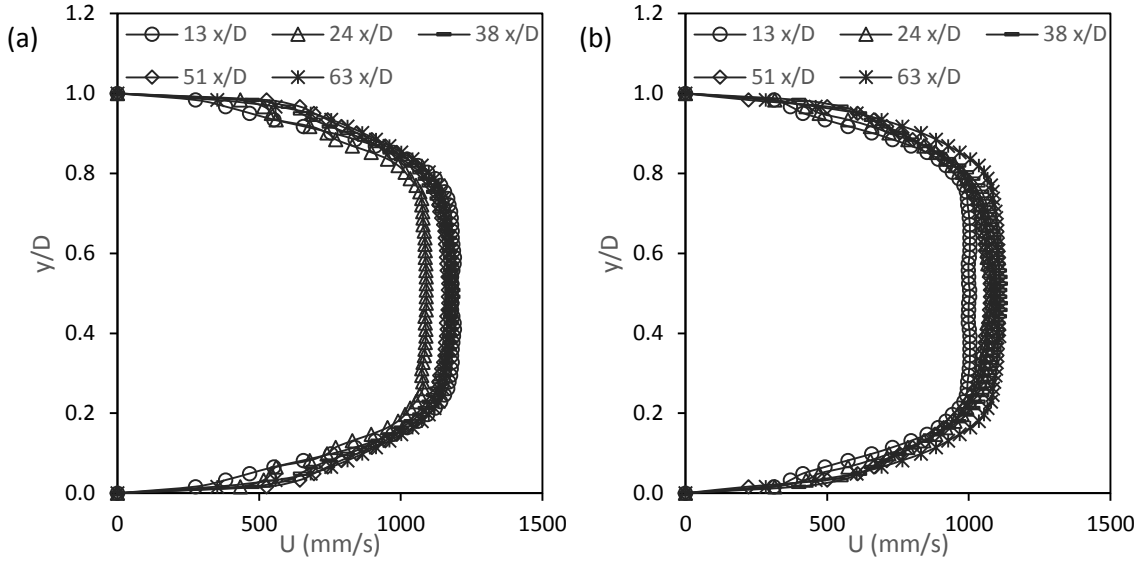

Figure 6.4: Time-average streamwise velocity profile for flow with 30% water cuts at pipeline constriction of (a) GC 0.50 (b) SC 0.50.

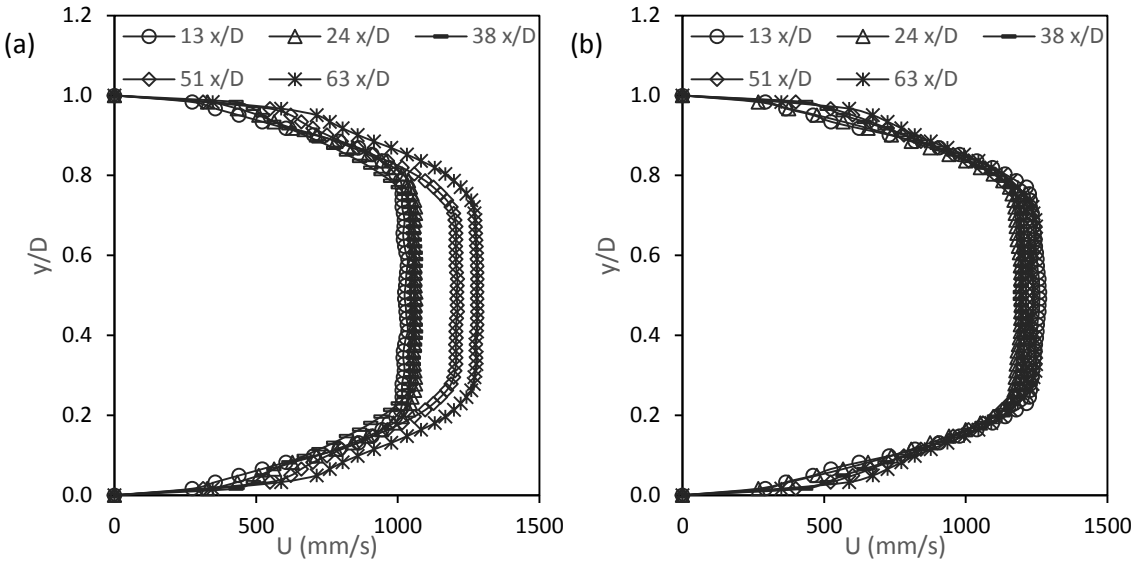

Figure 6.5: Time-average streamwise velocity profile for flow with 40% water cuts at pipeline constriction of (a) GC 0.50 (b) SC 0.50.

6.2 Wall Shear Stress

In the present work, wall shear stress (τ_w) is determined from Equation 6.1.

$$\tau_w = \mu \frac{\partial U}{\partial X} \tag{6.1}$$

where μ is the dynamic viscosity of the flowing fluid and $\frac{\partial U}{\partial X}$ is the shear rate of the flowing fluid in the main flow.

As introduced in Chapter 2, the Kinetic Energy Budget equations describe the energy transfer in the flow. From the equations, it is understood that shear production term (P) from the Kinetic Energy Budget equations is the only term that describes the generation of energy in the flow. The energy generated is known as turbulent kinetic energy. P is described as the product of Reynolds stresses and shear rate, as expressed in Equation 6.2.

$$P = \overline{u_i u_j} \frac{\partial U_i}{\partial X_j} \tag{6.2}$$

where $\overline{u_i u_j}$ represents the shear produced at the fluctuating part of the flow (known as Reynolds stresses) and $\frac{\partial U_i}{\partial X_j}$ represents the shear formed in the main flow (known as shear rate).

Equation 6.2 shows that energy is generated from the action of shear, and energy is indeed needed for the formation of emulsions. Hence, the analysis of shear will certainly serve as a measure to identify as well as to understand the correlation between the energy generated and the emulsification behaviour.

Although there are two shear components in the production term, this chapter only focuses on the shear formed in the main flow, which is the shear rate. As shown in Equation 6.1, τ_w is as a function of dynamic viscosity and shear rate, whereby the dynamic viscosity of fluid in the present study is constant (Newtonian fluid). So, the τ_w is directly proportional to the shear rate. This shows that analysis of the τ_w is a direct indication of the shear in the pipeline flow.

Besides, it is shown in Equation 6.2 that the shear rate is a vector, which means there are more than one shear rate components. However, in this study, only the streamwise velocity gradient ($\frac{du}{dy}$) is analyzed and used for the determination of τ_w. In order to determine the wall shear stress, the shear rate at the wall of the pipeline, which is $(\frac{du}{dy})_{y=0}$ is examined. It is understood as the streamwise velocity gradient at the wall of the pipe.

In the following discussion, the results are discussed based on the analyzed τ_w as it signifies not only the shear stress at the wall of the pipeline, but also denotes as the direct measure of the shear produced by the main flow as well. The τ_w presents in the

subsequent study is normalized in order to obtain dimensionless τ_w results for comparison. It is normalized by the diameter of the constriction (D), dynamic viscosity of the flowing fluid (μ) and average inlet velocity (U), as shown below:

$$Normalized \quad \tau_w = \frac{\tau_w D}{\mu U} \tag{6.3}$$

6.2.1 Effect of Water Cuts

Figure 6.6 (a) to **Figure 6.6 (**d) and **Figure 6.7** (a) to **Figure 6.7** (d) illustrate the wall shear stress as a function of water cuts at four different types of pipeline constrictions: they are, pipeline with gradual contraction with ratio of 0.50 (GC 0.50), pipeline with gradual contraction with ratio of 0.75 (GC 0.75), pipeline with sudden contraction with ratio of 0.50 (SC 0.50) and pipeline with sudden contraction with ratio of 0.75 (SC 0.75) for both the laminar inlet flow and transitional inlet flow, respectively. 13 *x/D*, 24 *x/D*, 38 *x/D*, 51 *x/D* and 63 *x/D* in the figures represent the measurement location along the pipeline test section.

For laminar inlet flow, the Reynolds number is between 1100 and 1800. As presented in **Figure 6.6** (a) to **Figure 6.6 (**d), the τ_w increases as the water cuts increase from 0% to 10%. Then, the τ_w decreases with the further increase in the water cuts from 10% to 40%. For transitional inlet flow, where the Reynolds number of the flowing fluid is between 2400 to 2800, it is observed that the τ_w increases with the increase in water cuts from 5% to 10% and then it decreases with further increase in the water cuts, as presented in **Figure 6.7** (a) to **Figure 6.7** (d). The results show that for both the laminar and transitional inlet flow, the change in the trend of τ_w with respect to water cuts happens at 10% WC.

The increase in τ_w with the increase in water cuts is believed to be due to different shear as a result of different amount of emulsions present in the flow. With higher water cuts, the amount of emulsions (dispersed water droplets) formed is higher as well, as has been

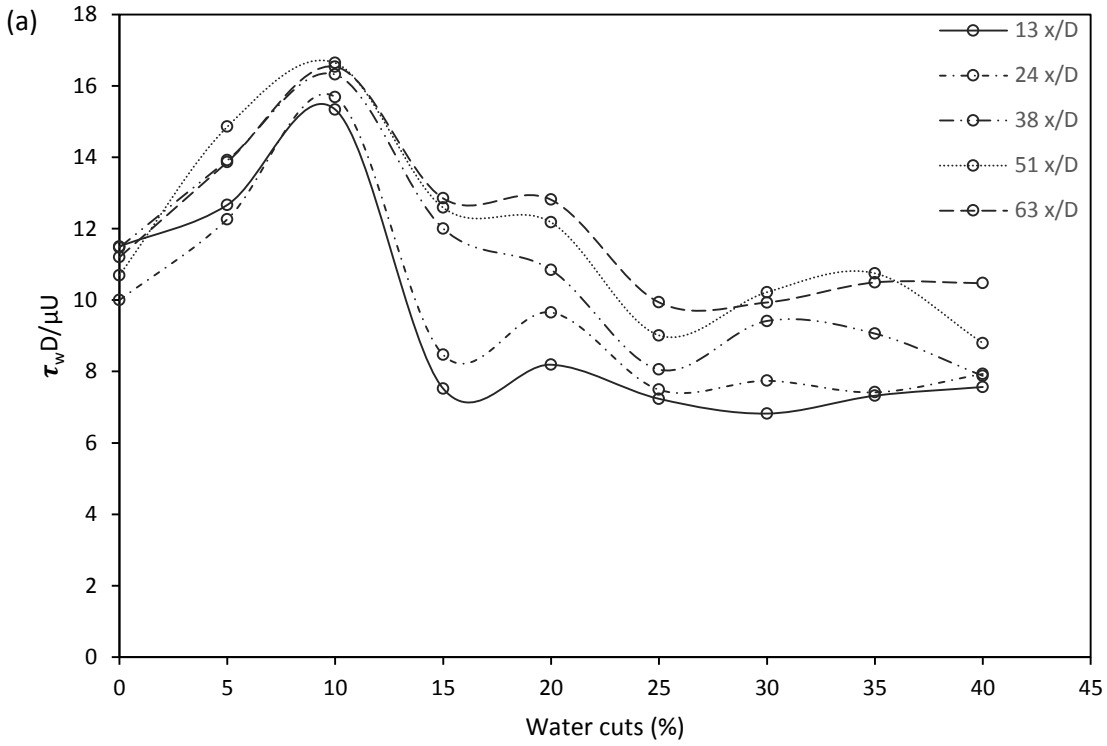
(a)
18
16
14
12
10
8
6
4
2
0
0
5
10
15
20
25
30
35
40
45
Water cuts (%)
$\tau_w D/\mu U$
13 x/D
24 x/D
38 x/D
51 x/D
63 x/D

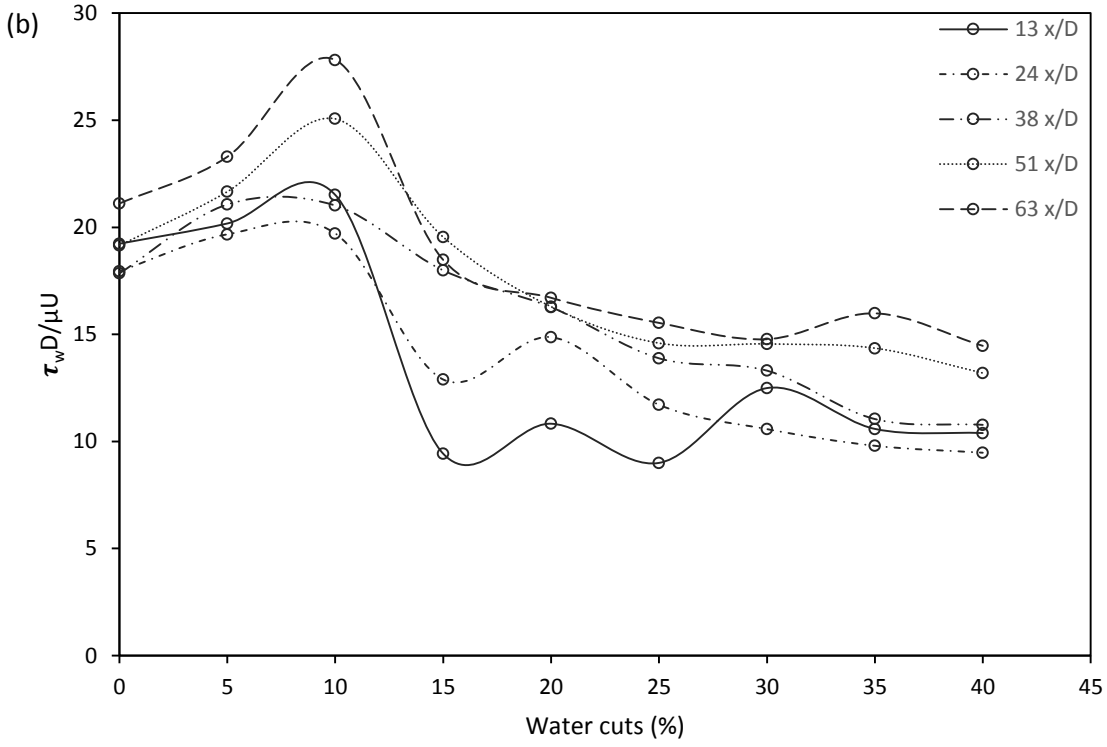
(b)
30
25
20
15
10
5
0
0
5
10
15
20
25
30
35
40
45
Water cuts (%)
$\tau_w D/\mu U$
13 x/D
24 x/D
38 x/D
51 x/D
63 x/D

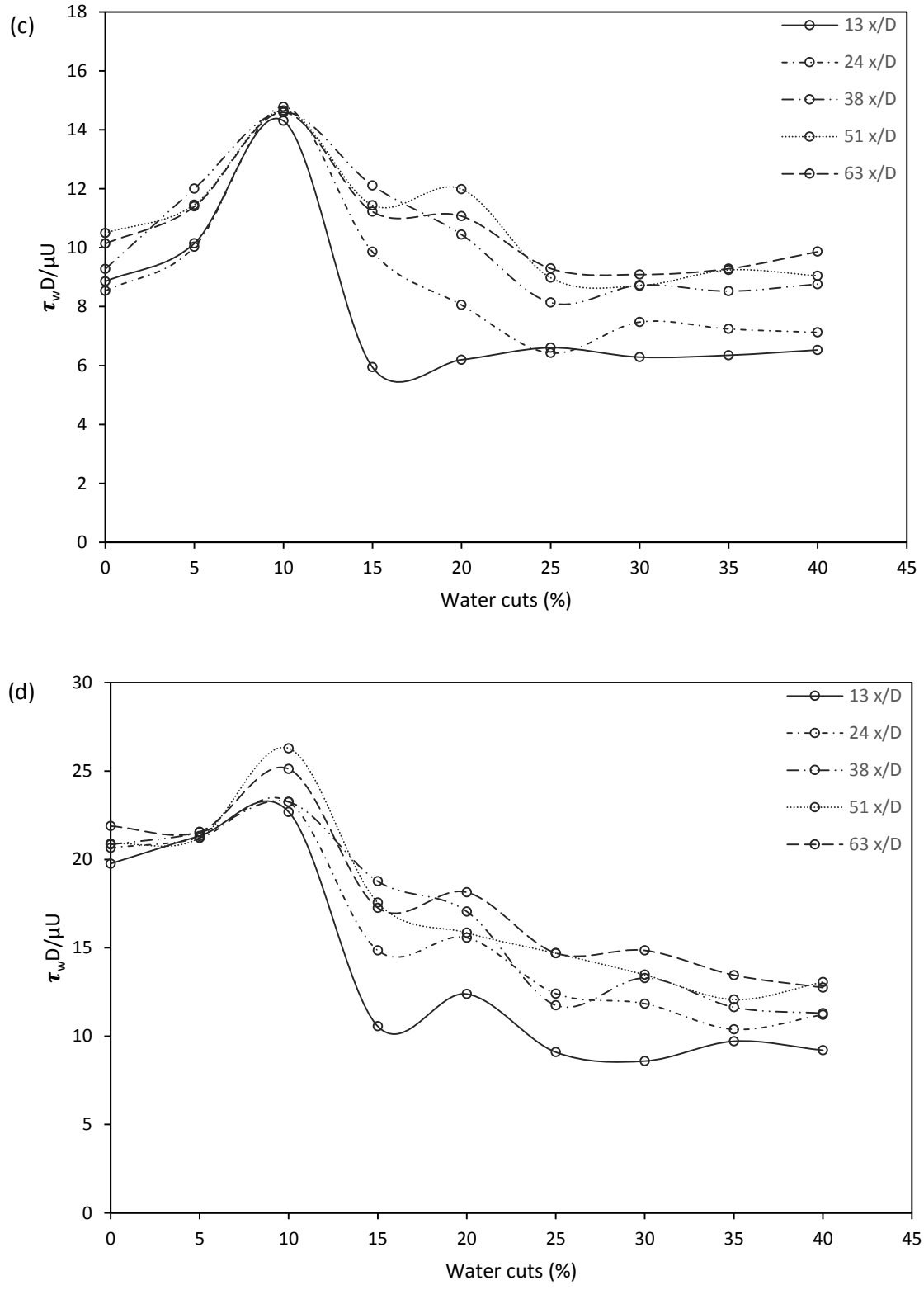

Figure 6.6: Normalized τ_w at different water cuts for pipeline constriction of (a) GC 0.50 (b) GC 0.75 (c) SC 0.50 and (d) SC 0.75 for laminar flow inlet (1100 < *Re* < 1800).

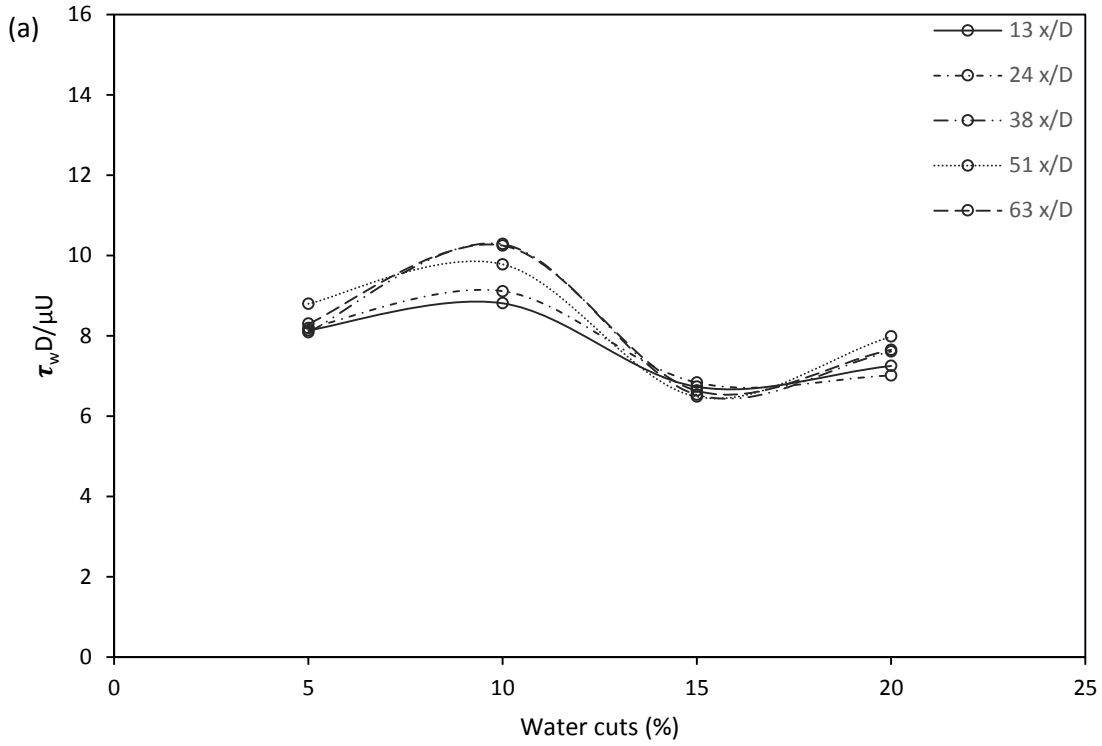
(a)
13 x/D
24 x/D
38 x/D
51 x/D
63 x/D
$\tau_w D/\mu U$
Water cuts (%)
0
2
4
6
8
10
12
14
16
0
5
10
15
20
25

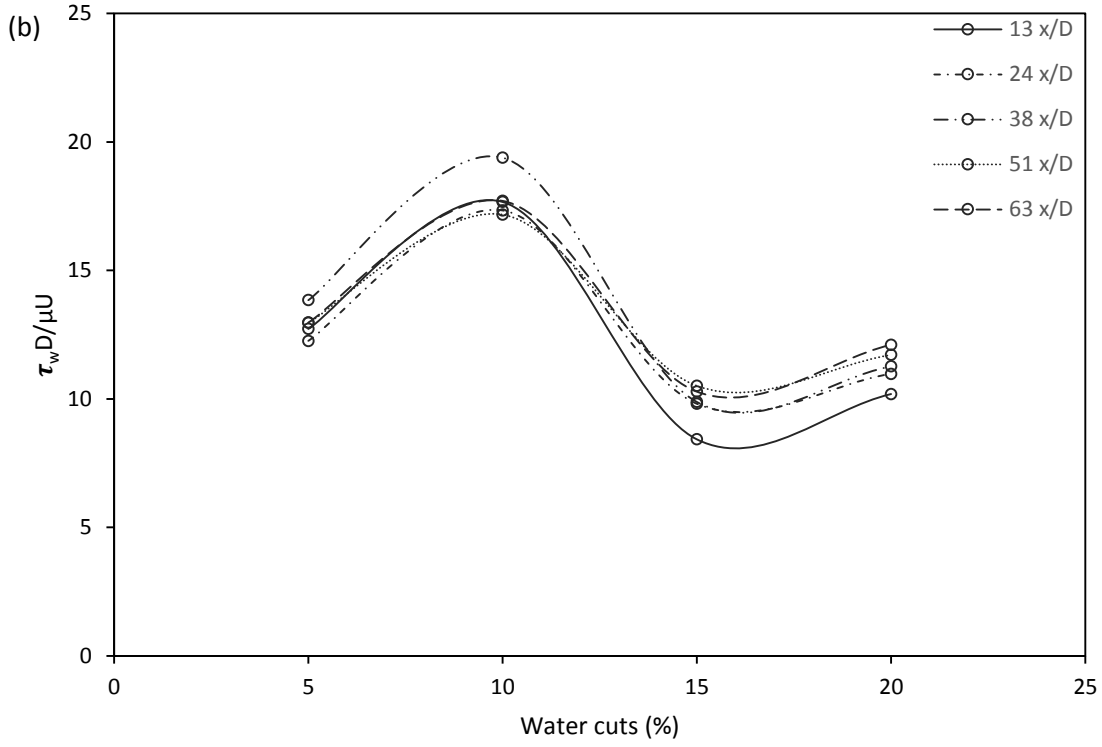
(b)
13 x/D
24 x/D
38 x/D
51 x/D
63 x/D
$\tau_w D/\mu U$
Water cuts (%)
0
5
10
15
20
25
0
5
10
15
20
25

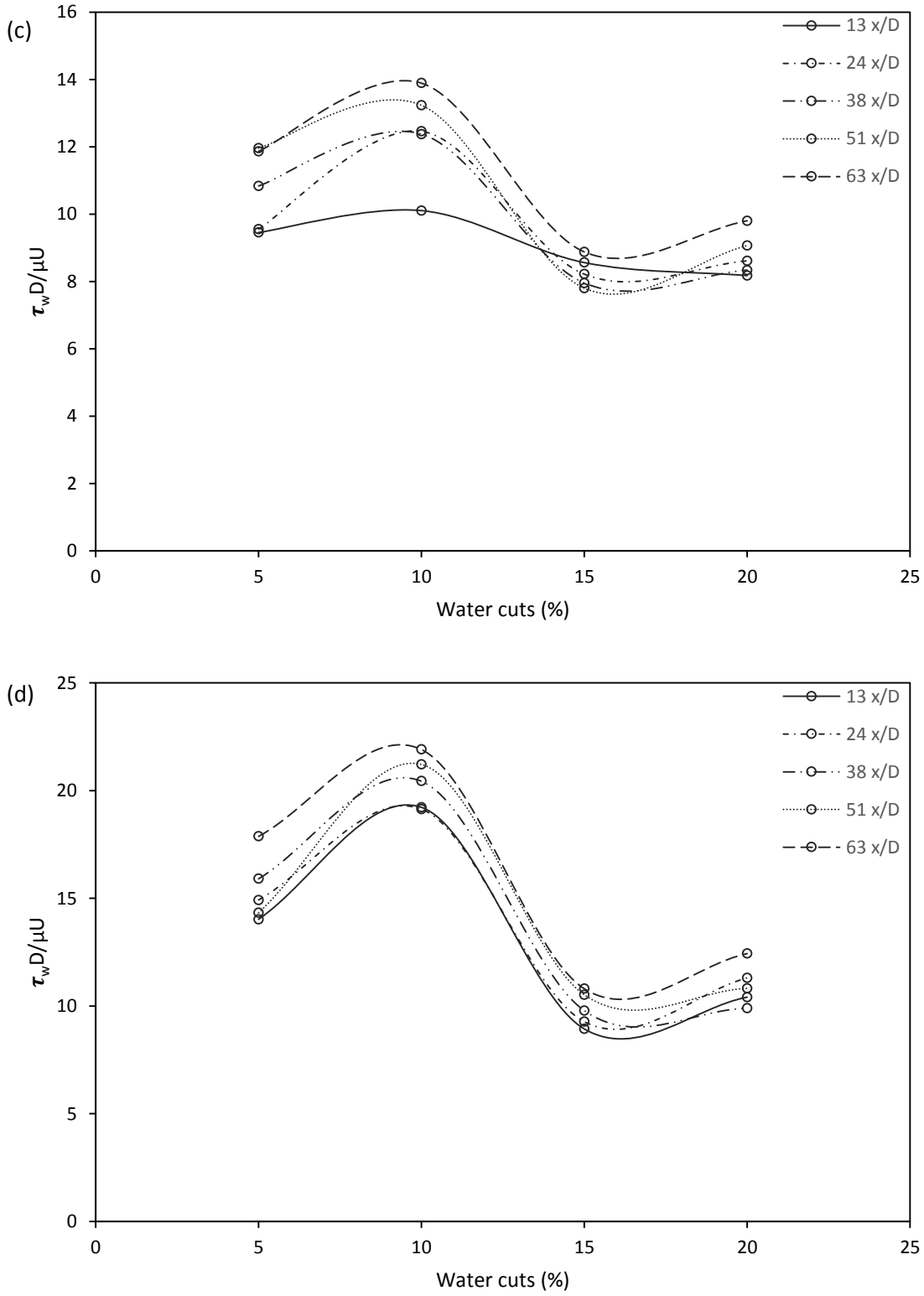

Figure 6.7: Normalized τ_w at different water cuts for pipeline constriction of (a) GC 0.50 (b) GC 0.75 (c) SC 0.50 and (d) SC 0.75 for transitional flow inlet (2400 < *Re* < 2800).

proved in the previous chapter. In other word, mixture with higher water cuts produces higher number of water droplets per unit volume as compared to the mixture with lower water cuts. When the dispersed water droplets per unit volume is higher, the collisions between the dispersed water droplets happen more frequently as compared to that of the lower droplets per unit volume. This is supported by the collision theory which has stated that increasing the concentration of the reactant particles will result in more collisions [113].

When one dispersed water droplet collides or hits with another dispersed water droplet in the flow, they will exert shear on one another. The same goes for the collisions between the emulsions with the fluid particles (the continuous phase fluid) around them. With the presence of more emulsions, the collision rate is increased, which leads to an increase in the shear. Consequently, the wall shear is affected. Wall shear will be larger when there are more emulsions because the collision rate of the emulsions increases with the amount of emulsions. Following the above discussion, the higher the amount of emulsions, the higher is the collision frequency and hence the higher is the shear rate. Therefore, the larger the wall shear stress with the increase in the water cuts.

However, beyond 10% WC, the effect of collisions is no longer significant. The results show that the τ_w decreases with the increase in the water cuts for both the laminar inlet flow and transitional inlet flow when the water cuts increases to above 10%. This is due to the drag reduction effect as a result of the presence of significant amounts of W/O emulsions in the flow. Drag reduction phenomenon caused by W/O emulsions has been reported elsewhere [17, 44]. The drag reduction phenomenon is believed to be caused by the suppression of turbulence as a result of dynamic break-up and coalescence of the dispersed droplets in the flow. The obtained results suggest that as the water cuts reaches beyond 10%, the amount of dispersed water droplets (emulsions) in the flow is sufficient to cause a significant effect on the turbulence suppression. As the water cuts increases, the amount of emulsions formed similarly increases. As a result of that, there are more dispersed water droplets to interact and suppress the turbulent eddies created at the pipeline constriction and this resulted in a higher degree of turbulence suppression. With

the increase in the turbulence suppression, the drag reduction is more profound as well. Therefore, the τ_w decreases as the water cuts increase beyond 10%.

Besides, the obtained results also suggest that regardless of the types of the inlet flow regime (either laminar or transitional), the flow develops into to turbulent flow after passing through the pipeline constriction. This is because turbulence suppression effect only present in the turbulent flow. However, this is determined in both the laminar and transitional inlet flow in the current research. This has further strengthened the result on the time-averaged velocity profiles presented in the previous section, which states that an increase in water cuts induces the flow to develop to turbulent flow after it passes through the pipeline constriction.

6.2.2 Effect of Reynolds Number

Figure 6.8, **Figure 6.9**, **Figure 6.10** and **Figure 6.11** compare the τ_w at different inlet flow regime (laminar and transitional) for GC 0.50, GC 0.75, SC 0.50 and SC 0.75, respectively. In each of these four figures, (a) to (e) represents the τ_w results at different measurement location of the pipeline, which are at 13, 24, 38, 51 and 63 *x/D* downstream of the pipeline constriction. From these figures, it is observed that the τ_w is lower in the transitional inlet flow (higher Reynolds number) as compared to laminar inlet flow (lower Reynolds number). This finding is observed in all types of pipeline constrictions and water cuts under examination.

Transitional inlet flow results in lower τ_w than the laminar inlet flow owing to the difference in the amount of energy in the flowing fluid. At a higher flow rate, there is more energy in the flow. As a result of that, emulsions are dispersed into smaller droplets as more energy is used for the dispersion of emulsions. As has been known earlier in the Kinetic Energy Budget of Turbulent Flow, the viscous dissipation term is the only term that dissipates the turbulent kinetic energy. Since viscous dissipation is the only term to dissipate energy and the Second Law of Thermodynamics states that energy in is equal to

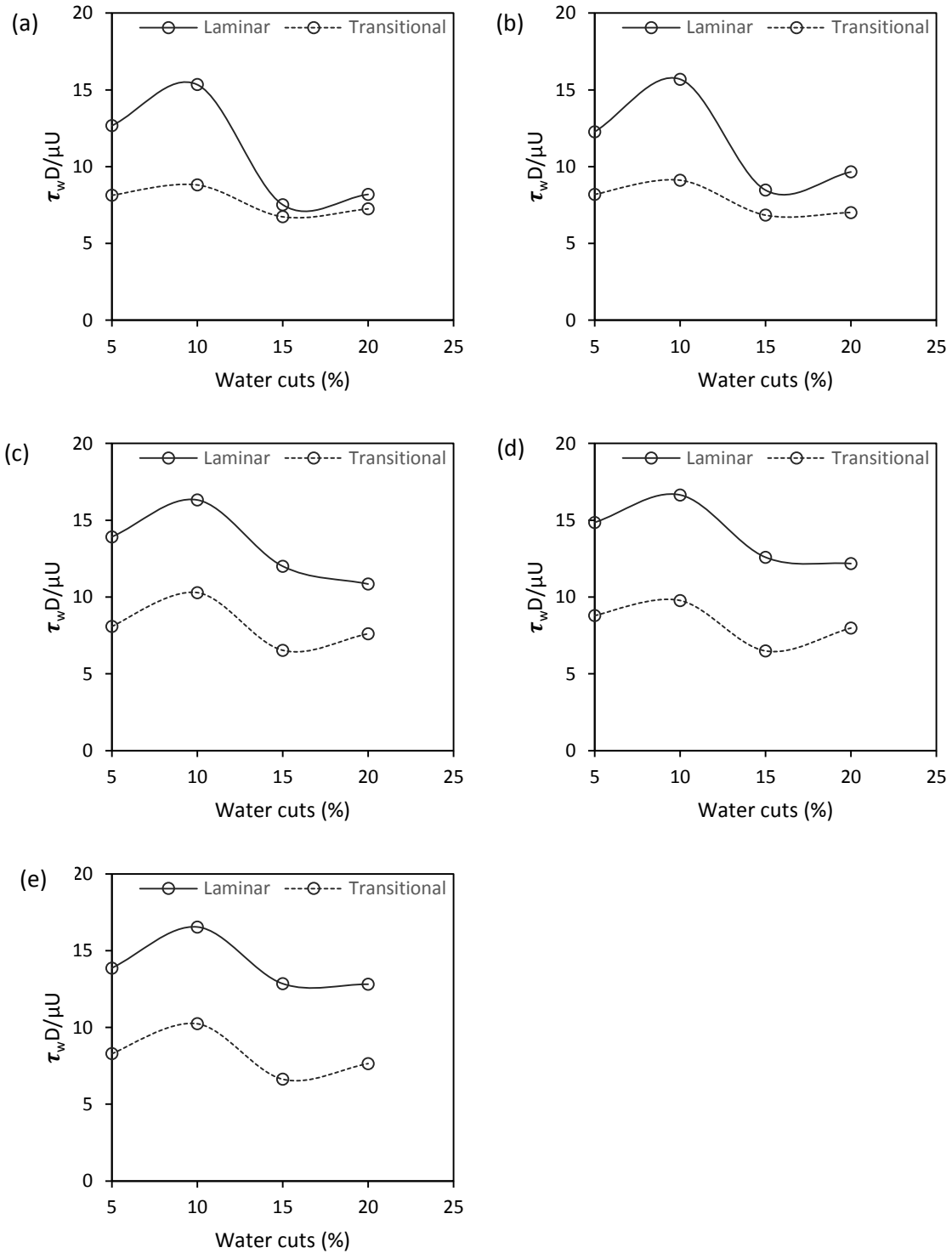

Figure 6.8: Normalized τ_w at different water cuts for different flow regime at (a) 13 (b) 24 (c) 38 (d) 51 and (e) 63 *x/D* downstream of GC 0.50 pipeline constriction.

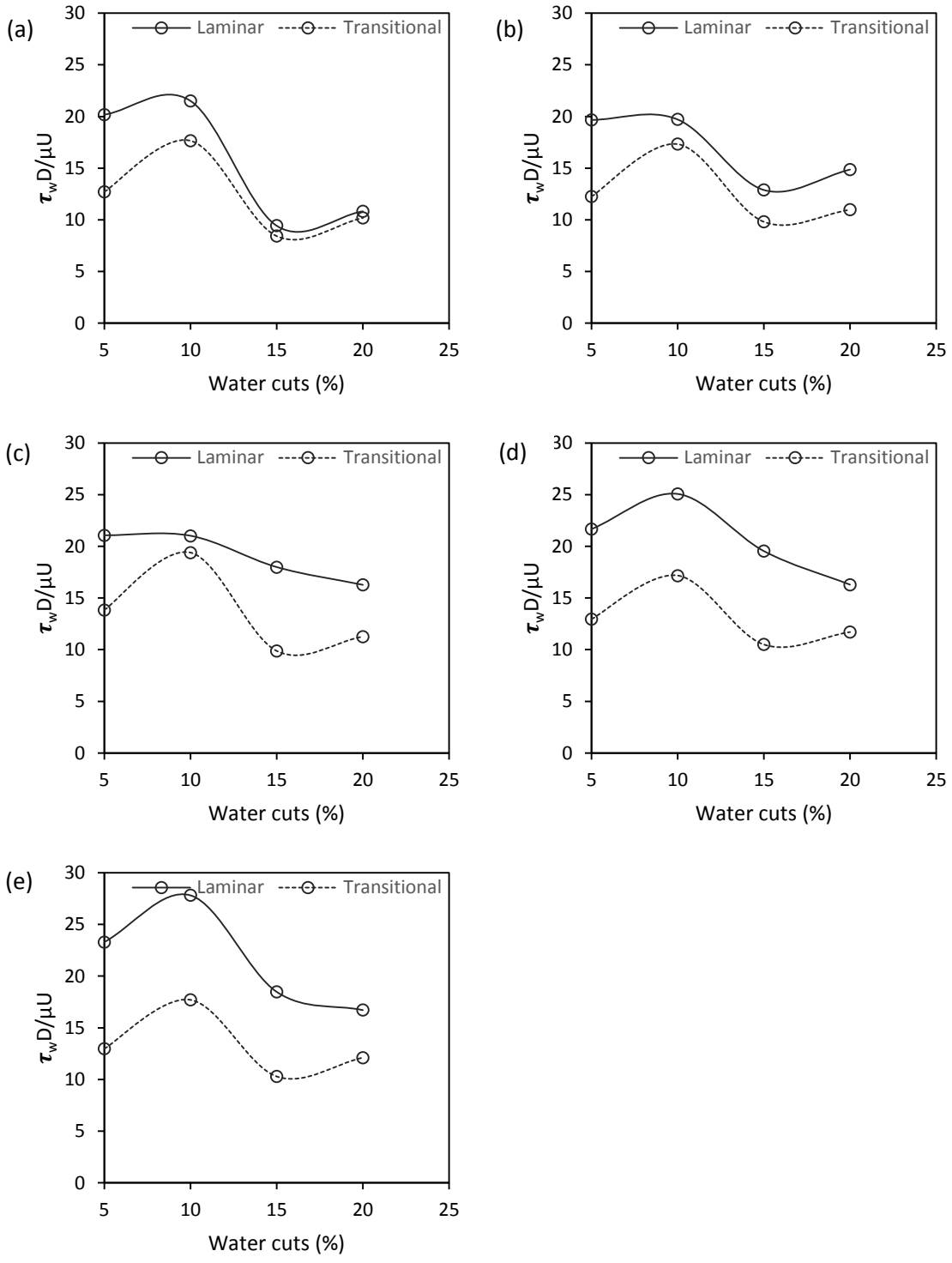

Figure 6.9: Normalized τ_w at different water cuts for different flow regime at (a) 13 (b) 24 (c) 38 (d) 51 and (e) 63 *x/D* downstream of GC 0.75 pipeline constriction.

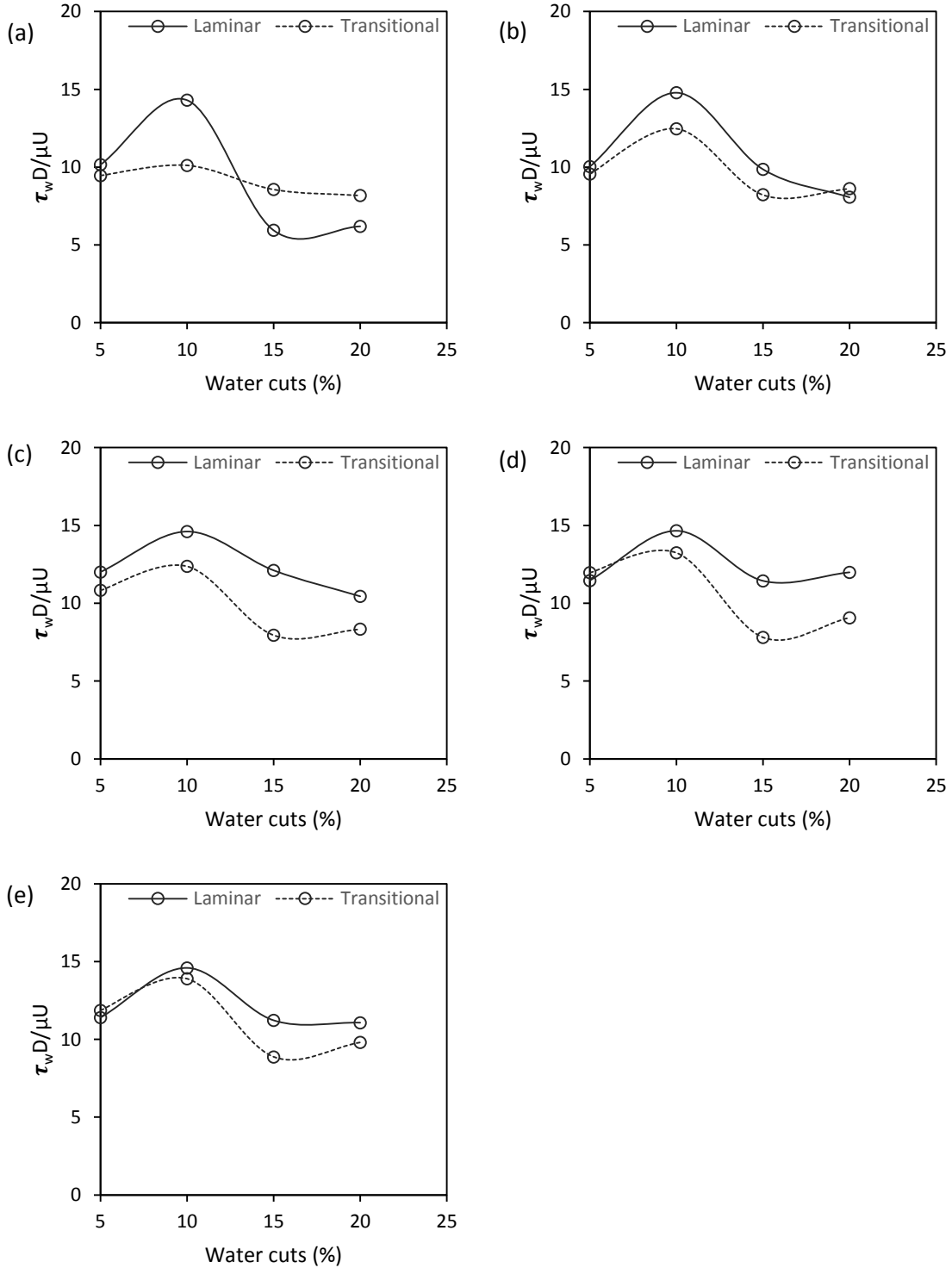

Figure 6.10: Normalized τ_w at different water cuts for different flow regime at (a) 13 (b) 24 (c) 38 (d) 51 and (e) 63 *x/D* downstream of SC 0.50 pipeline constriction.

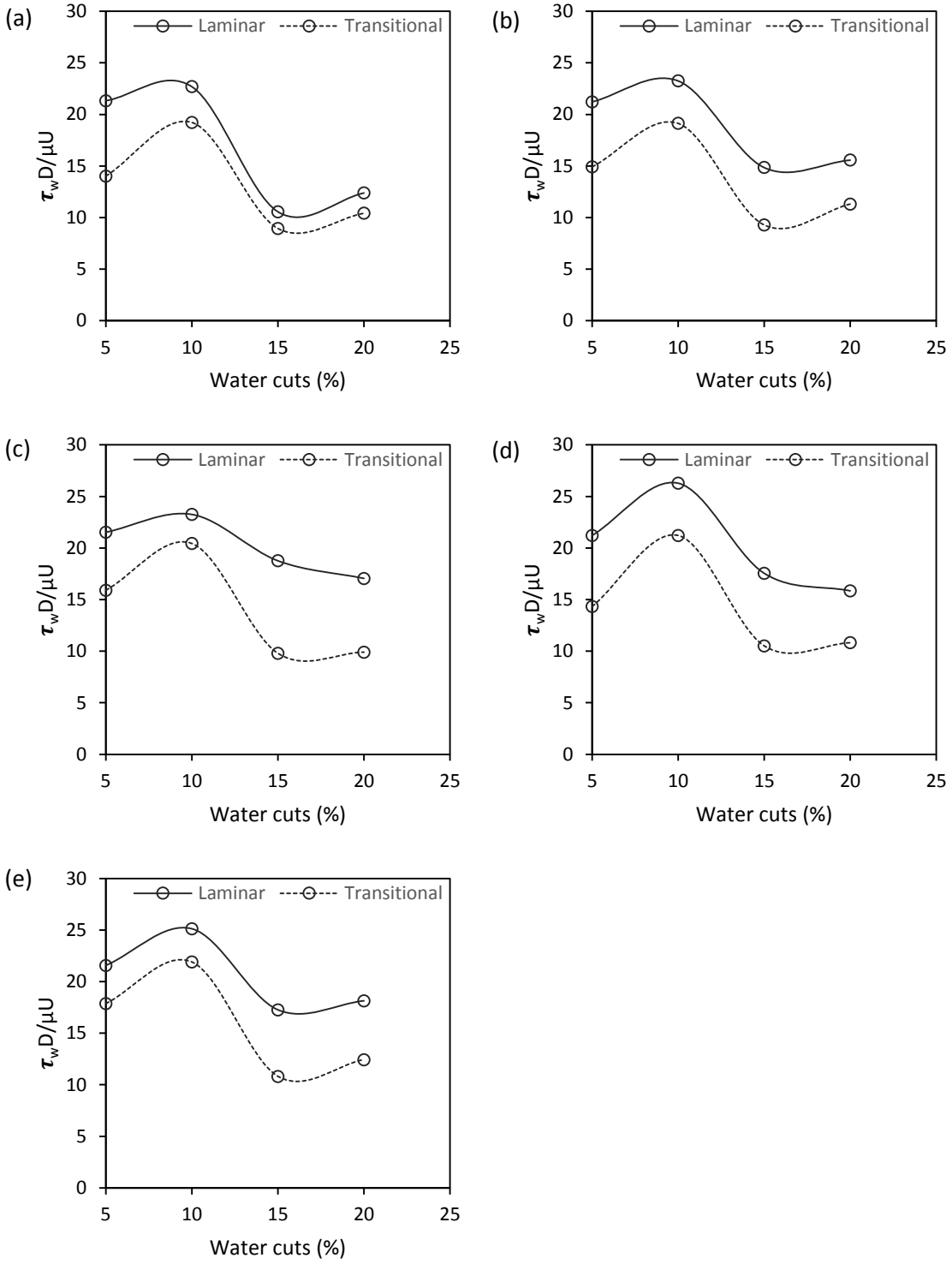

Figure 6.11: Normalized τ_w at different water cuts for different flow regime at (a) 13 (b) 24 (c) 38 (d) 51 and (e) 63 *x/D* downstream of SC 0.75 pipeline constriction.

energy out, it is safe to assume that the dissipation energy is representative of the production energy of the flow. Hence, higher dissipation energy signifies higher energy production. Therefore, in order to discover the role of energy in the emulsification behaviour in the respective flow regime (laminar and transitional inlet flow), the dissipation energy is examined. Previous studies [89, 114, 115] also have indicated the use of dissipation energy as the source of energy for the emulsification process. The dissipation energy rate is calculated using **Equation 6.4** [115].

$$\varepsilon = 2f\frac{U^3}{D} \tag{6.4}$$

Figure 6.12 compares the dissipation energy rate calculated for both the laminar and transitional flow inlet with respect to water cuts downstream of GC 0.50 pipeline constriction. From **Figure 6.12**, it is shown the dissipation energy rate of transitional inlet flow (higher flow rate) is higher than that of the laminar inlet flow (lower flow rate). The same dissipation energy results are obtained for pipeline constriction of GC 0.75, SC 0.50 and SC 0.75, hence the results are shown in Appendix C. Higher dissipation energy rate indicates that at higher flow rate, there is higher rate of interaction in between the dissipation eddies and the water droplets.

As mentioned in Chapter 2, energy is dissipated through turbulent eddies. During the dissipation action, the turbulent eddies interact with the water and shear them into smaller droplets. With higher dissipation energy rate, the water droplets are sheared and broken-up into finer dispersed droplets. This is supported by the previous study [115] which stated that small-scale eddies in the flow are responsible for the dispersion of emulsions into finer droplets. It is important to mention that the results are measured downstream the pipeline constriction. As the pipeline constriction causes a sudden change in the geometry, the flow is disrupted and this induces turbulence eddies to be created in the flow. At higher flow rate, there are more turbulence eddies created at the constriction owing to the more turbulent flow as a result of higher flow rate. As a direct consequence of that, there is more interaction (shearing) in between the emulsions and the turbulence eddies during the dissipation action. Consequently, the emulsions are broken into finer droplets in the higher flow rate.

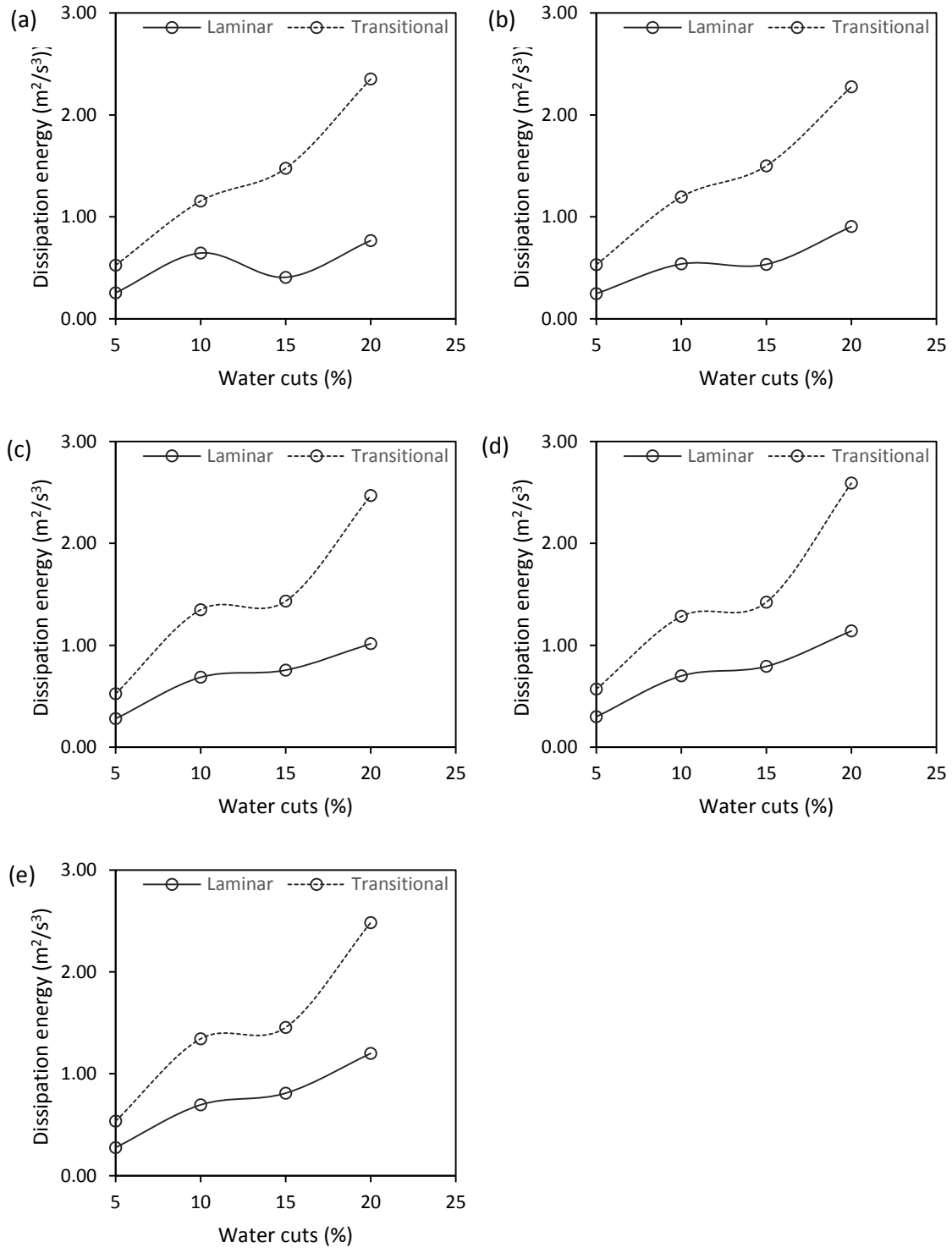

Figure 6.12: Dissipation energy as a function of water cuts for different flow regime at (a) 13 (b) 24 (c) 38 (d) 51 and (e) 63 *x/D* downstream of GC 0.50 pipeline constriction.

Decrease in droplets size with the increase in dissipation energy also has been reported elsewhere [116]. Study had revealed that the emulsion friction factor was reduced due to the reduction in the average dispersed phase droplet size of the emulsion [117]. Li *et. al.* [118] also reported a clear correlation between the mean diameter of dispersed droplet size and the friction coefficient, where mean friction coefficient is lower in the case with a smaller mean diameter of droplet size. This indicates that friction factor is directly correlated to the disperse droplet size.

From the above discussion, it is clear that higher flow rate results in dispersed droplets of finer size as compared to the one from lower flow rate owing to the higher dissipation energy rate. With finer dispersed droplets size, the friction factor is lower, which eventually results in lower τ_w. This explains the higher τ_w in transitional inlet flow (higher flow rate) as compared to the laminar inlet flow (lower flow rate).

6.2.3 Effect of Types of Pipeline Constriction

Figure 6.13 compares the τ_w results with different types of pipeline constrictions for laminar inlet flow ($1100 < Re < 1800$). The result shows that the effect of the geometry of constriction, which are gradual contraction and sudden contraction on τ_w, is not very significant. The τ_w comparisons among gradual contraction and sudden contraction type of pipeline constriction are very close to one another, as shown in **Figure 6.13**. However, it is observed that sudden contraction gives slightly higher τ_w. On the other hand, the effect of contraction ratio, which are contraction ratios of 0.50 and 0.75, shows a significant influence on the τ_w. Flowing fluid through the pipeline constriction with a contraction ratio of 0.75 is shown to exhibit higher τ_w as compared to the one of contraction ratio of 0.50. The results are consistent in all the measurement locations, which are 13 *x/D*, 24 *x/D*, 38 *x/D*, 51 *x/D* and 63 *x/D* downstream of the pipeline constriction (as shown in **Figure 6.13** (a) to **Figure 6.13** (e)).

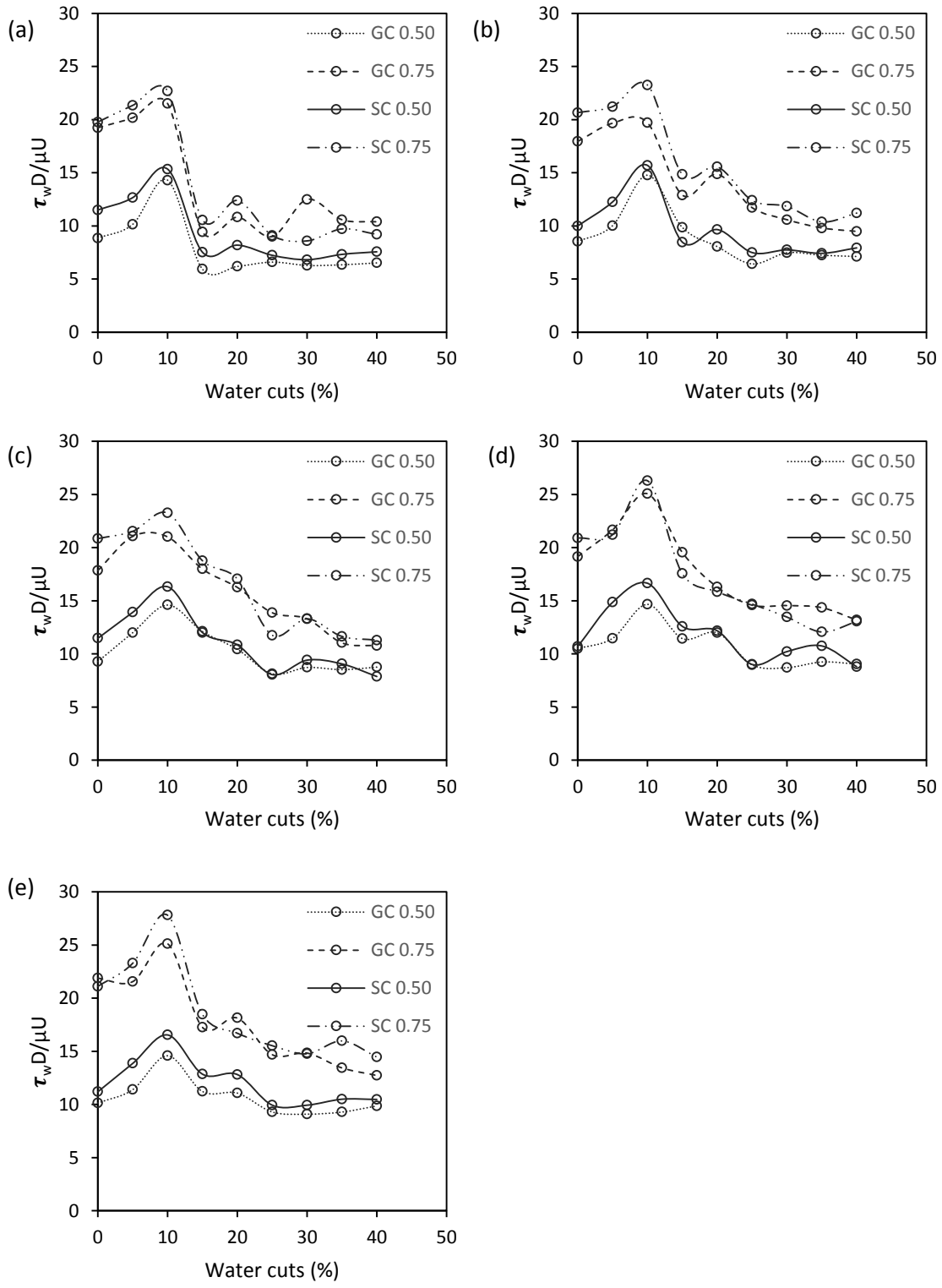

Figure 6.13: τ_w subject to various type pipeline constrictions at (a) 13 (b) 24 (c) 38 (d) 51 and (e) 63 *x/D* downstream of pipeline constriction for laminar flow inlet (1100 < *Re* < 1800).

Figure 6.14 presents the τ_w results from different types of pipeline constrictions for transitional inlet flow ($2400 < Re < 2800$). **Figure 6.14** (a) to **Figure 6.14** (e) clearly demonstrate that the τ_w results follow the same pattern of the one in the laminar flow, where both the gradual contraction and sudden contraction with a contraction ratio of 0.75 shows higher τ_w than the contraction ratio of 0.50. However, in transitional inlet flow, the effect of the geometry of the constriction has become more prominent. The results significantly show that the pipeline with sudden contraction gives higher τ_w compared to gradual contraction.

Fluid flowing through a pipeline constriction of smaller diameter (contraction ratio 0.50) results in higher τ_w is due to higher shear rate in the pipeline constriction with smaller diameter. Al-Yaari *et. al.* [117] stated that given the same Reynolds number, the shear rate in a pipe with half a diameter of another pipe is four times higher than the pipe with bigger size. As a result of higher shear in the constriction of smaller diameter, the water dispersed droplets are broken into smaller size owing to higher shearing rate. With the presence of smaller dispersed water droplets produced from the pipeline constriction of smaller diameter, the friction factor is lower. Hence, this resulted in the lower τ_w in the pipeline with contraction ratio of 0.50. Although no microscopic image of the droplet size distribution of W/O emulsions can be provided as an evidence for the proclamation on smaller pipeline constriction producing emulsions of finer average size, this statement can be supported by the stability results presented earlier in Chapter 5. As has been presented and discussed earlier, emulsions formed from pipeline constriction with lower contraction ratio (ratio 0.50) exhibit higher stability - indicating dispersed droplets of smaller average size. Likewise, it has been stated elsewhere [119] that higher stability emulsions is the result of the smaller average size of the dispersed phase droplets. This confirms that emulsions formed from pipeline constriction with smaller diameter exhibit smaller average droplets size (higher stability) resulting in lower friction. As a result of that, the τ_w is lower.

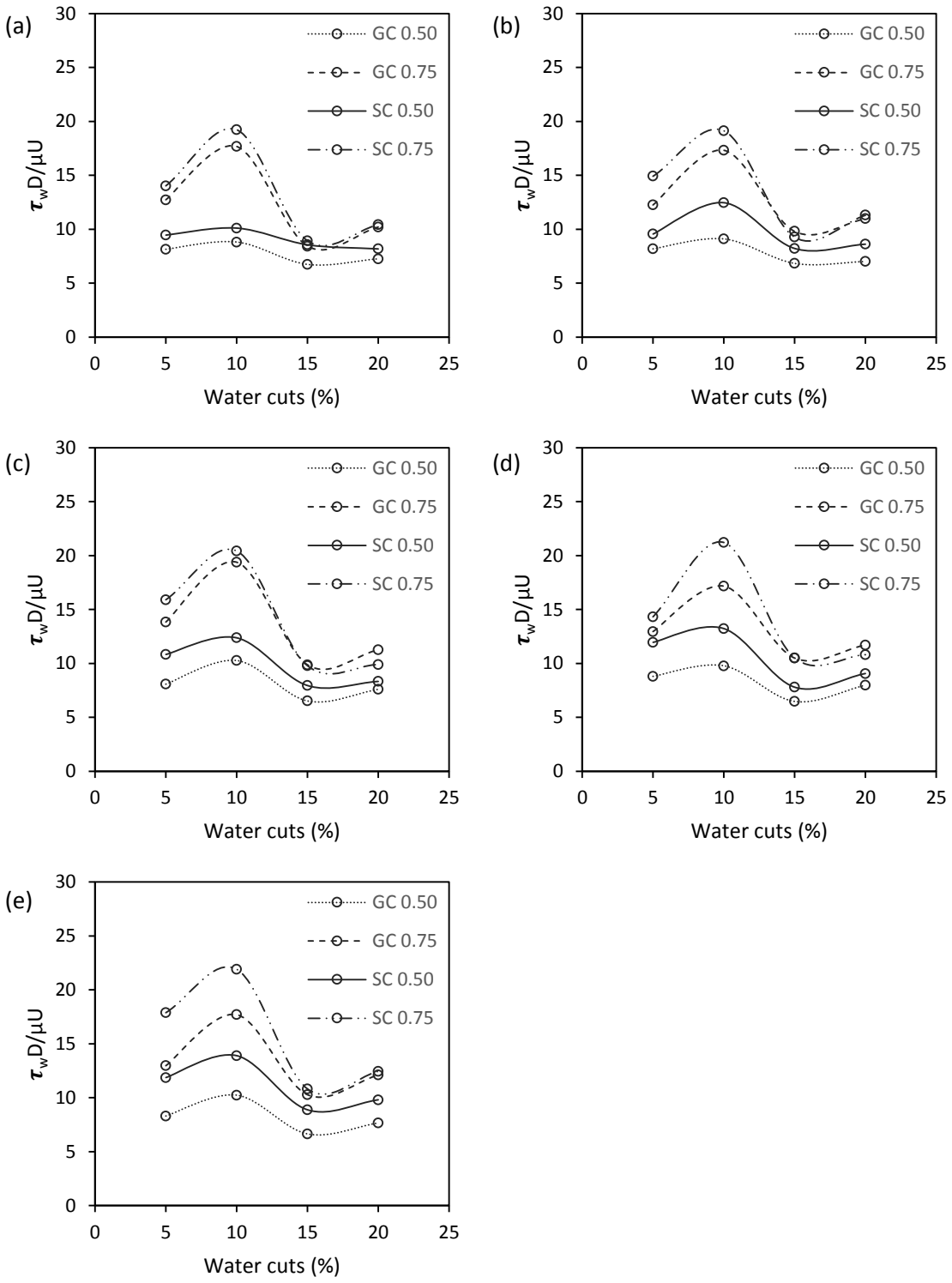

Figure 6.14: τ_w subject to various type pipeline constrictions at (a) 13 (b) 24 (c) 38 (d) 51 and (e) 63 *x/D* downstream of pipeline constriction for transitional flow inlet (2400 < *Re* < 2800).

As mentioned above, pipeline with the sudden contraction shows higher τ_w than the gradual pipeline contraction. As has been explained earlier in Chapter 5, the sudden constriction pipeline is expected to have a higher energy loss than the gradual constriction pipeline. Higher energy loss to the flow indicates that more energy is available for the formation of emulsions. As a result of that, more emulsions are formed through the sudden constriction pipeline as compared to the gradual constriction pipeline. Collision among droplets as well as with the pipeline wall will exert shear on one another. Thus, with the presence of more emulsions in sudden constriction pipeline, the collision rate is increased, leading to an increase in the shear (increase in the friction) and resulting in a higher τ_w.

It is pertinent to mention that, from the previous chapter, where the amount of emulsions formed is examined visually, determination on the amount of emulsions formed through different types of pipeline constrictions is the same. On the other hand, the τ_w results show that differences in types of pipeline constriction resulted in different τ_w, where this phenomenon is considered to be caused by the different amount of emulsions presence in the flow. This suggests that types of pipeline constrictions do affect the amount of emulsions formed in the pipeline.

6.2.4 Changes along the Pipeline

Figure 6.15 (a) to **Figure 6.15** (d) present the changes of τ_w along the pipeline (increase in the length of the pipeline) after the pipeline constriction for laminar inlet flow ($1100 < Re < 1800$). The measurement locations after the pipeline constriction were at 13 *x/D*, 24 *x/D*, 38 *x/D*, 51 *x/D* and 63 *x/D* along the horizontal pipeline. **Figure 6.16** (a) to **Figure 6.16** (d) depict the changes of τ_w along the pipeline after the pipeline constriction for transitional inlet flow ($2400 < Re < 2800$). The results demonstrate that τ_w increases with the increase in the pipe length after the pipeline constriction, for both laminar and transitional inlet flow.

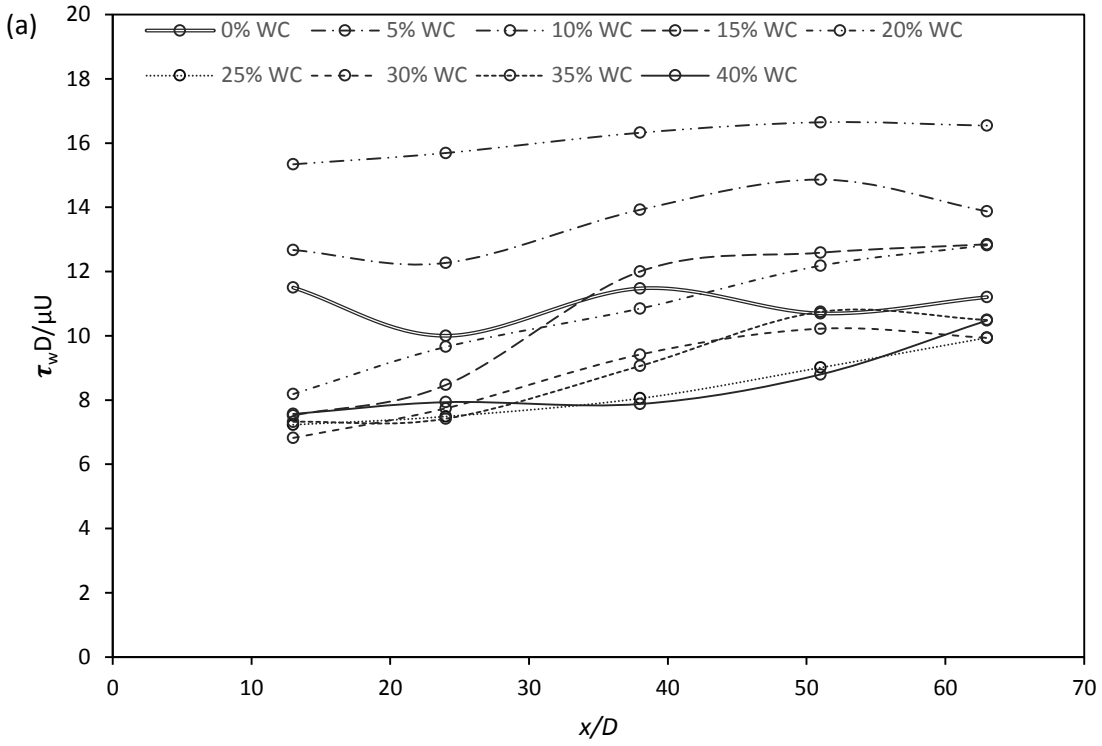
(a)
0% WC
5% WC
10% WC
15% WC
20% WC
25% WC
30% WC
35% WC
40% WC
$\tau_w D/\mu U$
x/D
0
2
4
6
8
10
12
14
16
18
20
0
10
20
30
40
50
60
70

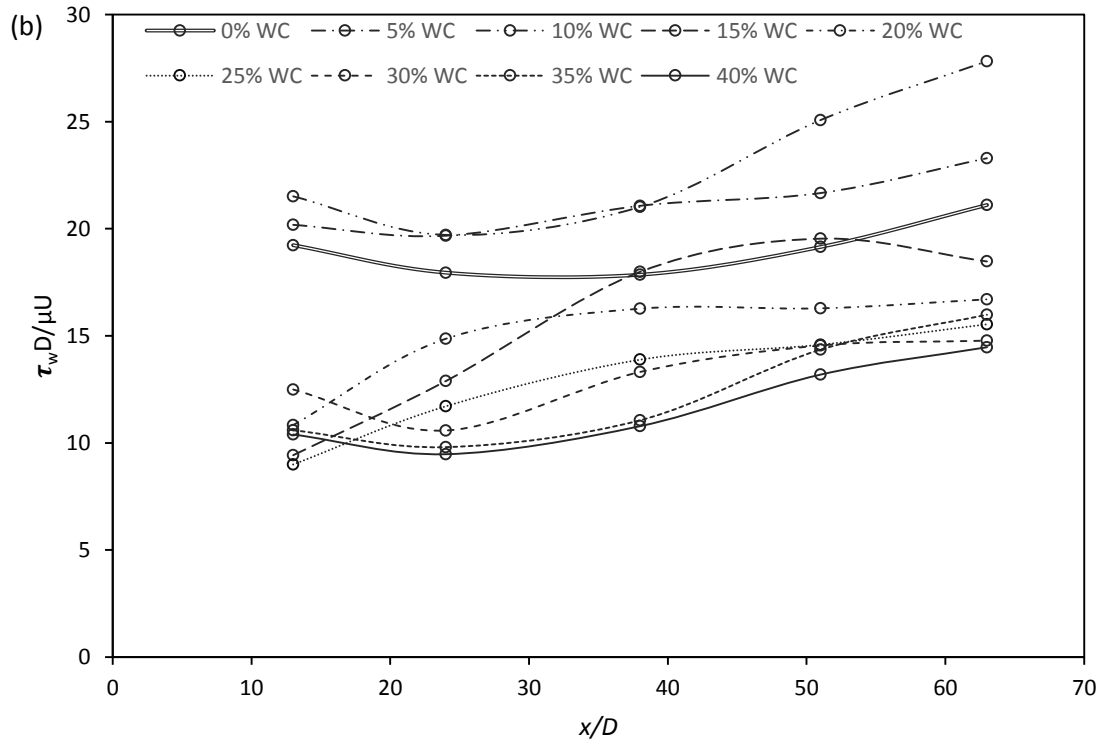
(b)
0% WC
5% WC
10% WC
15% WC
20% WC
25% WC
30% WC
35% WC
40% WC
$\tau_w D/\mu U$
x/D
0
5
10
15
20
25
30
0
10
20
30
40
50
60
70

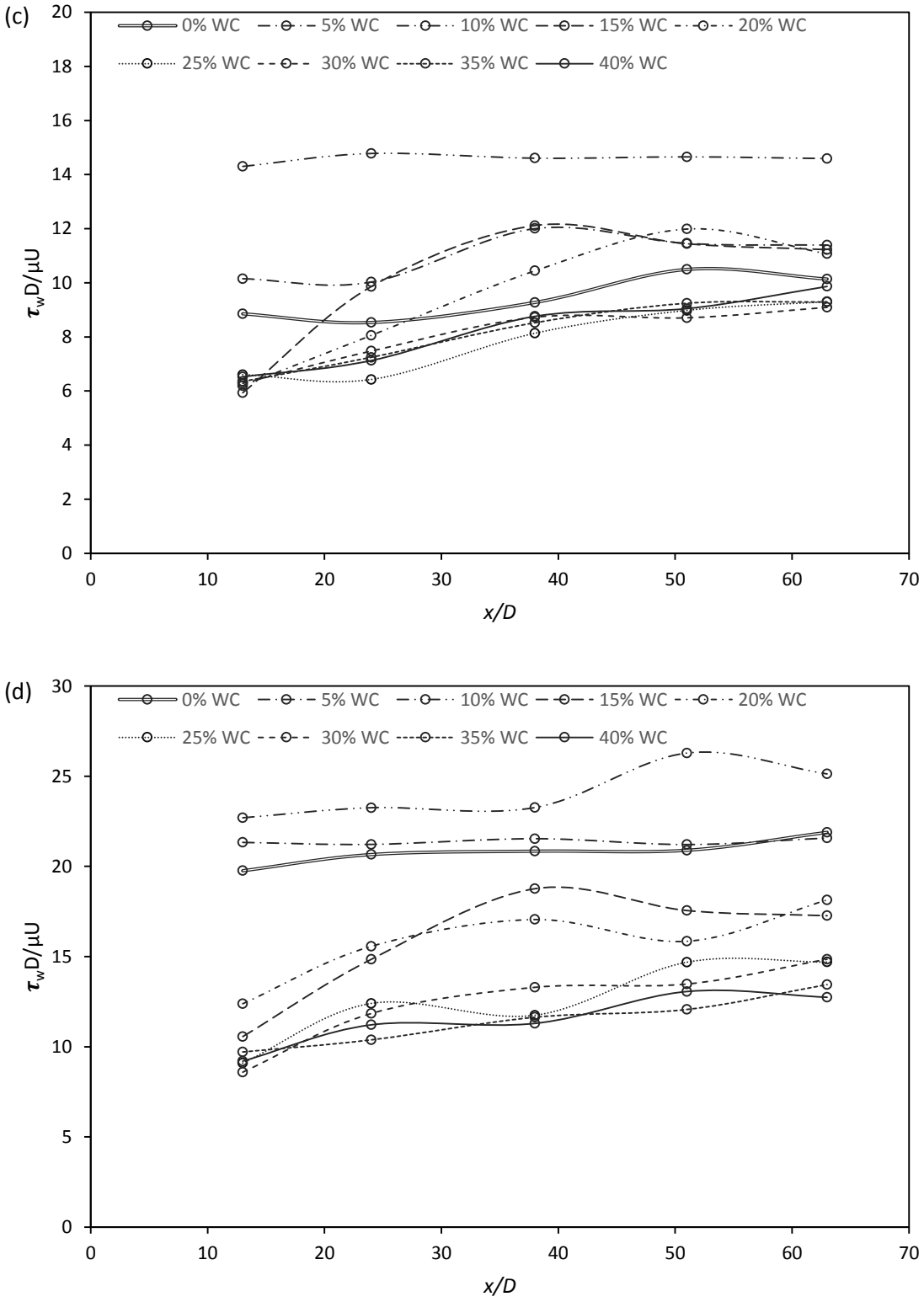

Figure 6.15: Changes of τ_w along the downstream of pipeline constriction of (a) GC 0.50 (b) GC 0.75 (c) SC 0.50 and (d) SC 0.75 for laminar flow inlet (1100 < *Re* < 1800).

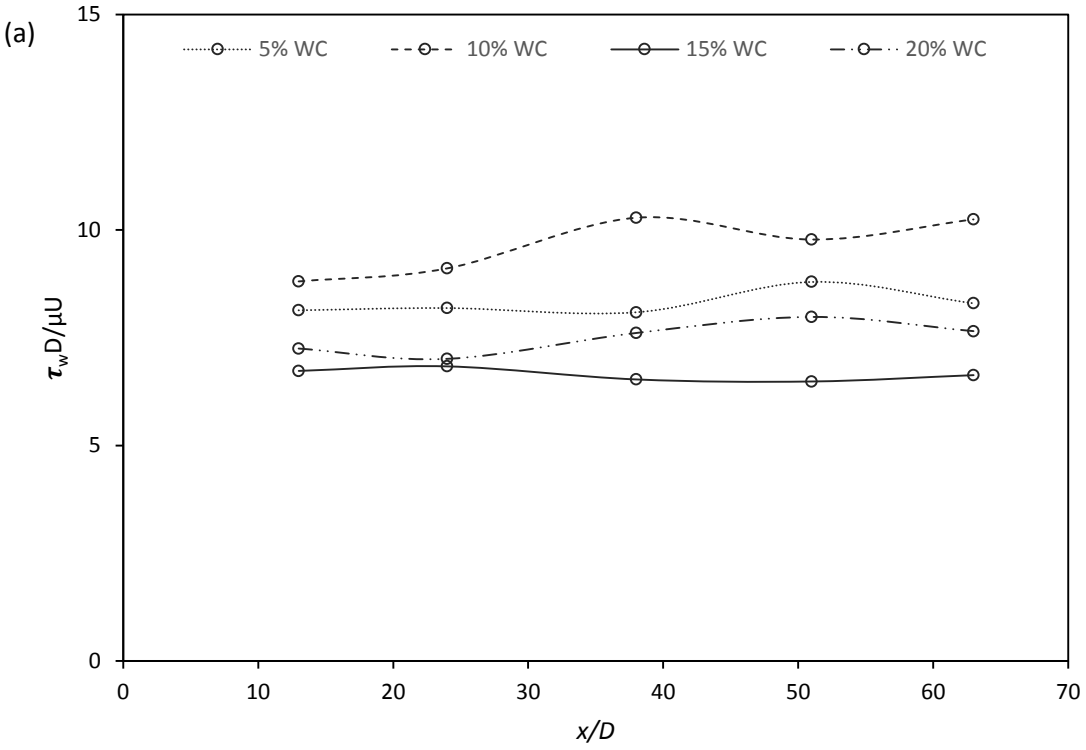
(a)
5% WC
10% WC
15% WC
20% WC
$\tau_w D/\mu U$
x/D
0
5
10
15
0
10
20
30
40
50
60
70

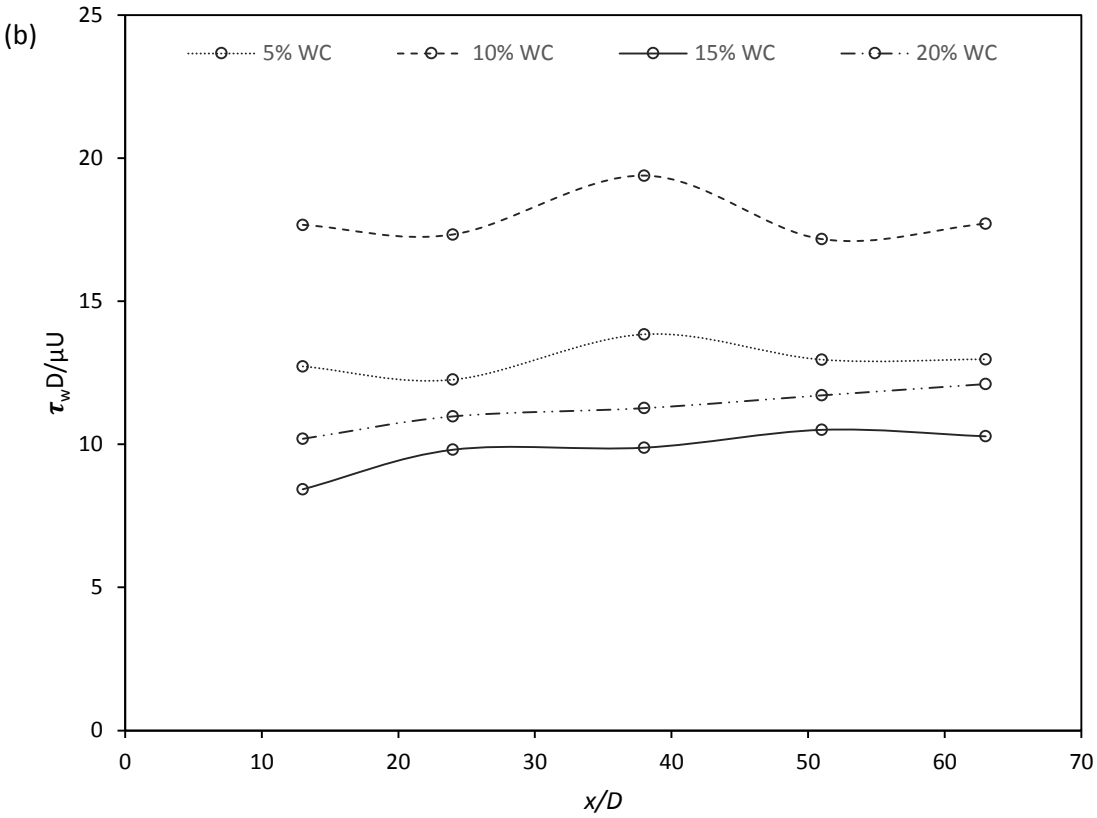
(b)
5% WC
10% WC
15% WC
20% WC
$\tau_w D/\mu U$
x/D
0
5
10
15
20
25
0
10
20
30
40
50
60
70

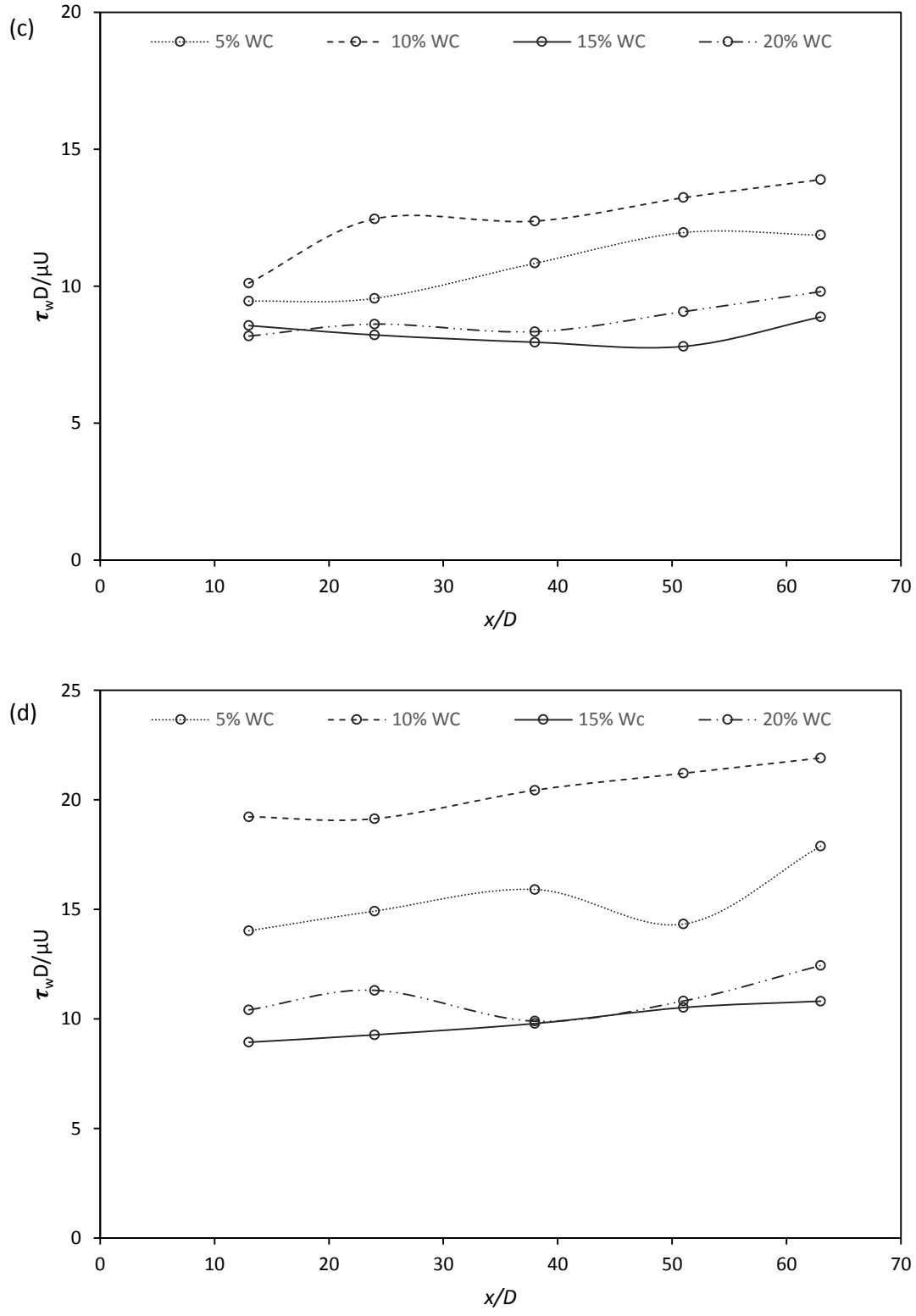

Figure 6.16: Changes of τ_w along the downstream of pipeline constriction of (a) GC 0.50 (b) GC 0.75 (c) SC 0.50 and (d) SC 0.75 for transitional flow inlet (2400 < *Re* < 2800).

The increase in τ_w with the increase in the pipe length downstream the pipeline constriction is due to the increase in the average dispersed water droplets (emulsions) size. In this study, the pipeline constriction acts as the dispersing zone for the emulsification process, where water is dispersed into small dispersed water droplets forming the W/O emulsions. It has been stated that the emulsions are at its finest size right after the dispersing zone [120].

According to Jafari *et. al.* [121], the newly formed emulsions are thermodynamically unstable and the interface of emulsions is not completely covered by emulsifier molecules, where these conditions lead to re-coalescence of the dispersed droplets. Tjaberinga *et. al.* [122] stated that the coalescence possibility is very low in the dispersing zone of an emulsification equipment as a result of longer continuous phase liquid drainage time in the contact region between the two colliding droplets (film drainage) than with the contact time between these droplets upon collision. Coalescence may occur as the dispersed droplets leave the dispersing zone due to the increase in contact time [120].

Since the newly formed emulsions are thermodynamically unstable tending to re-coalesce and re-coalesce probability is based on the contact time and as well as the film drainage time, the dispersed water droplets leaving the pipeline constriction (dispersing zone in this study) most likely to re-coalesce. This is because with the increase in the length of the pipeline after the constriction, the contact time of the dispersed water droplets is increased upon collision among the droplets. With the increase in the contact time of dispersed water droplets during collision, they are re-coalesced as one and formed a larger droplet due to the contact time exceeding the liquid drainage time. In other words, increase of contact time between the droplets that collide with one another allowing the droplets to have sufficient time to break the thin film that is separating them and thereafter resulting in the re-coalescence of the collided droplets. Thus, with the increase in the pipe length after the pipeline constriction (dispersing zone), which is from 13 *x/D* to 63 *x/D*, the contact time of the dispersed droplets increased. This leads to re-coalescence of the dispersed droplets along the way down the pipeline. As a result of that, the average dispersed droplets size increases with the increase in the pipe length.

The total surface area of dispersed water droplets (emulsions) is a function of the diameter of the dispersed droplets [120]. With the increase in the average dispersed droplets size, the total surface area of dispersed water droplets is decreased. The decrease of the total surface area of dispersed water droplets with the same amount of input energy (same shear force) leads to an increase in the shear stress. Therefore, τ_w increases as the fluid flows from 13 *x/D* to 63 *x/D* in the pipeline.

6.3 Summary of Chapter

In this chapter, the time-averaged streamwise velocity profiles are presented. From the velocity profiles, it is determined that as a result of pipeline constriction and emulsions effect, turbulent flow is triggered. This is followed by the analysis and discussion on the wall shear stress (τ_w) at different water cuts, different inlet flow regime, different type of pipeline constriction and its changes along the horizontal pipeline downstream the constriction. Based on the analysis, a few major conclusions are made. First, for water cuts of 0 to 40% (laminar inlet flow) and 5 to 20% (transitional inlet flow), the maximum τ_w is found to be at 10% water cuts for both the laminar and transitional flow. Beyond 10% water cuts, the emulsions exhibit drag-reducing behaviour. Next, for the study on the effect of Reynolds number, it is determined that the higher Reynolds number results in lower τ_w. Furthermore, for the effect of pipeline constriction, it is determined that pipeline constriction with contraction ratio of 0.75 results in higher τ_w than the contraction ratio of 0.50 for both the laminar and transitional inlet flow. The effect of gradual contraction and sudden contraction on τ_w is less significant in the laminar inlet flow. Nevertheless, the effect of gradual contraction and sudden contraction on τ_w is significantly observed in transitional inlet flow, where sudden constriction results in higher τ_w. Lastly, the τ_w is determined to have increased with the increase in the length of the pipeline downstream the pipeline constriction, for both laminar and transitional inlet flow.

CHAPTER 7

TURBULENCE CHARACTERISTICS STUDY OF THE EMULSIFIED FLOW

In chapter 6, the time-averaged streamwise velocity distribution profiles of the W/O emulsified flow have been presented. The time-averaged streamwise velocity distribution profiles have suggested that flow downstream of the pipeline constriction is developed into turbulence flow regardless of the inlet flow regime (either laminar or transitional flow). Besides, in Chapter 6, it is also stated that the formation of emulsions (dynamic break-up and coalescence of the dispersed droplets) tends to diminish the turbulence in the flow. This suggests that turbulence is consumed during the emulsification process. With reference to these findings in the previous chapter, it is known that the emulsified flow or formation of emulsions in the pipeline is closely related to turbulence. Hence, further investigation and additional analysis are needed to confirm the turbulence activities in the emulsified pipeline flow.

Therefore, this chapter will discuss the turbulence characteristics of the water-oil emulsions flow in order to have a better understanding on the roles of turbulence in the formation of emulsion in the pipeline flow. The turbulence characteristics of the water-oil emulsions flow in the pipeline are examined and discussed through the analysis of Reynolds stress and turbulence intensity of the flow field.

7.1 Reynolds Stress

Reynolds stress is one of the important characteristics in the study of turbulence activities. It is the shear generated in the fluctuating component of the flow and as has been known, shear is one of the important sources in producing turbulence. With reference to the Turbulent Kinetic Energy Budget, the Reynolds stress ($\overline{u_i u_j}$) term appears at the "loss to turbulence" term of mean kinetic energy equation and shear production term of turbulent kinetic energy equation. This shows the significant contribution of Reynolds stress to the transfer and production of turbulent energy in the flow. The Reynolds stress analysis in

this study will bring to an understanding on the transport of momentum due to the velocity fluctuation in the flow as a result of the pipeline constriction effect and also the W/O emulsions effects. The Reynolds stress in this study is presented in its normalized form. It is normalized by the averaged streamwise velocity of the flow, giving the normalized Reynolds stress - the $\frac{\overline{u'u'}}{U^2}$.

7.1.1 Reynolds Stress Comparisons along the Pipeline

Figure 7.1 (a) and (b) to **Figure 7.5** (a) and (b) present the normalized Reynolds stress ($\frac{\overline{u'u'}}{U^2}$) from the pipeline constriction type GC 0.50 at the pipeline location of 13 *x/D* and 63 *x/D* respectively, for 0 to 40% WC. The $\frac{\overline{u'u'}}{U^2}$ profiles for pipeline constrictions of GC 0.75, SC 0.50 and SC 0.75 are presented in Appendix D as they show about the same profiles.

From these figures, it is determined that the $\frac{\overline{u'u'}}{U^2}$ peak region at the location 13 *x/D* downstream the pipeline constriction is larger than that at 63 *x/D*. As shown in **Figure 7.1** (a) to **Figure 7.5** (a), the $\frac{\overline{u'u'}}{U^2}$ peak region for 0%, 10%, 20%, 30% and 40% WC covers about 0.35, 0.20, 0.45, 0.40 and 0.25 of the pipe radius (y/R) at the pipeline location of 13 *x/D*. As the fluid flows further downstream to location 63 *x/D* of the pipeline (increase in the pipe length), the results show that the $\frac{\overline{u'u'}}{U^2}$ peak region for 0 %, 10%, 20%, 30% and 40% WC reduces to 0.25, 0.15, 0.30, 0.10 and 0.10 y/R, respectively (as shown in **Figure 7.1** (b) to **Figure 7.5** (b)). This indicates that nearest to the pipeline constriction, the transport of momentum in the pipe that governs by the fluctuating components cover a larger cross-sectional area of the pipe since the $\frac{\overline{u'u'}}{U^2}$ peak region is larger. Further downstream the pipeline, the fluctuating components governs a smaller cross-sectional area of the pipe governs for the momentum transport. Only the flow near to the pipeline wall (y/R = 0) shows a significant momentum transport by the fluctuating component. This indicates that further downstream, the transport of flow is mostly governed by the main flow. With reference to these observations, it is understood that the fluctuating

components are most energetic at the location nearest to the constriction of the pipeline (13 *x/D*) and weaken with the increase in the pipe length. This suggests that the pipeline constriction is the source of turbulence production, where the largest amount of fluctuating components are observed there.

Besides, it is also determined that at location 13 *x/D*, the $\frac{\overline{u'u'}}{U^2}$ is fluctuating after the $\frac{\overline{u'u'}}{U^2}$ peak region, which is different from the phenomena observed at location 63 *x/D*. At 63 *x/D*, it is observed that the $\frac{\overline{u'u'}}{U^2}$ remains constant after the peak region. This indicates that with the increase in the pipe length (x-direction), the shear among the fluctuating components for transport of momentum is only dominant at very near to the pipe wall.

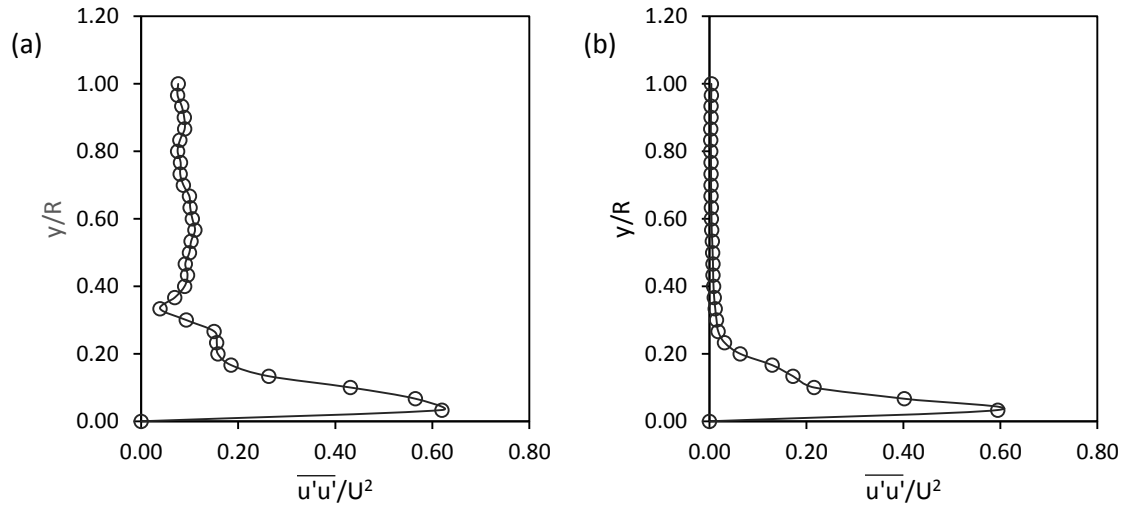

Figure 7.1: The $\overline{u'u'}/U^2$ profile at location (a) 13 *x/D* and (b) 63 *x/D* for pure crude after the pipeline constriction type GC 0.50.

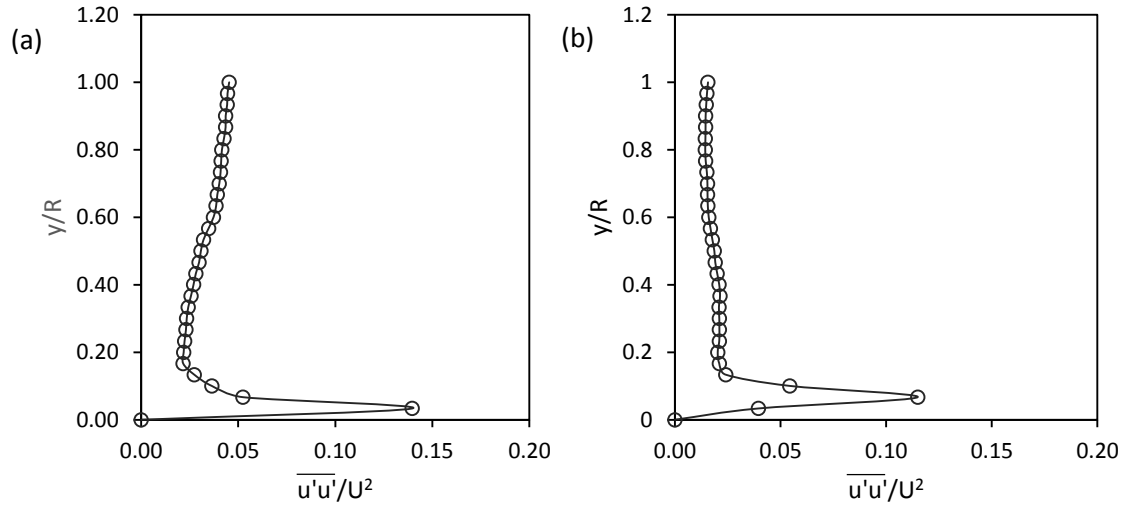

Figure 7.2: The $\overline{u'u'}/U^2$ profile at location (a) 13 *x/D* and (b) 63 *x/D* for 10% WC after the pipeline constriction type GC 0.50.

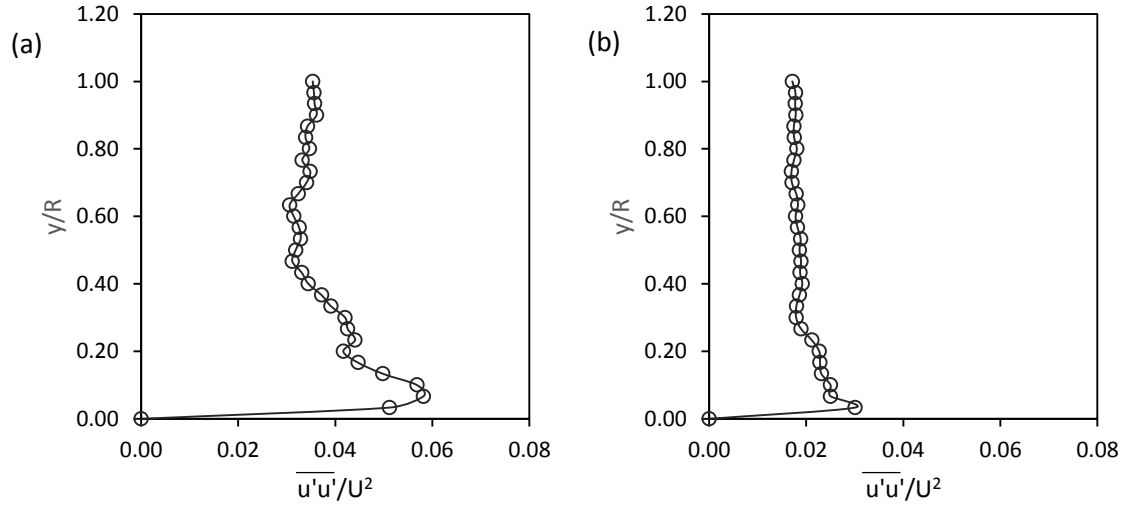

Figure 7.3: The $\overline{u'u'}/U^2$ profile at location (a) 13 *x/D* and (b) 63 *x/D* for 20% WC after the pipeline constriction type GC 0.50.

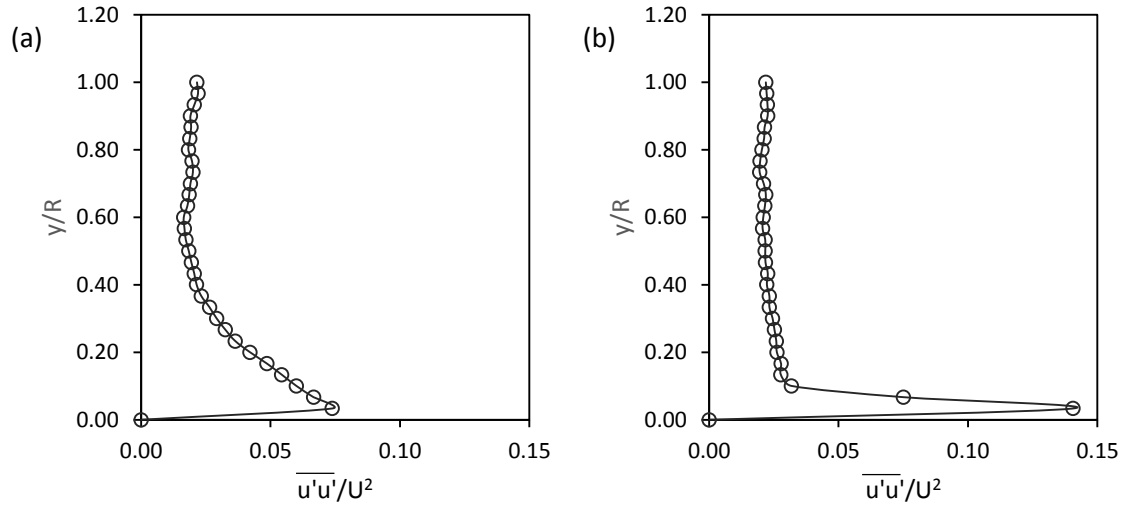

Figure 7.4: The $\overline{u'u'}/U^2$ profile at location (a) 13 *x/D* and (b) 63 *x/D* for 30% WC after the pipeline constriction type GC 0.50.

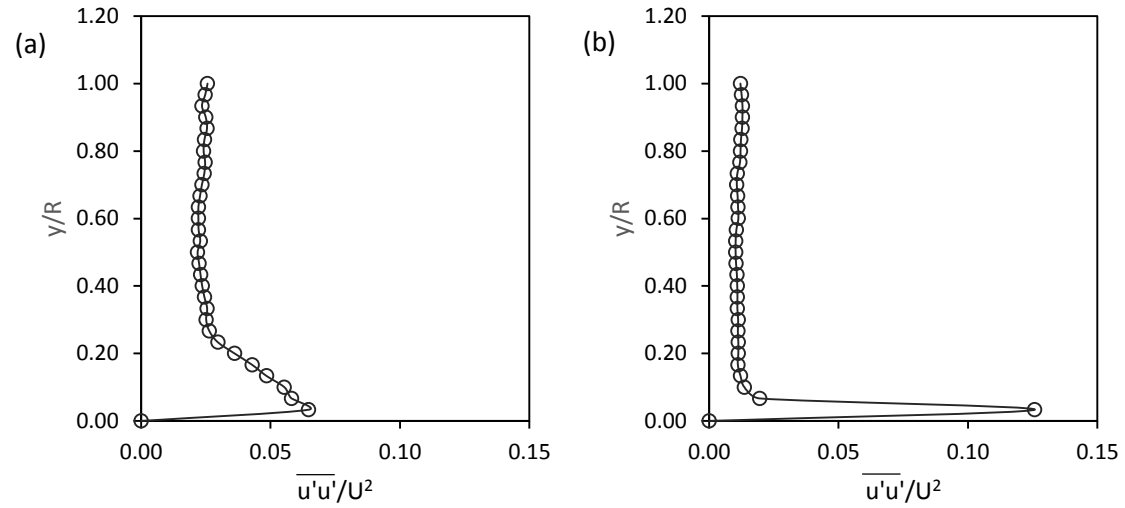

Figure 7.5: The $\overline{u'u'}/U^2$ profile at location (a) 13 *x/D* and (b) 63 *x/D* for 40% WC after the pipeline constriction type GC 0.50.

7.1.2 Reynolds Stress Comparison at Different Water Cuts

The normalized Reynolds stress ($\frac{\overline{u'u'}}{U^2}$) profiles from the sudden constriction 0.50 pipeline with water cuts of 0% to 40% are presented in **Figure 7.6** (a) to **Figure 7.6** (i). The Reynolds stress $\frac{\overline{u'u'}}{U^2}$ used for comparison are obtained from location 63 *x/D* in the pipeline for every water cuts. This is because Reynolds stresses are different in every location of the pipeline, as has been discussed in the previous section. So, for comparison purposes, the location to obtain $\frac{\overline{u'u'}}{U^2}$ is fixed. The $\frac{\overline{u'u'}}{U^2}$ profiles for pipeline constriction type GC 0.50, GC 0.75 and SC 0.75 presents a very similar pattern as the one of SC 0.50 being presented here. Hence, the $\frac{\overline{u'u'}}{U^2}$ profiles for another three types of pipeline constrictions are presented in Appendix E.

From **Figure 7.6** (a) to **Figure 7.6** (i), it is observed that the maximum $\frac{\overline{u'u'}}{U^2}$ decreases with the increase in the water cuts. As presented in **Figure 7.6** (a), the maximum $\frac{\overline{u'u'}}{U^2}$ for 0% WC is 1. As the water cuts increase to 5%, the maximum $\frac{\overline{u'u'}}{U^2}$ reduces to 0.45. With further increase in water cuts, 10% to 40%, the maximum $\frac{\overline{u'u'}}{U^2}$ reduces to about 0.1 to 0.2 only. Besides, it is also determined that the $\frac{\overline{u'u'}}{U^2}$ peak region decreases with the increase in the water cuts. As shown in **Figure 7.6** (a) and (b), for lower water cuts, the $\frac{\overline{u'u'}}{U^2}$ peak region covers up to 0.20 to 0.30 y/R. As the water cuts increases up to 30% and above, the $\frac{\overline{u'u'}}{U^2}$ peak region is reduced to as low as 0.05 y/R (as shown in **Figure 7.6** (g), (h) and (i)).

The $\frac{\overline{u'u'}}{U^2}$ results show that as the water cuts increases, the momentum transfer due to velocity fluctuation components is reduced. Likewise, the fluctuating components become less energetic as the water cuts increases. It has been extensively reported that turbulence suppression is one of the main factors that leads to the decrease in Reynolds stress [123-125]. Lower Reynolds stress indicates that there is less momentum transfer. This is because fluctuating velocity components in the turbulent flow induces lesser kinetic

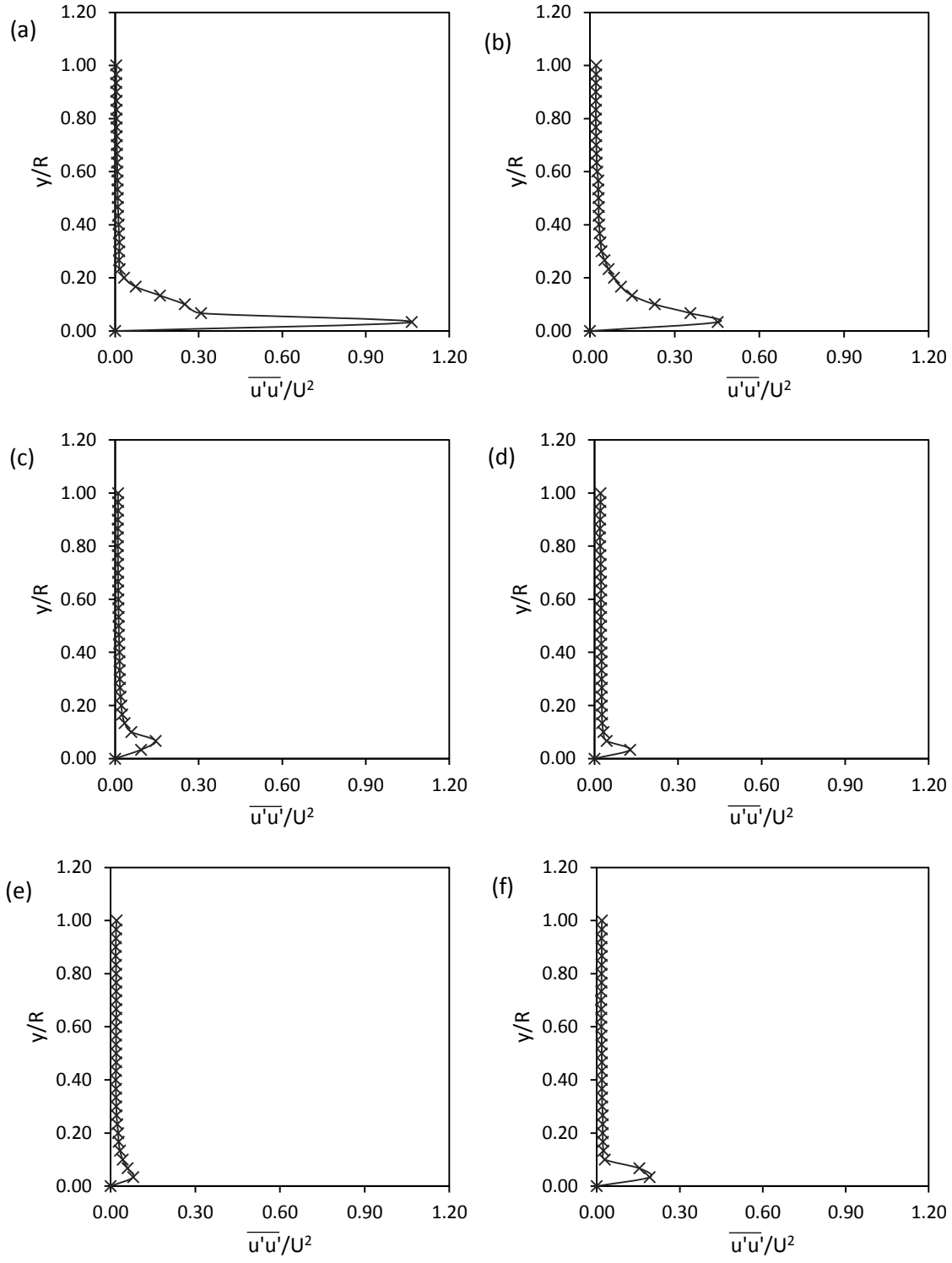
(a)
(b)
(c)
(d)
(e)
(f)
y/R
$\overline{u'u'}/U^2$
0.00
0.20
0.40
0.60
0.80
1.00
1.20
0.30
0.90

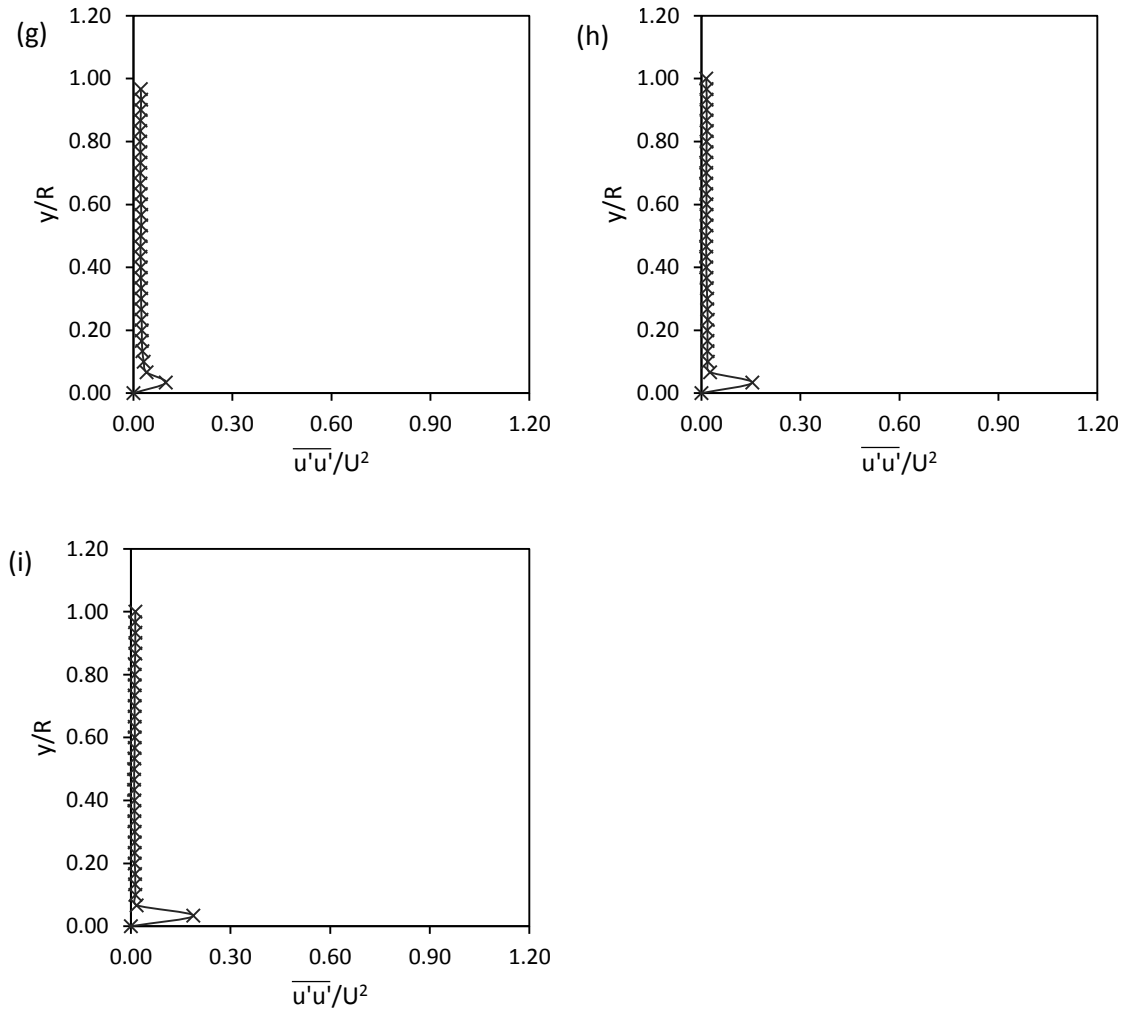

Figure 7.6: The Reynolds stress profile at 63 *x/D* after the pipeline constriction type SC 0.50 at water cuts (a) 0% (b) 5% (c) 10% (d) 15% (e) 20% (f) 25% (g) 30% (h) 35% (i) 40%.

energy. Since the results show that the $\frac{\overline{u'u'}}{U^2}$ decreases with the increase in water cuts, it is logical to suggest that the presence of emulsions is able to suppress the velocity fluctuation in the flow. Since turbulence is due to the fluctuation of the velocity component in the flow and emulsions are capable of suppressing the fluctuation, therefore increase in the water cuts (increase in emulsions) will directly lead to the diminishing of turbulence.

In the previous chapter, the effects of water cuts on τ_w is discussed to be due to the fact that turbulence is diminished as a result of contribution of the turbulence vortices to the dynamic break-up and coalescence of the dispersed droplets in the flow, which eventually leads to the drag-reduction effect and induces lower τ_w at higher water cuts. It is proclaimed that the degree of turbulence diminishing is higher with the presence of higher amount of emulsions (higher water cuts). The $\frac{\overline{u'u'}}{U^2}$ results have strengthened the discussion by evidence that the maximum $\frac{\overline{u'u'}}{U^2}$ is reduced with the increase in the water cuts (increase in the amount of emulsions), which indicates that the fluctuating components are less energetic (higher degree of diminishing of turbulence) as the amount of emulsions increases.

Next, in previous chapter, it also has been discussed that the stability of emulsions increases with the increase in the water cuts. To relate the stability of emulsions with the $\frac{\overline{u'u'}}{U^2}$ results (with the increase in water cuts) obtained in this chapter, it is understood that decrease in the maximum $\frac{\overline{u'u'}}{U^2}$ leads to the increase in the stability of emulsions.

7.2 Turbulence Intensity

Turbulence intensity analysis is used for the study of the turbulence characteristics of emulsified flow because it is a measure used for characterizing the turbulence level in term of percentage. In other words, turbulence intensity allows one to examine the turbulence level in the flow statistically. In this study, turbulence intensity is used to examine the fluctuations of the streamwise velocity component. A larger turbulence

intensity indicates a higher turbulence level and vice versa. In the present work, the turbulence intensity is calculated using Equation 7.1.

$$\text{Turbulence intensity} = \frac{u'}{\overline{U}} \tag{7.1}$$

where u' stands for root-mean-square of turbulent velocity fluctuation and $\overline{U}$ stands for the averaged streamwise mean velocity.

In this section, the turbulence intensity along the pipeline (increase in the pipe length) after the pipeline constriction and the turbulence intensity with respect to different water cuts are compared and discussed. The purpose is to understand the correlation in between the turbulence level of the flow with the emulsification behaviour as well as to confirm the proclamation made in Chapter 6 – an increase in water cuts leads to drag-reduction effect as a result of turbulence diminishing by the presence of emulsions, thereby resulted in the decrease of τ_w.

7.2.1 Turbulence Intensity Comparisons along the Pipeline

Figure 7.7 (a) and (b) to **Figure 7.14** (a) and (b) present the distribution of streamwise turbulence intensity ($\frac{u'}{\overline{U}}$) from the pipeline constriction type GC 0.50 at pipeline location of 13 *x/D* and 63 *x/D*, for 0 to 40% WC respectively. The streamwise $\frac{u'}{\overline{U}}$ profiles for pipeline constrictions of GC 0.75, SC 0.50 and SC 0.75 are presented in Appendix F, where similar profiles are observed. Hence, only one case is discussed here.

From **Figure 7.7** to **Figure 7.14**, it is observed that the streamwise $\frac{u'}{\overline{U}}$ peak region (fluctuation region) at pipeline location 13 *x/D* downstream the constriction is larger than that at the 63 *x/D* downstream constriction. For pure crude, it is determined that the streamwise $\frac{u'}{\overline{U}}$ peak region reduces from 0.35 to 0.25 of the pipe radius (y/R) as the flow flows from 13 *x/D* to 63 *x/D* (as shown in **Figure 7.7**). For emulsified flow with 10%, 15%, 20%, 25%, 30%, 35% and 40% WC, the results show that the $\frac{u'}{\overline{U}}$ peak region reduces from 0.20 to 0.15 y/R, 0.35 to 0.25 y/R, 0.40 to 0.25 y/R, 0.40 to 0.10 y/R, 0.40 to 0.10

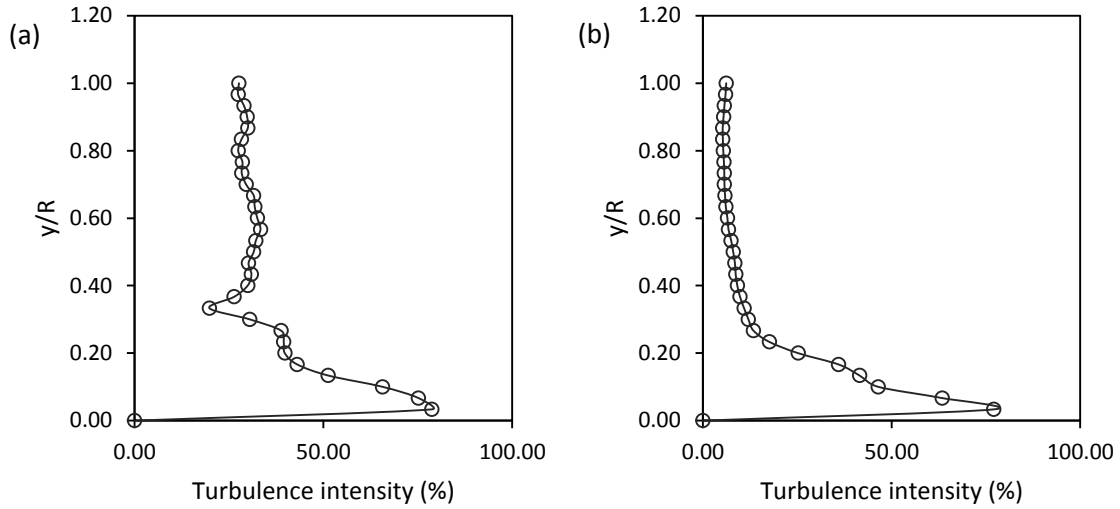

Figure 7.7: Streamwise $u'/\overline{U}$ distribution at (a) 13 *x/D* (b) 63 *x/D* for 0% WC after the pipeline constriction type GC 0.50.

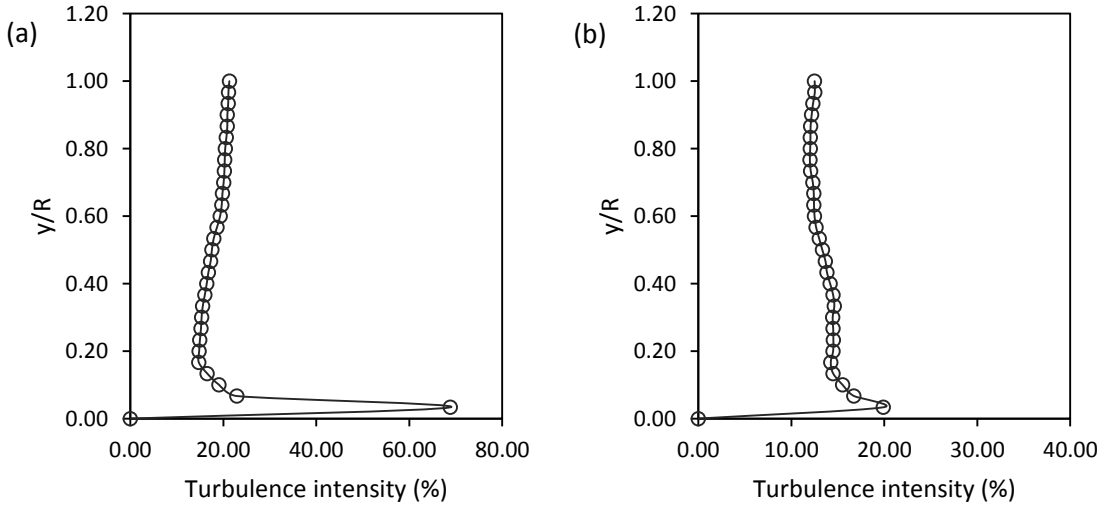

Figure 7.8: Streamwise $u'/\overline{U}$ distribution at (a) 13 *x/D* (b) 63 *x/D* for 10% WC after the pipeline constriction type GC 0.50.

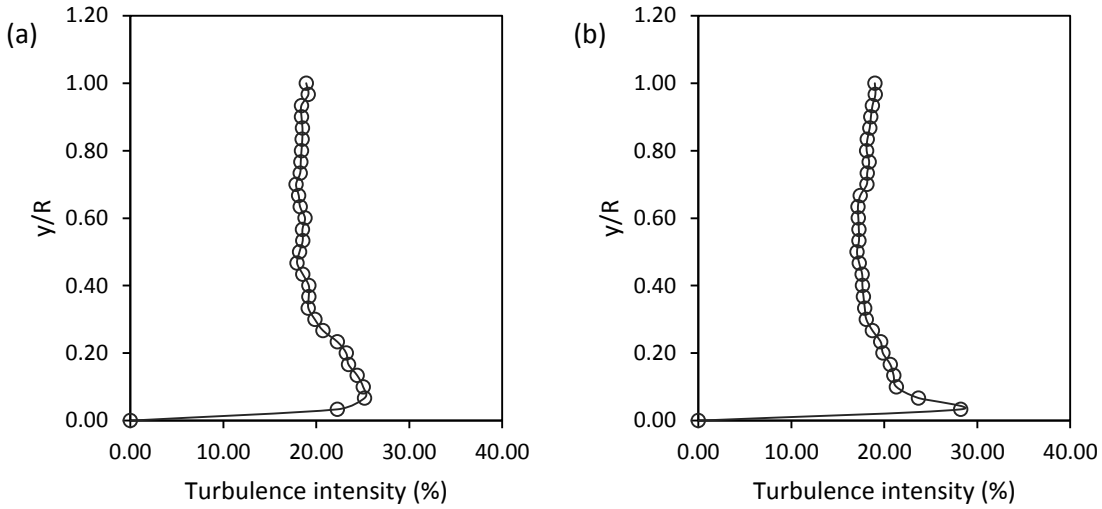

Figure 7.9: Streamwise $u'/\overline{U}$ distribution at (a) 13 *x/D* (b) 63 *x/D* for 15% WC after the pipeline constriction type GC 0.50.

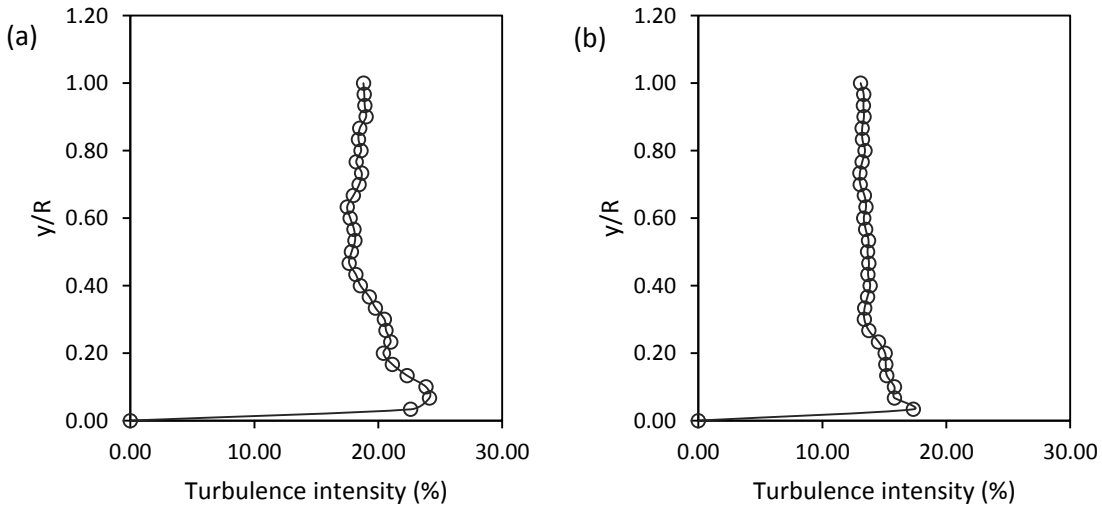

Figure 7.10: Streamwise $u'/\overline{U}$ distribution at (a) 13 *x/D* (b) 63 *x/D* for 20% WC after the pipeline constriction type GC 0.50.

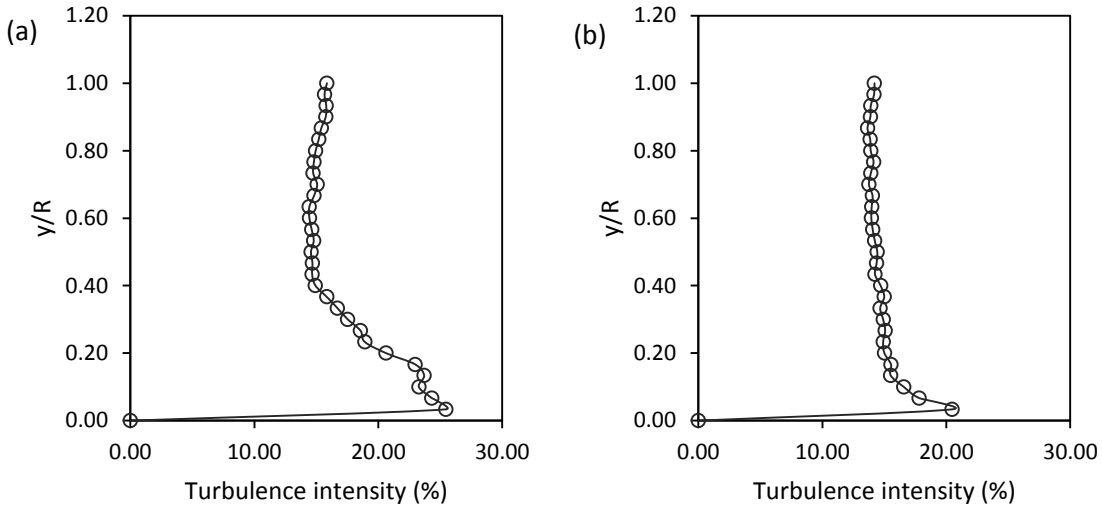

Figure 7.11: Streamwise $u'/\overline{U}$ distribution at (a) 13 *x/D* (b) 63 *x/D* for 25% WC after the pipeline constriction type GC 0.50.

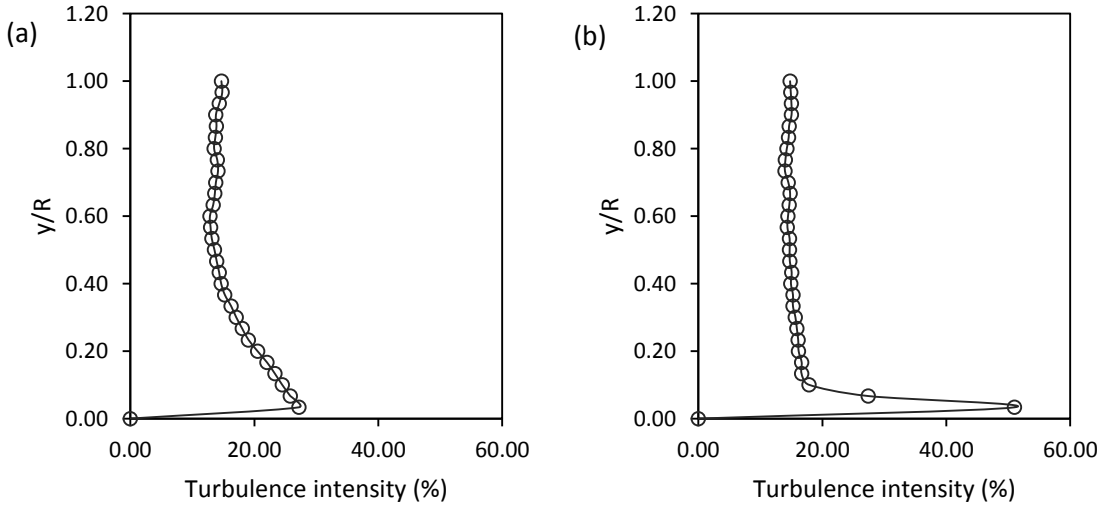

Figure 7.12: Streamwise $u'/\overline{U}$ distribution at (a) 13 *x/D* (b) 63 *x/D* for 30% WC after the pipeline constriction type GC 0.50.

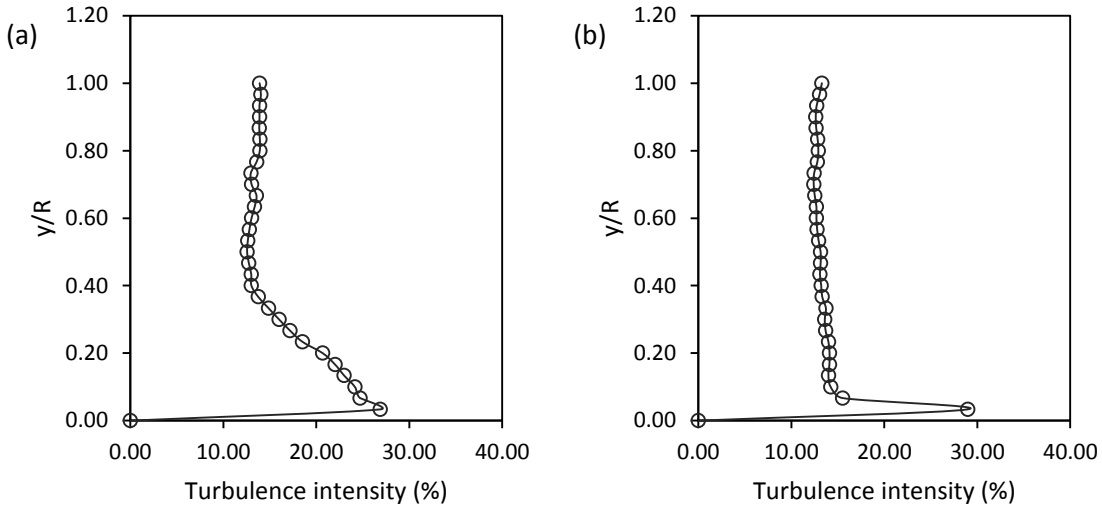

Figure 7.13: Streamwise $u'/\overline{U}$ distribution at (a) 13 *x/D* (b) 63 *x/D* for 35% WC after the pipeline constriction type GC 0.50.

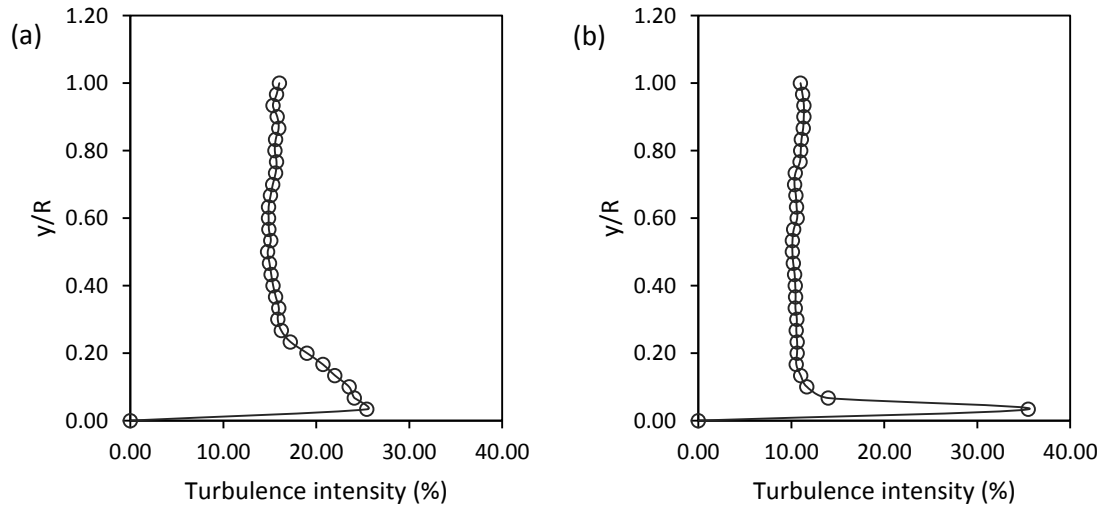

Figure 7.14: Streamwise $u'/\overline{U}$ distribution at (a) 13 *x/D* (b) 63 *x/D* for 40% WC after the pipeline constriction type GC 0.50.

y/R, 0.40 to 0.05 y/R and 0.30 to 0.10 y/R, respectively (as shown in **Figure 7.8** to **Figure 7.14)**.

The reduction in the streamwise $\frac{u'}{\bar{U}}$ fluctuation region as the flow flows further downstream indicates that the turbulence in the flow is diminished. Since the damping of streamwise $\frac{u'}{\bar{U}}$ is observed in both the pure crude and emulsified flow, the result in this section is unable to prove that turbulence in the flow is consumed for the formation of emulsions. However, the results do suggest that turbulence is induced at the constriction of the pipeline. This is because the results show that the streamwise $\frac{u'}{\bar{U}}$ fluctuation region is larger at 13 *x/D*, where this location is the nearest to the constriction of the pipeline.

From the above discussion, it is understood that the streamwise $\frac{u'}{\bar{U}}$ is reduced as the flow flows from 13 *x/D* to 63 *x/D* due to the decaying of turbulence as the flow flows further downstream of the pipeline. However, from **Figure 7.7** to **Figure 7.14**, it is observed that comparison between the maximum streamwise $\frac{u'}{\bar{U}}$ at 13 *x/D* and 63 *x/D* does not present a constant pattern. As shown in **Figure 7.7**, the maximum streamwise $\frac{u'}{\bar{U}}$ of pure crude at these two locations are nearly the same. For 10%, 20% and 25 % WC, the results show a decrease in the maximum streamwise $\frac{u'}{\bar{U}}$; for 15%, 30%, 35% and 40% WC, the results show an increase in the maximum $\frac{u'}{\bar{U}}$. This is most likely due to unequal distribution of energy between the fluctuation components. One of the fluctuating component, either u, v or w component gains energy from the mean flow. Then, the energy is redistributed among these fluctuating components. According to Brasseur and Lee [126], the pressure-strain-rate term is used for the inter-component energy transfer in the turbulent flow. The pressure-strain-rate term is one of the terms of Reynolds Stress Transport equations, which accounts for the redistribution of energy in between the fluctuating components so that the decaying turbulence is brought to isotropy. It happens during the interactions amongst the fluctuating components. Due to the function of this term, all the three components would have about the same order of kinetic energy magnitude, except when it is very close to the surface. This is because when it comes to very near to the surface, the normal fluctuation component will be suppressed by the kinematic boundary condition thereby

leading to an unequal distribution of energy near the pipe wall. Hence, the comparisons for maximum streamwise $\frac{u'}{\overline{U}}$, which is located at very near to the pipe wall among different water cuts, do not give a constant pattern; neither increasing nor decreasing with the changes in water cuts.

Next, from these figures, it can be seen that the maximum streamwise $\frac{u'}{\overline{U}}$ is located at approximately 0.05 y/R from the pipe wall. The location of maximum streamwise $\frac{u'}{\overline{U}}$ is shown to remain the same at 0.05 y/R for both the 13 *x/D* and 63 *x/D* despite the changes in the streamwise $\frac{u'}{\overline{U}}$ peak region. This indicates that the damping of turbulence intensity near the pipe wall is always the least, resulting in the highest fluctuation near to the pipe wall.

7.2.2 Turbulence Intensity Comparisons at Different Water Cuts

The distribution of streamwise turbulence intensity ($\frac{u'}{\overline{U}}$) profiles for 0% to 40% WC at 13 *x/D* is presented in **Figure 7.15** (a) to (i). As mentioned earlier in this chapter, the turbulence intensities at different water cuts are calculated and compared in order to determine the correlation between the turbulence level and the emulsions formed in the flow. More specifically, it is to understand the relationship between the amounts of emulsions formed in the pipeline with the turbulence level. This is because the τ_w results in Chapter 6 have suggested that the presence of emulsions is capable of diminishing the turbulence in the flow.

Figure 7.15 (a) to (i) clearly shows that the maximum streamwise turbulence intensity decreases with the increase in the water cuts from 0% to 40%. With the increase in water cuts from 0% to 40%, the maximum streamwise turbulence intensity decreases from 100% to about 25% only. The decrease in the maximum streamwise turbulence intensities with the increase in water cuts indicates that the turbulence level in the flow with higher water cuts is lower. This is because at higher water cuts, the amounts of emulsions formed are higher as well. As a result of that, the frequency of emulsion-emulsion collision is increased due to the increase in the compactness of the emulsions in the flow. This is

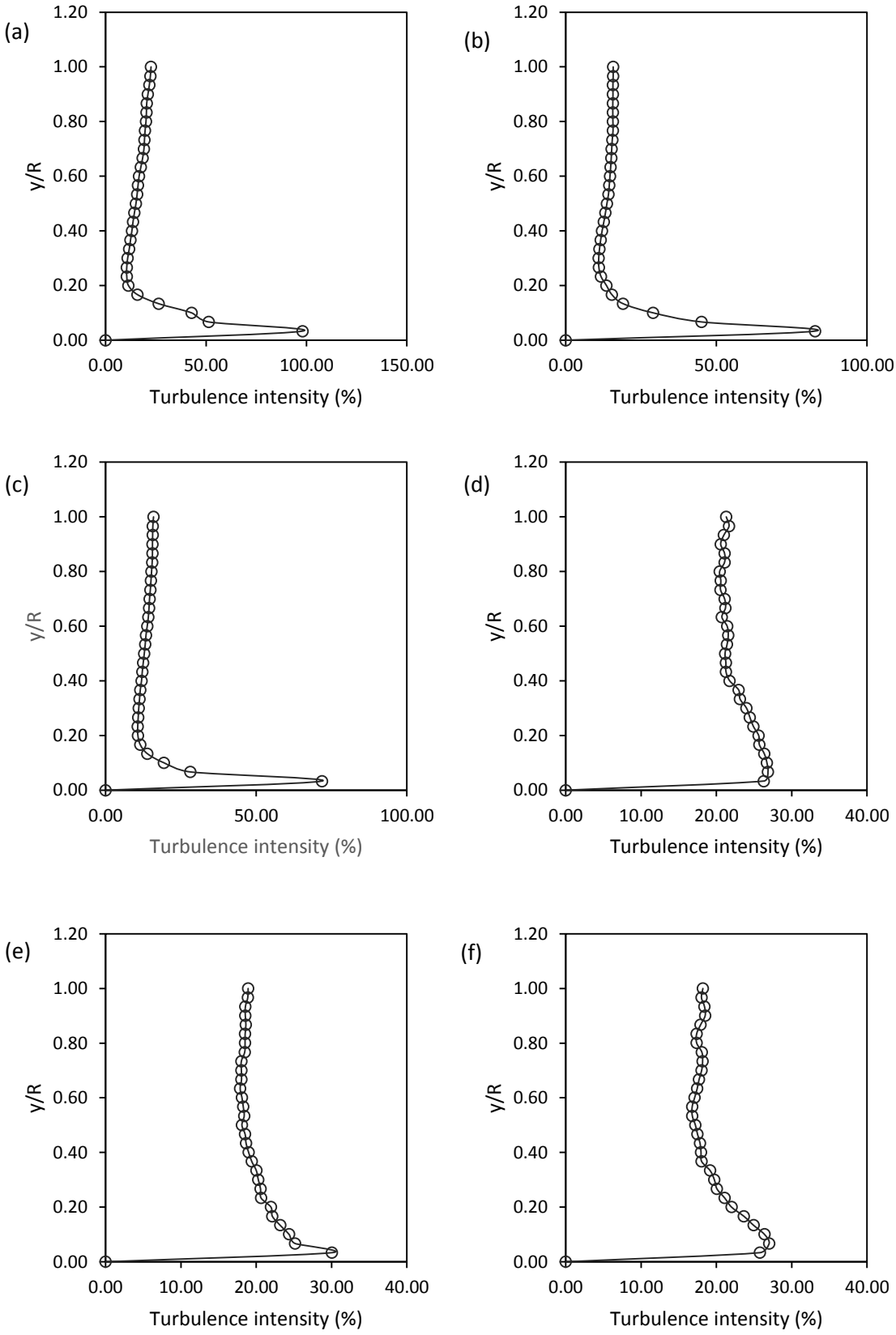
(a)
y/R
Turbulence intensity (%)
(b)
y/R
Turbulence intensity (%)
(c)
y/R
Turbulence intensity (%)
(d)
y/R
Turbulence intensity (%)
(e)
y/R
Turbulence intensity (%)
(f)
y/R
Turbulence intensity (%)

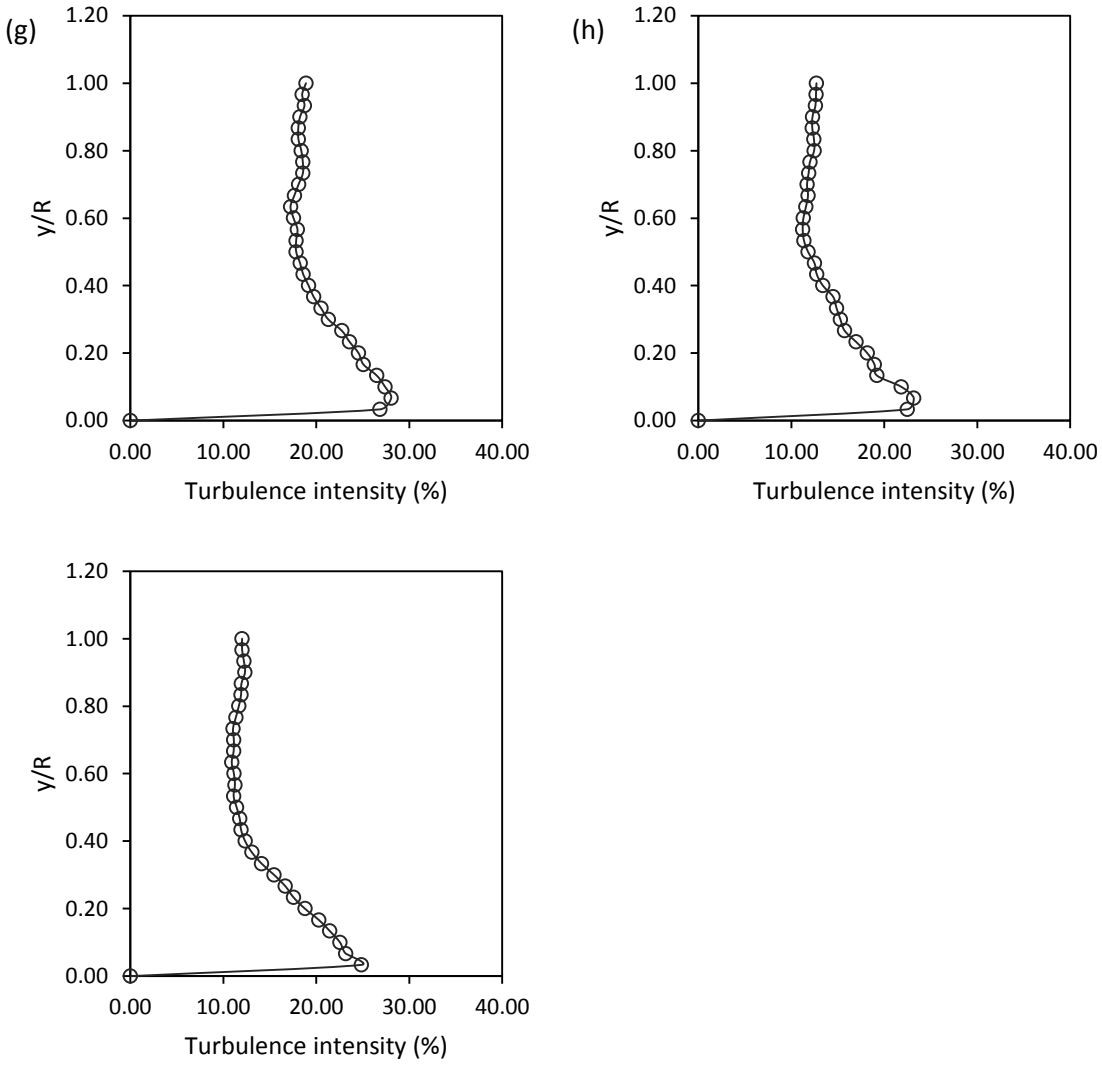

Figure 7.15: Streamwise turbulence intensity distribution for pipeline constriction SC 0.75 at (a) 0% (b) 5% (c) 10% (d) 15% (e) 20% (f) 25% (g) 30% (h) 35% (i) 40% WC.

supported by Varaksin *et. al.* [127] whose report has stated that the intensive exchange of momentum between the particles during the particle-particle collisions will lead to the proximity of their velocities, resulting in the decrease of the velocity fluctuation. This means that an increase in the water cuts (amount of emulsions) will lead to the decrease in the velocity fluctuation owing to more exchange of momentum between the emulsions. Thus, the turbulence level in the flow reduces with the increase in the input of water cuts, as presented by the results shown here. The results suggest that the presence of emulsions diminishes the turbulence in the flow. As a result of diminishing in turbulence, drag in the flow is reduced, leading to a drag the reduction effect with the increase in the water cuts. This has confirmed the discussion in the previous chapter that the drag reduction phenomenon is caused by the diminishing in turbulence due to the presence of emulsions.

Besides, the results also show that the flow with 0% to 10% WC presents a much higher turbulence level as compared to the flow with 15% to 40% WC. From 0% to 5% WC, the maximum streamwise turbulence intensity decreases from 100% to 83%. From 5% to 10% WC, the maximum streamwise turbulence intensity decreases from 83% to 73%. Beyond 10% WC (15% to 40%), the maximum streamwise turbulence intensities reduce drastically to about 25% only. This indicates that the turbulence diminishing behaviour is much stronger when the water cuts reaches 15% and above. Through the above analysis, it is concluded that the water cuts (amount of emulsions present in the flow) can alter the fluid flow significantly. For water cuts of 5% to 10%, the presence of emulsions lowers the turbulence level by 20% to 30% only; but for water cuts of 15% and above, the turbulence level is decreased by about 75% as compared to the pure crude (0% WC). This indicates that emulsions from 5% to 10% WC consume much lesser turbulence compared to that of 15% to 40%. Relate this to the τ_w results presented in Chapter 6, it is understood that the increase in τ_w for water cuts from 0 to 10% is due to the presence of higher turbulence energy in the flow. Meanwhile, for water cuts above 10%, it is evidently shown that the turbulence level is greatly reduced. This confirms the discussion made in the previous chapter that an increase in the amounts of emulsions leads to a decrease in the turbulence level (drag-reduction effect).

Next, the streamwise turbulent intensities results also provide an understanding of the changes in τ_w with the variations in water cuts. As can be understood from the results, the reduction in maximum streamwise turbulent intensities by about 30% as compared to the turbulent intensity of pure crude does not induce the reduction in τ_w. The τ_w is shown to increase with the increase in emulsions (up to 10% water cuts) regardless of the reduction in turbulent intensity of about 30%. However, as the turbulent intensity reduced by 75% as compared to the turbulent intensity of pure crude, a significant effect on the τ_w is determined. As presented in the previous chapter, the τ_w has shown a sudden reduction at 15% water cuts, where turbulent intensity is reduced by 75% as compared to pure crude oil.

Another observation made from **Figure 7.15** (a) to (i) is, the pattern of streamwise turbulence intensity profiles of 0% to 10% WC differs from the one of water cuts beyond 10%. As shown in **Figure 7.15** (a) to (c), for 0 to 10% water cuts, the streamwise turbulence intensities are increased gradually towards the 1.0 y/D (center of the pipe) after the peak region near to the pipe wall. On the other hand, for 15% to 40% WC, the streamwise turbulence intensities remain constant after the peak region. This shows that by observing the streamwise turbulence intensities in terms of the cross-sectional area of the pipe for different water cuts, the overall flow is getting less fluctuation when the input of water cuts is higher than 10%.

In Chapter 5, it has been presented that the stability of emulsions increases with the increase in the water cuts. Meanwhile in this section, it has been clearly presented that the maximum streamwise turbulence intensity decreases with the increase in the water cuts from 0% to 40%. By correlating both of these results, it is understood that the decrease in the maximum streamwise turbulence intensity results in the increase of emulsions stability.

7.3 Summary of Chapter

In order to confirm the postulation made in the previous chapter that turbulence is diminished with the increase in the water cuts (increase in the amount of emulsions), this chapter has investigated the turbulence characteristics statistically. The normalized Reynolds stress ($\frac{\overline{u'u'}}{U^2}$) and the streamwise turbulence intensity ($\frac{u'}{\bar{U}}$) are analyzed. The results presented in this chapter provide an insight into the roles or contribution of turbulence in the emulsification process. Through the examination on the $\frac{\overline{u'u'}}{U^2}$ and $\frac{u'}{\bar{U}}$, it has been demonstrated that the turbulence is the source for the formation of emulsions and turbulence is induced from the constriction of pipeline. Both the $\frac{\overline{u'u'}}{U^2}$ and $\frac{u'}{\bar{U}}$ have shown to support the discussion made in the Chapter 6.

CHAPTER 8

CONCLUSIONS AND RECOMMENDATIONS

This chapter concludes the key findings on the characterization of W/O emulsions, effect of emulsions to the pipeline flow and the turbulence characteristics of emulsified flow. This chapter also covers the recommendations for future work in this research area.

8.1 Conclusions

Emulsions Characterization Study

The rheological behaviour of Miri light crude (MLC) is examined. It is determined that MLC is a Newtonian fluid. The viscosity remains constant at 0.00733 Pa.s at shear rates of 0 to1000 s^{-1}. Next, the rheological behaviour of emulsions and stability of the W/O emulsions are studied. The emulsions are shown to exhibit a non-Newtonian fluid property, which is, shear-thinning behaviour at shear rates below 200 s^{-1} (for 5-30% WC) and 350 s^{-1} (for 35 – 90% WC). Above the stated shear rates for the respective water cuts, the emulsions are shown to exhibit Newtonian fluid property. Besides, from the rheological study, it is determined that phase inversion of MLC from W/O emulsions to O/W emulsions happens at 40% WC.

From the study of the stability of W/O emulsions, it is concluded that the stability of the emulsions increases with the increase in the water cuts and flow rate. Also, it is determined that the emulsions formed from the pipeline constriction type GC 0.50 and SC 0.50 are more stable than the emulsions formed from GC 0.75 and SC 0.75.

For the study on the formation of emulsions based on the amount of emulsions formed, it is concluded that the amount of emulsions formed increases with the increase in the water cuts and flow rate. The amount of emulsions formed from different types of pipeline constriction could not be determined, which is most likely due to the difference in the amount of emulsions is too small to be captured visually.

Effect of W/O Emulsions on Wall Shear Stress

From the time-averaged streamwise velocity profiles measured at different location at the horizontal pipeline, it is determined that the flow is induced to turbulent flow after the constriction. With the increase in the input of water cuts, the representation of turbulent flow is more significant as the velocity profiles become less parabolic and flatter.

Next, the wall shear stress (τ_w) is calculated by using the velocity gradient at the pipe wall obtained from the time-averaged streamwise velocity profiles. Based on the analysis, it is concluded that the τ_w increases with the increase in the water cuts from 0 to 10% (laminar inlet flow) and 5 to 10% (transitional inlet flow). Above 10% WC, the τ_w decreases with the increase in the water cuts, up to 40% (for laminar inlet) and up to 20% (for transitional inlet). The decrease in the τ_w is due to drag reduction phenomenon, which is believed to be caused by the dying of turbulence as a result of dynamic break-up and coalescence of the dispersed droplets in the flow.

Besides, it is determined that the τ_w of emulsified flow is lower for the inlet flow with higher velocity. This is because higher velocity (higher energy) results in dispersed droplets of smaller size due to higher dissipation energy. As a result of smaller size dispersed droplets, lower friction is induced, resulting in lower τ_w.

Furthermore, it is determined that pipeline constriction with a contraction ratio of 0.50 results in a lower τ_w as compared to the contraction ratio of 0.75 for both the laminar and transitional inlet flow. This phenomenon is because of the smaller pipeline diameter offering higher shearing rates, which then resulted in smaller dispersed droplet size. Again, with dispersed droplets of smaller size, the friction factor is lower, and hence resulted in lower τ_w in pipeline constriction of smaller diameter (contraction ratio of 0.50). Meanwhile, comparison between pipeline with the gradual contraction and the sudden contraction showed that sudden contraction resulted in higher τ_w than the gradual contraction. This is due to more emulsions that are produced in sudden constriction

pipeline because of higher energy loss in the flow. More emulsions lead to the increase in the collision rate, bringing about an increase in the shear and in turn results in the higher τ_w.

Moreover, it is examined that the τ_w increases with the increase in the length of the pipe after the constriction (from 13 *x/D* to 63 *x/D*). This is because dispersed droplets tend to re-coalesce and formed a larger droplet as the flowing fluid flows downstream the pipeline (away from the dispersing zone). As a result of larger droplets, the total surface area of dispersed water droplets is reduced and thereafter resulted in higher τ_w.

Turbulence Characteristics Study of the Emulsified Flow

In the study of turbulence characteristics of emulsified flow, the normalized Reynolds stress ($\frac{\overline{u\prime u\prime}}{U^2}$) and the streamwise turbulence intensity ($\frac{u\prime}{\bar{U}}$) are investigated. They are investigated in order to confirm the discussion in the previous chapter. From the $\frac{\overline{u\prime u\prime}}{U^2}$ and $\frac{u\prime}{\bar{U}}$ analysis, it was confirmed that pipeline constriction is where the turbulence was produced. Next, the results have shown that turbulence in the flow decreases with the increase in the input of water cuts (increase in the emulsions formed). This proved that the turbulence in the flow is the source for the formation of emulsions, with which the more the emulsions formed, the more turbulence is consumed, thereby resulting in lower turbulence level with the increase in the input of water cuts.

On the whole, the results obtained from this research study will enable the oil industry to provide a better strategy in treating the emulsification phenomena in the pipeline transportation system. In Malaysia offshore brownfields, most of the transporting pipelines carry around 10% to 50% of water [128]. As stated before, emulsions bring a number of negative effects to the industry. Although water cuts present in the crude oil from offshore brownfield could not be controlled, effect of emulsions to the transportation can still be controlled by varying the Reynolds number (through flow rate) and types of choke valves (represents using the pipeline constrictions in this study) use. From this study, it is recommended the crude oil be delivered at a higher Reynolds number (higher

flow rate). Pipeline constrictions used in this study, which serves to replicate the usage of choke valves in the oil and gas industry have shown that gradual constriction with contraction ratio of 0.50 (GC 0.50) is the best amongst the four different types of constrictions used for comparison. Higher Reynolds number and pipeline constriction type GC 0.50 are suggested to be used because they result in the lowest wall shear stress. Lower wall shear stress is desirable because lower wall shear stress indicates lower friction in the flow and therefore pressure drop in the flow can be reduced. This helps in minimizing the energy losses during the transportation of crude in the pipeline.

8.2 Recommendations

Throughout the course of this study, a few recommendations for future research have been identified.

The first recommendation is to improve the experimental rig. In this study, experiments were terminated once the increase in temperature was more than 15 ℃. The experiments can only be resumed after the temperature was reduced to room temperature. So, it is recommended that a temperature control system be installed to the current experimental rig. This improvement will not only reduce the period of experimentations, it will also provide a more consistent result because temperature difference would have had an effect on the properties of the fluid.

Next, it is recommended that different types of pure crude be examined, *e.g.* heavy crude, using the same controlling parameters of this study. This would allow a direct comparison to be made between light crude and heavy crude.

In this research, only one velocity component was measured owing to the number limitation of UVP probe. To have a statistical result that can better represent turbulent flow, it is recommended that two or three-dimensional velocity measurements be carried out. This is because by measuring two or three velocity components, parameters such as Reynolds stress tensor and turbulence intensity from more velocity components can be determined. Also, turbulence production terms can be calculated so that the turbulence energy in the flow can be correlated with the behaviour of emulsions in the pipeline flow.

Furthermore, it is recommended to study the droplet breakage mechanism (microscopic study) in order to have a better understanding or explanation for the emulsions formation as well as the emulsions stability.

Last but not least, it is also recommended to carry out optimization study for the parameters – Reynolds number and pipeline constriction types, in order to determine the optimum case for producing least stable emulsion and at the same time resulting in the lowest wall shear stress.

APPENDIX A

Table A.1: Flow meters comparison.

No	Vendor Name	Flow Meter Type	Price	Remarks	Reason of Technical Rejection
1	Moseb Engineering	Macnaught Oval Gear Flowmeter With digital meter and totalizer Model: MX25S-1SD	RM 5740 (Delivery in 4 – 6 weeks)	Flow Range: 6 – 120 LPM Body: Steel Rotor: PPS Seal: Viton Port Size: 1" BSP Female Accuracy: +- 0.5% of reading Repeatability: +- 0.003% Temperature limit of 80 °C Max pressure of 2000 psi (137.895 bar)	REJECTED. Max measured flow is only 120 LPM. This is lower than the flow velocity of 1 m/s in our flow loop (equivalent to 121.53 LPM).
2	Moseb Engineering	A100 GPI Digital Type Meter With flowrate and totalizer display Light weight and compact design, turbine meter	RM 3140 (Stock Available)	Flow Range: 10 – 190 LPM Body: Aluminum Rotor: PVDF Bearing: Ceramic Shaft: Tungsten Carbide Rings: SS 316 Port Size: 1" NPT Accuracy: +- 1.5% of reading Repeatability: +- 0.2%	NA

				Temperature limit of 121 °C Max pressure of 300 psi (21 bar)	
3	Forwell O & G	Fill-Rite Mechanical Flowmeter Model: 901L1.5	RM 1450 (Stock Available)	Flow Range: 23 – 151 LPM Body: Aluminum Seal: Viton & Buna Internal: SS & Polyester Port Size: 1.5" NPT Temperature limit of 121 °C Max pressure of 50 psi (3.5 bar)	REJECTED. Min measured flow is only 23 LPM. This is higher than the flow velocity of 0.1 m/s in our flow loop (equivalent to 12.17 LPM). Also, mechanical flow meter has very low accuracy and sensitivity.
4	Forwell O & G	Fill-Rite, TN Series Mechanical Flowmeter High Pressure and Viscosity Model: TN860AN1CAB1LAC	RM 5780 (Delivery in 6 – 10 weeks)	Flow Range: Max 209 LPM Seals: Fluorocarbon Port Size: 1.5" NPT Accuracy: +- 2% of reading Repeatability: +- 0.25% Temperature limit of 121 °C Max pressure of 150 psi (10 bar)	NA
5	Pascal Control	TRIMEC 1" Aluminum PD oval gear type flow meter	RM 5175 (Stock Available)	Flow Range: 10 – 150 LPM Body: Aluminum	NA

	Model: MG025A-001-211-RT40 RT40 large LCD flow rate totalizer (Allloy housing)	Rotor: PPS – Teflon filled O-ring: Viton Port Size: 1” BSP Female Threaded Accuracy: +- 0.5% of reading Repeatability: +- 0.03% Temperature limit of 120 °C Max pressure of 435 psi (30 bar)

APPENDIX B

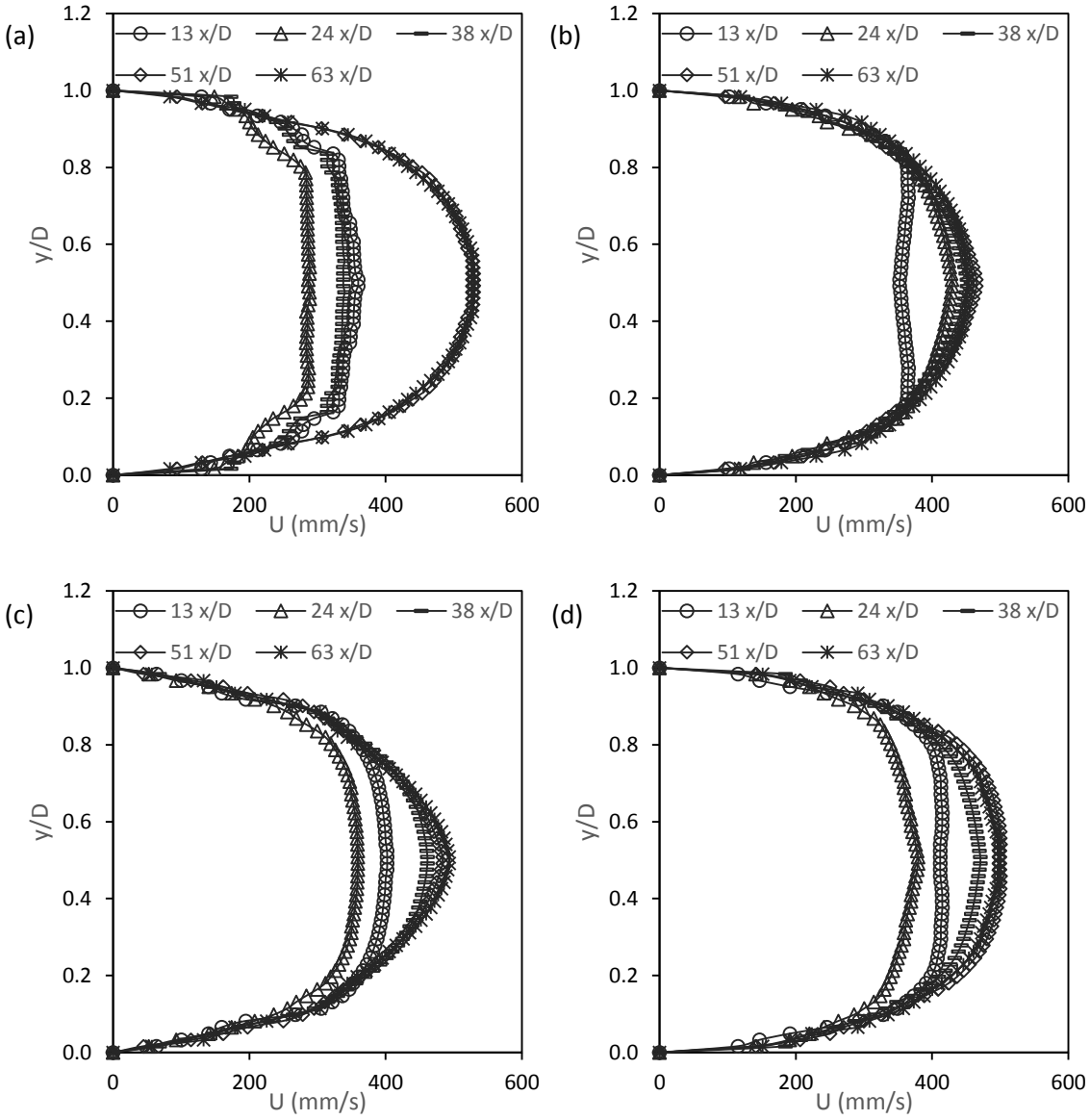

Figure B.1: Time-average streamwise velocity profile for flow with pure crude at pipeline constriction of (a) GC 0.50 (b) GC 0.75 (c) SC 0.50 (d) SC 0.75.

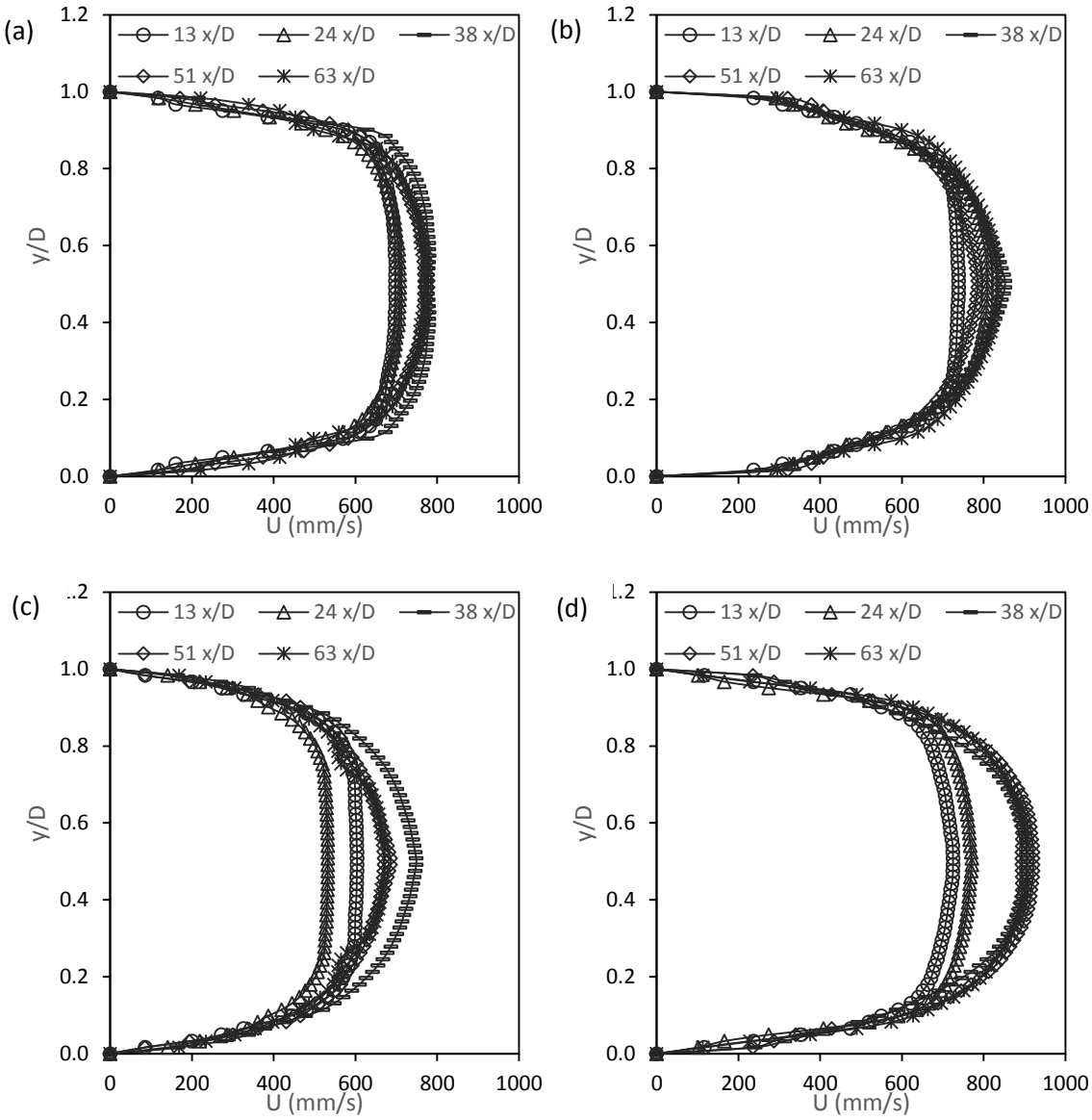

Figure B.2: Time-average streamwise velocity profile for flow with 5 % water cuts at pipeline constriction of (a) GC 0.50 (b) GC 0.75 (c) SC 0.50 (d) SC 0.75.

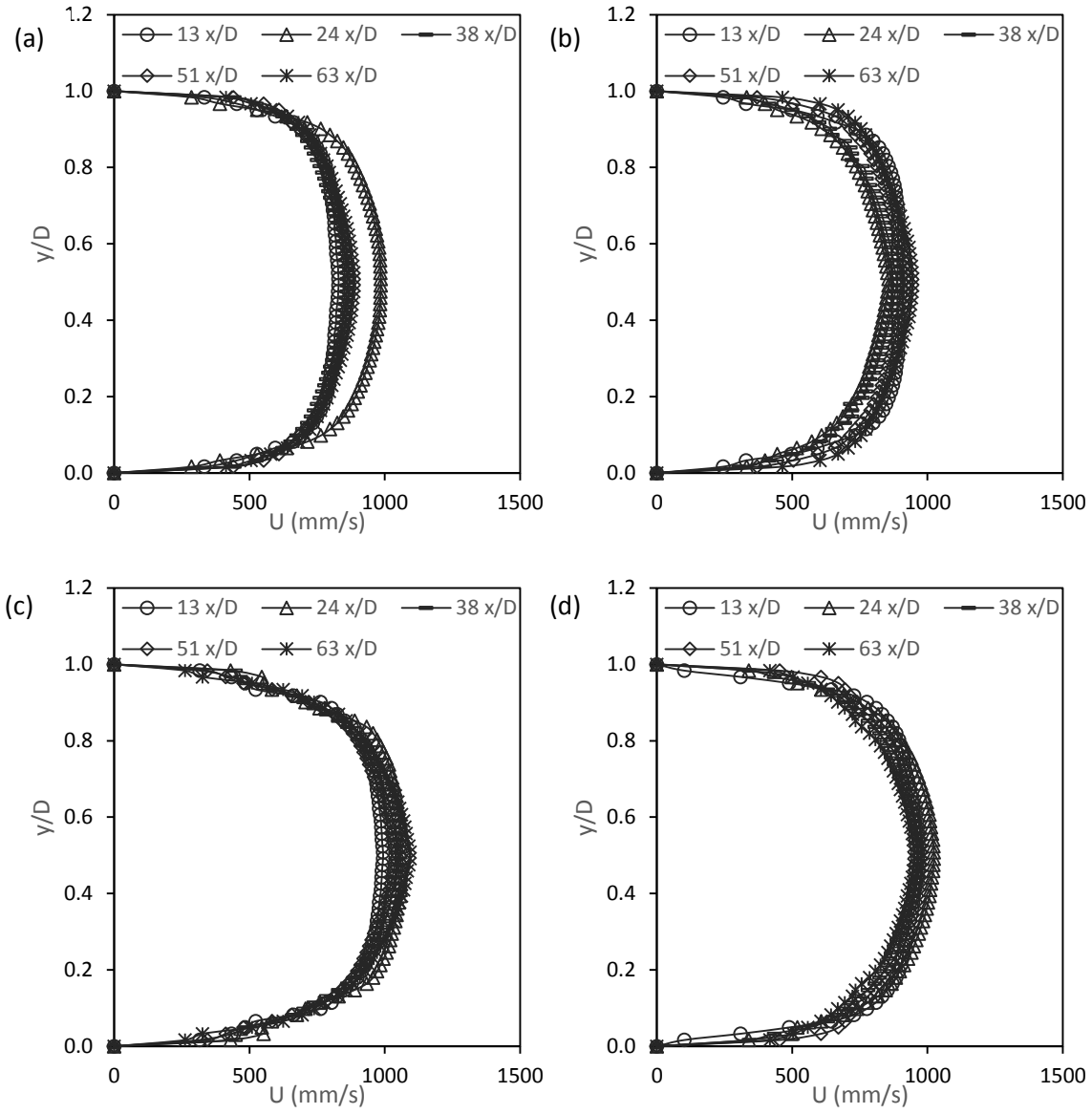

Figure B.3: Time-average streamwise velocity profile for flow with 10 % water cuts at pipeline constriction of (a) GC 0.50 (b) GC 0.75 (c) SC 0.50 (d) SC 0.75.

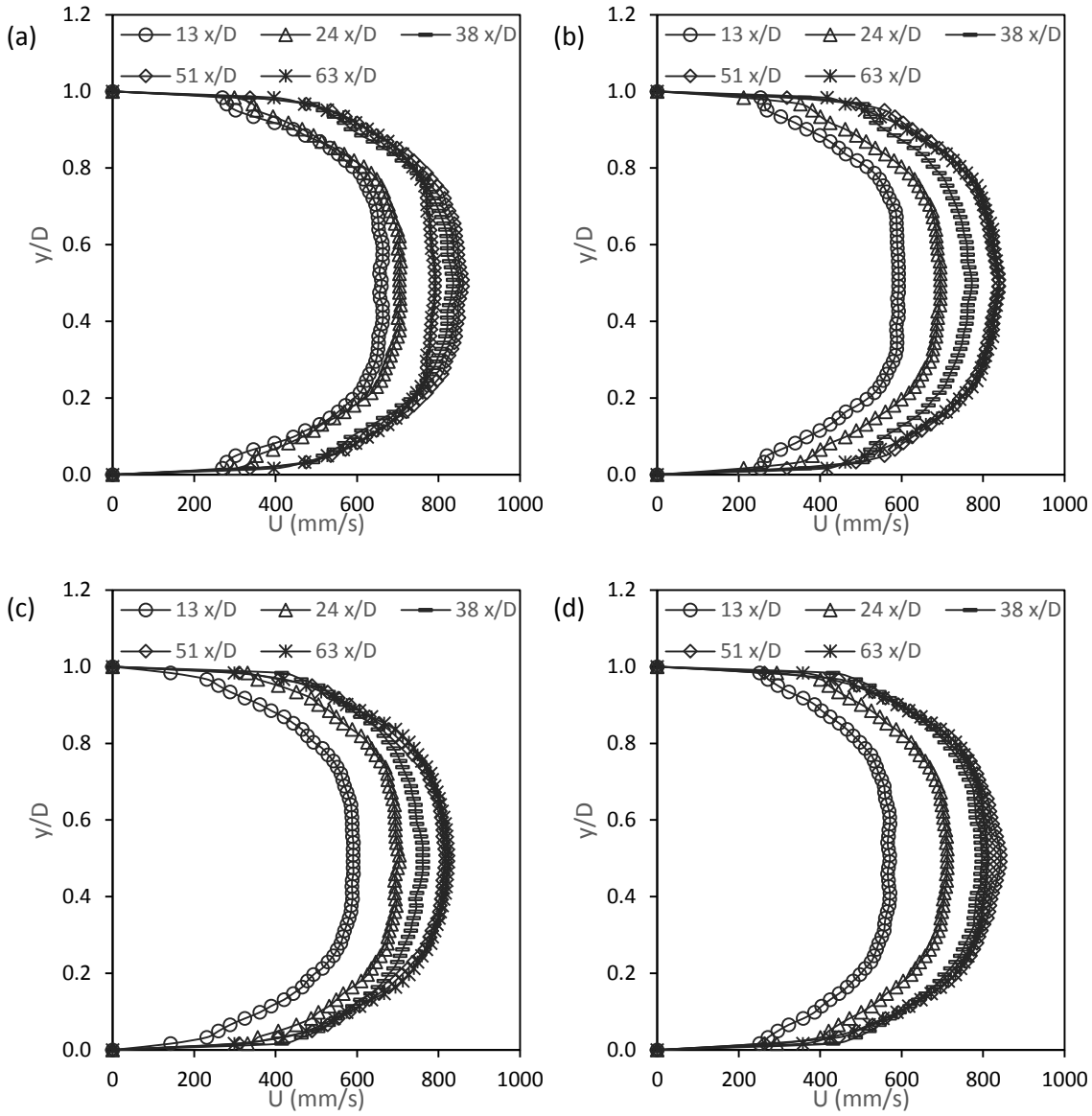

Figure B.4: Time-average streamwise velocity profile for flow with 15 % water cuts at pipeline constriction of (a) GC 0.50 (b) GC 0.75 (c) SC 0.50 (d) SC 0.75.

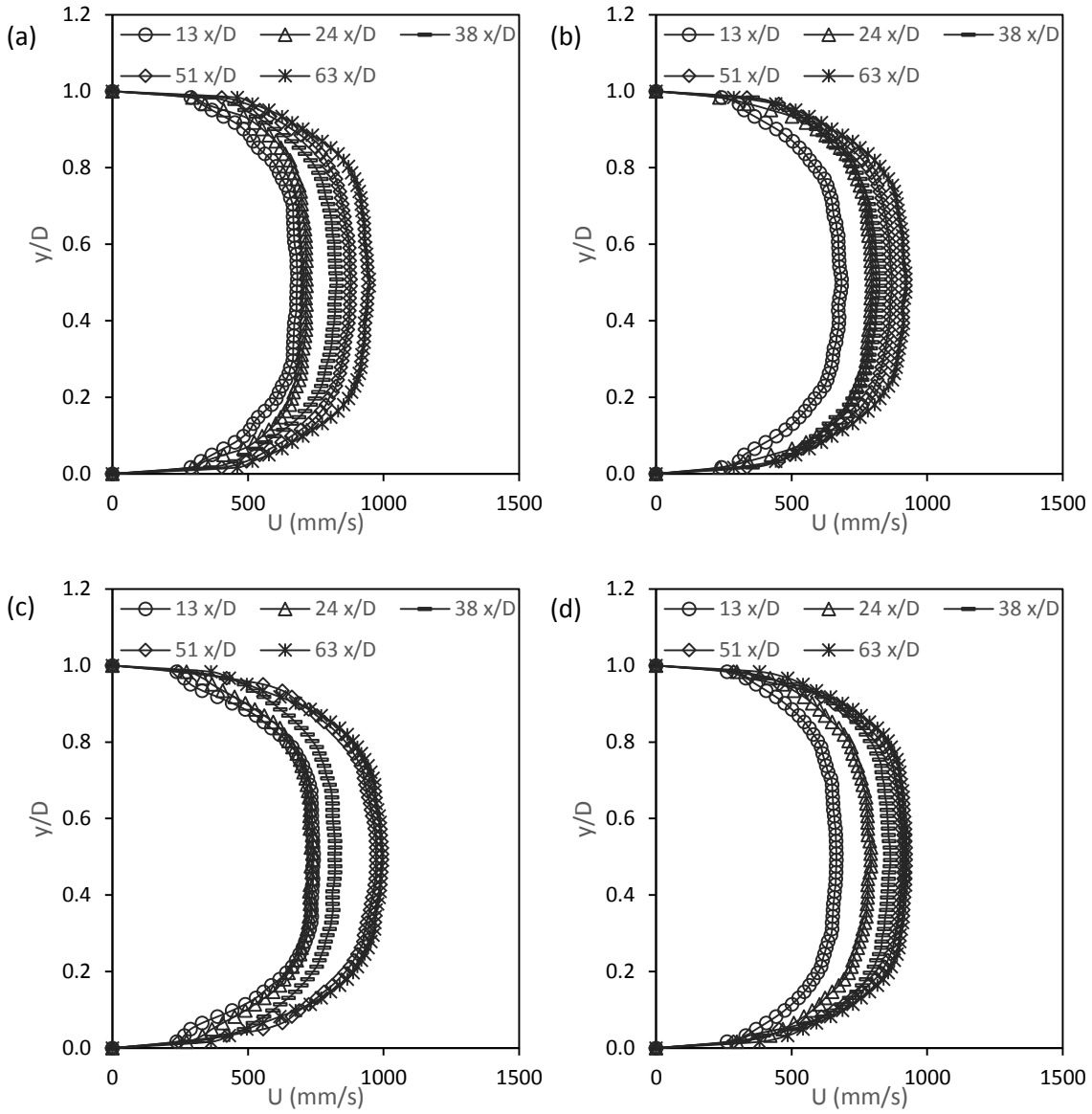

Figure B.5: Time-average streamwise velocity profile for flow with 20 % water cuts at pipeline constriction of (a) GC 0.50 (b) GC 0.75 (c) SC 0.50 (d) SC 0.75.

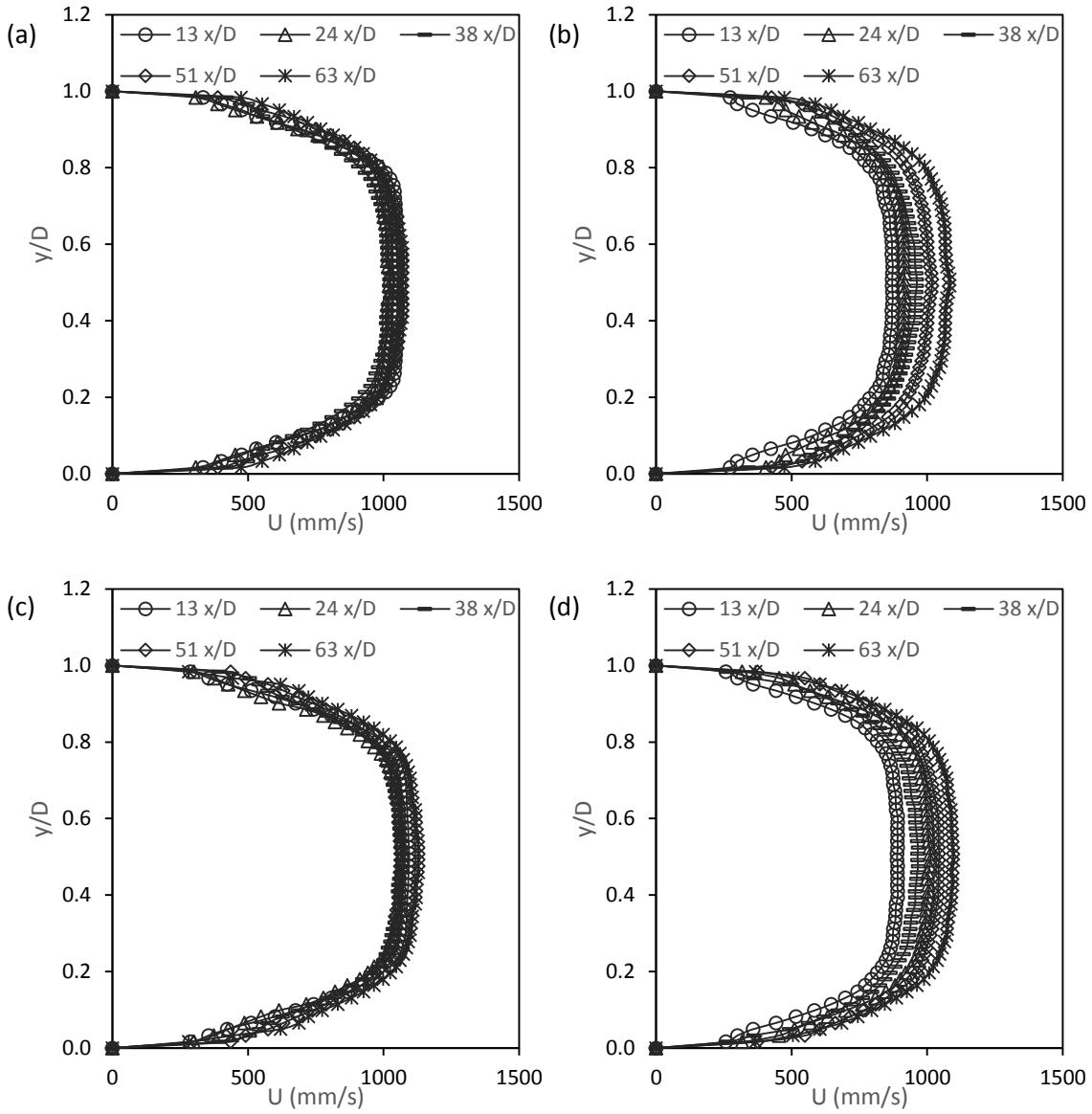

Figure B.6: Time-average streamwise velocity profile for flow with 25 % water cuts at pipeline constriction of (a) GC 0.50 (b) GC 0.75 (c) SC 0.50 (d) SC 0.75.

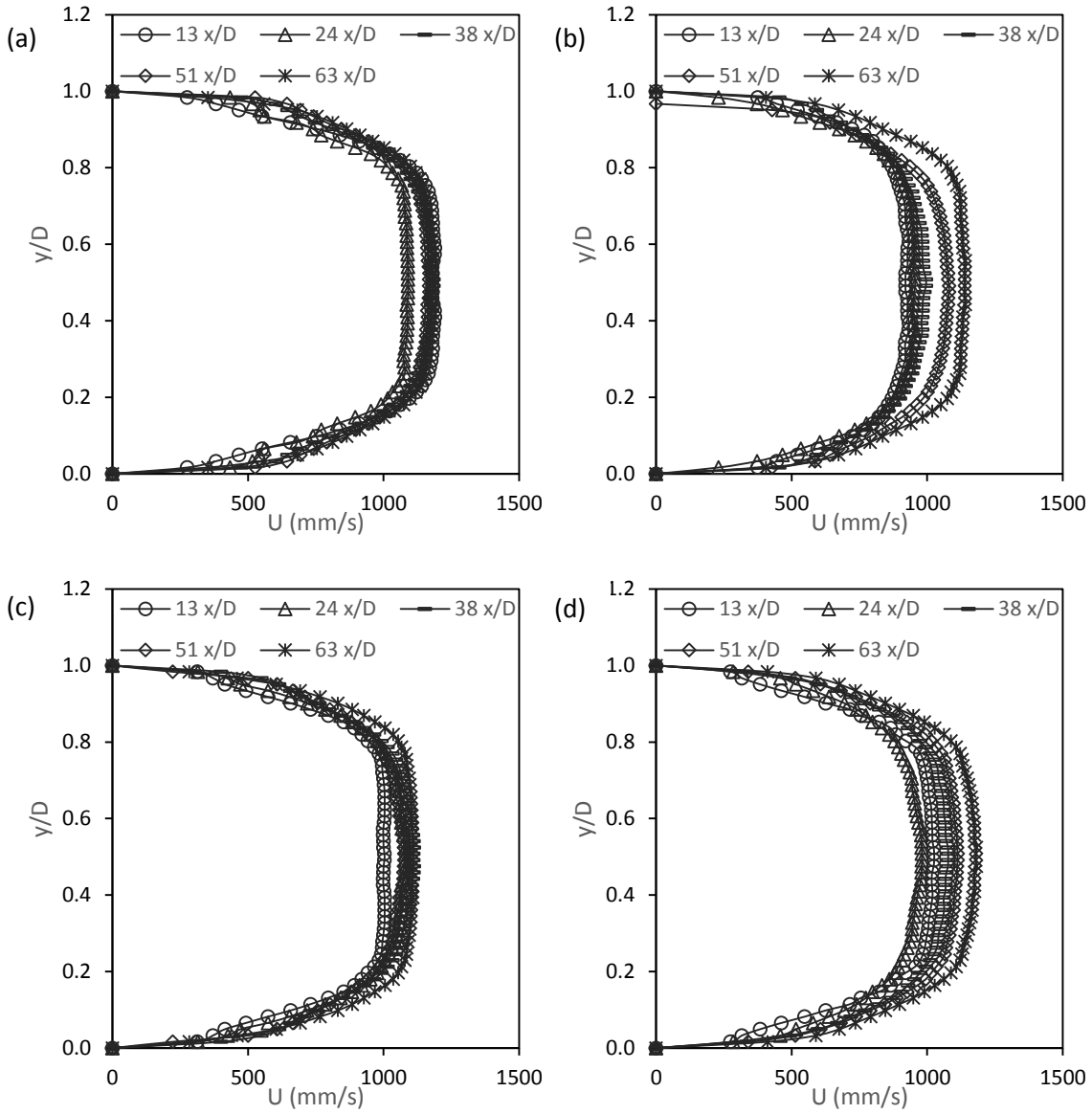

Figure B.7: Time-average streamwise velocity profile for flow with 30 % water cuts at pipeline constriction of (a) GC 0.50 (b) GC 0.75 (c) SC 0.50 (d) SC 0.75.

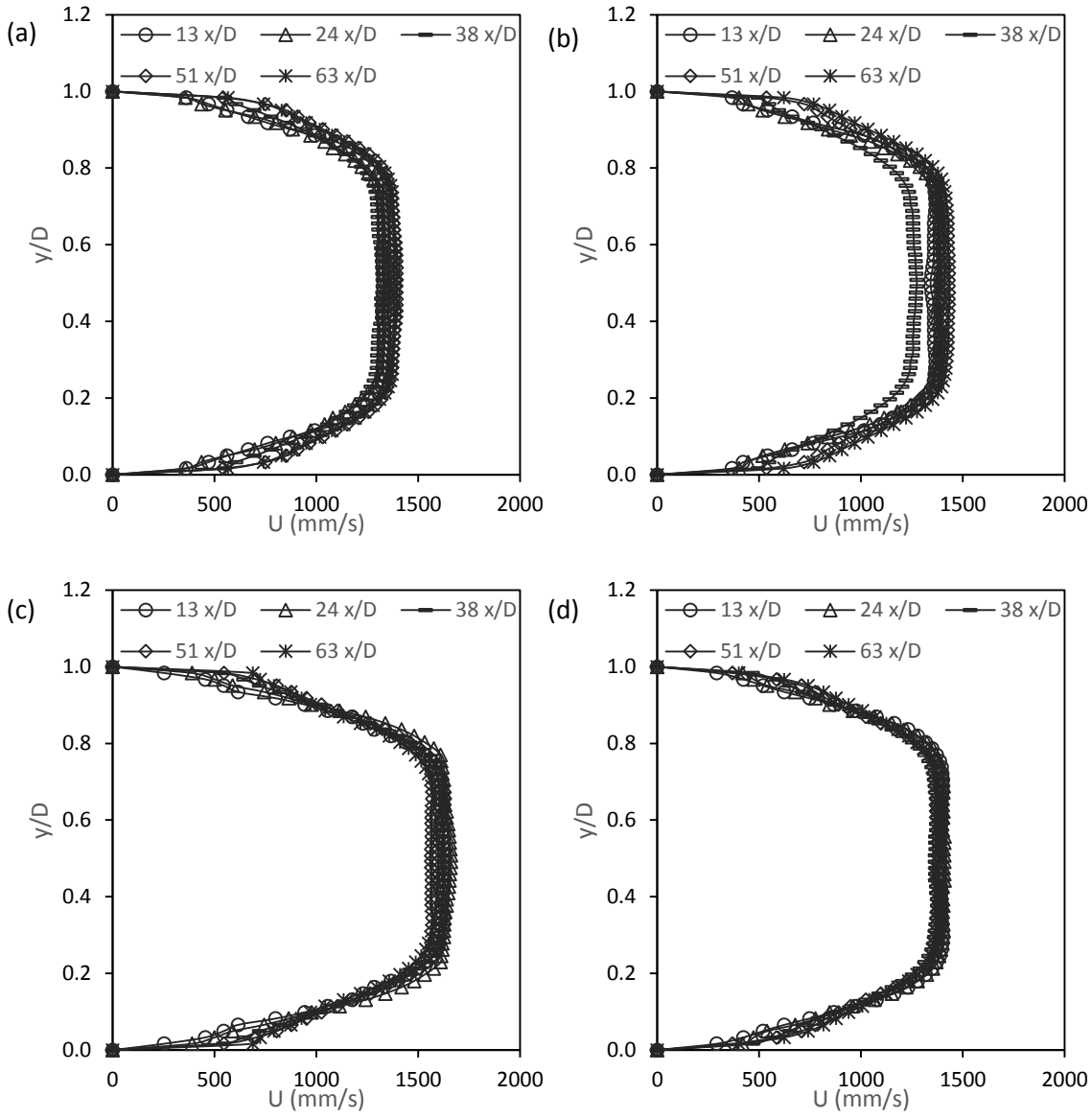

Figure B.8: Time-average streamwise velocity profile for flow with 35 % water cuts at pipeline constriction of (a) GC 0.50 (b) GC 0.75 (c) SC 0.50 (d) SC 0.75.

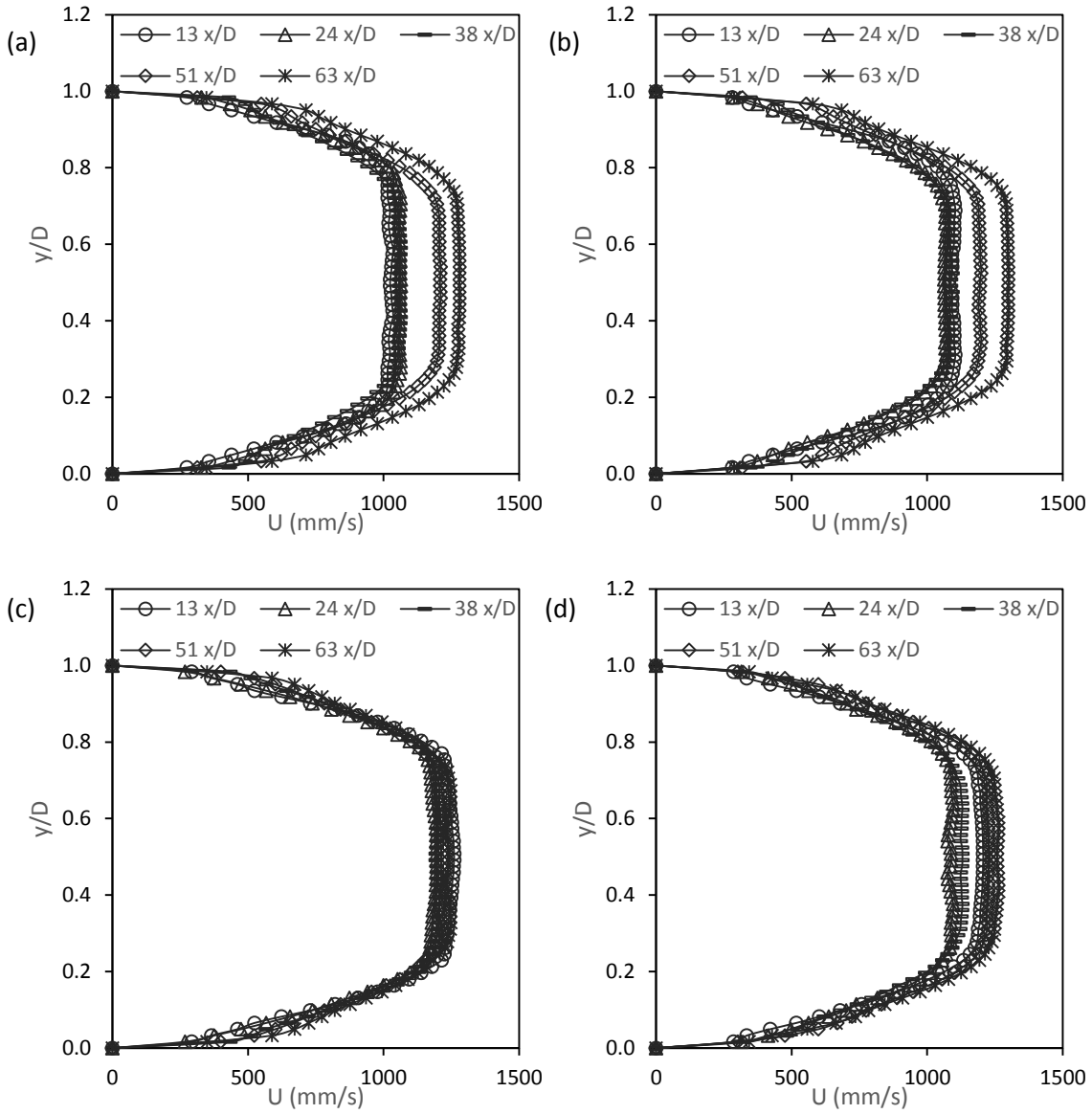

Figure B.9: Time-average streamwise velocity profile for flow with 40 % water cuts at pipeline constriction of (a) GC 0.50 (b) GC 0.75 (c) SC 0.50 (d) SC 0.75.

APPENDIX C

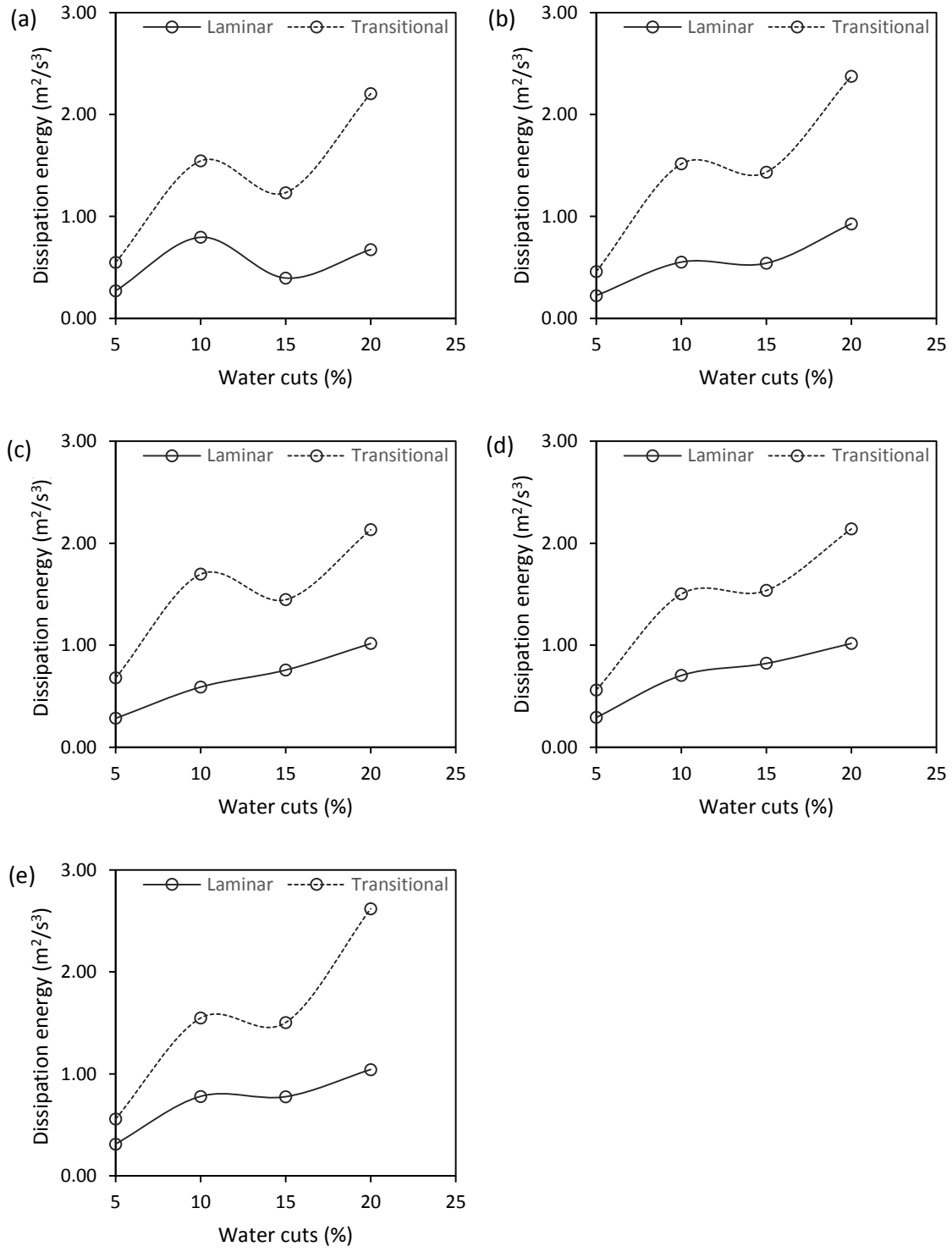

Figure C.1: Dissipation energy as a function of water cuts for different flow regime at (a) 13 (b) 24 (c) 38 (d) 51 and (e) 63 *x/D* downstream of GC 0.75 pipeline constriction.

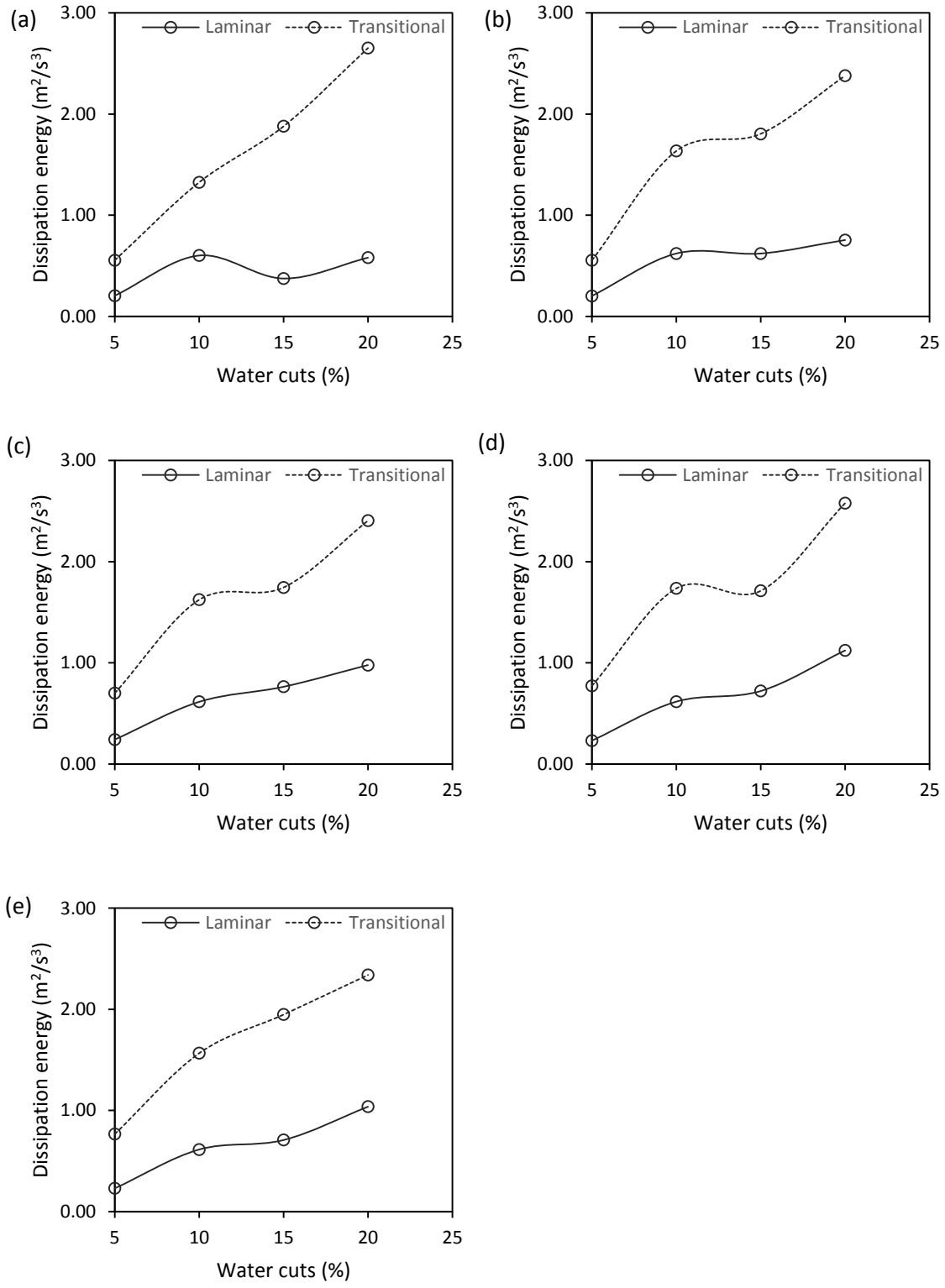

Figure C.2: Dissipation energy as a function of water cuts for different flow regime at (a) 13 (b) 24 (c) 38 (d) 51 and (e) 63 *x/D* downstream of SC 0.50 pipeline constriction.

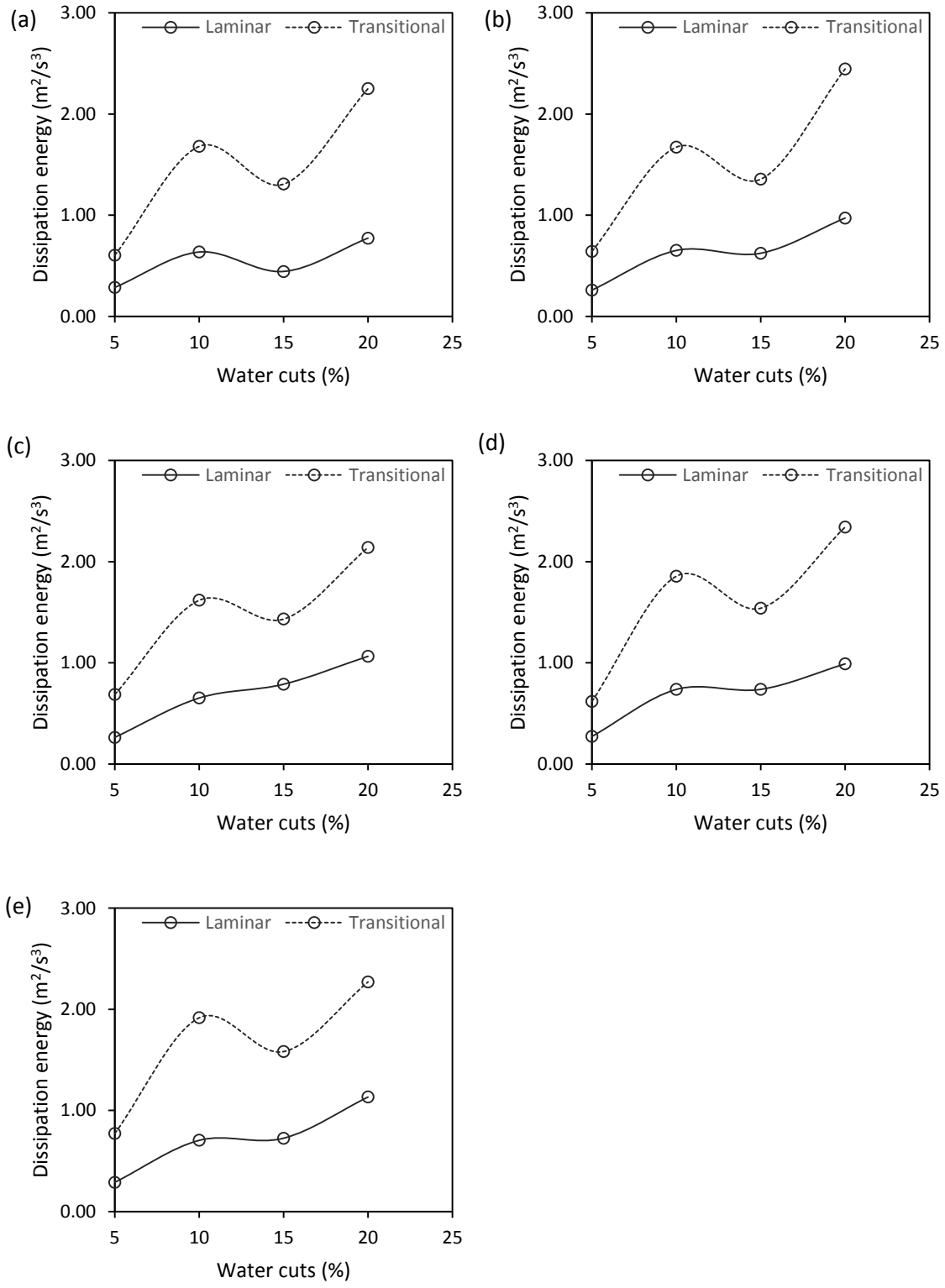

Figure C.3: Dissipation energy as a function of water cuts for different flow regime at (a) 13 (b) 24 (c) 38 (d) 51 and (e) 63 *x/D* downstream of SC 0.75 pipeline constriction.

APPENDIX D

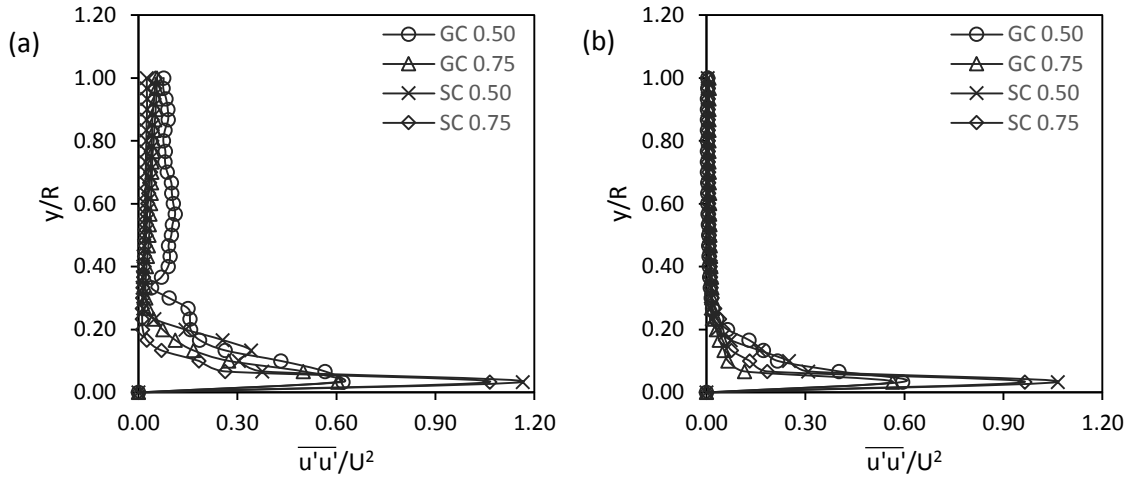

Figure D.1: The $\overline{u'u'}/U^2$ at location (a) 13 *x/D* and (b) 63 *x/D* for all the pipeline constriction at 0% WC.

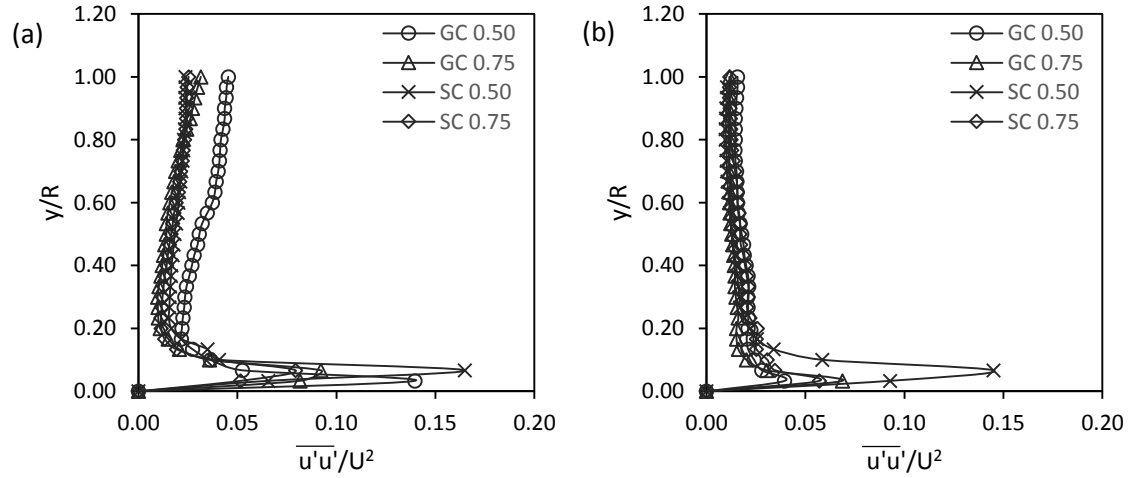

Figure D.2: The $\overline{u'u'}/U^2$ at location (a) 13 *x/D* and (b) 63 *x/D* for all the pipeline constriction at 10% WC.

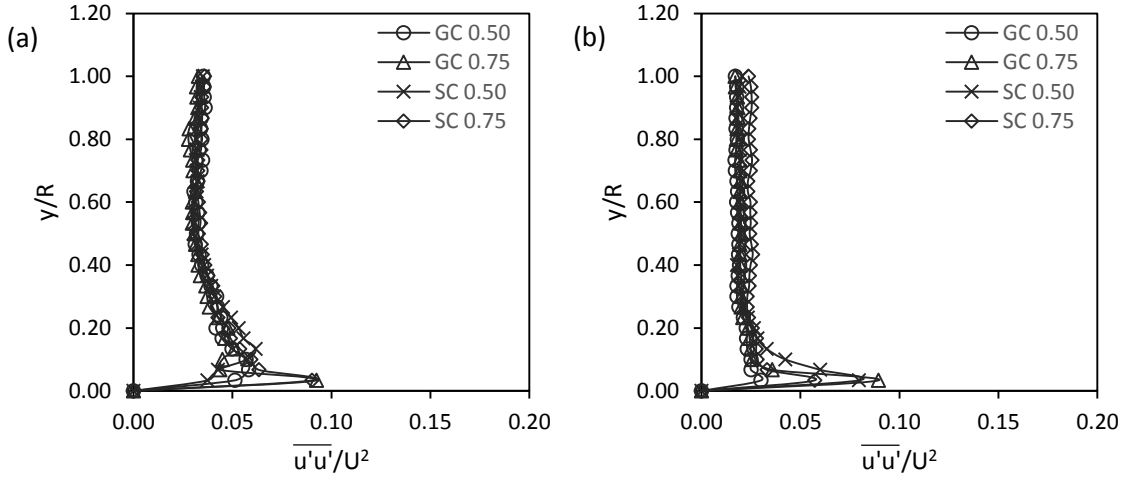

Figure D.3: The $\overline{u'u'}/U^2$ at location (a) 13 *x/D* and (b) 63 *x/D* for all the pipeline constriction at 20% WC.

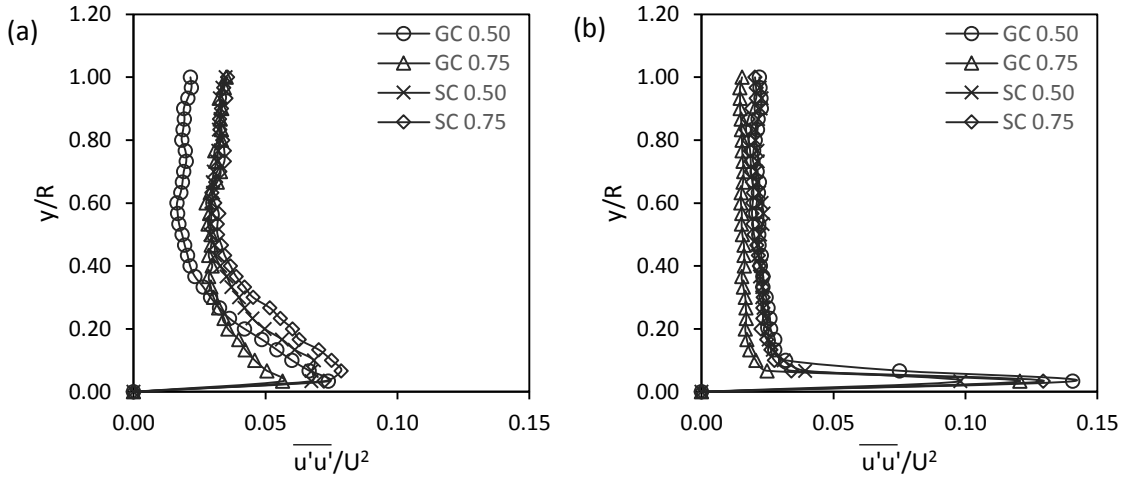

Figure D.4: The $\overline{u'u'}/U^2$ at location (a) 13 *x/D* and (b) 63 *x/D* for all the pipeline constriction at 30% WC.

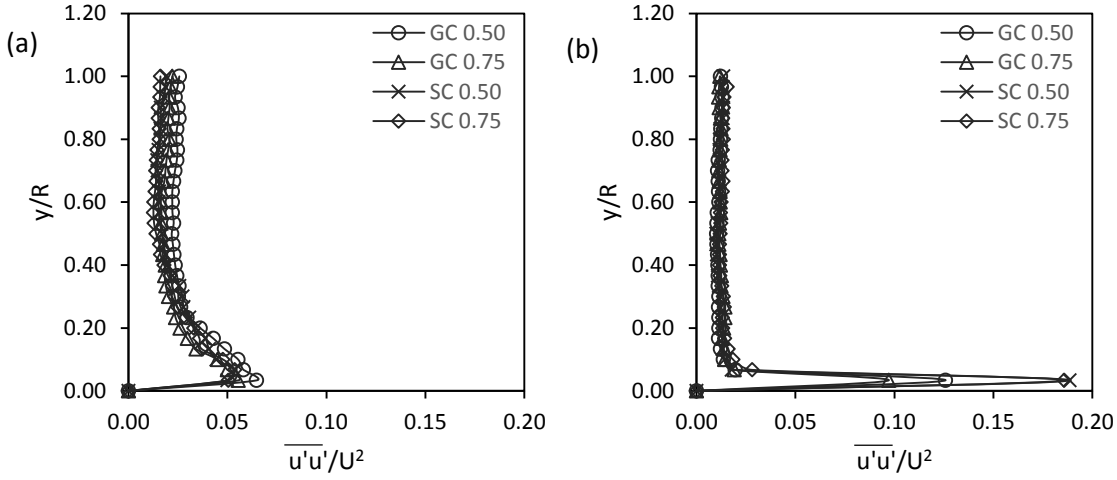

Figure D.5: The $\overline{u'u'}/U^2$ at location (a) 13 *x/D* and (b) 63 *x/D* for all the pipeline constriction at 40% WC.

APPENDIX E

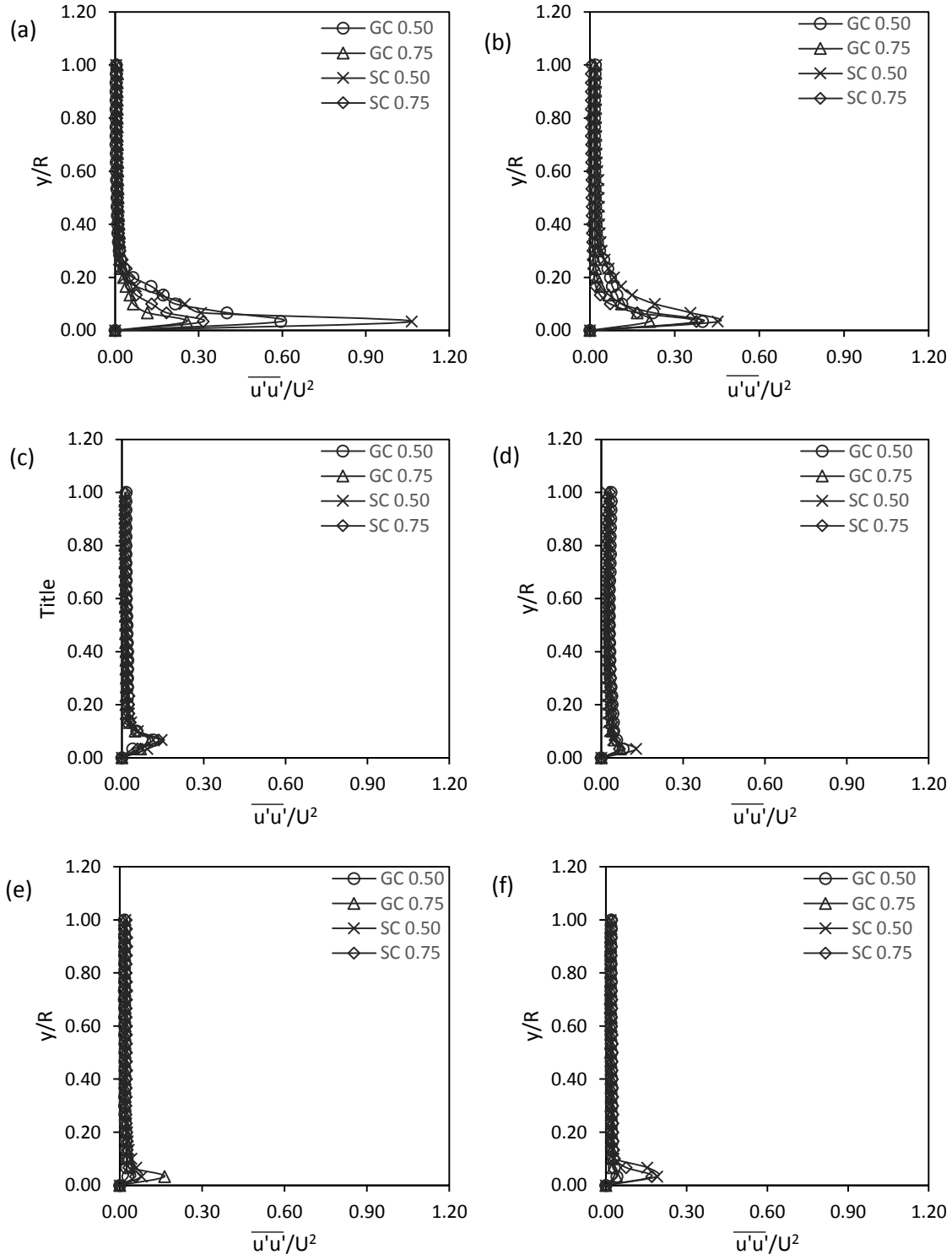
(a)
(b)
(c)
(d)
(e)
(f)
GC 0.50
GC 0.75
SC 0.50
SC 0.75
y/R
Title
$\overline{u'u'}/U^2$
0.00
0.20
0.40
0.60
0.80
1.00
1.20
0.30
0.90

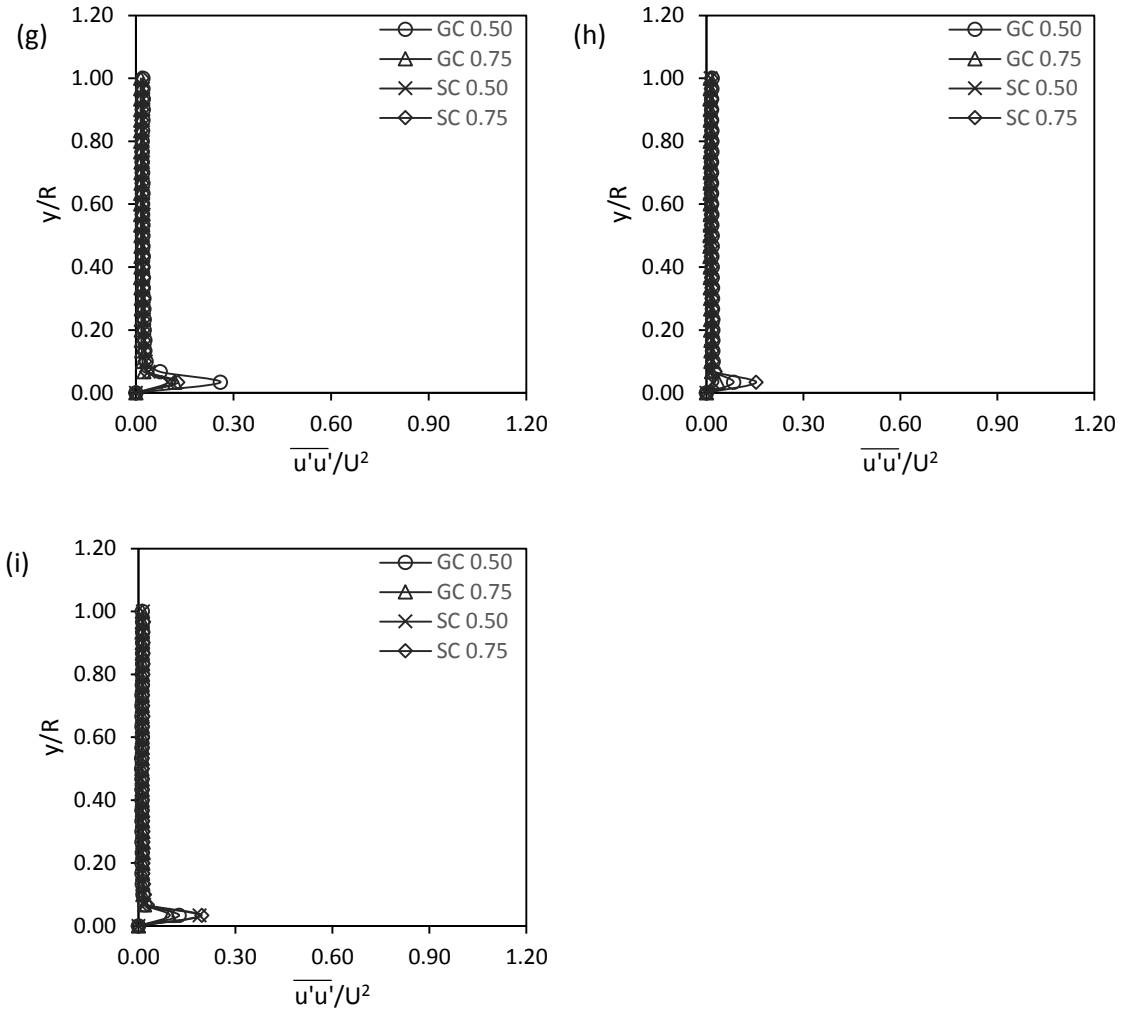

Figure E.1: Reynolds stress profile for all the pipeline constriction at water cuts (a) 0% (b) 5% (c) 10% (d) 15% (e) 20% (f) 25% (g) 30% (h) 35% (i) 40%, at pipeline location 63 *x/D*.

APPENDIX F

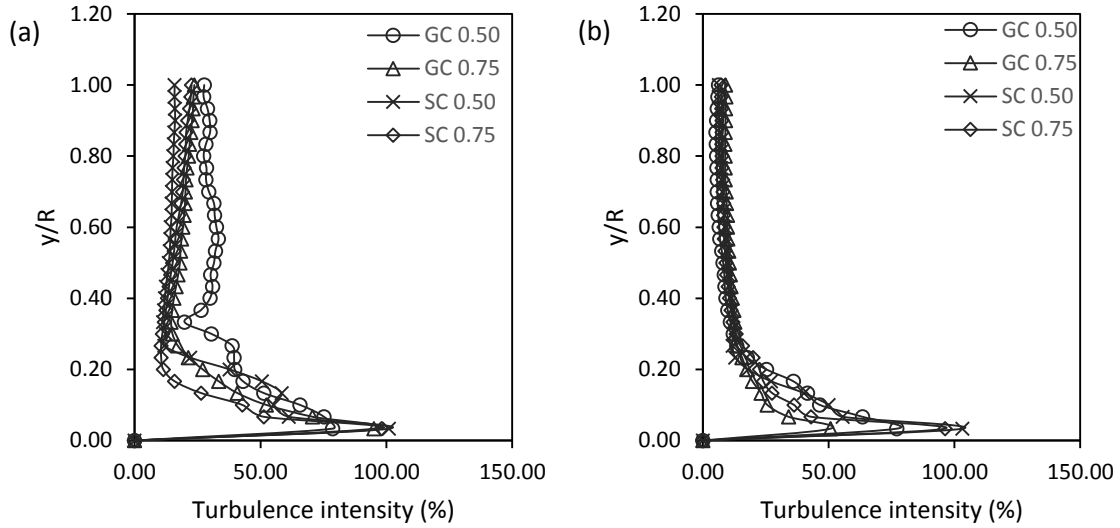

Figure F.1: Streamwise turbulence intensity distribution for 0% water cuts (pure crude) at (a) 13 *x/D* (b) 63 *x/D* after the pipeline constriction, for all the pipeline constriction.

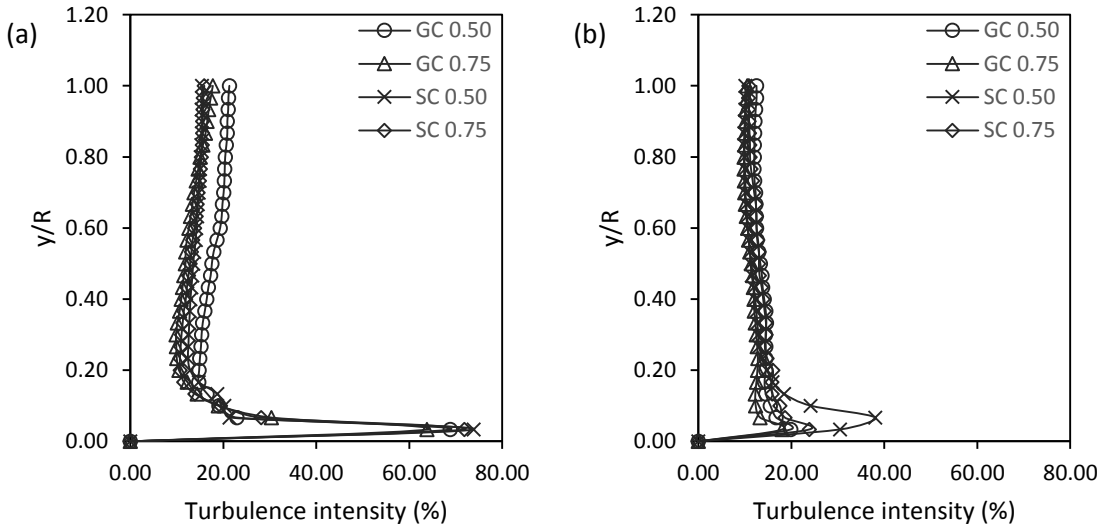

Figure F.2: Streamwise turbulence intensity distribution for 10% water cuts at (a) 13 *x/D* (b) 63 *x/D* after the pipeline constriction, for all the pipeline constriction.

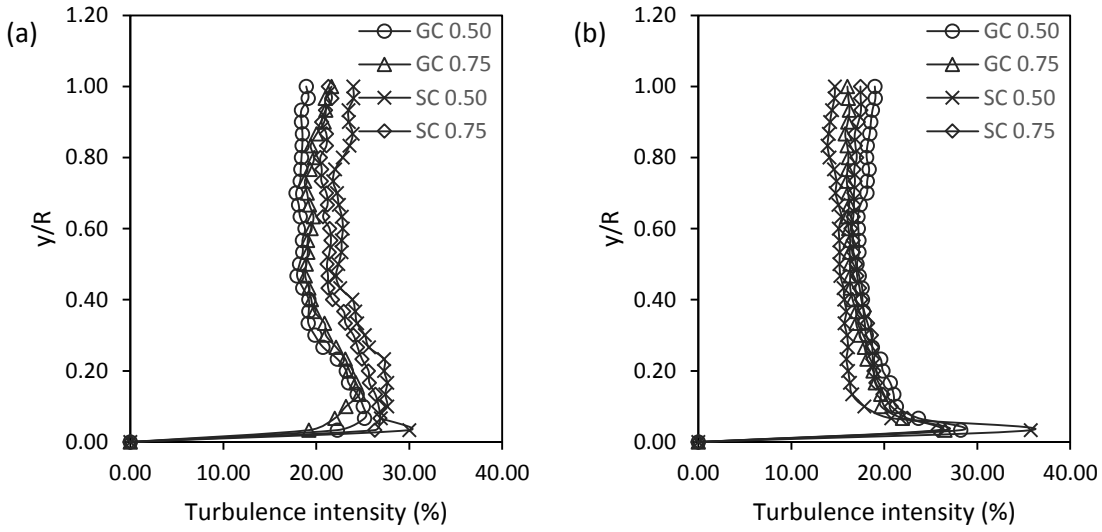

Figure F.3: Streamwise turbulence intensity distribution for 15% water cuts at (a) 13 *x/D* (b) 63 *x/D* after the pipeline constriction, for all the pipeline constriction.

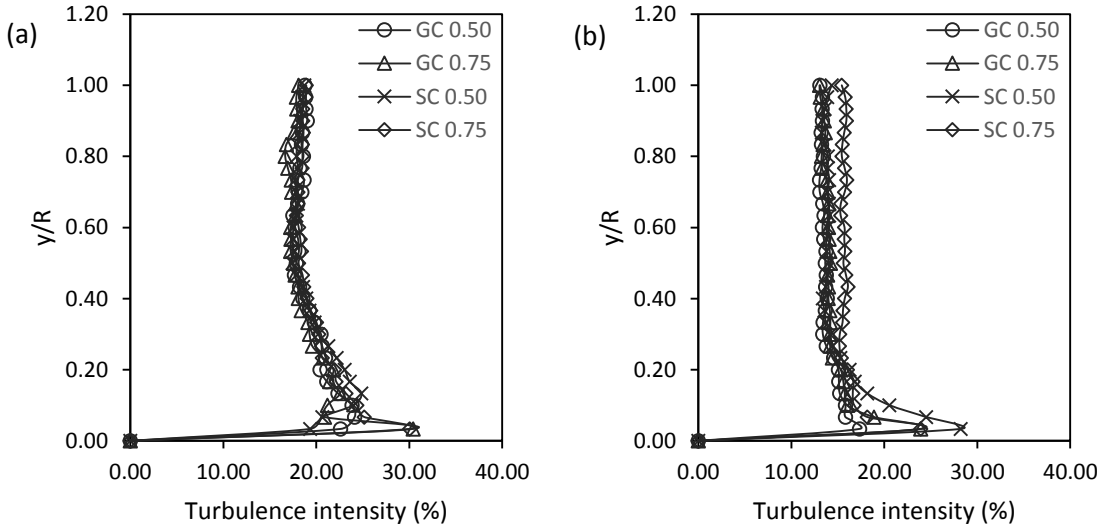

Figure F.4: Streamwise turbulence intensity distribution for 20% water cuts at (a) 13 *x/D* (b) 63 *x/D* after the pipeline constriction, for all the pipeline constriction.

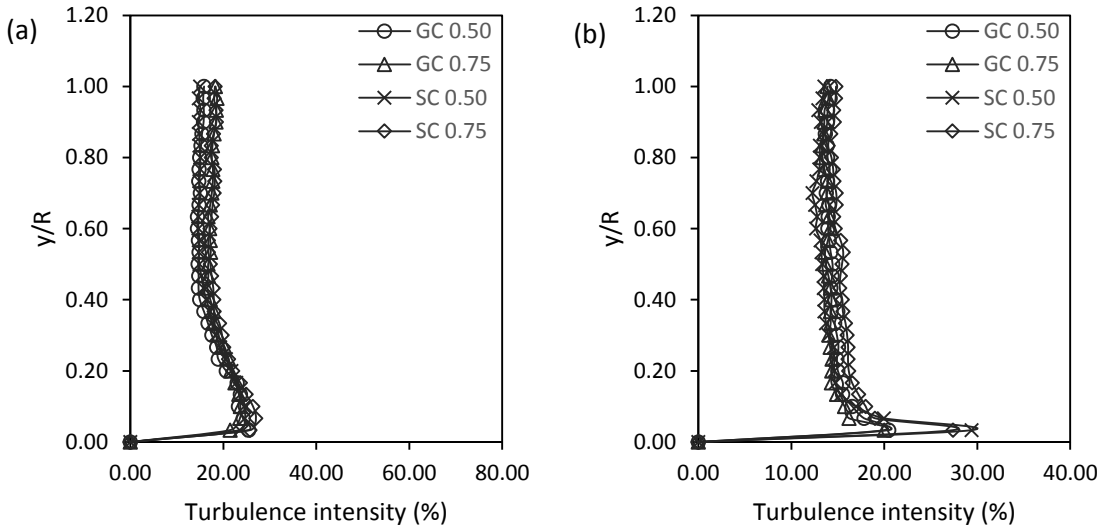

Figure F.5: Streamwise turbulence intensity distribution for 25% water cuts at (a) 13 *x/D* (b) 63 *x/D* after the pipeline constriction, for all the pipeline constriction.

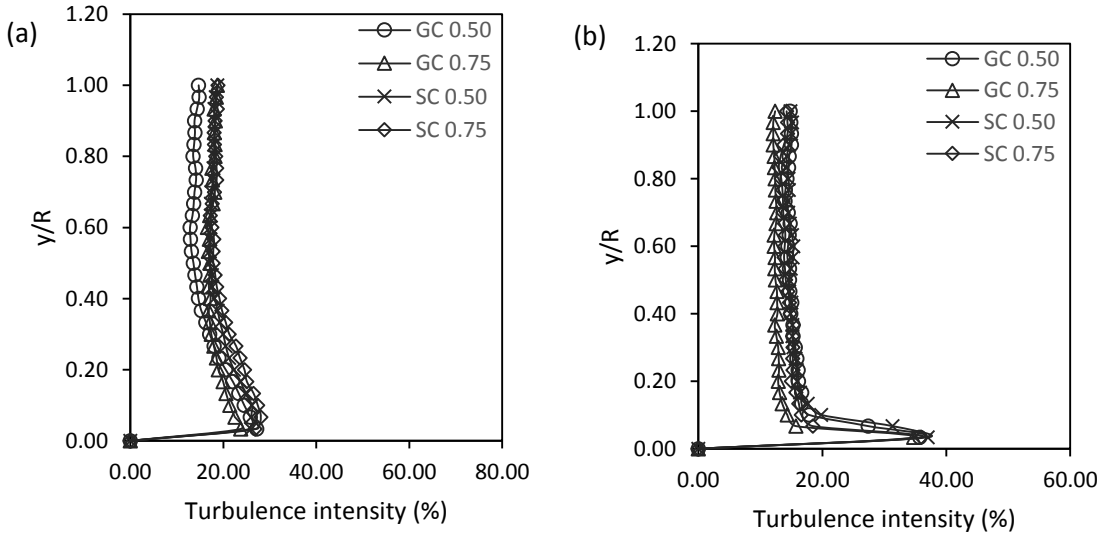

Figure F.6: Streamwise turbulence intensity distribution for 30% water cuts at (a) 13 *x/D* (b) 63 *x/D* after the pipeline constriction, for all the pipeline constriction.

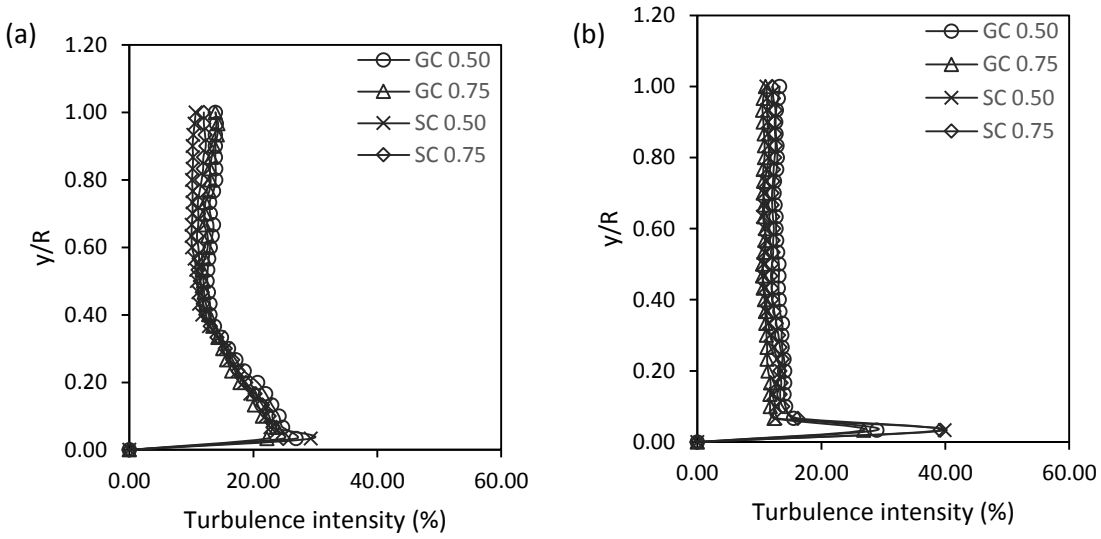

Figure F.7: Streamwise turbulence intensity distribution for 35% water cuts at (a) 13 *x/D* (b) 63 *x/D* after the pipeline constriction, for all the pipeline constriction.

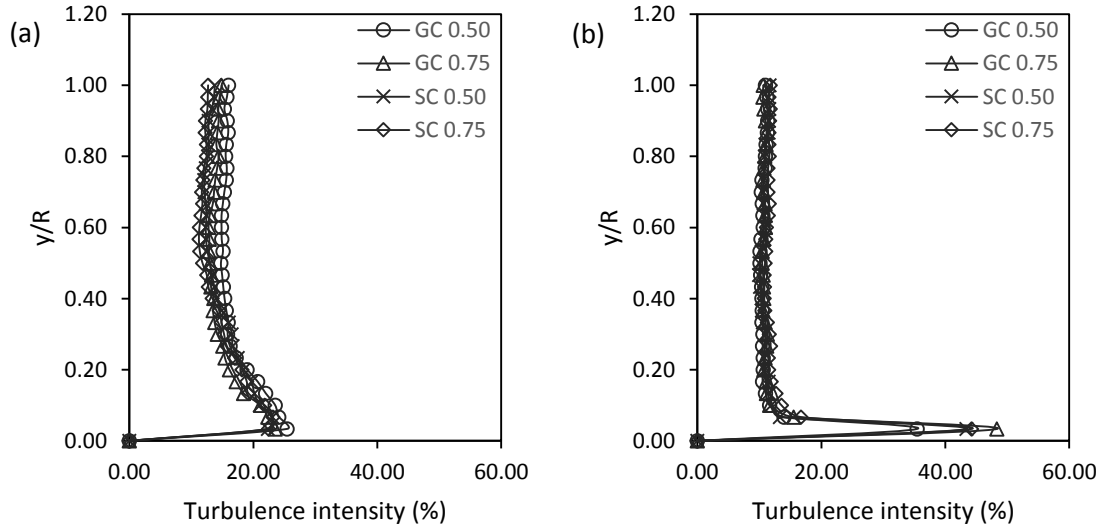

Figure F.8: Streamwise turbulence intensity distribution for 40% water cuts at (a) 13 *x/D* (b) 63 *x/D* after the pipeline constriction, for all the pipeline constriction.

APPENDIX G

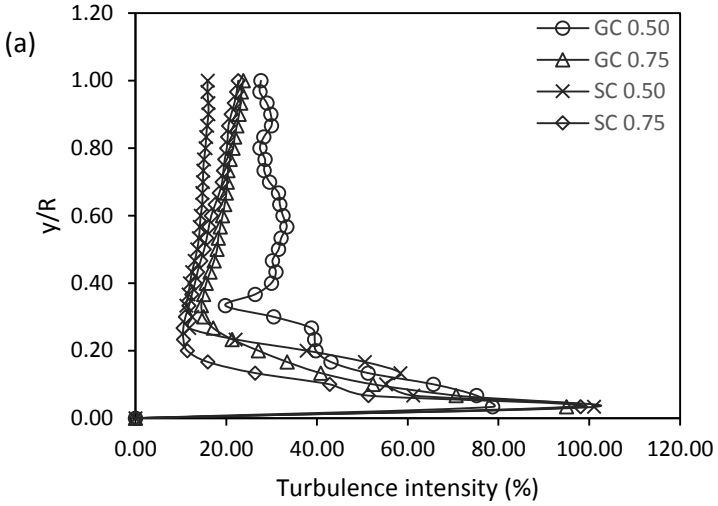
(a)
GC 0.50
GC 0.75
SC 0.50
SC 0.75
y/R
1.20
1.00
0.80
0.60
0.40
0.20
0.00
0.00
20.00
40.00
60.00
80.00
100.00
120.00
Turbulence intensity (%)

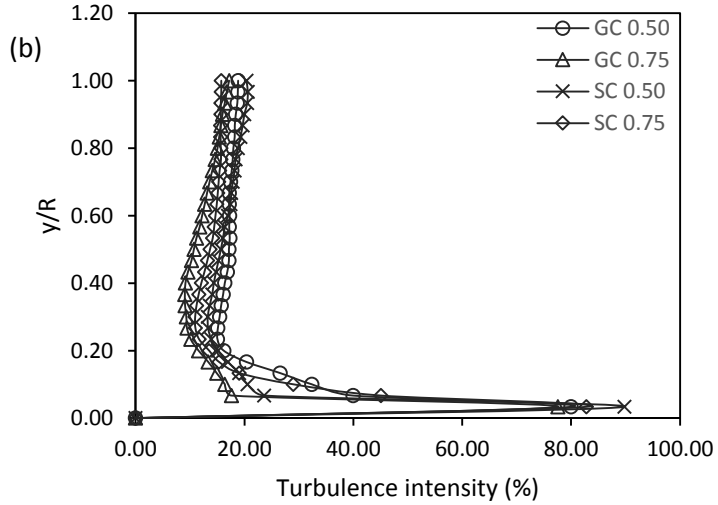
(b)
GC 0.50
GC 0.75
SC 0.50
SC 0.75
y/R
1.20
1.00
0.80
0.60
0.40
0.20
0.00
0.00
20.00
40.00
60.00
80.00
100.00
Turbulence intensity (%)

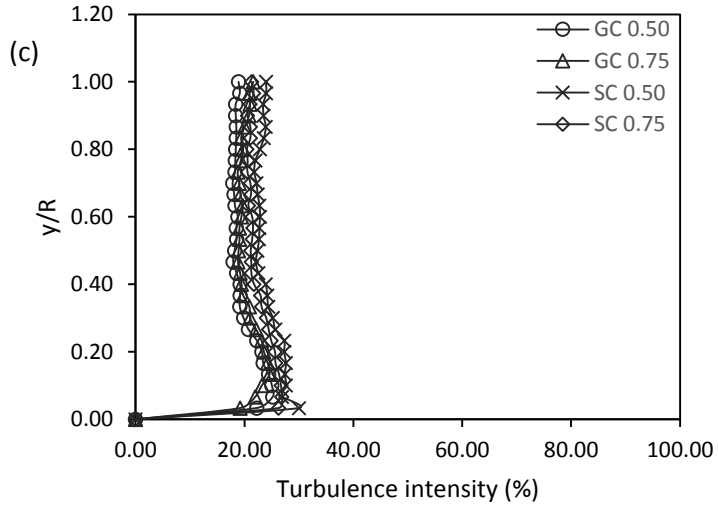
(c)
GC 0.50
GC 0.75
SC 0.50
SC 0.75
y/R
1.20
1.00
0.80
0.60
0.40
0.20
0.00
0.00
20.00
40.00
60.00
80.00
100.00
Turbulence intensity (%)

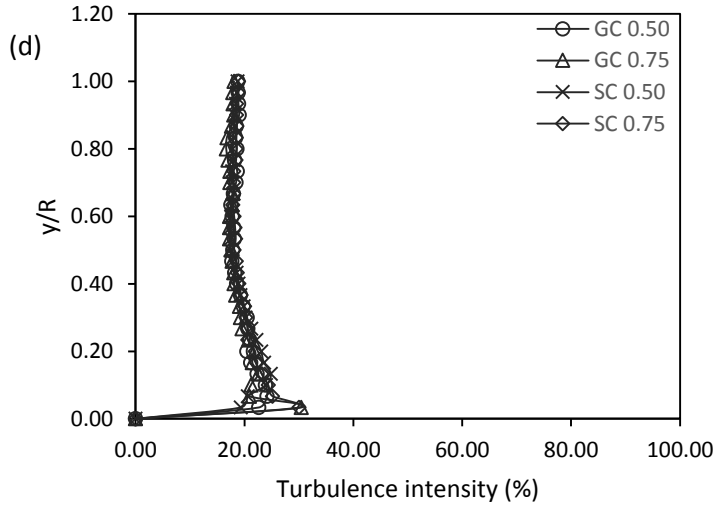
(d)
GC 0.50
GC 0.75
SC 0.50
SC 0.75
y/R
1.20
1.00
0.80
0.60
0.40
0.20
0.00
0.00
20.00
40.00
60.00
80.00
100.00
Turbulence intensity (%)

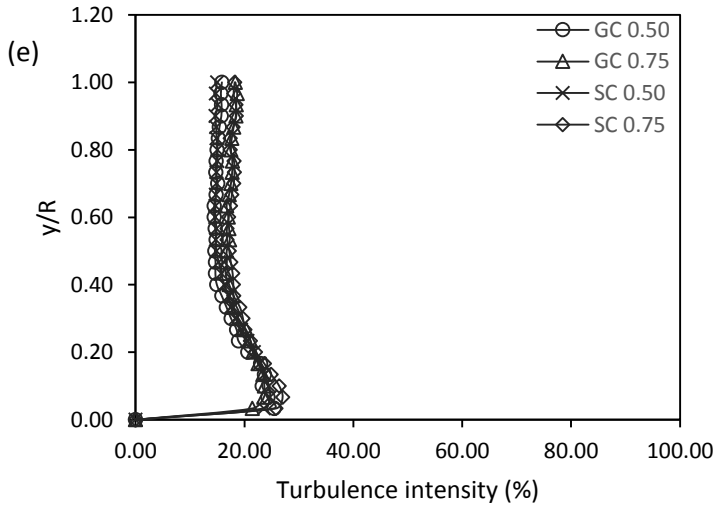
(e)
GC 0.50
GC 0.75
SC 0.50
SC 0.75
y/R
1.20
1.00
0.80
0.60
0.40
0.20
0.00
0.00
20.00
40.00
60.00
80.00
100.00
Turbulence intensity (%)

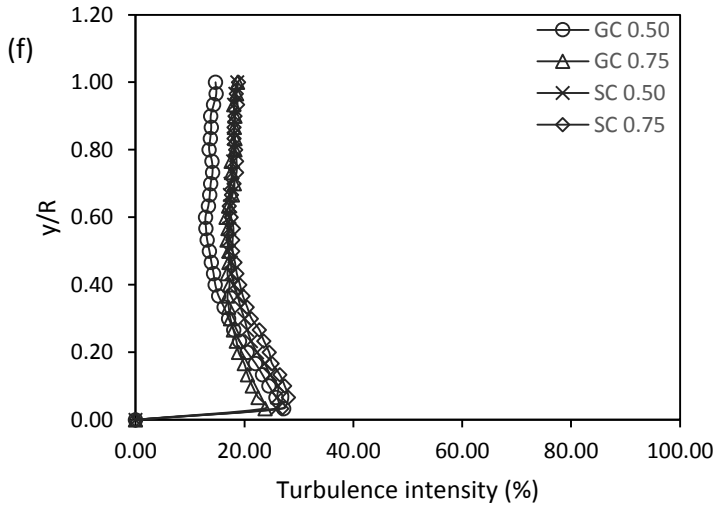
(f)
GC 0.50
GC 0.75
SC 0.50
SC 0.75
y/R
1.20
1.00
0.80
0.60
0.40
0.20
0.00
0.00
20.00
40.00
60.00
80.00
100.00
Turbulence intensity (%)

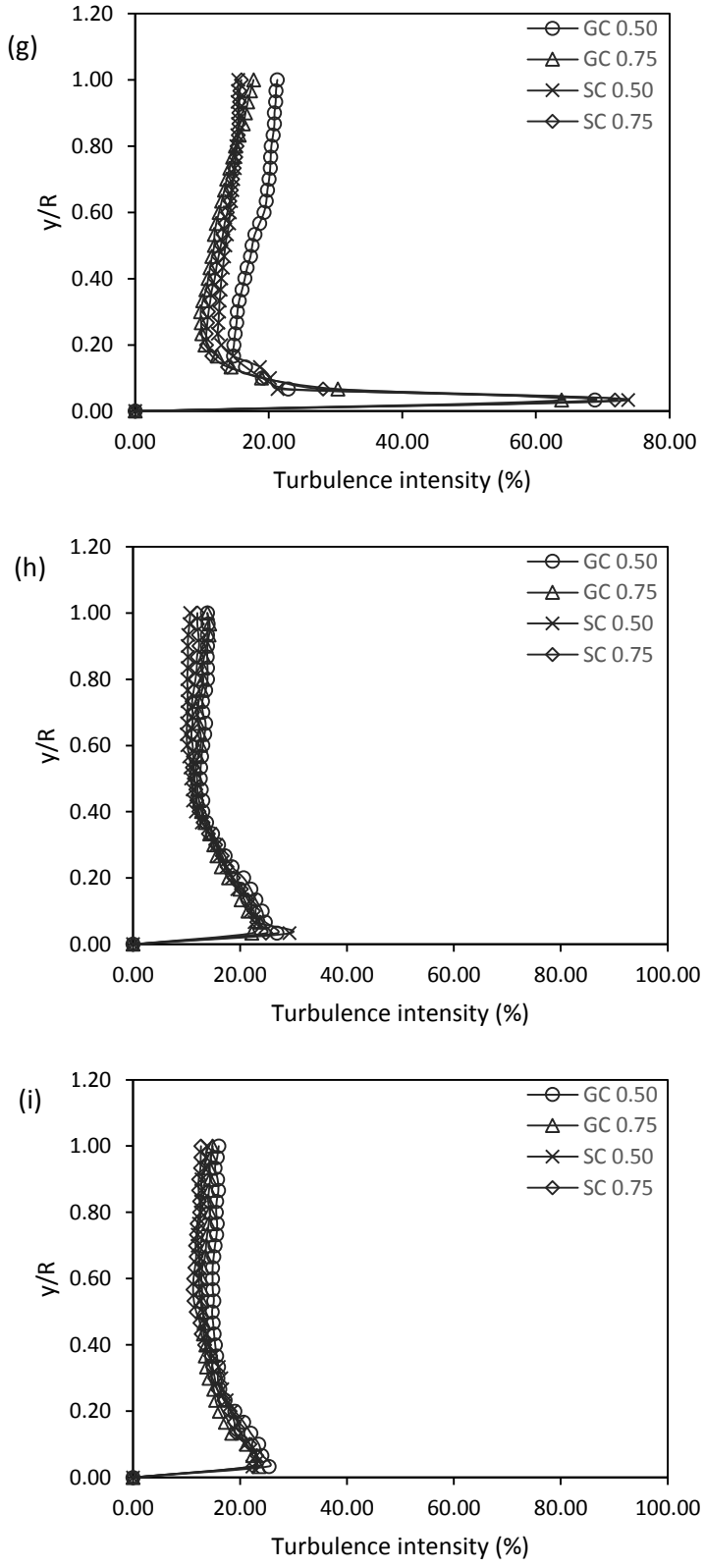

Figure G.1: Streamwise turbulence intensity distribution for water cuts (a) 0% (b) 5% (c) 10% (d) 15% (e) 20% (f) 25% (g) 30% (h) 35% (i) 40%.

REFERENCES

1. *History of Oil and Gas in Malaysia*. 2014; Available from: http://www.mprc.gov.my/industry/history-of-oil-gas-in-malaysia.

2. *Malaysia Investment Performance Report 2013*. 2013, Malaysian Investment Development Authority: Malaysia. p. 9.

3. Lim, J.S., S.F. Wong, M.C. Law, Y. Samyudia, and S.S. Dol, *A Review on the Effects of Emulsions on Flow Behaviours and Common Factors Affecting the Stability of Emulsions.* Journal of Applied Sciences, 2015. **15**: p. 167-172.

4. *Shale Oil Processing*. 2014 [cited 2015 05.02.]; Available from: http://www.bakerhughes.com/capabilities/shale-oil-processing.

5. Wong, S.F., J.S. Lim, and S.S. Dol, *Crude oil emulsion: A review on formation, classification and stability of water-in-oil emulsions.* Journal of Petroleum Science and Engineering, 2015. **135**: p. 498-504.

6. SP, A. and R. K, *Physical Pharmacy*. 2007: p. 177-186.

7. Broboana, D. and C. Balan, *Investigations of the rheology of water-in-crude oil emulsions.* U.P.B. Sci. Bull., Series B, 2007. **69**(3).

8. Julio, L.M., V.Y. Ixtaina, M.A. Fernández, R.M.T. Sánchez, J.R. Wagner, S.M. Nolasco, and M.C. Tomás, *Chia seed oil-in-water emulsions as potential delivery systems of ω-3 fatty acids.* Journal of Food Engineering, 2015. **162**: p. 48-55.

9. Nielloud, F. and G. Marti-Mestres, *Pharmaceutical emulsions and suspensions: revised and expanded*. 2000: CRC Press.

10. Fingas, M., B. Fieldhouse, M. Bobra, and E. Tennyson. *The Physics and Chemistry of Emulsions*. in *Proceedings of the Workshop on Emulsions*. 1993. Marine Spill Response Corporation, Washington, D.C.

11. Mat, H., A. Samsuri, W.A. Wan Rahman, and I.R. Siti, *Study on Demulsifier Formulation for Treating Malaysian Crude oil Emulsion.* Universiti Teknologi Malaysia, 2006.

12. Russell, T.W.F., G.W. Hodgson, and G.W. Govier, *Horizontal Pipeline Flow of Mixtures of Oil and Water*. THE CANADIAN JOURNAL OF CHEMICAL ENGINEERING 1959. **37**(1): p. 9-17.

13. Pal, R., *Pipeline flow of unstable and surfactant-stabilized emulsions.* AIChE Journal, 1993. **39**(11): p. 1754-1764.

14. Nädler, M. and D. Mewes, *Flow Induced Emulsification in the Flow of Two Immiscible Liquids in Horizontal Pipes.* International Journal of Multiphase Flow 1997. **23**(1): p. 55-68.

15. Keleşoğlu, S., B.H. Pettersen, and J. Sjöblom, *Flow properties of water-in-North Sea heavy crude oil emulsions.* Journal of Petroleum Science and Engineering, 2012. **100**(0): p. 14-23.

16. Som, S.K. and G. Biswas, *Introduction to fluid mechanics and fluid machines*. 2nd Ed. ed. 2003, New Delhi: Tata McGraw-Hill.

17. Omer, A.O.A., *Pipeline Flow Behavior of Water-In-Oil Emulsions,* in *Chemical Engineering*. 2009, University of Waterloo: Waterloo, Ontario, Canada. p. 184.

18. Plasencia, J., B. Pettersen, and O.J. Nydal, *Pipe flow of water-in-crude oil emulsions: Effective viscosity, inversion point and droplet size distribution.* Journal of Petroleum Science and Engineering, 2013. **101**(0): p. 35-43.

19. Khan, B.A., N. Akhtar, H.M.S. Khan, K. Waseem, T. Mahmood, A. Rasul, M. Iqbal, and H. Khan, *Basics of pharmaceutical emulsions: A review* African Journal of Pharmacy and Pharmacology, 2011. **5**(25): p. 2715-2725.

20. Fingas, M. and B. Fieldhouse, *Studies of the formation process of water-in-oil emulsions.* Marine Pollution Bulletin, 2003. **47**(9–12): p. 369-396.

21. Fingas, M. and B. Fieldhouse, *Formation of water-in-oil emulsions and application to oil spill modelling.* Journal of Hazardous Materials, 2004. **107**(1–2): p. 37-50.

22. Fingas, M., *Water-in-oil emulsion formation: A review of physics and mathematical modelling.* Spill Science & Technology Bulletin, 1995. **2**(1): p. 55-59.

23. Wang, Z., M. Fingas, C. Yang, and J.H. Christensen, *16 - Crude Oil and Refined Product Fingerprinting: Principles,* in *Environmental Forensics*, R.D. Morrison and B.L. Murphy, Editors. 2005, Academic Press: Burlington. p. 339-407.

24. Zaki, N., P.-C. Schoriing, and I. Rahimian, *Effect of Asphaltene and Resins on the Stability of Water-in-Waxy Oil Emulsions.* Petroleum Science and Technology, 2000. **18**(7-8): p. 945-963.

25. Berridge, S.A., R.A. Dean, R.G. Fallows, and A. Fish, *The properties of persistent oils at sea.* Journal of Institute of Petroleum, 1968. **54**: p. 300-309.

26. Bridie, A.L., T.H. Wanders, W. Zegveld, and H.B. Van Der Heijde, *Formation, prevention and breaking of sea water in crude oil emulsions 'chocolate mousses'.* Marine Pollution Bulletin 11, 1980: p. 343-348.

27. Mackay, D. and W. Zagorski, *Studies of the formation of water-in-oil emulsions.* In Proceedings of the Fourth Annual Arctic Marine Oilspill Program Technical Seminar, Environment Canada, Ottawa, Ontario, 1981: p. 75-86.

28. Mackay, D. and W. Zagorski, *Studies of water-in-oil emulsions.* Environment Canada Manuscript Report EE-34, Ottawa, Ontario,, 1982a: p. 93.

29. Mackay, D. and W. Zagorski, *Water-in-oil emulsions: a stability hypothesis.* In Proceedings of the Fifth Annual Arctic Marine Oilspill Program Technical Seminar, Environment Canada, Ottawa, Ontario, 1982b: p. 61-74.

30. Nesterova, M.P., O.S. Moehalova, and A.B. Mamayev, *Transformation of oil-in-water emulsion into solid tar balls in the sea.* Oceanology, 1983. **23**: p. 734-737.

31. Canvari, G.P., *Marine Pollution Bulletin.* 1982. **13**: p. 49-54.

32. Schubert, H. and H. Armbruster, *Principles of Formation and Stability of Emulsions.* International Chemical Engineering 1992. **32**: p. 14-28.

33. Fingas., M.F., *Water-in-Oil Emulsions: Formation and Prediction.* Journal of Petroleum Science Research, 2014. **3**(1): p. 38-49.

34. Haegh, T. and T. Ellingsen, *The Effect of Breaking Waves on Oil Spills; 1. Emulsification of Crude Oil at Sea.* SINTEF, The Foundation of Scientific and Industrial Research at the University of Trondbeim, Norway, 1977: p. 23.

35. Wang, H. and C.P. Huang, *The effect of turbulence on oil emulsification.* The Physical Behavior of Oil in The Marine Environment, Princeton University, Princeton, New Jersey, 1979: p. 81-100.

36. Fingas, M., B. Fieldhouse, P. Lambert, Z. Wang, J. Noonan, J. Lane, and J.V. Mullin, *Water-in-oil emulsions formed at sea, in test tanks, and in the laboratory*. Environment Canada Manuscript Report EE-170, Ottawa, Ont., 2002.

37. Fingas, M., B. Fieldhouse, and Z. Wang, *The Long Term Weathering of Water-in-Oil Emulsions.* Spill Science and Technology Bulletin, 2003. **8**(2): p. 137–143.

38. Darby, R., *Chemical engineering: Fluid mechanics*. 1996, New York: Marcel Dekker.

39. Wilkes, J.O., *Fluid Mechanics for Chemical Engineers*. 1999: Prentice Hall.

40. Davidson, L., *Fluid mechanics, turbulent flow and turbulence modeling*, in *Department of Applied Mechanics*. 2015, Chalmers University of Technology: SE-412 96 G¨oteborg, Sweden. p. 348.

41. Van Dyke, M. and M. Van Dyke, *An album of fluid motion*. Vol. 176. 1982: Parabolic Press Stanford.

42. Beltramini, J.N. and G.Q. Lu, *Processing of Primary and Secondary Fuels: Perspective on Petroleum Refining*, in *Encyclopedia of Life Support Systems*. 2002, Eolss Publishers: Eolss Publishers Paris, UNESCO; Oxford, UK. p. 619 - 634.

43. Pal, R., *Emulsions: Pipeline Flow Behavior, Viscosity Equations and Flow Measurement*. 1987, University of Waterloo: Ontario.

44. Omer, A. and R. Pal, *Effects of Surfactant and Water Concentrations on Pipeline Flow of Emulsions.* Industrial & Engineering Chemistry Research, 2013. **52**(26): p. 9099-9105.

45. Cengel, J.A., A.A. Faruqui, J.W. Finnigan, C.H. Wright, and J.G. Kundsen, *Laminar and turbulent flow of unstable liquid-liquid emulsions.* AIChE Journal, 1962. **8**(3): p. 335-339.

46. Pal, R., *Mechanism of Turbulent Drag Reduction in Emulsions and Bubbly Suspensions.* Industrial & Engineering Chemistry Research, 2007. **46**(2): p. 618-622.

47. Omer, A. and R. Pal, *Pipeline Flow Behavior of Water-in-Oil Emulsions with and without a Polymeric Additive in the Aqueous Phase.* Chemical Engineering & Technology, 2010. **33**(6): p. 983-992.

48. Zakin, J.L., R. Pinaire, and M.E. Borgmeyer, *Transport of Oils as Oil-in-Water Emulsions.* Journal of Fluids Engineering, 1979. **101**(1): p. 100-104.

49. Sherman, P., *Industrial Rheology*. 1970, London: Academic Press.

50. Tadros, T.F. and B. Vincent, *Emulsion stability*, in *Encyclopaedia of emulsion technology*, P. Becher, Editor. 1983, Marcel Dekker: New York.

51. Ashrafizadeh, S.N., E. Motaee, and V. Hoshyargar, *Emulsification of heavy crude oil in water by natural surfactants.* Journal of Petroleum Science and Engineering, 2012. **86–87**: p. 137–143.

52. Otsubo, Y. and R.K. Prud'homme, *Effect of drop size distribution on the flow behaviour of oil-in-water emulsions.* Rheologica Acta, 1994. **33**: p. 303–306.

53. Pal, R. and E. Rhodes, *Viscosity / Concentration Relationships for Emulsions.* Journal of Rheology, 1989. **33**(7): p. 1021-1045.

54. Kokal, S.L., *Crude Oil Emulsions: A State-Of-The-Art Review.*

55. Krieger, I.M. and T.J. Dougherty, *A Mechanism for Non-Newtonian Flow in Suspensions of Rigid Spheres.* Transactions of The Society of Rheology, 1959. **3**(1): p. 137-152.

56. Lee, D.I., *The viscosity of concentrated suspensions.* Transactions of The Society of Rheology: Journal of Rheology, 1969. **13**: p. 273–288.

57. Charles, M.E., G.W. Govier, and G.W. Hodgson, *The horizontal pipeline flow of equal density oil-water mixtures.* The Canadian Journal of Chemical Engineering, 1961. **39**(1): p. 27-36.

58. Marsden, S.S. and R. Raghaven, *A system for producing and transporting crude oil as oil/water emulsions.* Journal of the Institute of Petroleum, 1973. **59**: p. 573.

59. T.R., S., *Method of transporting viscous hydrocarbons*. 1981.

60. Simon, R. and P. W.G., *Pipelining oil/water mixtures*. 1970.

61. Lamb, M.S. and W.C. Simpson. *Pipeline transportation of wax-laden crude oil as water suspensions*. in *Proceedings of the Sixth World Petroleum Congress*. 1973. Frankfurt, Germany, Section VII.

62. Ahmed, N.S., A.M. Nassar, N.N. Zaki, and H.K. Gharieb, *Formation of fluid heavy oil - in-water emulsions for pipeline transportation.* Journal of Fuel, 1999. **78**: p. 593–600.

63. Ashrafizadeh, S.N. and M. Kamran, *Emulsification of heavy crude oil in water for pipeline transportation.* Journal of Petroleum Science and Engineering, 2010. **71**(3): p. 205-211.

64. Yaghi, B. and A. Al-Bemani, *Heavy crude oil viscosity reduction for pipeline transportation.* Energy Sources, 2002. **24**(2): p. 93-102.

65. Zhang, J., D. Chen, D. Yan, X. Yang, and C. Shen, *Pipelining of Heavy Crude Oil as Oil-in-Water Emulsions*. Society of Petroleum Engineers.

66. Messick, M.A., *Pipeline transportation of heavy crude oil*. 1982.

67. Chen, G. and D. Tao, *An experimental study of stability of oil–water emulsion.* Fuel Processing Technology, 2005. **86**(5): p. 499-508.

68. Bhardwaj, A. and S. Hartland, *Studies on build up of interfacial film at the crude oil/water interface.* Journal of Dispersion Science and Technology, 1998. **19**(4): p. 465-473.

69. Ortega, F., H. Ritacco, and R.G. Rubio, *Interfacial microrheology: Particle tracking and related techniques.* Current Opinion in Colloid & Interface Science, 2010. **15**(4): p. 237-245.

70. Aguileraa, B.M., J.G. Delgadob, and A.L. Cárdenas, *Water-in-Oil Emulsions Stabilized by Asphaltenes Obtained from Venezuelan Crude Oils.* Journal of Dispersion Science and Technology, 2010. **31**(3): p. 359-363.

71. McLean, J.D. and P.K. Kilpatrick, *Effects of Asphaltene Solvency on Stability of Water-in-Crude-Oil Emulsions.* Journal of Colloid and Interface Science, 1997. **189**: p. 242-253.

72. Nghiem, L.X., M.S. Hassam, R. Nutakki, and A.E.D. George, *Efficient Modelling of Asphaltene Precipitation.* Society of Petroleum Engineers Journal 1993. **5**: p. 375-384.

73. Bobra, M.A., *A study of the formation of water-in-oil emulsions.* In Proceedings of the Thirteenth Annual Arctic Marine Oil Spill Program Technical Seminar, Environment Canada, Ottawa, Ontario, 1990: p. 87-117.

74. Bobra, M.A., *Water-in-oil emulsification: a physicochemical study.* International Oil Spill Conference Proceedings, 1991. **1**: p. 483-488.

75. Bobra, M.A., *A study of water-in-oil emulsification.* Environment Canada Manuscript Report EE-32, 1992.

76. *Rheological Analysis Of Dispersions By Frequency Sweep Testing Using Equipment From Malvern Instruments*. 2005 10 September 2013 [cited 2014 17 March 2014].

77. Maia Filho, D.C., J.B.V.S. Ramalho, G.M.S. Lucas, and E.F. Lucas, *Aging of water-in-crude oil emulsions: Effect on rheological parameters.* Colloids and Surfaces A: Physicochemical and Engineering Aspects, 2012. **405**(0): p. 73-78.

78. Derkach, S.R., *Rheology of emulsions.* Adv. Colloid Interface Sci. , 2009. **151**: p. 1-23.

79. Briceno, M.I., M. Ramirez, J. Bullón, and J.L. Salager. *Customizing drop size distribution to change emulsion viscosity*. in *2nd World Congress on Emulsion - 2ème Congrès Mondial de l'Emulsion CME2*. 1997. Bordeaux, France.

80. Pal, R., Y. Yan, and J.H. Masliyah, *Emulsions: fundamentals and applications in the petroleum industry*, ed. L.L. Schramm. 1992, Washington, DC: American Chemical Society.

81. Zaki, N.N., *Surfactant stabilized crude oil-in-water emulsions for pipeline transportation of viscous crude oils.* Colloids and Surfaces A: Physicochemical and Engineering Aspects, 1997. **125**(1): p. 19-25.

82. Sakka, S., *Sol–gel science and technology: Topics in fundamental research and applications*, ed. S. Sakka. Vol. 1. 2002, New York: Springer US.

83. Yang, F., Q. Niu, Q. Lan, and D. Sun, *Effect of dispersion pH on the formation and stability of Pickering emulsions stabilized by layered double hydroxides particles.* Journal of Colloid and Interface Science, 2007. **306**(2): p. 285-295.

84. Tambe, D.E. and M.M. Sharma, *Factors Controlling the Stability of Colloid-Stabilized Emulsions: I. An Experimental Investigation.* Journal of Colloid and Interface Science, 1993. **157**(1): p. 244-253.

85. Sjöblom, J., L. Mingyuan, H. Höiland, and E.J. Johansen, *Water-in-crude oil emulsions from the norwegian continental shelf part III. A comparative destabilization of model systems.* Colloids and Surfaces, 1990. **46**(2): p. 127-139.

86. Grace, R., *Commercial Emulsion Breaking*, in *Emulsions fundamentals and applications in the petroleum industry*. 1992, American Chemical Society: Washington DC. p. 313-339.

87. Binks, B.P., *Surfactant monolayers at the oil-water interface.* Chemistry and Industry 1993. **14**: p. 537-541.

88. Kobayashi, I., M. Yasuno, S. Iwamoto, A. Shono, K. Satoh, and M. Nakajima, *Microscopic observation of emulsion droplet formation from a polycarbonate membrane.* Colloids and Surfaces A: Physicochemical and Engineering Aspects, 2002. **207**(1): p. 185-196.

89. Johnsen, E.E. and H.P. Rønningsen, *Viscosity of 'live' water-in-crude-oil emulsions: experimental work and validation of correlations.* Journal of Petroleum Science and Engineering, 2003. **38**(1–2): p. 23-36.

90. Farah, M.A., R.C. Oliveira, J.N. Caldas, and K. Rajagopal, *Viscosity of water-in-oil emulsions: Variation with temperature and water volume fraction.* Journal of Petroleum Science and Engineering, 2005. **48**(3–4): p. 169-184.

91. Dan, D. and G. Jing, *Apparent viscosity prediction of non-Newtonian water-in-crude oil emulsions.* Journal of Petroleum Science and Engineering, 2006. **53**(1–2): p. 113-122.

92. Anisa, A.N.I. and A. H.Nour, *Affect of Viscosity and Droplet Diameter on water-in-oil (w/o) Emulsions: An Experimental Study*. World Academy of Science, Engineering and Technology, 2010. **38**: p. 4.

93. Munson, B.R., D.F. Young, T.H. Okiishi, and W.W. Huebsch, *Fundamentals of Fluid Mechanics*. Sixth ed. 2010: John Wiley & Sons (Asia) Pte Ltd.

94. Zhang, X.G., *Galvanic corrosion*. Uhlig's Corrosion Handbook, ed. R.W. Revie. 2000, New York John Wiley & Sons.

95. Metflow, *UVP Monitor – Model UVP-XW, Users guide*. 2000: Met-flow SA, Lausanne, Switzerland

96. Geisler, T., *Ultrasonic Velocity Profile Measurements in Experimental Hydraulics*, in *Institute of Hydraulic Structures and Water Resources Management* 2001, Graz University of Technology: Graz, Austria p. 95.

97. Wong, S.F., M.C. Law, Y. Samyudia, and S.S. Dol, *Rheology study of water-in-crude oil emulsions.* Chemical Engineering Transactions, 2015. **45**: p. 1411-1416.

98. Auflem, I.H., *Influence of asphaltene aggregation and pressure on crude oil emulsion stability*. 2002, Norwegian University of Science and Technology.

99. Al-Yaari, M., I. Hussein, A. Al-Sarkhi, M. Abbad, F. Chang, and B. Abu-Sharkh, *Effect of Water Fraction on Surfactant Stabilized Water-in-Oil Emulsion Flow Characteristics.* Society of Petroleum Engineers Journal.

100. Ariffin, T.S.T., E. Yahya, and H. Husin. *The Rheology of Light Crude Oil and Water-in-Oil Emulsion*. in *Procedia Engineering*. 2016.

101. Stern, F., M. Muste, M.-L. Beninati, and W.E. Eichinger, *Summary of Experimental Uncertainty Assesment Methodology with Example*, in *IIHR Technical Report No. 406* 1999 Iowa Institute of Hydraulic Research College of Engineering, The University of Iowa Iowa City, Iowa 52242 p. 37.

102. Khandpur, R.S., *Handbook of Analytical Instruments*. McGraw Hill Education (India) Private Limited.

103. Coleman, H.W. and W.G. Steele, *Experimentation, Validation, and Uncertainty Analysis for Engineers*. 2009: Wiley.

104. Nadkarni, R.A.K., *Guide to ASTM Test Methods for the Analysis of Petroleum Products and Lubricants*. 2nd Edition ed. 2007: ASTM International, West Conshohocken, PA.

105. George, H.F. and F. Qureshi, *Newton's Law of Viscosity, Newtonian and Non-Newtonian Fluids*, in *Encyclopedia of Tribology*. 2013, Springer. p. 2416-2420.

106. Hebert, D.A. and S.M. de Bruyn Kops, *Relationship between vertical shear rate and kinetic energy dissipation rate in stably stratified flows.* Geophysical research letters, 2006. **33**(6).

107. Sanchez, L.E. and J.L. Zakin, *Transport of viscous crudes as concentrated oil-in-water emulsions.* Industrial & engineering chemistry research, 1994. **33**(12): p. 3256-3261.

108. Langevin, D., S. Poteau, I. Hénaut, and J. Argillier, *Crude oil emulsion properties and their application to heavy oil transportation.* Oil & gas science and technology, 2004. **59**(5): p. 511-521.

109. Ronningsen, H.P., *Rheology of petroleum fluid.* Annual Transaction of the Nordic Rheology Society, 2012. **20**: p. 11-18.

110. Auflem, I.H., *Influence of asphaltene aggregation and pressure on crude oil emulsion stability*. Norwegian University of Science and Technology. Doktor Ingeniør Thesis, 2002.

111. Al-Yaari, M., I. Hussein, A. Al-Sarkhi, M. Abbad, F. Chang, and B. Abu-Sharkh, *Effect of Water Fraction on Surfactant Stabilized Water-in-Oil Emulsion Flow Characteristics*. Society of Petroleum Engineers.

112. Fincham, A., T. Maxworthy, and G. Spedding, *Energy dissipation and vortex structure in freely decaying, stratified grid turbulence.* Dynamics of Atmospheres and Oceans, 1996. **23**(1-4): p. 155-169.

113. Boundless, *The Collision Theory*, in *Boundless Chemistry Boundless*. 2016.

114. Abiev, R.S. and M.P. Vasilev, *Pulsating flow type apparatus: Energy dissipation rate and droplets dispersion.* Chemical Engineering Research and Design, 2016. **108**: p. 101-108.

115. Walsh, J.M., *The Savvy Separator Series: Part 5. The Effect of Shear on Produced Water Treatment.* Oil and Gas Facilities, 2016. **5**(01): p. 16-23.

116. Gomaa, H.G., J. Liu, R. Sabouni, and J. Zhu, *Operational characteristics of oscillatory micro-screen emulsifier: Coupling effects and energy dissipation.* Chemical Engineering Science, 2014. **117**: p. 161-172.

117. Al-Yaari, M., I.A. Hussein, and A. Al-Sarkhi, *Pressure drop reduction of stable water-in-oil emulsions using organoclays.* Applied Clay Science, 2014. **95**: p. 303-309.

118. Gong, J. *Study On Flow Friction of Hydrate Slurry Under Water-in-Oil Emulsions Condition*. in *The Twentieth International Offshore and Polar Engineering Conference*. 2010. International Society of Offshore and Polar Engineers.

119. Jackson, J., R. Harrington, and D. Manko, *Emulsion Tendency Studies --Understanding Method, Inhibitors And Water Cut*. NACE International.

120. Karbstein, H. and H. Schubert, *Developments in the continuous mechanical production of oil-in-water macro-emulsions.* Chemical Engineering and Processing: Process Intensification, 1995. **34**(3): p. 205-211.

121. Jafari, S.M., E. Assadpoor, Y. He, and B. Bhandari, *Re-coalescence of emulsion droplets during high-energy emulsification.* Food hydrocolloids, 2008. **22**(7): p. 1191-1202.

122. Tjaberinga, W., A. Boon, and A. Chesters, *Model experiments and numerical simulations on emulsification under turbulent conditions.* Chemical engineering science, 1993. **48**(2): p. 285-293.

123. Li, F.-C., B. Yu, J.-J. Wei, and Y. Kawaguchi, *Turbulent drag reduction by surfactant additives*. 2012: John Wiley & Sons.

124. Li, F.-C., Y. Kawaguchi, and K. Hishida, *Investigation on the characteristics of turbulence transport for momentum and heat in a drag-reducing surfactant solution flow.* Physics of Fluids, 2004. **16**(9): p. 3281-3295.

125. Virk, P.S., *Drag reduction fundamentals.* AIChE Journal, 1975. **21**(4): p. 625-656.

126. Brasseur, J.G. and M.J. Lee, *Local structure of intercomponent energy transfer in homogeneous turbulent shear flow*. 1987.

127. Varaksin, A.Y., Y.V. Polezhaev, and A.F. Polyakov, *Effect of particle concentration on fluctuating velocity of the disperse phase for turbulent pipe flow.* International journal of heat and fluid flow, 2000. **21**(5): p. 562-567.

128. PETRONAS, *Annual Crude Pipeline Network Capacity Report (Internal Report)*. 2015.